UC Santa Cruz

UC Santa Cruz Electronic Theses and Dissertations

Title

Redefining the Role of the P3 Peptide in the Amyloid Cascade Hypothesis

Permalink

https://escholarship.org/uc/item/2kq736s5

Author

Kuhn, Ariel Jade

Publication Date

2021

Copyright Information

This work is made available under the terms of a Creative Commons Attribution License, available at https://creativecommons.org/licenses/by/4.0/

Peer reviewed|Thesis/dissertation

eScholarship.org Powered by the California Digital Library
University of California

UNIVERSITY OF CALIFORNIA
SANTA CRUZ

REDEFINING THE ROLE OF THE P3 PEPTIDE IN THE AMYLOID CASCADE HYPOTHESIS

A dissertation submitted in partial satisfaction
of the requirements for the degree of

DOCTOR OF PHILOSOPHY

in

CHEMISTRY

by

Ariel Jade Kuhn

December 2021

The dissertation of Ariel Jade Kuhn
is approved:

_____
Professor Jevgenij Raskatov, Chair

_____
Professor R. Scott Lokey

_____
Professor Seth Rubin

_____
Peter F. Biehl
Vice Provost and Dean of Graduate Studies

Copyright © by

Ariel Jade Kuhn

2021

TABLE OF CONTENTS

Page

List of Figures……...vi

Abstract……...viii

Acknowledgements……..xii

Dedication……...xvi

Chapter 1. Introduction

1.1 Role of intrinsically disordered proteins in Alzheimer's Disease……..…2

1.2 Background on the p3 peptide…….5

1.3 Specific Aims…….11

Aim 1. Determine aggregation kinetics and resulting morphology of aggregates formed by the C-terminal fragment of Aβ, the p3 peptide……..11

Aim 2. Discern colocalization and seeding effects between of p3 with Aβ to establish a heterogenous Amyloid aggregation model……12

Aim 3. Relationships between uptake and toxicity for p3 and Aβ, and associated mixtures……..12

Aim 4. Devise novel methods for combating challenges associated with studying aggregation-prone, intrinsically disordered proteins such as Aβ & p3……..13

1.4 Reprint: Is the p3 peptide (Aβ17-40, Aβ17-42) relevant to the pathology of Alzheimer's Disease……14

Chapter 2. Biophysical and morphological characterization of the p3 peptide

2.1 Introduction……27

2.1 Reprint: Alzheimer's Disease "Non-amyloidogenic" p3 peptide revisited: A case for Amyloid-α……..29

Chapter 3. Biophysical and biological properties of heterogenous mixtures of p3 and Aβ

3.1 Reprint: Mixing of Aβ and p3 Results in Fibrilization Enhancement, Unique Intermediate Formation, and Suppression of Toxicity …….36

Chapter 4. Tools to evade the challenges of studying intrinsically disordered proteins

4.1 Introduction…….……69

4.2 Reprint: Using mirror-image peptides to enhance robustness and reproducibility in studying the amyloid-β protein……...75

4.3 Reprint: New insights into differential aggregation of enantiomerically pure and racemic Aβ40 systems……..87

4.4 Reprint: Chirality dependence of amyloid-β cellular uptake and a new mechanistic perspective……...94

4.5 Reprint: A Crystal-Structural Study of Pauling-Corey Rippled Sheets…...99

References

Appendix

A. RightsLinks……...138

B. Supporting Information (SI) for reprinted publications

B.1 Alzheimer's Disease "Non-amyloidogenic" p3 peptide revisited: A case for Amyloid-α ……...142

B.2. Mixing of Aβ and p3 Results in Fibrilization Enhancement, Unique Intermediate Formation, and Suppression of Toxicity……..156

B.3. New insights into differential aggregation of enantiomerically pure and racemic Aβ40 systems……174

B.4. Chirality dependence of amyloid-β cellular uptake and a new mechanistic perspective…….182

B.5. A Crystal-Structural Study of Pauling-Corey Rippled Sheets…….199

LIST OF FIGURES

Chapter 1. Introduction

Figure 1. Two major processing pathways of the Amyloid-β Precursor Protein (AβPP)……...4

Figure 2. Comparison in quantity of papers discussing p3 vs Aβ over time.…6

Figure 3. Comparison in quantity of papers discussing p3 vs non-amyloidogenicity……7

Figure 4. Binding sites of various Amyloid-targeting AD therapeutics along the Aβ sequence…….9

Figure 5. Isolation of p3 from plaques…….10

Chapter 2. Biophysical and morphological characterization of the p3 peptide

Figure 6. Sequence and structural information for Aβ1-40 and p3(17-40)…….……28

Chapter 3. Biophysical and biological properties of heterogenous mixtures of p3 and Aβ

Figure 7. Hydropathy profile of Aβ42 and p3…….39

Figure 8. Confocal microscopy images……...41

Figure 9. ThT-monitored kinetics and SEM images……43

Figure 10. PICUP SDS-PAGE gel and TEM images……..45

Figure 11. Cellular viability, ROS production and LDH release…….48

Figure 12. Flow cytometry quantitation ……..51

Chapter 4. Tools to evade the challenges of studying intrinsically disordered proteins

Figure 13. Nucleation-dependent, self-assembly of Aβ……..70

Figure 14. Multi-step purification protocol of the p3 peptide…….71

ABSTRACT

REDEFINING THE ROLE OF THE P3 PEPTIDE IN THE AMYLOID CASCADE HYPOTHESIS

Ariel Jade Kuhn

Alzheimer's Disease (AD) is the 6th leading cause of death in the United States and affects over 6 million Americans. Surprisingly, dementia-related deaths have increased by over 16% during the SARS-CoV-2 pandemic, making finding a cure more now important than ever. AD is characterized by two major pathological hallmarks: amyloid plaques, rich in the intrinsically disordered, aggregation-prone Amyloid-β (Aβ) peptide, and neurofibrillary tau tangles. The transmembrane protein that produces Aβ, the Amyloid-β Precursor Protein (AβPP), is cleaved by β- (BACE1) and γ-secretases. While much of the Aβ-focused therapeutic and academic efforts have targeted late-stage, insoluble Aβ fibrils, interest has shifted to the more toxic intermediate oligomers. These transient, rapidly interconverting oligomers are exceptionally challenging to study and therapeutically target, a fact made abundantly clear by the succession of devastating drug trial failures.

AβPP can be alternatively processed by other lesser-known enzymes, such as α-secretase, to produce alternative peptidic fragments. One such fragment, the p3 peptide, is a C-terminal fragment of Aβ, and spans residues 17-40/42, the segment most

attributed to Aβ's amyloidogenicity. Despite this, p3 has traditionally been described as non-amyloidogenic and neuroprotective. Consequently, the biological and biophysical properties of p3 have been sparsely studied. The studies described in this thesis aim to provide an extensive *in vitro* characterization of p3, to better understand its role, if any, in AD.

In Chapter 1, we aim to summarize and deconvolute the small pool of conflicting findings in the literature surrounding the p3 peptide. According to PubMed, since 1984, there have been 56,502 papers that mention Aβ, and only 921 that mention p3, an over 60-fold difference (Figure 2). Of the small pool of papers published discussing p3 since the mid-1980s, only a handful investigate the properties of the peptide, while most simply state that it is non-amyloidogenic, or that its production precludes the production of Aβ. Despite this, a few rarely discussed papers, primarily published in the 1990s and early 2000s, expose amyloidogenic properties of p3. Our work, discussed in Chapters 2 and 3, builds on these early studies.

In Chapter 2, we employed advanced chemical biological techniques to assess whether p3 is truly non-amyloidogenic, as indicated by the literature. We found that p3 self-assembles to form oligomers and fibrils morphologically indistinguishable from Aβ, and that these resultant aggregates share confirmational similarities with Aβ. Additionally, we determined that the rate of p3 fibril formation is significantly faster than that of Aβ. These results highlight the solubilizing effect of the N-terminus of Aβ, and the importance of hydrophobic contacts in amyloid formation.

In Chapter 3, we investigated the kinetic and biological consequences of mixing p3 and Aβ, to simulate the endogenous heterogeneity of amyloid aggregation in the brains of AD patients. We observed fibrillar colocalization of Aβ and p3, and enhanced aggregation propensity of Aβ upon introduction of p3. This enhancement in stable, insoluble, heterogenous fibril formation resulted in reduced cellular toxicity. We found that under fibril forming conditions, mixtures of Aβ and p3 produced unique oligomers not observed in the homogenous preparations. Additionally, fibril formation proved favorable even under oligomer forming conditions. The enhanced fibril formation resulted in suppression of toxicity and ROS production in both PC12 and SH-SY5Y cells. Additionally, we found that at an early timepoint, TAMRA-Aβ and TAMRA-p3 uptake was comparable, while at a later timepoint, internalization of labeled-peptide was nearly 6x higher for the TAMRA-Aβ treated cells. However, no augmentation of uptake was observed upon addition of unlabeled p3 into TAMRA-Aβ treated cells.

In Chapter 4, we discuss challenges in the field of intrinsically disordered proteins (IDPs), and offer novel methods to improve reproducibility. We first propose the benefits of employing all mirror-image peptides to both rigorously control peptide quality, and to probe complicated mechanisms in aggregation and toxicity of Aβ and related peptides. Through comparing the uptake of L- and D-Aβ, we observed that cellular uptake of Aβ is highly stereospecific, indicating that Aβ uptake is likely a receptor-driven process. We also demonstrated "chiral inactivation", a technique previously developed by the Raskatov lab to abolish toxicity of Aβ42, with the Aβ40 system, which we monitored with ^{1}H NMR. This chapter also presents a structural

study of the long-orphaned Pauling-Corey rippled β-sheet. Current knowledge on rippled sheets is limited to a small pool of studies that combined partial experimental structures with theoretical modeling. At the end of Chapter 4, we report a high-resolution crystal structure, in which racemic (L,L,L)- and (D,D,D)-triphenylalanine form dimeric antiparallel rippled sheets, packed into herringbone layers.

Overall, the studies described herein highlight the challenges and controversies in probing IDPs, and a few ways to overcome them. Special attention is paid to p3, a peptidic fragment of Aβ previously described as non-amyloidogenic and innocuous. We urge the field of AD-related research to expand the Amyloid Cascade Hypothesis (ACH) in light of these findings, to account for alternative proteolytic fragments of AβPP, and their resultant biological properties.

ACKNOWLEDGEMENTS

I would first like to acknowledge and thank my graduate research advisor, Professor Jevgenij A. Raskatov for his mentorship and infectious, unwavering passion for science. I greatly appreciate the freedom he afforded me to explore my individual scientific interests, even when they veered away from the general interest of the lab. He has instilled in me the courage to face complex and often controversial scientific challenges. Through his weekly journal club, I have learned to critically read scientific literature, a skill that has made me the curious scientist I am today. Jevgenij has encouraged me to present my research findings at several conferences around the United States, a great privilege which has allowed me to hone my scientific communication skills.

I would also like to acknowledge all of the exceptional labmates I had the pleasure of working with during my time in the Raskatov Lab: Prof. Subrata Dutta, Dr. Luis Alejandro Rodriguez Foley, Dr. Amaruka Hazari, graduate students: Thomas Finn and Ka Chan, as well as undergraduate students: Stella Knowlton, Kareem Bdeir, Jon Brodie, Timothy Kung, and Marleigh Fansler. I specifically would like to thank Subrata and Alejandro for mentoring me as an early graduate student, and teaching me several of the techniques described in this thesis. In addition, I had the great pleasure of mentoring Stella, Kareem, and Jon, during their undergraduate educations. I look forward to watching each of them reach their career goals in future years.

I also extend my gratitude to my thesis committee, Prof. Scott Lokey and Prof. Seth Rubin, for their continued support and feedback throughout my entire PhD. I

would especially like to thank both Scott and Seth for the numerous letters of recommendation they have written for me over the years. I would also like to thank my outside committee member from University of California Irvine, Prof. Charles Glabe for offering crucial feedback on my research ideas and most importantly, for sharing my enthusiasm for the controversial p3 peptide. I would also like to thank Prof. Carrie Partch, without whom I would not have an NIH fellowship. Of this, I am certain. She took the time out of her busy schedule on several occasions to critically review my proposal drafts, and exponentially improved them with each consecutive revision. Additional thanks to Prof. David Kliger and Dr. Eefei Chen for always making themselves available to hear about my projects, and for allowing me to use their lab for my light-sensitive PICUP experiments. In addition, I would like to acknowledge Prof. Timothy Johnstone and Prof. Scott Oliver for their invaluable insights and guidance on the rippled β-sheet projects. I would like to thank many of the outstanding facility directors at UCSC, without whom, these projects would have been impossible: Dr. Hsiau-Wei (Jack) Lee for extensive help with NMR, Dr. Benjamin Abrams for training, guidance, and data analysis on literally every single microscope that UCSC has to offer (if UCSC housed more microscopes, I would have asked Ben for help with those too), Bari Holm Nazario for help with tissue culture and flow cytometry, Dr. Vitor Serrão for Cryo-EM sample preparation and future sample analysis (fingers crossed), and Qiangli (Li) Zhang for help with Mass Spectrometry. I would also like to thank Prof. Jeremy Lee from the MCD Biology Dept., for being an unofficial mentor, and spotting another fisherman at sea in the vast and complicated research field that is Alzheimer's

Disease. Furthermore, I would like to thank David States for his helpful suggestions and revisions on my grant proposals.

I would also like to acknowledge my undergraduate research advisors, Prof. William Karney and Prof. Claire Castro. William and Claire have created a learning environment in which both student growth and scientific advancement receive equal attention.

I would like to extend my immense gratitude to the dedicated administrators and support staff at UCSC: Karen Meece, Katie Crampton, Patti Schell, Derek DeMarco, and Janet Jones. In particular, I would like to thank Karen, who always makes herself available and goes above and beyond for the chemistry graduate students at UCSC. I am confident that every Chemistry graduate student at UCSC feels the same.

My research project was made possible by a Ruth L. Kirschstein Predoctoral Individual National Research Service Award (F31) through the National Institute on Aging at the National Institute of Health (NIH). This funding has afforded me the freedom to explore my independent ideas and pursue high-risk projects.

Furthermore, I would like to thank all of the wonderful friends I have made while at UCSC, including but not limited to, Jenny (and *de facto* Mackie), Pamela, Victor, Anam, Anna, David[2], Tommy, Jocelyn, Kaitlyn, Fran, Melissa, Duy, Pat, Jerah, Tannia, and of course my lovely housemates and friends, Bia, Ray, Lena and Ed. Also, a big thanks to my much furrier housemates, Cake, Jiji, and Jake. Because of these folks (and creatures), I have countless incredible memories from graduate school other

than long nights in lab. I hope to maintain these friendships as we continue down our respective scientific paths. Best of luck to all of the friends listed above (and the many I undoubtedly forgot to mention).

None of this would have been possible without the love and support of my family - both chosen and blood. Thanks to my mom, who is resilient beyond words. Thanks to all of my incredible grandparents; I was lucky enough to have six grandparents in my life, and I would not be who I am today without each and every one of them. They believed in me when no one else would, and for that I am eternally grateful. And a very special thanks to my chosen family and best friends, Jackie, Vicky, Aggie, and Eileen. These girls have been everything to me for over a decade, and I shudder to think where I would be without their unwavering love and support.

I especially would like to acknowledge and thank Ezra Clark, one of the most intelligent, attentive, creative, and weirdest human beings I have ever known. I had the great pleasure of watching Ezra metamorphosize from a stressed-out second-year graduate student at UC Berkeley to an even more stressed-out assistant Professor at Pennsylvania State University. He is my best friend and my life-partner and my backpacking buddy all wrapped up into one very tall package (both literally and figuratively), and I would not have it any other way.

DEDICATION

To my friends, family, and all the dogs I have not yet adopted.

CHAPTER 1: Introduction

This chapter contains text and figures from the following manuscripts: Kuhn, A.J.; Raskatov, R. A. *J. Alz. Dis.* **2020**.; Gowing, E.; Ball, M. J.; et. al. *J. Biol. Chem.* **1994.**; and Lalowski, M.; Wisniewski, T.; et. al. *J. Biol. Chem.* **1996**. See appendix for RightsLinks.

1.1 Role of Intrinsically Disordered Proteins in Alzheimer's Disease

Intrinsically disordered proteins (IDPs) lack defined tertiary structures under physiological conditions, or in the case of intrinsically disordered protein regions (IDPRs), include structureless extended regions. Unlike typical proteins in which strong structure-function relationships can be interpreted and mimicked, IDPs, also known as natively unfolded proteins, offer unique challenges preventing their exploration. This is due, in part, to their significant confirmational heterogeneity and relatively smooth energy landscapes. While many proteins undergo an energetically favorable native folding process, either spontaneously or under the guidance of chaperones, IDPs sample a wide array of rapidly interconvertible confirmations. Surprisingly, approximately 32% of proteins in the human proteome are IDPS, 19% contain IDRPs, leaving only 49% ordered proteins.[1]

IDPs often contain hydrophobic central regions[2] and large net negative charges at either the N- or C-termini, generally attributed to the presence of lysine and/or aspartic acid.[3] The absence of a defined tertiary structure promotes binding promiscuity.[4] In fact, some IDPs fold into different tertiary structures upon specific target binding.[5] For these reasons, diseases related to IDPs, of which there are many, have garnered significant attention from the scientific community. In particular, aggregation prone IDPs are frequently associated with neurodegenerative diseases. Examples include: Amyloid-β (Aβ) and tau in Alzheimer's Disease (AD), α-synuclein in Parkinson's Disease, and amylin in Type 2 Diabetes mellitus.

Alzheimer's Disease (AD), the most prevalent form of dementia, is the 6th leading cause of death in the U.S, affecting 10% of seniors over the age of 65. Alzheimer's Disease is characterized by two major pathological hallmarks: neurofibrillary tau tangles and Aβ-rich amyloid plaques. Aβ is an aggregation-prone IDP, produced by the proteolytic cleavage of Amyloid-β Precursor Protein (AβPP), a transmembrane protein with unknown endogenous function (Figure 1), by β-secretase (BACE1) and γ-secretase (Figure 1). Consequently, free Aβ is released from the cell membrane, after which it self-assembles to form transient oligomers and, eventually, stable fibrils (Figure 1). This pathway is presumed to cause AD, and is referred to as the "Amyloid Cascade Hypothesis". The Amyloid Cascade has been a major target of therapeutic efforts, primarily through β-secretase inhibitors and Aβ aggregation modulators. Unfortunately, all of these efforts have been met with disappointment, which the exception of the recent approval of the controversial drug, Aducanumab.[6,7]

Figure 1 (*Next Page*). Two major processing pathways of the Amyloid-β Precursor Protein (AβPP). A) Sequences of Aβ(1-40/42), including two alternative β-secretase cleavage sites (3-40/42 and 11-40/42), and the sequence of p3(17-40/42), produced by α-secretase. B) Two proteolytic processing pathways of AβPP: the Amyloidogenic pathway, in which sAβPPβ and Aβ are produced by the sequential cleavages by β- and γ- secretases. Aβ is an aggregation-prone peptide that undergoes self-assembly to form transient oligomers, and late-stage fibrils. Alternatively, the so-called "Non-Amyloidogenic" pathway produces sAβPPα and p3, via α- and γ- secretases. The aggregation pathway for p3 is denoted with a "?", as p3 has traditionally been described as "non-aggregation-prone". *Adapted with permission from:* Kuhn, A. J.; Raskatov, J. Is the P3 Peptide (Aβ17-40, Aβ17-42) Relevant to the Pathology of Alzheimer's Disease? *J Alzheimer's Dis* **2020**.[8] See appendix for RightsLink.

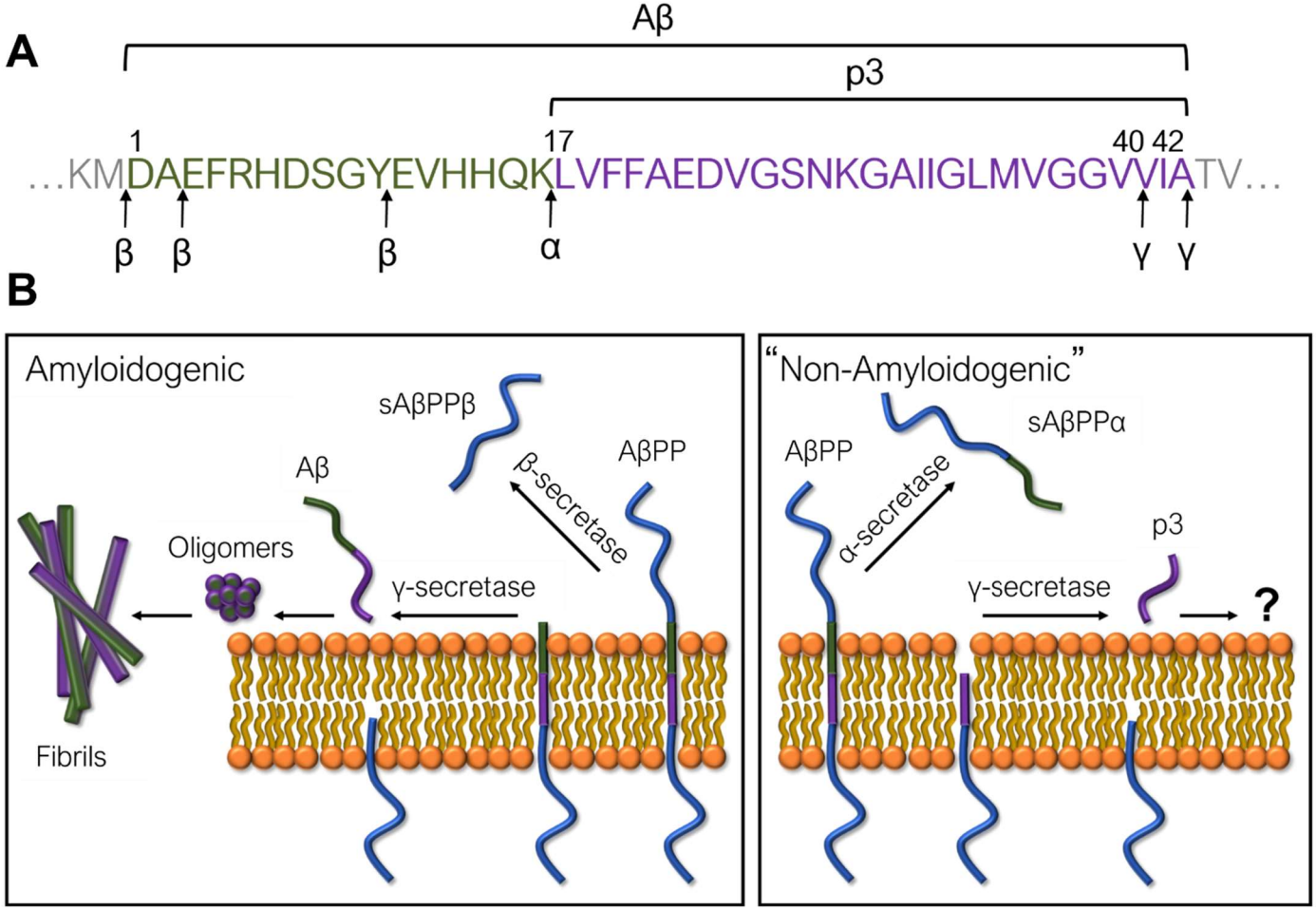
A
Aβ
p3
1
17
40 42
…KMDAEFRHDSGYEVHHQKLVFFAEDVGSNKGAIIGLMVGGVVIATV…
β
β
β
α
γ
γ
B
Amyloidogenic
sAβPPβ
AβPP
Aβ
β-secretase
Oligomers
γ-secretase
Fibrils
"Non-Amyloidogenic"
sAβPPα
AβPP
α-secretase
p3
γ-secretase
?

1.2 Background on the p3 peptide

Moreover, AβPP has additional proteolytic processing pathways, featuring enzymes other than β-secretase, such as α-, δ- and η-secretases.[9–11] The α-secretase pathway, attributed to ADAM9, ADAM10, and/or ADAM17,[11] produces the p3 peptide, a major focus of this thesis. p3 is the C-terminal fragment of Aβ, spanning residues 17-40/42 (Figure 1). This pathway is thought to be the more prominent endogenous processing pathway of AβPP, yet has received significantly less mentions in the literature (Figure 2). Specifically, in 2020, there were 64 papers on p3, which is starkly contrasted against the 4406 papers on Aβ, a nearly 69-fold difference (Figure 2). In addition, most of these studies that mention p3 refer to it as "non-amyloidogenic" and "neuroprotective" (Figure 3), despite little to no evidence to support this. Since 1984, there have been 56,502 papers that mention Aβ, and only 921 that mention p3, an over 60-fold difference (Figure 2). Of the small pool of papers published discussing p3 since the mid-1980s, only a handful investigate the properties of the peptide, as most simply state that it is non-amyloidogenic, or that its production precludes the production of Aβ. These numbers are staggering when one considers that p3 is the more prominently produced fragment of AβPP, and that it is supposedly "neuroprotective". Given this, it is perplexing that there have not been more significant efforts to understand this peptide, specifically, how much is produced in healthy vs AD patients, and how these values are affected upon therapeutic intervention. However, the studies specifically aimed at understanding the biophysical and/or biological properties offer very conflicting accounts. This topic is discussed in more detail in the reprinted

manuscript at the end of this chapter: Kuhn, A. J. Raskatov, R. A. Is the p3 (Aβ17-40, Aβ17-42) peptide relevant to the pathology of Alzheimer's Disease? *J. Alz. Dis.* **2020**, 74 (1), 43-53.

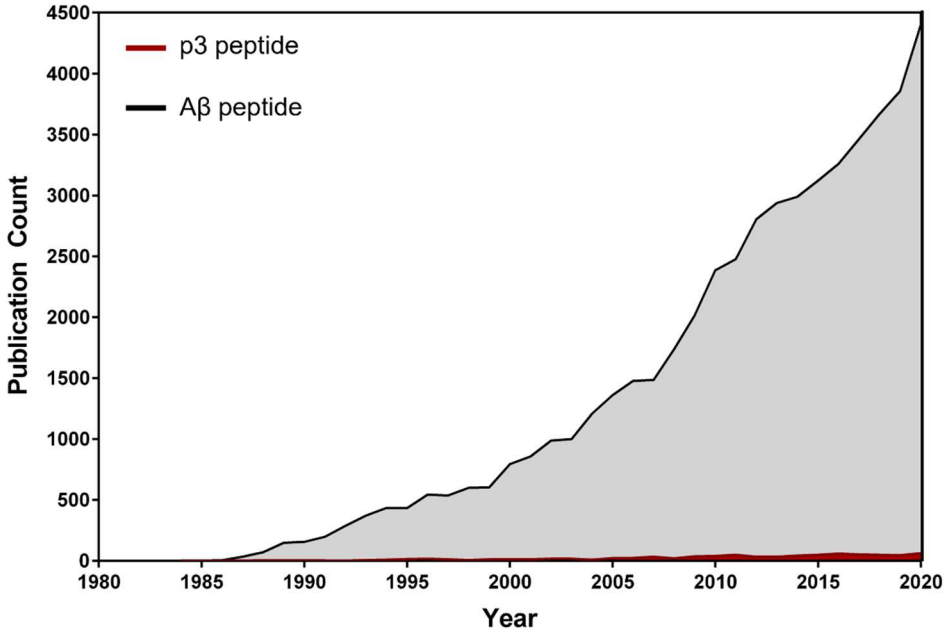

Figure 2. Comparison in quantity of papers discussing p3 vs Aβ over time. A PubMed search was conducted in which the following search terms were used for p3: "p3" AND "Alzheimer's Disease" OR "non-amyloidogenic" AND "Alzheimer's Disease". The following search terms were used for Aβ: "Amyloid-β" AND "Alzheimer's Disease" OR "Aβ" AND "Alzheimer's Disease".

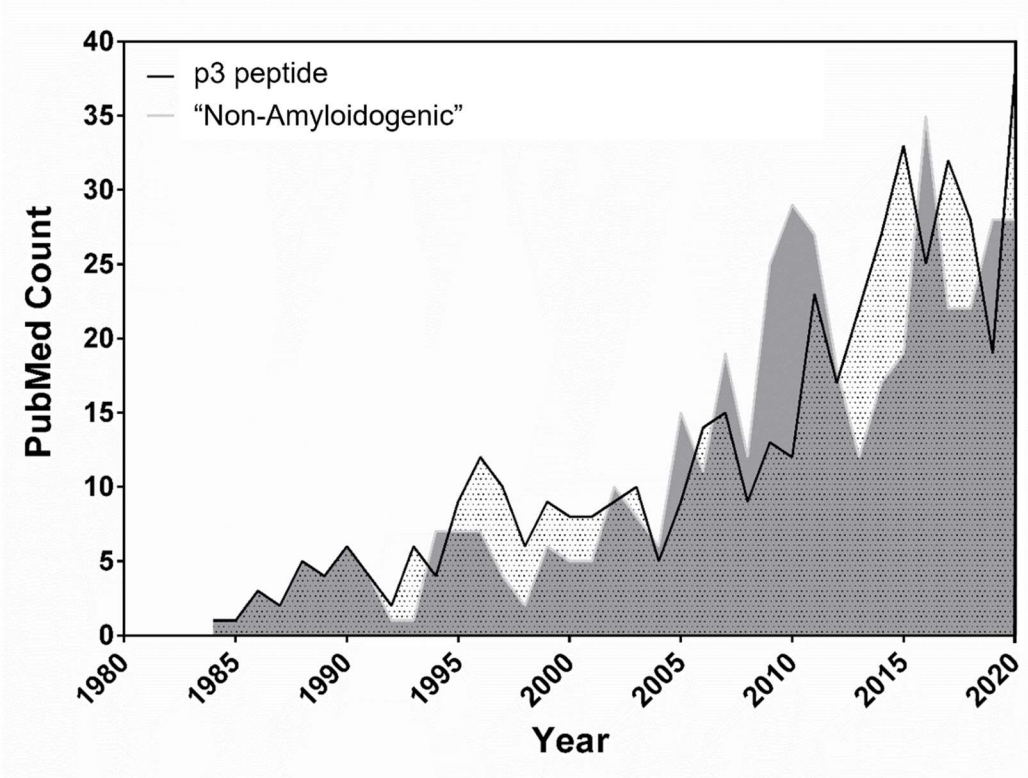

Figure 3. Comparison in quantity of papers discussing p3 vs non-amyloidogenicity. A PubMed search was conducted in which the following search terms were used for p3: "p3" AND "Alzheimer's Disease". The following search terms were used for non-amyloidogenic: "non-amyloidogenic" AND "Alzheimer's Disease".

Despite the myriad Alzheimer's Disease therapeutics targeting the production and clearance of the Aβ peptide, a cure is yet to be identified. While there are likely a myriad of reasons for this, given the vast complexity of the disease, one possible explanation is that the amyloid model only seeks to understand the properties of two predominant isoforms of Aβ – comprised of 40 or 42 amino acids. As a consequence, many proposed amyloid-targeting AD therapeutics bind the N-terminus of Aβ, the segment absent in p3 (Figure 4). Thus, if p3 or any of the other fragments of Aβ are in fact pathogenic or are in some way cooperatively involved in aggregation of Aβ, these therapeutics may be rendered ineffective.

Figure 4 (next page). Binding sites of various Amyloid-targeting AD therapeutics along the Aβ sequence.

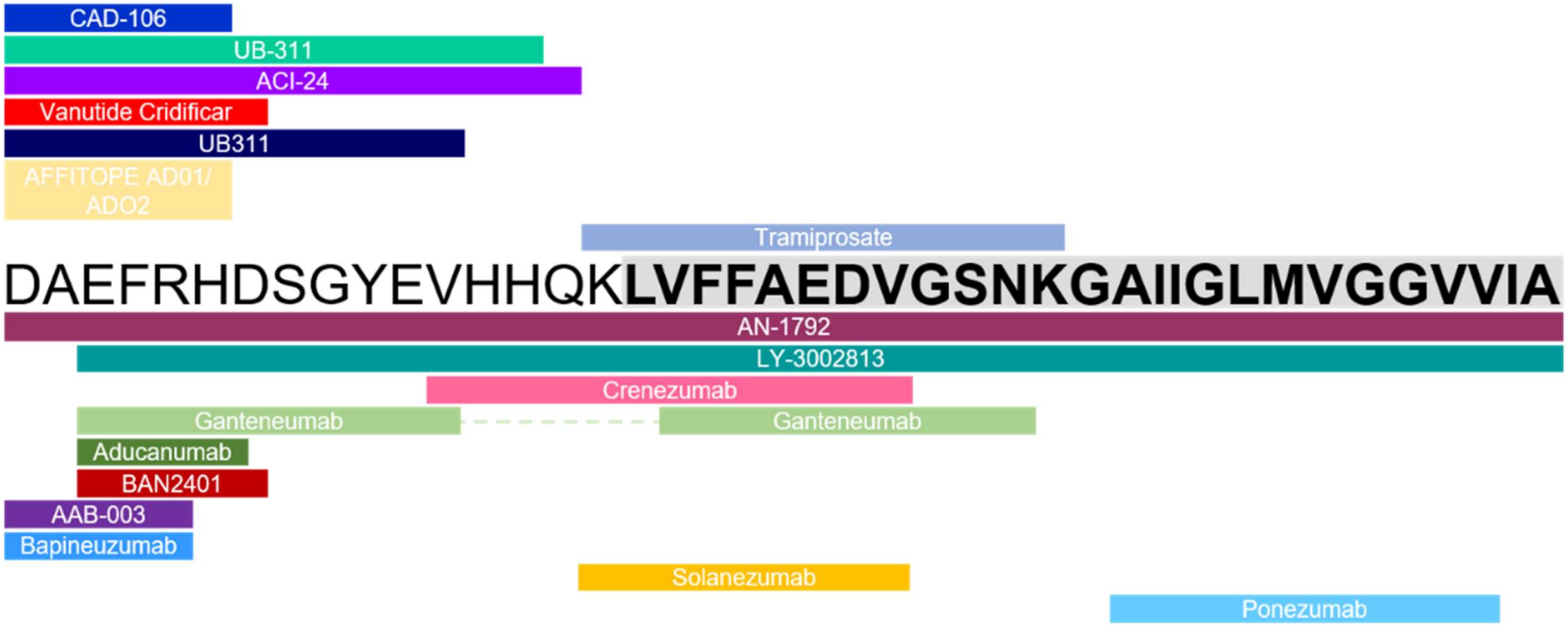
CAD-106
UB-311
ACI-24
Vanutide Cridificar
UB311
AFFITOPE AD01/ ADO2
Tramiprosate
DAEFRHDSGYEVHHQKLVFFAEDVGSNKGAIIGLMVGGVVIA
AN-1792
LY-3002813
Crenezumab
Ganteneumab
Ganteneumab
Aducanumab
BAN2401
AAB-003
Bapineuzumab
Solanezumab
Ponezumab

In addition, plaques isolated from the brains of Alzheimer's patients contain a variety of Aβ peptides and over 900 unique proteins (approximately 200 of which are found consistently across many patient samples).[12,13] Given that p3 may be a predominant processing product of AβPP, and as described in Chapter 1, it rapidly forms amyloidogenic aggregates, presumably, p3 is one of these 900 proteins. Interestingly, p3 is a major component of "diffuse" amyloid plaques in AD patients and cerebellar preamyloid in those with Down Syndrome (Figure 5).[14,15] Aside from these studies, little is known about what happens to p3 in the brains of Alzheimer's patients in terms of aggregation, clearance and pathogenesis. To ensure that future AD therapeutics are more effective, we urgently need to understand how the different isoforms and fragments of Aβ and AβPP collectively contribute to the very complex disease that is AD.

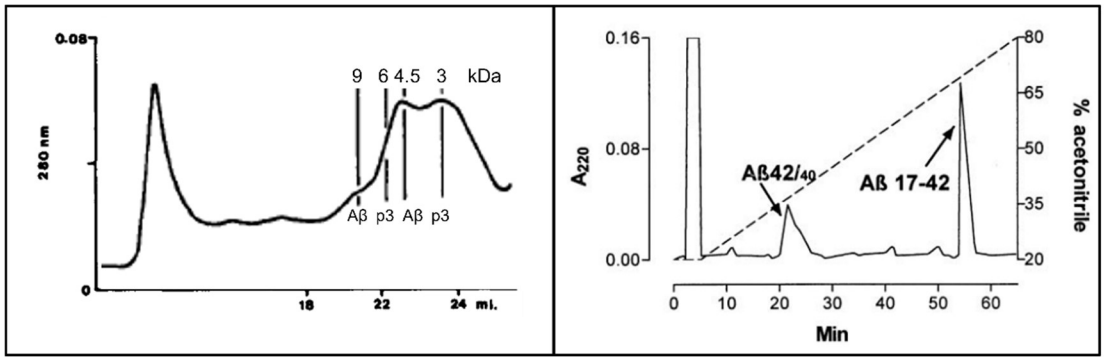

Figure 5. Isolation of p3 from plaques. Left panel: LCMS chromatogram of diffuse amyloid isolate from the brain of an AD patient.[14] The two peaks labeled 3 and 6 kDa were determined to be p3, and the two peaks labeled 4.5 and 9 kDa correspond to Aβ. Right panel: LCMS chromatogram of cerebellar preamyloid from the brain of a person with Down Syndrome.[15] The peak labeled Aβ17-42 is p3, and Aβ42/40 is Aβ. *Images adapted with permission from:* Gowing, E.; Ball, M. J.; et. al. *J. Biol. Chem.* **1994** and Lalowski, M.; Wisniewski, T.; et. al. *J. Biol. Chem.* **1996**. See appendix for RightsLinks.

1.3 Specific Aims

The purpose of the research described herein is to elucidate the mechanisms by which β-Amyloid (Aβ) and one of its variants contribute *collectively* to the pathology of Alzheimer's Disease. To meet this end, our lab has pioneered an efficient and large-scale method for producing exceptionally pure Aβ and related peptides,[16] putting us in a unique position to study their biophysical and biological properties.

The major goal of this work was to characterize the aggregation and mechanism of toxicity of p3 to elucidate its role in amyloid fibril formation. My hypothesis was that the p3 fragment forms amyloid fibrils capable of imparting drastic changes on the aggregation of the well-studied Aβ peptide. The current amyloid model can be significantly improved by understanding the collective contribution of all Aβ-related peptides

Aim 1. Determine aggregation kinetics and resulting morphology of aggregates formed by the C-terminal fragment of Aβ, the p3 peptide

Characterizing the mechanism and morphology of p3 aggregates is crucial to establishing its role, if any, in Alzheimer's Disease. Given that p3 is primarily hydrophobic and contains 100% of sequence segments of Aβ attributed to amyloidogenicity, the lack of current literature focused on its aggregation is surprising. My results indicate that p3 exhibits expedited aggregation propensity and forms oligomers and fibrils morphologically indistinguishable from those formed by Aβ. In

addition, I have demonstrated that p3 binds OC and Congo Red, both probes specific for β-sheet-rich amyloid fibrils.

Aim 2. Discern colocalization and seeding effects between of p3 with Aβ to establish a heterogenous Amyloid aggregation model.

To date, most structural work on Aβ aggregation exclusively explores homogenous aggregates comprised of Aβ. However, this approach must be expanded to include other isoforms given the diversity in plaque content. I found that TAMRA-labeled p3 and FAM-labeled Aβ colocalize in heterogenous aggregates. I also found that p3 seeds Aβ, resulting in fibril formation enhancement. In addition, heterogenous mixtures of p3 and Aβ form new oligomeric species not observed in the respective homogenous preparations.

Aim 3. Relationships between uptake and toxicity for p3 and Aβ, and associated mixtures

Despite the enormous body of work focused on the aggregation of Aβ, the mechanism by which Aβ exerts its toxicity remains elusive, despite many proposed pathways, ranging from inflammation to calcium dysregulation. Our lab, among others, has demonstrated a correlation between cellular uptake and toxicity of Aβ, indicating that uptake may be a compulsory step of toxic action. My findings indicate that p3 is less toxic and cell permeable as compared to Aβ. Surprisingly, I also found that p3 rescues viability of cells dosed with toxic concentrations of Aβ.

Aim 4. Devise novel methods for combating challenges associated with studying aggregation-prone, intrinsically disordered proteins such as Aβ and p3

IDPs are exceptionally challenging to study, making it difficult to acquire reproducible, reliable data. Aβ, in particular, is extremely sensitive to small perturbations, impurities, and deviations in synthetic and isolation methodologies. This is reflected in the inconsistent and often controversial findings across the Aβ literature. To evade these challenges, aside from adopting extensive purification, filtration, and pre-treatment protocols, our lab has employed all-D enantiomeric peptides as a biophysical and biological control to improve rigor and reproducibility in Aβ studies. This approach has allowed us to induce oligomer-to-fibril conversion in the aggregation profile of Aβ. Additionally, we have employed chirality as a tool to study the mechanism of cellular uptake of Aβ. Through these explorations, we have resolved a high-resolution crystal structure of an antiparallel, rippled β-sheet, a structural motif first theorized by Pauling and Corey in 1953. A subsequent PDB search uncovered three orphaned rippled sheets among racemic protein crystal structures.

By providing key insights into the aggregation properties and biological activity of p3, the described work demonstrates how p3 interacts with Aβ, and how it affects the well-studied amyloid model.

1.4 Reprint: Is the p3 peptide (Aβ17-40, Aβ17-42) relevant to the pathology of Alzheimer's Disease: Reprinted with permission from IOS Press (*J. Alz. Dis.* **2020**, 74 (1), 43-53). This publication is available at IOS Press through http://dx.doi.org/10.3233/JAD-191201.

Journal of Alzheimer's Disease 74 (2020) 43–53
DOI 10.3233/JAD-191201
IOS Press

Review

Is the p3 Peptide (Aβ17-40, Aβ17-42) Relevant to the Pathology of Alzheimer's Disease?[1]

Ariel J. Kuhn and Jevgenij Raskatov*
Department of Chemistry and Biochemistry, University of California Santa Cruz, Physical Sciences Building, Santa Cruz, CA, USA

Handling Associate Editor: Annelise Barron

Accepted 30 December 2019

Abstract. Despite the vast heterogeneity of amyloid plaques isolated from the brains of those with Alzheimer's Disease (AD), the basis of the Amyloid Cascade Hypothesis targets a single peptide, the amyloid-β (Aβ) peptide. The countless therapeutic efforts targeting the production and aggregation of this specific peptide have been met with disappointment, leaving many to question the role of Aβ in AD. An alternative cleavage product of the Amyloid-β protein precursor, called the p3 peptide, which has also been isolated from the brains of AD patients, has been largely absent from most Aβ-related studies. Typically referred to as non-amyloidogenic and even suggested as neuroprotective, the p3 peptide has garnered little attention aside from some conflicting findings on cytotoxicity and potential self-assembly to form higher order aggregates. Herein, we report an extensive analysis of the findings surrounding p3 and offer some evidence as to why it may not be as innocuous as previously suggested.

Keywords: Amyloid-β, amyloids, intrinsically disordered proteins, p3, peptides

BACKGROUND ON ALZHEIMER'S DISEASE

Alzheimer's Disease (AD) is a debilitating, neurological disease responsible for an annual worldwide financial burden of over $818 billion US dollars [1]. While a definitive cause of the disease remains elusive, even in lieu of successive drug trial failures, significant evidence still supports the Amyloid Cascade Hypothesis. The basis of the Amyloid Cascade Hypothesis is that an intrinsically disordered protein, called amyloid-β (Aβ), aggregates to form intermediate, soluble oligomers, and eventually late-stage, insoluble fibrils that accumulate in the brains of patients, eventually leading to dementia [2, 3]. While the AD brain is riddled with plaques rich in Aβ fibrils, substantial evidence points to the metastable oligomers as the neurotoxic species of Aβ responsible for cognitive decline [3–6].

The processing of the Amyloid-β protein precursor (AβPP) occurs via two main enzymatic routes (Fig. 1): the amyloidogenic pathway and an alternative pathway, commonly referred to as "non-amyloidogenic". In the amyloidogenic pathway, AβPP is cleaved by β- and γ- secretases to produce Aβ. Alternatively, in the "non-amyloidogenic pathway", AβPP is cleaved by α- rather than β-secretase to produce an N-terminally truncated version of Aβ, called p3 [Aβ (17-40/42) or p3 (17-40/42)] (Fig. 1B). The p3-producing pathway is thought to

[1]In memoriam Christopher M. Dobson

*Correspondence to: Jevgenij Raskatov, Department of Chemistry and Biochemistry, University of California Santa Cruz, Physical Sciences Building, 1156 High Street, Santa Cruz, CA 95064, USA. Tel.: 831 459 2978; E-mail: jraskato@ucsc.edu.

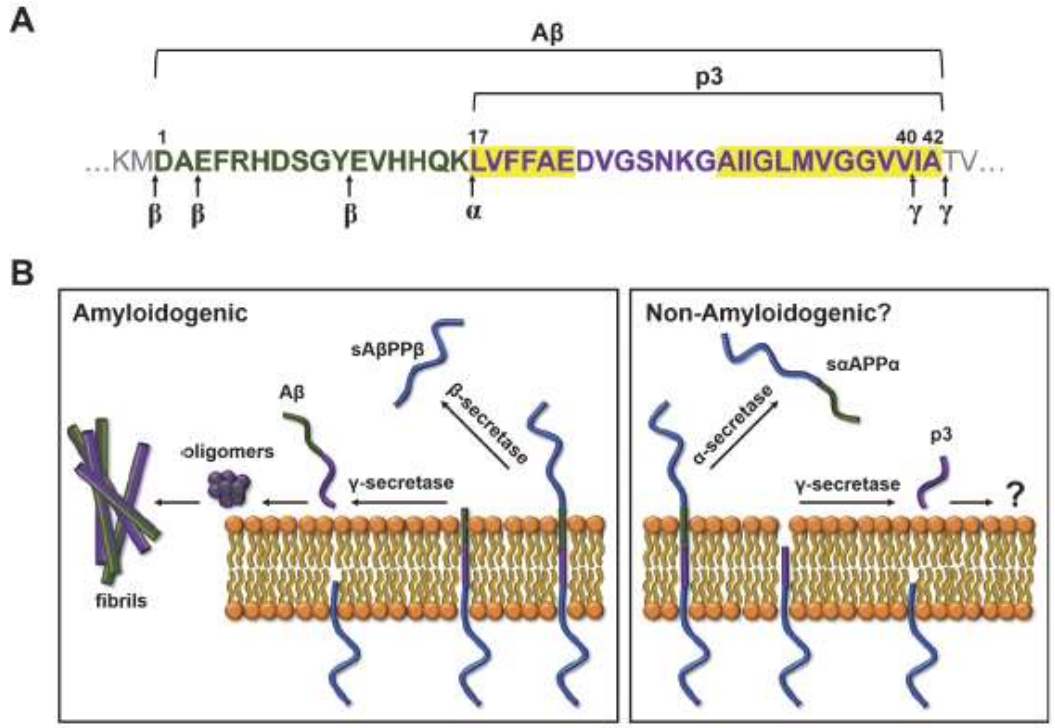

Fig. 1. Processing pathways of AβPP. A) The sequences of Aβ (1-40/42), including two alternative β-secretase cleavage sites (3-40/42 and 11-40/42), and the sequence of p3 (17-40/42), produced by α-secretase. The highlighted regions of the sequence (17-22 and 30-42) denote aggregation "hot spots" of Aβ (1-42) as determined by the web-based prediction software, AGGRESCAN [8]. B) The two major pathways of AβPP processing: the Amyloidogenic pathway, in which sAβPPβ and Aβ are produced by the sequential cleavages by β- and γ-secretases. Aβ is an aggregation-prone peptide that undergoes self-assembly to form transient oligomers, and late-stage fibrils. Alternatively, the so-called "Non-Amyloidogenic" pathway produces sAβPPα and p3, via α- and γ- secretases.

be favored, as p3 is released from cultured neurons approximately 2-fold more frequently than Aβ [7]. While most consider the p3-producing pathway to be neuroprotective given that it precludes the production of Aβ, little is known about the biological and biophysical properties of p3. Despite this, upon employing a web-based software for the prediction of aggregation-prone regions of polypeptides [8], we found that 100% of the predicted "hot spots" calculated for Aβ (1-42) were found within the p3 region (residues 17-42) (Fig. 1A). It begs the question as to why further studies have not been conducted to understand whether or not p3 plays a pathogenic role in AD.

SUCCESSIVE DRUG TRIAL FAILURES

Due to the strong link between Aβ levels and cognitive dysfunction, many therapeutic efforts have aimed to reduce Aβ levels in the brain, either by targeting Aβ directly, or indirectly through intervention into enzymatic processing of AβPP [9, 10]. To date, most treatments aimed to cure AD have failed Phase III clinical trials [9], aside from Biogen's recent revisited analysis of the anti-amyloid antibody drug, aducanumab, which is currently seeking FDA approval [11]. Moreover, current treatments for AD symptoms include cholinesterase inhibitors and N-methyl-D-aspartate (NMDA) receptor antagonists [12]. These successive failures have led many to question the relevance of Aβ with respect to disease treatment [13]. In fact, several β-secretase inhibitors have actually made patients cognitively worse when compared with the placebo groups [9, 14–16], indicating that a new approach is urgently needed. Ultimately, AD is a complex disease that will likely require a treatment that is multifaceted in nature. Since Aβ is an intrinsically disordered protein, it can

form a diverse landscape of aggregates with varied morphologies and toxicities, making it exceptionally difficult to target with therapeutics [17–19]. In addition, a factor rarely considered in drug design is the heterogeneity of amyloid plaques [20–23]. Proteomic studies have revealed that amyloid plaques isolated from the brains of patients with AD are comprised of on average 913 different proteins, and 279 of these were found consistently in all patients in the study [21]. It is not known what portion of these proteins contribute to plaque formation directly versus proteins that are absorbed at a later point. However, it is clear that Aβ is not the sole contributor to plaque formation.

DEFINING "AMYLOIDOGENIC"

When trying to understand whether p3 should be classified as amyloidogenic, it is important to first define what the term "amyloidogenic" actually means. To provide some historical context, the term "amyloid" was originally implemented by a botanist named Matthias Schleiden in 1838 to describe starch-like structures found in plants [24]. It was later applied to medicine by Rudolf Virchow in 1854 to describe disease-related deposits sensitive to sulfuric acid and iodine staining [25]. Today however, the term is applied more generally to a variety of different disease-related protein deposits, both *in* and *ex vivo* in nature. To provide some clarity, the Nomenclature Committee of the International Society of Amyloidosis defines an amyloid as "extracellular deposits of protein fibrils with a characteristic appearance in electron microscopy, a typical X-ray diffraction pattern and an affinity for Congo red with concomitant green birefringence" [26,27]. A thorough analysis of the small body of literature surrounding p3, primarily from the 1990s, reveals conflicting findings on whether p3 fulfills this definition of amyloidogenic.

DEBATE ON THE AMYLOIDOGENIC PROPERTIES OF P3

Presence of p3 in plaques and cerebrospinal fluid

Despite receiving little attention, p3 has been detected in plaques removed from the postmortem brains of patients with AD [23, 28–30]. In fact, it has been identified as the major component of Down's Syndrome diffuse plaques [28], which are thought to precede the formation of mature, senile plaques [31, 32]. This is of interest because AβPP is located on chromosome 21, so people with Down's Syndrome produce excess AβPP, and thus experience plaque deposition beginning in their 30s [33]. People with Down's Syndrome almost invariably get AD, making the identification of substantial p3 content in plaques seem like an unlikely coincidence. Interestingly, these patients also experience elevated oxidative stress [34]. The finding that p3 is localized in diffuse plaques may provide a snapshot into the early events of Aβ aggregation, which remain elusive in late-onset AD.

Aside from the handful of studies cited above, p3 is rarely mentioned as a product from brain homogenate extractions. However, this does not necessarily mean that p3 is not present in plaques, but rather that there may be detection limits for p3 that must be overcome. Factors that influence levels of certain isoforms of Aβ in postmortem brains may be antibody sensitivity, extraction protocols, and brain extraction locations. Specifically, a commonly used immunohistochemistry antibody, 6E10, binds to amino acids 5–7 on Aβ, [35] thus precluding p3 binding. In contrast, 4G8 binds amino acids 17–24 [35], which binds both Aβ and p3 indiscriminately. The use of 4G8 would prevent any distinction between p3 and Aβ, leading to the incorrect assignment of p3 as Aβ. Also, since p3 lacks a hydrophilic region, it is likely that different protocols and buffers are required for its extraction from brain homogenates. It is also unclear what effect the harsh conditions used in plaque purifications, such as high salt concentration, protease treatment and urea, have on the peptides of interest. In addition, unlike Aβ, p3 is devoid of any tyrosine residues, reducing the extinction coefficient at 280 nm, making UV-Vis detection less straightforward for this fragment.

Furthermore, since amyloid plaque deposition occurs in aging, healthy brains without AD symptoms, it has been suggested that clearance of Aβ plays a pivotal role in AD progression [36–39]. Mawuenyega and coworkers found that, compared to cognitively normal controls, patients with AD showed reduced clearance of Aβ from the brain to the cerebrospinal fluid (CSF) [39]. Since p3 has not been implicated in AD, aside from one study that found elevated p3 levels in the CSF of patients with mild cognitive impairment [40], p3 is largely absent from studies on Aβ clearance. This is problematic because p3 (and/or other Aβ isoforms and fragments) may be an essential element to unlocking the

AD puzzle, either through its effect on Aβ aggregation or clearance. Perhaps there is a substantial difference in clearance of p3 between healthy controls and demented patients. Or perhaps p3 seeds or sequesters Aβ, resulting in altered clearance rates. Without these data, these critical questions remain unanswered.

Fibril formation

A discrepancy exists as to whether or not p3 forms amyloid fibrils, or even fibrils at all (Fig. 2). Early efforts to explore the fibril forming ability of p3 (17-40/42) presented electron microscopy (EM) images of what they consistently described to be

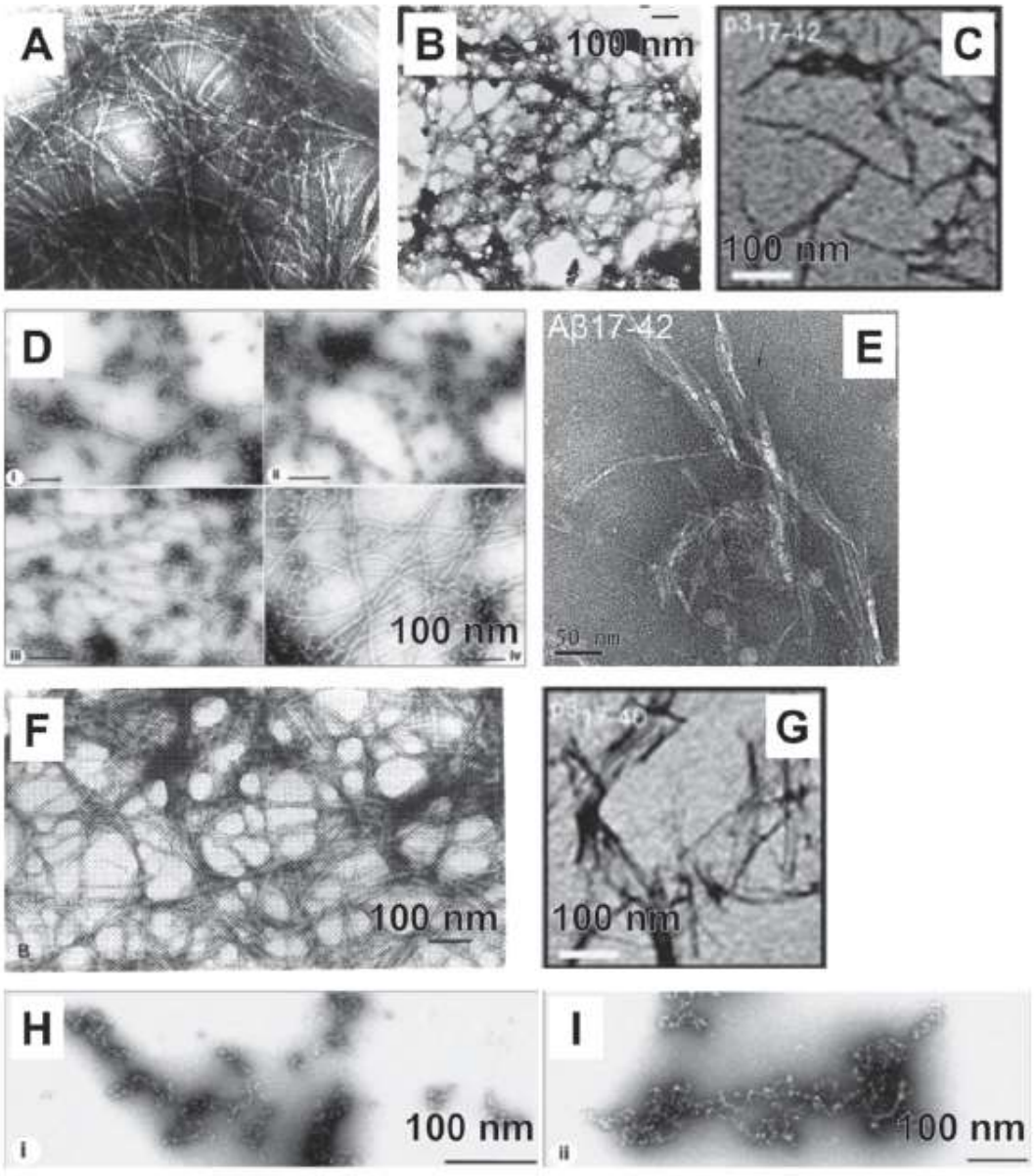

Fig. 2. Published TEM images of fibrillar A-E) p3 (17-42) and F-I) p3 (17-40). A) [41], B) [28], C) [46], D) [44], E) [43], F) [42], G) [46], H-I) [44]. Reproduced with permission.

amorphous aggregates or lattices of dense polymers (Fig. 2A, B, F) [28, 41, 42]. These authors noted differences in morphologies as compared with Aβ, such as shorter fibril lengths, narrower diameter, and more heterogeneity [28, 41, 42]. However, two of these studies did not provide any images of Aβ for comparison [28, 41], making it difficult to assess any differences. Several subsequent publications also published EM images of p3 (17-40/42), but noted less differences other than reduced twisting and a slight irregular morphology (Fig. 2C–E, 2G–I) [43–46]. In each of these studies, drastically different fibril forming conditions were employed, which is not unusual in the field of AD. The concentrations ranged from 5–500 μM, incubation times ranged from 1 hour – 2 weeks, temperatures ranged from 25–37 °C, buffer contents and pH differed, and some samples were shaken while others were kept quiescent. Like Aβ, p3 is an intrinsically disordered protein, and thus will be exceptionally sensitive to assay conditions. Each of these conditions will individually exert effects on the morphologies of any aggregates formed. For example, shaking during fibril formation has been shown to sometimes produce shorter, thicker fragments [47]. Moreover, from these published EM images, it is clear that p3 exhibits fibril-like morphology, but whether or not p3 shares structural characteristics with Aβ is unclear.

p3 lacks the hydrophilic N-terminus of Aβ, leaving behind a peptide comprised, to a large degree, of hydrophobic residues (Fig. 1A). This alone suggests that under aqueous, physiological conditions, p3 should be capable of self-assembly to a higher degree than Aβ. As shown in Figure 1A, the aggregation-prone regions of Aβ (17-22 and 30-42) are all found in the p3 peptide, as determined by AGGRESCAN [8]. In fact, only a couple of the recently published cryo-EM structures of amyloid fibrils include the presence of the N-terminus as a critical part of the fibril stability [48, 49]. Aside from these examples, most published structures of fibrillar Aβ to date omit the N-terminus entirely, or describe it as structurally disordered when compared with the C-terminus [49–51]. In support of this, Török et al. found via site-directed spin labeling that amino acids 30–40 produce the core region of Aβ fibrils [52].

Moreover, significantly smaller regions of Aβ than p3 have been shown to exhibit amyloidogenic properties. The KVLFF region has been shown to self-assemble to form β-sheet rich, fibrillar species [53, 54] and to competitively bind to full-length Aβ [55–57]. Even more surprising, Adler-Abramovich et al. demonstrated that individual phenylalanine molecules can self-assemble into well-ordered, cytotoxic, disease- relevant, amyloid-like fibrils that exhibit birefringence under polarized light when stained with Congo Red [58]. However, in the context of p3, these findings are typically overlooked.

Absence of binding sites to potential molecular chaperones of Aβ in p3

Furthermore, it has been proposed that the following binding partners of Aβ participate in amyloid plaque formation: heparin sulfate proteoglycans, Cu, Al, Fe, Zn, and the collagen-like AD amyloid plaque component [59]. Many of these are thought to interact with the N-terminus of Aβ [59], which is absent from p3. However, the necessity of the N-terminus of Aβ in the aggregation pathway to form toxic species has been heavily debated since the 1990s [59–61]. Ali et al. concluded with electrospray mass spectrometry that p3 does not bind Cu^{2+} at pH 7.2 when compared with $Aβ_{40}$ [62]. Despite this, Jang et al. demonstrated that p3 forms ion channels in cell membranes of human cortical neurons, leading to calcium dysregulation and ultimately neurite degeneration [63]. Thus, perhaps even in the absence of the HHQKL region, other hydrophobic regions of p3 are capable of interacting with lipids. Further studies are needed to understand the potential for p3 to interact with the other chaperones of Aβ aggregation.

Structural characterization of p3

Secondary structure analyses of Aβ and related peptides have revealed that under physiological conditions, they are primarily composed of β-sheets at various states of self-assembly [64]. Circular dichroism and ATR-FTIR studies have revealed predominant β-sheet character for p3 at physiological pH, similar to what has been published for Aβ [41, 44, 46, 62]. Schmechel et al. [44] and Vandersteen et al. [46] found that p3 (17-40) and p3 (17-42) had less pronounced β-sheet character, while Pike et al. [41] found that the β-sheet content was the same regardless of N-terminus presence. In contrast, Ali et al. [62] found that the β-sheet character of p3 (17-40) was substantially enhanced when compared with $Aβ_{40}$.

Aside from characterizing morphology of fibrils, other techniques commonly used to identify β-sheet rich fibril formation are Thioflavin T (ThT) and Congo red. ThT is a small molecule that exhibits a

fluorescence enhancement upon binding β-sheet rich fibrils. However, there are certain limitations to the ThT assay including inconsistent fluorescence upon incubation with the Osaka mutation of Aβ [65, 66], and the recent finding that ThT can bind a cross-α structure [67]. Of the fibril EM images shown in Figure 2, four publications determined that p3 is ThT positive, one of which demonstrated a very low fluorescence intensity, and one additional publication determined that p3 is ThT negative [28, 42, 43, 46, 68]. Congo red is a dye that exhibits birefringence under polarized light upon binding amyloid fibrils. Lalowski et al. stated that the p3 structures exhibited "characteristic apple-green birefringence" in some foci [28]; however, the images were published in black and white, so it is difficult to verify these findings, and Milton et al. demonstrated Congo red binding but did not mention birefringence [45].

Kinetics of p3 fibril formation

Efforts to understand the kinetics of fibril formation for p3 have revealed that p3 aggregates more rapidly than Aβ via ThT and sedimentation assays [41, 46]. In addition, p3 exhibited substantially more sedimentation of aggregates when compared with Aβ (80% for p3 as compared to 40% for Aβ) [41]. This is in stark contrast with the claims that p3 is soluble and preferentially exists as a monomer [34, 69].

Intermediate oligomer formation

While not mentioned directly in the definition of an amyloid as defined by the Nomenclature Committee of the International Society of Amyloidosis, oligomers are widely considered to be the more relevant toxic species in AD rather than fibrils [3–6]. There is conflicting evidence as to whether or not p3 forms transient oligomers during the transition from monomer to fiber. Vandersteen et al. found that p3 binds A11 [46], the oligomer-specific antibody [70]. However, two other groups were unable to trap intermediate oligomers using oligomer forming conditions typically applied for Aβ [43, 71]. The mechanism by which p3 aggregates remains unclear aside from theoretical calculations employing Molecular Dynamics [63, 71–75]. For example, Cheon et al. determined that p3 forms U-shaped protofilaments from disordered oligomers via a series of PRIME20/DMD simulations [75].

Furthermore, as mentioned by Chiti and Dobson, toxic, intermediate oligomers of Aβ have large hydrophobic regions exposed on the external surface [76]. The micelle-like, external hydrophobicity of oligomers is thought to be driven by an interaction with lipid-rich regions of cell membranes [77, 78]. Jang et al. [63] found that p3 (17-42) forms annular, channel-like structures that protrude from the membrane of lipid bilayers, similar to the membrane-associated oligomers formed by $A\beta_{40/42}$ [77, 78]. Given the extensive hydrophobic content of p3, it seems plausible that a similar confirmation could be achieved for p3. Further work is needed to understand what intermediates are formed during the aggregation of p3.

POTENTIAL SYNERGY BETWEEN Aβ AND P3

Another question yet to be answered is whether or not p3 and Aβ can interact with each other. The propensity of Aβ to interact with other molecules through hydrophobic contacts has been well established and includes other proteins, such as the prion protein [79], the islet amyloid polypeptide [80], α-synuclein [81, 82], as well as other non-polar species, such as cholesterol [83], or even carbon nanotubes [84]. This suggests that Aβ is a promiscuous peptide capable to interacting and possibly aggregating with other molecules, thus forming heterogenous species. This should not come as a surprise given the heterogenous nature of amyloid plaques [20–23]. In fact, substantial studies have shown that the pyroglutamate modifications of Aβ truncations, Aβ (pE3-40/42) and Aβ (pE11-40/42), can both seed and interact with Aβ [85–89]. Despite this, to the best of our knowledge, no studies have been conducted investigating the co-aggregation and or seeding effects between p3 and Aβ.

Moreover, a lysine to asparagine heterozygous, missense mutation of AβPP (K16N), located at the α-secretase cleavage site, reduces the production of the p3 peptide by 40–50% [90]. People with this mutation are more likely to experience early onset dementia, which is attributed to the production of cytotoxic, heterogenous, proteolysis resistant aggregates and enhanced production of Aβ from AβPP. However, the AβK16N mutant will also have distinct biophysical and biological properties from Aβ, so that no direct comparison can be made. This mutation may indicate that the ratio of p3:Aβ is an important factor to consider when attempting to understand the role of p3 in AD.

BIOLOGICAL CHARACTERISTICS OF P3 COMPARED WITH Aβ

Despite the non-amyloidogenic designation that p3 has received, several publications have reported that it exhibits toxicity [41, 63, 91, 92] and elicits a biological response [63, 92, 93]. Similar to much of the work surrounding p3, there are varied findings on the toxicity of p3 when compared with Aβ [91, 92]. Pike et al. [41] found that fibrillar p3 (17-40/42) was substantially more toxic than Aβ (40/42) in cultured hippocampal neurons. The same was true for freshly prepared p3 (17-40) versus Aβ (1-40). Wei et al. [92] supported these findings that p3 (17-40) is more toxic than Aβ (1-40) in SH-SY5Y and IMR-32 cells. In contrast, Liu et al. [91] found that fibrillar p3 (17-40) and Aβ (1-40) are equally toxic to SH-SY5Y cells. However, interestingly, Pike et al. [41] also found that freshly prepared p3 (17-42) was substantially less toxic than Aβ (1-42) in hippocampal neurons. While it is clear that both p3 (17-40) and p3 (17-42) exhibit toxicity in a variety of tissue culture cell lines, it is unclear how this toxicity compares with Aβ given the discrepancies described above. Walsh and coworkers found that synthetic p3 at a concentration of 11.5 nM did not block hippocampal long-term potentiation (LTP) [4]. However, it is not clear why this concentration was chosen, especially because significantly higher concentrations are typically used for experiments of this nature [94, 95].

Calcium dysregulation is thought to play a role in the cell toxicity of Aβ [96]. Jang and coworkers found that p3 forms ion channels and disrupts calcium regulation, inducing death in human cortical neurons [63]. Also, Szczepanik and coworkers found that similar to Aβ, p3 is a pro-inflammatory glial modulator by initiating production of cytokines interleukin (IL)-1α, IL-1β, IL-6, tumor necrosis factor-α (TNF-α), and MCP-1 [93].

PRODUCTION OF P3 AND IDENTITY OF α-SECRETASE

The N-terminus of p3 is generated by an α-secretase cleavage of AβPP in the plasma membrane and trans golgi network [97]. This cleavage also produces an ectodomain, AβPPα, which has been described as neuroprotective [98–100]. This may be an underlying reason why p3 has also been considered neuroprotective.

α-secretase is thought to be ADAM 10, of the disintegrin and metalloprotease family, which is a type I transmembrane protein containing 750 residues [101, 102]. ADAM 10 knock-out results in early embryonic lethality presumably due to loss of Notch signaling [102]. Thus, if p3 were implicated in AD, complete inhibition of α-secretase would not be a plausible treatment.

There is evidence indicating competition between α- and β-secretase activity, possibly attributed to the difference in cellular locations of AβPP processing [103]. This could potentially contribute to the vast number of failed β-secretase inhibitors if α-secretase activity is enhanced upon inhibition of β-secretase. Further studies should be done to quantify the levels of all products of AβPP in the blood and CSF during clinical trials to identify if alternative processing pathways are altered upon inactivation of β-secretase.

CONCLUDING REMARKS

In summary, there is some evidence that the "non-amyloidogenic" designation of p3 should be revisited, as it seems to share some of the amyloid-like properties of Aβ. The published cytotoxicity and aggregation studies, while incredibly conflicting, elude to the possibility of this peptide playing a larger role than previously described in the aggregation of amyloids in AD brains. Further effort should be aimed at understanding the complex biological and biophysical properties of p3, both with respect to its role alone and its effect on full-length Aβ. Once a clear relationship between Aβ and the other relevant AβPP processing products is established, a multifaceted therapeutic approach can be achieved.

DISCLOSURE STATEMENT

Authors' disclosures available online (https://www.j-alz.com/manuscript-disclosures/19-1201r1).

REFERENCES

[1] Prince M, Wilmo A, Guerchet M, Ali G-C, Wu Y-T, Prina M (2015) *World Alzheimer Report 2015: The Global Impact of Dementia*. Alzheimer's Disease International, London.

[2] Hardy JA, Higgins GA (1992) Alzheimer's disease: The amyloid cascade hypothesis. *Science* **256**, 184-185.

[3] Hardy J, Selkoe DJ (2002) The amyloid hypothesis of Alzheimer's disease: Progress and problems on the road to therapeutics. *Science* **297**, 353-356.

[4] Walsh DM, Klyubin I, Fadeeva JV, Cullen WK, Anwyl R, Wolfe MS, Rowan MJ, Selkoe DJ (2002) Naturally

secreted oligomers of amyloid β protein potently inhibit hippocampal long-term potentiation in vivo. *Nature* **416**, 535-539.

[5] Mclean CA, Cherny RA, Fraser FW, Fuller SJ, Smith MJ, Beyreuther K, Bush AI, Masters CL (1999) Soluble pool of Aβ amyloid as a determinant of severity of neurodegeneration in Alzheimer's disease. *Ann Neurol* **46**, 860-866.

[6] Lue L, Kuo Y, Roher AE, Brachova L, Shen Y, Sue L, Beach T, Kurth JH, Rydel RE, Rogers J (1999) Soluble amyloid beta peptide concentration as a predictor of synaptic change in Alzheimer's disease. *Am J Pathol* **155**, 853-862.

[7] Moghekar A, Rao S, Li M, Ruben D, Mammen A, Tang X, O'Brien RJ (2011) Large quantities of Aβ peptide are constitutively released during amyloid precursor protein metabolism in vivo and in vitro. *J Biol Chem* **286**, 15989-15997.

[8] Conchillo-Solé O, de Groot NS, Avilés FX, Vendrell J, Daura X, Ventura S (2007) AGGRESCAN: A server for the prediction and evaluation of "hot spots" of aggregation in polypeptides. *BMC Bioinformatics* **8**, 1-17.

[9] Knopman DS (2019) Lowering of amyloid-beta by β-secretase inhibitors – some informative failures. *N Engl J Med* **380**, 11-13.

[10] De Strooper B, Vassar R, Golde T (2010) The secretases: enzymes with therapeutic potential in Alzheimer disease. *Nat Rev Neurol* **6**, 99-107.

[11] Schneider L (2019) A resurrection of aducanumab for Alzheimer's disease. *Lancet Neurol* **4422**, 9-10.

[12] Parsons CG, Danysz W, Dekundy A, Pulte I (2013) Memantine and cholinesterase inhibitors: Complementary mechanisms in the treatment of Alzheimer's disease. *Neurotox Res* **24**, 358-369.

[13] Karran E, Strooper B De (2016) The amyloid cascade hypothesis: are we poised for success or failure? *J Neurochem* **139**, 237-252.

[14] Egan MF, Kost J, Voss T, Mukai Y, Aisen PS, Cummings JL, Tariot PN, Vellas B, Van Dyck CH, Boada M, Zhang Y, Li W, Furtek C, Mahoney E, Mozley LH, Mo Y, Sur C, Michelson D (2019) Randomized trial of verubecestat for prodromal Alzheimer's disease. *N Engl J Med* **380**, 1408-1420.

[15] Egan MF, Kost J, Tariot PN, Aisen PS, Cummings JL, Vellas B, Sur C, Mukai Y, Voss T, Furtek C, Mahoney E, Mozley LH, Vandenberghe R, Mo Y, Michelson D (2018) Randomized trial of verubecestat for mild-to-moderate Alzheimer's disease. *N Engl J Med* **378**, 1691-1703.

[16] Henley D, Raghavan N, Sperling R, Aisen P, Raman R, Romano G (2019) Preliminary results of a trial of atabecestat in preclinical Alzheimer's disease. *N Engl J Med* **380**, 1483-1485.

[17] Teplow DB, Lazo ND, Bitan G, Bernstein S, Wyttenbach T, Bowers MT, Baumketner A, Shea JE, Urbanc B, Cruz L, Borreguero J, Stanley HE (2006) Elucidating amyloid β-protein folding and assembly: A multidisciplinary approach. *Acc Chem Res* **39**, 635-645.

[18] Ono K, Condron MM, Teplow DB (2009) Structure-neurotoxicity relationships of amyloid beta-protein oligomers. *Proc Natl Acad Sci U S A* **106**, 14745-14750.

[19] Roychaudhuri R, Yang M, Hoshi MM, Teplow DB (2009) Amyloid-β protein assembly and Alzheimer disease. *J Biol Chem* **284**, 4749-4753.

[20] Duong DM, Peng J, Rees HD, Wang J, Liao L, Levey AI, Gearing M, Lah JJ, Cheng D, Losik TG (2004) Proteomic characterization of postmortem amyloid plaques isolated by laser capture microdissection. *J Biol Chem* **279**, 37061-37068.

[21] Drummond E, Nayak S, Faustin A, Pires G, Hickman RA, Askenazi M, Cohen M, Haldiman T, Kim C, Han X, Shao Y, Safar JG, Ueberheide B, Wisniewski T (2017) Proteomic differences in amyloid plaques in rapidly progressive and sporadic Alzheimer's disease. *Acta Neuropathol* **133**, 933-954.

[22] Tekirian TL, Saido TC, Markesbery WR, Russell MJ, Wekstein DR, Patel E, Geddes JW (1998) N-terminal heterogeneity of parenchymal and cerebrovascular aβ deposits. *J Neuropathol Exp Neurol* **57**, 76-94.

[23] Saido TC, Yamao-Harigaya W, Iwatsubo T, Kawashima S (1996) Amino- and carboxyl-terminal heterogeneity of β-amyloid peptides deposited in human brain. *Neurosci Lett* **215**, 173-176.

[24] Schleiden M (1838) Einige Bemerkungen uber den vegetabilischen Faserstoff und sein Verhaltniss zum Starkemehl. *Ann Phys* **119**, 391-397.

[25] Virchow R (1854) Zur Zellulose-Frage. *Arch für Pathol Anat und Physiol und für Klin Med* **6**, 416-426.

[26] Benson MD, Buxbaum JN, Eisenberg DS, Merlini G, Saraiva MJM, Sekijima Y, Sipe JD, Westermark P (2018) Amyloid nomenclature 2018: Recommendations by the International Society of Amyloidosis (ISA) nomenclature committee. *Amyloid* **25**, 215-219.

[27] Westermark P, Benson MD, Buxbaum JN, Cohen AS, Ikeda S, Masters CL, Merlini G, Maria J, Sipe JD (2005) Amyloid: Toward terminology clarification Report from the Nomenclature Committee of the International Society of Amyloidosis. *Amyloid* **12**, 1-4.

[28] Lalowski M, Golabek A, Lemere CA, Selkoe DJ, Wisniewski HM, Beavis RC, Frangione B, Wisniewski T (1996) The "Nonamyloidogenic" p3 fragment (amyloid beta 17-42) is a major constituent of down's syndrome cerebellar preamyloid. *J Biol Chem* **271**, 33623-33631.

[29] Higgins LS, Murphy GM, Forno LS, Catalano R, Cordell B (1996) P3 beta-amyloid peptide has a unique and potentially pathogenic immunohistochemical profile in Alzheimer's disease brain. *Am J Pathol* **149**, 585-596.

[30] Gowing E, Roher AE, Woods AS, Cotter RJ, Chaney M, Little SP, Ball MJ (1994) Chemical characterization of Aβ 17-42 peptide, a component of diffuse amyloid deposits of Alzheimer disease. *J Biol Chem* **269**, 10987-10990.

[31] Giaccone G, Tagliavini F, Linoli G, Bouras C, Frigerio L, Frangione B, Bugiani O (1989) Down patients: Extracellular preamyloid deposits precede neuritic degeneration and senile plaques. *Neurosci Lett* **97**, 232-238.

[32] Mann DMA (1989) Cerebral amyloidosis, ageing and Alzheimer's disease; a contribution from studies on Down's syndrome. *Neurobiol Aging* **10**, 397-399.

[33] Wisniewski KE, Wisniewski HM, Wen GY (1985) Occurrence of neuropathological changes and dementia of Alzheimer's disease in Down's syndrome. *Ann Neurol* **17**, 278-282.

[34] Butterfield DA, Swomley AM, Sultana R (2013) Amyloid beta-peptide (1-42)-induced oxidative stress in Alzheimer disease: Importance in disease pathogenesis and progression. *Antioxid Redox Signal* **19**, 823-835.

[35] Baghallab I, Reyes-Ruiz JM, Abulnaja K, Huwait E, Glabe C (2018) Epitomic characterization of the specificity of the anti-amyloid Aβ monoclonal antibodies 6E10 and 4G8. *J Alzheimers Dis* **66**, 1235-1244.

[36] Demattos RB, Bales KR, Cummins DJ, Dodart J, Paul SM, Holtzman DM (2001) Peripheral anti-Aβ antibody alters CNS and plasma Aβ clearance and decreases brain Aβ burden in a mouse model of Alzheimer's disease. *Proc Natl Acad Sci U S A* **98**, 8850-8855.

[37] Shibata M, Yamada S, Kumar SR, Calero M, Bading J, Frangione B, Holtzman DM, Miller CA, Strickland DK, Ghiso J, Zlokovic BV (2000) Clearance of Alzheimer's amyloid-Beta 1-40 peptide from brain by LDL receptor – related protein-1 at the blood-brain barrier. *J Clin Invest* **106**, 1489-1499.

[38] Ghersi-Egea JF, Gorevic PD, Ghiso J, Frngione B, Patlak CS, Fenstermacher JD (1996) Fate of cerebrospinal fluid-borne amyloid beta-peptide: Rapid clearance into blood and appreciable accumulation by cerebral arteries. *J Neurochem* **67**, 880-883.

[39] Mawuenyega KG, Sigurdson W, Ovod V, Munsell L, Kasten T, Morris JC, Yarasheski KE, Bateman RJ (2010) Decreased clearance of CNS β-amyloid in Alzheimer's disease. *Science* **330**, 1774.

[40] Abraham JD, Prome S, Salvetat N, Rubrecht L, Cobo S, du Paty E, Galea P, Mathieu-Dupas E, Ranaldi S, Caillava C, Cremer GA, Rieunuer F, Robert P, Molina F, Laune D, Checler F, Fareh J (2013) Cerebrospinal Aβ 11-x and 17-x levels as indicators of mild cognitive impairment and patients' stratification in Alzheimer's disease. *Transl Psychiatry* **3**, 1-8.

[41] Pike CJ, Overman MJ, Cotman CW (1995) Amino-terminal deletions enhance aggregation of β-amyloid peptides in vitro. *J Biol Chem* **270**, 23895-23899.

[42] Naslund J, Jensen M, Tjernberg LO, Thyberg J, Terenius L, Nordstedt C (1994) The metabolic pathway generating p3, an Aβ peptide fragment, is probably non-amyloidogenic. *Biochem Biophys Res Commun* **204**, 780-787.

[43] Shi JM, Zhang L, Liu EQ (2017) Dissecting the behaviour of β-amyloid peptide variants during oligomerization and fibrillation. *J Pept Sci* **23**, 810-817.

[44] Schmechel A, Zentgraf H, Scheuermann S, Fritz G, Reed J, Beyreuther K, Bayer TA, Multhaup G (2003) Alzheimer beta -amyloid homodimers facilitate Aβ fibrillization and the generation of conformational antibodies. *J Biol Chem* **278**, 35317-35324.

[45] Milton NGN, Harris JR (2009) Polymorphism of amyloid-β fibrils and its effects on human erythrocyte catalase binding. *Micron* **40**, 800-810.

[46] Vandersteen A, Hubin E, Sarroukh R, De Baets G, Schymkowitz J, Rousseau F, Subramaniam V, Raussens V, Wenschuh H, Wildemann D, Broersen K (2012) A comparative analysis of the aggregation behavior of amyloid-β peptide variants. *FEBS Lett* **586**, 4088-4093.

[47] Petkova AT, Leapman RD, Guo Z, Yau W-M, Mattson MP, Tycko R (2005) Self-propagating, molecular-level polymorphism in Alzheimer's beta-amyloid fibrils. *Science* **307**, 262-266.

[48] Kollmer M, Close W, Funk L, Rasmussen J, Bsoul A, Schierhorn A, Schmidt M, Sigurdson CJ, Jucker M, Fändrich M (2019) Cryo-EM structure and polymorphism of Aβ amyloid fibrils purified from Alzheimer's brain tissue. *Nat Commun* **10**, 1-8.

[49] Gremer L, Scholzel D, Schenk C, Reinartz E, Labahn J, Ravelli RBG, Tusche M, Lopez-Iglesias C, Hoyer W, Heise H, Willbold D, Schroder GF (2017) Fibril structure of amyloid beta 1-42 by cryoelectron microscopy. *Science* **358**, 116-119.

[50] Xiao Y, Ma B, McElheny D, Parthasarathy S, Long F, Hoshi M, Nussinov R, Ishii Y (2015) Aβ(1-42) fibril structure illuminates self-recognition and replication of amyloid in Alzheimer's disease. *Nat Struct Mol Biol* **22**, 499-505.

[51] Wälti MA, Ravotti F, Arai H, Glabe CG, Wall JS, Böckmann A, Güntert P, Meier BH, Riek R (2016) Atomic-resolution structure of a disease-relevant Aβ(1-42) amyloid fibril. *Proc Natl Acad Sci U S A* **113**, E4976-E4984.

[52] Török M, Milton S, Kayed R, Wu P, McIntire T, Glabe CG, Langen R (2002) Structural and dynamic features of Alzheimer's Aβ peptide in amyloid fibrils studied by site-directed spin labeling. *J Biol Chem* **277**, 40810-40815.

[53] Krysmann MJ, Castelletto V, Kelarakis A, Hamley IW, Hule RA, Pochan DJ (2008) Self-assembly and hydrogelation of an amyloid peptide fragment. *Biochemistry* **47**, 4597-4605.

[54] Bortolini C, Klausen LH, Hoffmann SV, Jones NC, Saadeh D, Wang Z, Knowles TPJ, Dong M (2018) Rapid growth of acetylated Aβ(16-20) into macroscopic crystals. *ACS Nano* **12**, 5408-5416.

[55] Arai T, Sasaki D, Araya T, Sato T, Sohma Y (2014) A cyclic KLVFF-derived peptide aggregation inhibitor induces the formation of less-toxic off-pathway amyloid-beta oligomers. *ChemBioChem* **15**, 2577-2583.

[56] Turner JP, Lutz-rechtin T, Moore KA, Rogers L, Bhave O, Moss MA, Servoss SL (2014) Rationally designed peptoids modulate aggregation of amyloid- beta 40. *ACS Chem Neurosci* **5**, 552-558.

[57] Tjernberg LO, Na J, Lindqvist F, Johansson J, Karlstro AR, Thyberg J (1996) Arrest of beta-amyloid fibril formation by a pentapeptide ligand. *J Biol Chem* **271**, 8545-8549.

[58] Adler-Abramovich L, Vaks L, Carny O, Trudler D, Magno A, Caflisch A, Frenkel D, Gazit E (2012) Phenylalanine assembly into toxic fibrils suggests amyloid etiology in phenylketonuria. *Nat Chem Biol* **8**, 701-706.

[59] Larner AJ (1999) Hypothesis: Amyloid beta-peptides truncated at the N-terminus contribute to the pathogenesis of Alzheimer's disease. *Neurobiol Aging* **20**, 65-69.

[60] Urbanc B (2017) Flexible N-termini of amyloid beta protein oligomers: A link between structure and activity? *Isr J Chem* **57**, 651-664.

[61] Williamson MP, Suzuki Y, Bourne NT, Asakura T (2006) Binding of amyloid β-peptide to ganglioside micelles is dependent on histidine-13. *Biochem J* **397**, 483-490.

[62] Ali F, Thompson AJ, Barrow CJ (2000) The p3 peptide, a naturally occurring fragment of the amyloid-β peptide (Aβ) found in Alzheimer's disease, has a greater aggregation propensity in vitro than full-length Aβ, but does not bind Cu2+. *Aust J Chem* **53**, 321-326.

[63] Jang H, Arce FT, Ramachandran S, Capone R, Azimova R, Kagan BL, Nussinov R, Lal R (2010) Truncated β-amyloid peptide channels provide an alternative mechanism for Alzheimer's Disease and Down syndrome. *Proc Natl Acad Sci U S A* **107**, 6538-6543.

[64] Kirschner D, Abraham C, Selkoe DJ (1986) X-ray diffraction from intraneuronal paired helical filaments and extraneuronal amyloid fibers in Alzheimer's Disease indicates cross-Beta confirmation. *Proc Natl Acad Sci U S A* **83**, 503-507.

[65] Ovchinnikova OY, Finder VH, Vodopivec I, Nitsch RM, Glockshuber R (2011) The Osaka FAD mutation E22Δ leads to the formation of a previously unknown type of

amyloid β fibrils and modulates Aβ neurotoxicity. *J Mol Biol* **408**, 780-791.

[66] Kulic L, McAfoose J, Welt T, Tackenberg C, Späni C, Wirth F, Finder V, Konietzko U, Giese M, Eckert A, Noriaki K, Shimizu T, Murakami K, Irie K, Rasool S, Glabe C, Hock C, Nitsch RM (2012) Early accumulation of intracellular fibrillar oligomers and late congophilic amyloid angiopathy in mice expressing the Osaka intra-Aβ APP mutation. *Transl Psychiatry* **2**, 1-14.

[67] Tayeb-Fligelman E, Tabachnikov O, Moshe A, Goldshmidt-tran O, Sawaya MR, Coquelle N, Colletier J, Landau M (2017) The cytotoxic Staphylococcus aureus PSMα3 reveals a cross-α amyloid-like fibril. *Science* **355**, 831-833.

[68] Pike CJ, Overman MJ, Cotman CW (1995) Amino-terminal deletions enhance aggregation of β-amyloid peptides in vitro. *J Biol Chem* **270**, 23895-23898.

[69] Querfurth HW, LaFerla FM (2010) Alzheimer's disease. *N Engl J Med* **362**, 329-344.

[70] Kayed R, Head E, Thompson JL, Mcintire TM, Milton SC, Cotman CW, Glabe CG (2003) Amyloid oligomers implies common mechanism of pathogenesis. *Science* **300**, 486-490.

[71] Dulin F, Léveillé F, Ortega JB, Mornon JP, Buisson A, Callebaut I, Colloc'h N (2008) p3 peptide, a truncated form of Aβ devoid of synaptotoxic effect, does not assemble into soluble oligomers. *FEBS Lett* **582**, 1865-1870.

[72] Zheng J, Jang H, Ma B, Tsai C-J, Nussinov R (2007) Modeling the Alzheimer Aβ17-42 fibril architecture: tight intermolecular sheet-sheet association and intramolecular hydrated cavities. *Biophys J* **93**, 3046-3057.

[73] Cheon M, Kang M, Chang I (2016) Polymorphism of fibrillar structures depending on the size of assembled Aβ17-42 peptides. *Sci Rep* **6**, 38196.

[74] Streltsov VA, Varghese JN, Masters CL, Nuttall SD (2011) Crystal structure of the amyloid-β p3 fragment provides a model for oligomer formation in Alzheimer' disease. *J Neurosci* **31**, 1419-1426.

[75] Cheon M, Hall CK, Chang I (2015) Structural conversion of Aβ17-42 peptides from disordered oligomers to U-shape protofilaments via multiple kinetic pathways. *PLoS Comput Biol* **11**, 1-23.

[76] Chiti F, Dobson CM (2009) Amyloid formation by globular proteins under native conditions. *Nat Chem Biol* **5**, 15-22.

[77] Lin H, Bhatia R, Lal R (2001) Amyloid β protein forms ion channels: Implications for Alzheimer's disease pathophysiology. *FASEB J* **15**, 2433-2444.

[78] Quist A, Doudevski I, Lin H, Azimova R, Ng D, Frangione B, Kagan B, Ghiso J, Lal R (2005) Amyloid ion channels: A common structural link for protein-misfolding disease. *Proc Natl Acad Sci U S A* **102**, 10427-10432.

[79] Zou WQ, Xiao X, Yuan J, Puoti G, Fujioka H, Wang X, Richardson S, Zhou X, Zou R, Li S, Zhu X, McGeer PL, McGeehan J, Kneale G, Rincon-Limas DE, Fernandez-Funez P, Lee HG, Smith MA, Petersen RB, Guo JP (2011) Amyloid-β42 interacts mainly with insoluble prion protein in the Alzheimer brain. *J Biol Chem* **286**, 15095-15105.

[80] O'Nuallain B, Williams AD, Westermark P, Wetzel R (2004) Seeding specificity in amyloid growth induced by heterologous fibrils. *J Biol Chem* **279**, 17490-17499.

[81] Mandal PK, Pettegrew JW, Masliah E, Hamilton RL, Mandal R (2006) Interaction between Aβ peptide and alpha-synuclein: Molecular mechanisms in overlapping pathology of Alzheimer's and Parkinson's in dementia with Lewy body disease. *Neurochem Res* **31**, 1153-1162.

[82] Tsigelny IF, Crews L, Desplats P, Shaked GM, Sharikov Y, Mizuno H, Spencer B, Rockenstein E, Trejo M, Platoshyn O, Yuan JXJ, Masliah E (2008) Mechanisms of hybrid oligomer formation in the pathogenesis of combined Alzheimer's and Parkinson's diseases. *PLoS One* **3**, e3135.

[83] Yao ZX, Papadopoulos V (2002) Function of β-amyloid in cholesterol transport: a lead to neurotoxicity. *FASEB J* **16**, 1677-1679.

[84] Luo J, Wärmländer SKTS, Yu CH, Muhammad K, Gräslund A, Pieter Abrahams J (2014) The Aβ peptide forms non-amyloid fibrils in the presence of carbon nanotubes. *Nanoscale* **6**, 6720-6726.

[85] Barritt JD, Younan ND, Viles JH (2017) N-terminally truncated amyloid-$\beta_{(11\text{-}40/42)}$ cofibrillizes with its full-length counterpart: Implications for Alzheimer's disease. *Angew Chemie Int Ed* **56**, 9816-9819.

[86] Tomaselli S, Pagano K, D'Arrigo C, Molinari H, Ragona L (2017) Evidence of molecular interactions of Aβ1-42 with N-terminal truncated beta amyloids by NMR. *ACS Chem Neurosci* **8**, 759-765.

[87] Schilling S, Lauber T, Schaupp M, Manhart S, Scheel E, Bo G, Demuth H (2006) On the seeding and oligomerization of pGlu-amyloid peptides (in vitro). *Biochemistry* **45**, 12393-12399.

[88] DeMattos RB, Lu J, Tang Y, Racke MM, DeLong CA, Tzaferis JA, Hole JT, Forster BM, McDonnell PC, Liu F, Kinley RD, Jordan WH, Hutton ML (2012) A plaque-specific antibody clears existing β-amyloid plaques in Alzheimer's disease mice. *Neuron* **76**, 908-920.

[89] Hao X, Zheng J, Sun Y, Dong X (2019) Seeding and cross-seeding aggregations of Aβ40 and its N-terminal-truncated peptide Aβ11-40. *Langmuir* **35**, 2821-2831.

[90] Kaden D, Harmeier A, Weise C, Munter LM, Althoff V, Rost BR, Hildebrand PW, Schmitz D, Schaefer M, Lurz R, Skodda S, Yamamoto R (2012) Novel APP/Aβ mutation K16N produces highly toxic heteromeric Aβ oligomers. *EMBO Mol Med* **4**, 647-659.

[91] Liu R, McAllister C, Lyubchenko Y, Sierks MR (2004) Residues 17-20 and 30-35 of beta-amyloid play critical roles in aggregation. *J Neurosci Res* **75**, 162-171.

[92] Wei W, Norton DD, Wang X, Kusiak JW (2002) Aβ 17-42 in Alzheimer's disease activates JNK and caspase-8 leading to neuronal apoptosis. *Brain* **125**, 2036-2043.

[93] Szczepanik AM, Rampe D, Ringheim GE (2001) Amyloid-beta peptide fragments p3 and p4 induce pro-inflammatory cytokine and chemokine production *in vitro* and *in vivo*. *J Neurochem* **77**, 304-17.

[94] Puzzo D, Privitera L, Leznik E, Fà M, Staniszewski A, Palmeri A, Arancio O (2008) Picomolar amyloid-β positively modulates synaptic plasticity and memory in hippocampus. *J Neurosci* **28**, 14537-14545.

[95] Raskatov JA (2019) What is the "relevant" amyloid β42 concentration? *ChemBioChem* **95064**, 1725-1726.

[96] Marx J (2007) Fresh evidence points to an old suspect: Calcium. *Science* **318**, 384-386.

[97] Lichtenthaler SF (2011) Alpha-secretase in Alzheimer's disease: Molecular identity, regulation and therapeutic potential. *J Neurochem* **116**, 10-21.

[98] Furukawa K, Sopher BL, Rydel RE, Begley JG, Pham DG, Martin GM, Fox M, Mattson MP (1996) Increased activity-regulating and neuroprotective efficacy of α-secretase-derived secreted amyloid precursor protein

conferred by a C-terminal heparin-binding domain. *J Neurochem* **67**, 1882-1896.

[99] Meziane H, Dodart JC, Mathis C, Little S, Clemens J, Paul SM, Ungerer A (1998) Memory-enhancing effects of secreted forms of the β-amyloid precursor protein in normal and amnestic mice. *Proc Natl Acad Sci U S A* **95**, 12683-12688.

[100] Stein TD, Anders NJ, DeCarli C, Chan SL, Mattson MP, Johnson JA (2004) Neutralization of transthyretin reverses the neuroprotective effects of secreted amyloid precursor protein (APP) in APPSw mice resulting in tau phosphorylation and loss of hippocampal neurons: Support for the amyloid hypothesis. *J Neurosci* **24**, 7707-7717.

[101] Kuhn PH, Wang H, Dislich B, Colombo A, Zeitschel U, Ellwart JW, Kremmer E, Roßner S, Lichtenthaler SF (2010) ADAM10 is the physiologically relevant, constitutive α-secretase of the amyloid precursor protein in primary neurons. *EMBO J* **29**, 3020-3032.

[102] Jorissen E, Prox J, Bernreuther C, Weber S, Schwanbeck R, Serneels L, Snellinx A, Craessaerts K, Thathiah A, Tesseur I, Bartsch U, Weskamp G, Blobel CP, Glatzel M, De Strooper B, Saftig P (2010) The disintegrin/metalloproteinase ADAM10 is essential for the establishment of the brain cortex. *J Neurosci* **30**, 4833-4844.

[103] Vassar R, Bennett BD, Babu-Khan S, Kahn S, Mendiaz EA, Denis P, Teplow DB, Ross S, Amarante P, Loeloff R, Luo Y, Fisher S, Fuller J, Edenson S, Lile J, Jarosinski MA, Biere AL, Curran E, Burgess T, Louis JC, Collins F, Treanor J, Rogers G, Citron M (1999) β-Secretase cleavage of Alzheimer's amyloid precursor protein by the transmembrane aspartic protease BACE. *Science* **286**, 735-741.

Chapter 2. Biophysical and morphological characterization of the p3 peptide

This chapter contains text and figures from the following manuscript: Kuhn, A.J.; Abrams, B.S..; Knowlton, S.; Raskatov, R. A. *ACS Chem. Neuro.* **2020.** See appendix for RightsLinks.

2.1 Introduction

There is mounting evidence that the full 40-42 residues of Aβ are not required for fibril formation. Aβ fragments, such as pyroglutamate-truncated-Aβ (AβpE3-40/42 and AβpE11-40/42)[17,18] and Aβ4-40/42,[19,20] exhibit enhanced aggregation propensity,[19,21–23] cellular toxicity,[21] and can even stimulate rapid fibril formation of Aβ.[24] In addition, the segments of full-length Aβ attributed to amyloid fibril formation, as determined by an amyloid prediction software, AGGRESCAN,[25] span Aβ17-22 and Aβ30-40/42 (highlighted in yellow in Fig 6).[26] Both of these segments are found in the C-terminal, p3 portion of Aβ. Additional studies exist on significantly smaller segments of Aβ able to form amyloid fibrils, such as the KLVFF (Aβ16-20)[27–29] and FF (Aβ19-20) segments.[30–32] Furthermore, most of the atomic-resolution structures of Aβ, such as 2M4J shown in Figure 6[33], reveal the N-terminus as flexible, while the C-terminus makes up the fibril core to shield the hydrophobic residues from water. Given all of this, the non-amyloidogenic descriptor designated to p3 seems perplexing, which provided the motivation for the work described in this Chapter.

The Nomenclature Committee of the International Society of Amyloidosis defines an amyloid as "extracellular deposits of protein fibrils with a characteristic appearance in electron microscopy, a typical X-ray diffraction pattern, and an affinity for Congo red with concomitant green birefringence".[34,35] Our findings indicate that p3 fulfills these requirements, and thus is in fact amyloidogenic.

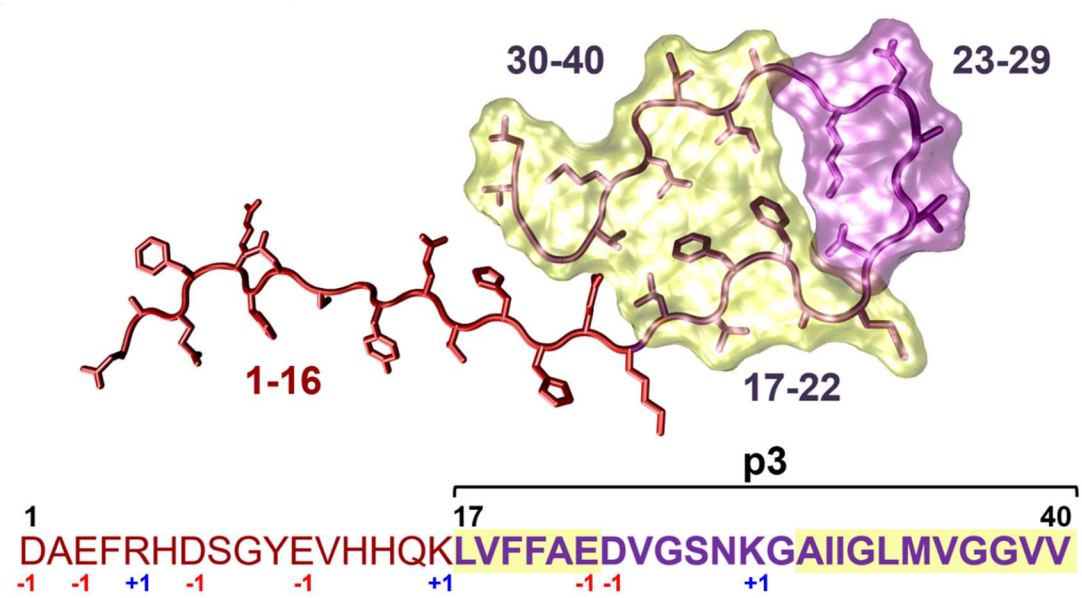

Figure 6. Sequence and structural information for Aβ1-40 and p3(17-40). Upper panel: ssNMR structure of Aβ1-40 fibril (2M4J).[33] Lower panel: sequences of Aβ1-40 and p3(17-40) with associated charges. Segments highlighted in yellow (Aβ17-22 and Aβ30-40) designate amyloidogenic regions, calculated by AGGRESCAN.[25,26] *Reprinted with permission from:* Kuhn, A.J.; Abrams, B.S..; Knowlton, S.; Raskatov, R. A. *ACS Chem. Neuro.* **2020**. See Appendix for RightsLink.

2.2 Reprint

Reprinted with permission from (*ACS Chem. Neuro.* **2020**, 11 (1), 1539-1544). See RightsLink in Appendix.

ACS Chemical Neuroscience

pubs.acs.org/chemneuro Letter

Alzheimer's Disease "Non-amyloidogenic" p3 Peptide Revisited: A Case for Amyloid-α

Ariel J. Kuhn, Benjamin S. Abrams, Stella Knowlton, and Jevgenij A. Raskatov*

Cite This: ACS Chem. Neurosci. 2020, 11, 1539−1544 Read Online

ACCESS | Metrics & More | Article Recommendations | Supporting Information

ABSTRACT: Amyloid-β (Aβ) is an intrinsically disordered peptide thought to play an important role in Alzheimer's disease (AD). It has been the target of most AD therapeutic efforts, which have repeatedly failed in clinical trials. A more predominant peptidic fragment, formed through alternative processing of the amyloid precursor protein, is the p3 peptide. p3 has received little attention, which is possibly due to the prevailing view in the AD field that it is "non-amyloidogenic." By probing the self-assembly of this peptide, we found that p3 aggregates to form oligomers and fibrils and, when compared with Aβ, displays enhanced aggregation rates. Our findings highlight the solubilizing effect of the N-terminus of Aβ and the favorable formation of structures formed through C-terminal hydrophobic peptide interfaces. Based on our findings, we suggest a reevaluation of the current therapeutic approaches targeting only the β-secretase pathway of AD, given that the α- secretase pathway is also amyloidogenic.

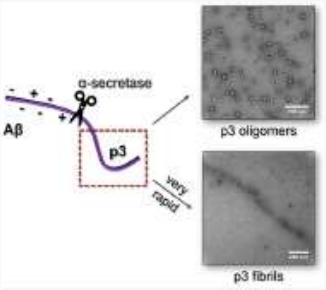

KEYWORDS: *Alzheimer's disease, amyloid-β, amyloid-α, oligomer, fibril, aggregation*

Alzheimer's Disease (AD) is a debilitating neurological disease characterized by amyloid plaques and neurofibrillary tau tangles, currently affecting almost 50 million people worldwide.[1] Although amyloid plaques may contain up to 900 unique proteins, with approximately 200 found consistently,[2,3] the target of most therapeutic efforts to date has been the amyloid-β peptide (Aβ).[4,5] Aβ has been the subject of thousands of publications annually since 2000, a figure that is exponentially rising (Figure S1). Yet, in 2020, all Phase III drugs designed to reduce Aβ production or aggregation have failed,[6] and we are far from an effective treatment for AD.[5−9] Thus, it is critical to investigate the contribution of other plaque-associated peptides to amyloid deposition in the brain.

In light of recent findings that fragments of Aβ exhibit enhanced aggregation propensity,[10,11] we sought to understand the predominant cleavage product of the amyloid precursor protein (APP),[12] cleaved by α- rather than β-secretase. This peptide, termed p3, has received remarkably little attention, and it is largely regarded as benign. However, its biophysical and biological properties remain unclear and inconsistent, as discussed in our recent review[13] and summarized in Table S1. Some have described p3 as neuroprotective,[14] while others have demonstrated that p3 exhibits significant cytotoxicity.[15,16] Whereas p3 is often referred to as soluble and "non-amyloidogenic,"[17−22] several studies found that p3 formed "amorphous aggregates" and "lattice-like" networks[19,23] and, possibly, amyloid fibrils.[24,25] One study, conducted by Vandersteen et al.,[25] revealed what were described as fibrillar fragments, shorter and dissimilar to those formed by Aβ. Despite the aforementioned studies revealing fibrillar-like morphologies for p3, potentially indicative of amyloidogenicity, the field still recognizes p3 production as an alternative, neuroprotective, and "non-amyloidogenic" pathway of APP processing.[17,19−22] To deconvolute these conflicting claims, we sought out to investigate the aggregation propensity of p3. We hypothesized, based on the hydrophobicity and large regions of predicted amyloidogenicity,[13] that p3 could aggregate to form oligomers and fibrils.

To probe our hypothesis that, despite lacking the first 16 amino acids, p3 shares amyloidogenic properties with Aβ, p3 and Aβ (Figure 1A) were synthesized and purified using our published protocols[26] (Figures S2 and S3). To evaluate fibrillogenicity, p3 was incubated under fibril-forming conditions and compared alongside Aβ. TEM analysis of p3 fibrils (Figure 1B; S9A-B) revealed long, twisted fibrillar structures that closely resemble the fibrils formed by Aβ (Figure 1C). For both p3 and Aβ, the resultant fibril morphologies bear semblance to published quiescently formed Aβ fibrils.[27] Thus, the absence of the hydrophilic, disordered N-terminus did not preclude fibril formation in p3, contrary to the previous claims that p3 is "non-amyloidogenic."[18,19] In addition, p3

Received: March 25, 2020
Accepted: May 15, 2020
Published: May 15, 2020

ACS Publications © 2020 American Chemical Society

https://dx.doi.org/10.1021/acschemneuro.0c00160
ACS Chem. Neurosci. 2020, 11, 1539−1544

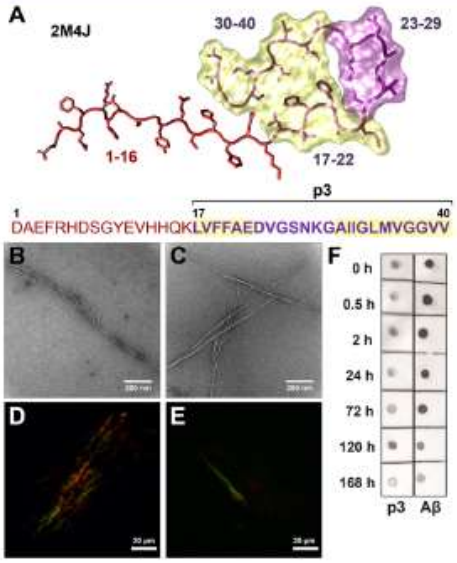

Figure 1. Fibrillogenicity of p3 compared with Aβ. (A) Fibril structure[35] and sequence of Aβ(1−40), with p3(17−40) indicated in purple. Highlighted regions (17−22 and 30−40) indicate the amyloidogenic regions of Aβ, calculated by AGGRESCAN.[13] TEM images of fibrillar (B) p3 and (C) Aβ. Polarized light microscopy images of CR stained (D) p3 and (E) Aβ fibrils. (F) Dot blots stained for OC binding for Aβ and p3. All peptide samples were prepared at 20 μM and incubated for 7 days at 37 °C in PBS (pH 7.4).

fibrils exhibited characteristic green birefringence typical for cross-β-sheet amyloid structures,[28,29] under polarized light upon incubation with Congo Red (CR) (Figure 1D), again indistinguishable from Aβ (Figure 1E). The presence of β-sheet-rich structures formed by p3 revealed by the CR assay are in agreement with the circular dichroism results obtained by Ali et al.[30]

Our results agree with the findings of Sawaya et al. that large hydrophobic residue patches frequently associate to form "steric zippers".[31] A hydrophobic steric zipper is plausible in the case of p3 given that the two amyloidogenic, hydrophobic patches of Aβ (LVFFAE and AIIGLMVGGVV)[13] are also found in p3 (Figure 1A). To further investigate if fibrillar Aβ and p3 have conformational similarities, the OC antibody, which recognizes conformation-specific epitopes of amyloid fibrils,[32] was employed (Figure 1F). The dot blots reveal OC binding for both p3 and Aβ across all time points, confirming the presence of conformational similarities in the fibril structures for both peptides, again highlighting the importance of the hydrophobic C-terminal regions for fibril formation.[31] Together, these findings of shared fibril morphology with Aβ, CR birefringence, and OC-binding establish that p3 is amyloidogenic as defined by the Nomenclature Committee of the International Society of Amyloidosis.[33,34]

We next studied fibril formation kinetics of p3 via the Thioflavin T (ThT) and TAMRA-quenching assays.[36] The ThT assay (Figure 2A) revealed that the fibrilization of p3 was significantly more rapid than that for Aβ. The p3 kinetic profile was absent of a characteristic sigmoidal growth profile beginning with a "lag phase" that is typically seen for Aβ.

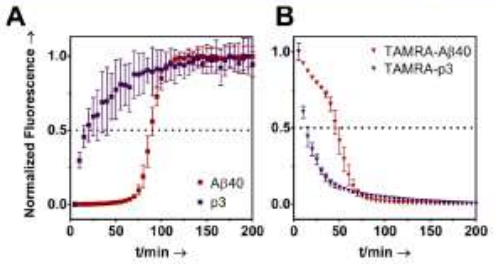

Figure 2. Kinetics of fibril formation. (A) ThT (20 μM) monitored aggregation kinetics of Aβ and p3. (B) TAMRA quenching assay. Peptides were prepared at 20 μM and incubated at 37 °C in PBS (pH 7.4) with continuous shaking. Each data point is an average of four replicates with error bars representing standard deviation.

This indicates that the nucleation phase of the fibril formation mechanism was expedited for p3. Moreover, a ThT-monitored seeding assay revealed that Aβ fibrillization can be enhanced by seeding of preformed p3 fibrils (Figure S10).

To validate the kinetic trends seen in the ThT assays, TAMRA dye was conjugated to the N-termini of p3 and Aβ (Figures S6 and S7), and the fluorescence signal suppression, indicative of aggregation,[36] was monitored. As shown in Figure 2B, TAMRA-p3 fluorescence decayed more rapidly than TAMRA-Aβ, further revealing that p3 forms fibrils more rapidly than Aβ. The ion-rich 1−16 region of Aβ therefore appears to provide a solubilizing function for Aβ, which attenuates amyloid fibril formation. This may also explain why p3 is a major component of preamyloid plaques found in the brains of those with Down syndrome.[19] Fibril formation of TAMRA-p3 was confirmed with TEM (Figures S8 and S9). Together, these results indicate that p3 may play an important role in amyloid deposition in the brains of those with AD.

Evidence is growing that the toxicity of Aβ is not from the accumulation of insoluble fibrils, but rather from the soluble oligomeric intermediates.[37] Oligomers have been shown to disrupt neuronal function,[38] long-term potentiation,[39] neuronal microRNA expression,[40] and memory.[41,42] Oligomers vary in size and shape and are difficult to characterize given their transient nature. Following the trapping protocol by Ahmed et al.,[43] we trapped and imaged p3 oligomers, which are indistinguishable from those shown in TEM images of Aβ published by Ahmed. et al.[43] The TEM images displayed in Figure 3A and B (Figure S11) reveal round particles ranging from 10 to 85 nm in diameter for both p3 and Aβ. No elongated, fibrillar species were identified in the oligomeric TEM images, as reflected in the histograms shown in Figure 3C. The average particle diameter for p3 was determined to be 26.6 ± 11.2 nm which is within error of the value calculated for Aβ, 23.4 ± 11.5 nm (Figure 3C). The histograms shown in Figure 3C reveal very similar particle size distributions for both peptides. However, the histogram for Aβ exhibits some tailing, representative of larger structures (60−100 nm), not prevalently seen for p3. The formation of large nonspherical, elongated structures seen for Aβ but not p3 may be due to micelle formation, promoted by the amphipathic, surfactant-like build of Aβ,[44] a property not shared with p3 (Figure 1A). To the best of our knowledge, these are the first TEM images of oligomers formed by p3, refuting the previous claim that p3 does not form oligomers.[45] Our findings that p3 forms

https://dx.doi.org/10.1021/acschemneuro.0c00160
ACS Chem. Neurosci. 2020, 11, 1539−1544

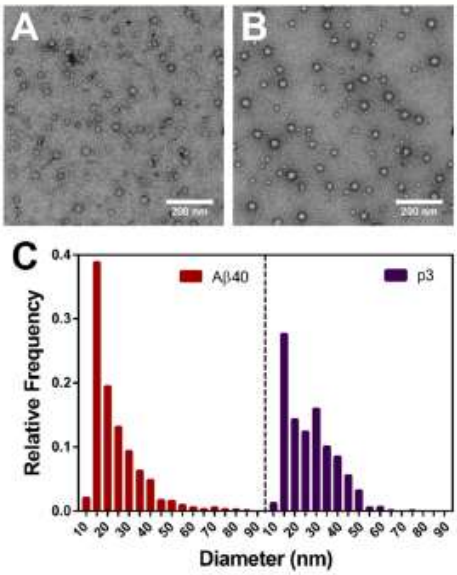

Figure 3. Oligomer characterization. TEM images of 20 μM (A) Aβ and (B) p3 incubated at 4 °C in PBS (pH 7.4) for 6 h. (C) Histograms displaying size distributions of oligomers formed by Aβ and p3 calculated from (A) and (B) and Figure S11.

oligomers similar to those formed by Aβ agree with the MD simulations conducted by Miller et al. indicating that p3 oligomers can form both parallel and antiparallel β-sheets.[46] Moreover, since several studies have demonstrated cellular toxicity for both monomeric and fibrillar p3,[15,16,23,47] we probed the toxicity of oligomeric p3 (Figure S12). We found that, at 50 μM, p3 reduced SH-SY5Y cell viability to approximately 80%, in comparison to 50% for Aβ-treated cells (Figure S12). We attribute the higher viability of p3-treated cells to the rapidity of p3 fibrillization, as shown in Figure 2.

To further characterize early stages of self-assembly of p3, photoinduced cross-linking[48] was utilized to provide a snapshot of the short-lived, metastable oligomers. Two modified variants of p3 were synthesized given that tyrosine is required for cross-linking[49] (Figure 4A): $p3_{F19Y}$ and $p3_{F20Y}$. The SDS-PAGE gel shown in Figure 4B reveals monomeric, dimeric, trimeric, and tetrameric oligomers resulting from covalent cross-linking for both $p3_{F19Y}$ and $p3_{F20Y}$. Aβ also formed similar assembly sizes in addition to faint signals corresponding to higher order structures (20−30 kDa), which may be related to the presence of larger oligomers formed by Aβ but not p3, as seen in TEM (Figures 3 and S11). The presence of low-N oligomers identified with TEM and SDS-PAGE demonstrates that p3 can form transient intermediates broadly similar in size and shape as Aβ. These findings are important in the context of AD because cellular toxicity of Aβ oligomers has been attributed to an excess of hydrophobic surface exposure of oligomers in cell membranes.[50] Given that p3 is almost entirely hydrophobic (Figure 1A), p3 oligomers could potentially play an important role in amyloid-related neurotoxicity.

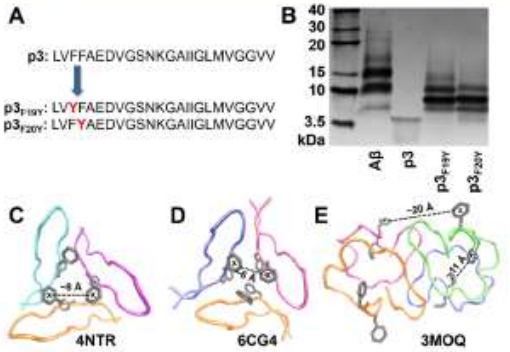

Figure 4. Oligomer characterization. (A) Sequences of p3 peptides with Phe → Tyr substitutions. (B) SDS-PAGE gel of cross-linked samples of Aβ, p3, $p3_{F19Y}$, and $p3_{F20Y}$ (20 μM). Control, non-cross-linked samples are shown in Figure S13. Crystal structures displaying possible trimeric (C,[51] D[52]) and tetrameric (E[53]) assemblies of p3 peptidic fragments, with representative centroid-to-centroid distances between phenylalanines from neighboring units indicated.

ThT kinetic curves for both $p3_{F19Y}$ and $p3_{F20Y}$ are shown in Figure S14, indicating that tyrosine substitution did not prevent fibril formation. Interestingly, the kinetic profile for $p3_{F20Y}$ closely matched that of p3, while $p3_{F19Y}$ exhibited a slightly attenuated onset of aggregation. This may indicate a favorable interaction between F19 and another residue, reinforced by the discovery that a F19P mutation abolishes Aβ aggregation.[54] Moreover, our findings are supported by Bitan et al. showing that truncations of residues 1−9 of Aβ do not inhibit oligomer formation.[49] Aβ also formed similar assembly sizes in addition to faint signals corresponding to high-N structures (20−30 kDa).

Furthermore, the enhanced staining for trimers and tetramers for p3 shown in Figure 4B may reveal initial steps in the mechanism of p3 aggregation. Crystal structures of similar species are shown in Figure 4C−E,[51−53] indicating possible structures of the prominent species shown in Figure 4B.

In summary, we have demonstrated that the "non-amyloidogenic" p3 peptide, in fact, does exhibit substantial amyloidogenic properties. Given this, and its similarity to Aβ, we propose to rename p3 to amyloid-α (Aα). Our results revealed OC-positive, CR birefringent, p3 fibrils that formed more rapidly than Aβ. We also found that, contrary to previous literature,[45] p3 aggregated to form intermediate oligomers that share a similar size distribution with Aβ. Overall, this work suggests that p3 may not be as innocuous as previously suggested, and further analysis is needed to understand the role of p3 in Alzheimer's Disease.

METHODS

Additional experimental methods can be found in the Supporting Information.

Peptide Synthesis. All peptides were synthesized by SPPS using Fmoc chemistry, following our previously published protocols[55] on Tentagel S PHB resin (Rapp Polymere GmbH, cat. no. RA1327).

Fibril Growth. Lyophilized peptide (Aβ40 or p3) was dissolved in 20 mM NaOH and sonicated for 30 s and then diluted to 20 μM in PBS. The samples were incubated either (1) at 37 °C for 24 h with mild agitation or (2) at 37 °C quiescently for 7 days. For TEM imaging, 3 μL sample aliquots were spotted onto freshly glow-

https://dx.doi.org/10.1021/acschemneuro.0c00160
ACS Chem. Neurosci. 2020, 11, 1539−1544

discharged carbon-coated electron microscopy grids (Ted Pella, cat. no. 01701-F). The grids were rinsed with Milli-Q water after 1 min incubation, followed by staining with 30 μL of 1% uranyl acetate.

Congo Red. Since CR crystals can exhibit false-positive birefringence, a protocol from Nakka et al.[56] was adapted. Either Aβ40 or p3 fibrils were grown quiescently as described above at 20 μM. Fibrils were centrifuged at 14000*g* for 15 min and washed with Milli-Q H_2O × 2. Next, 5 μL of the CR stock solution (7 mg of CR in 1 mL Milli-Q H_2O) was added to 1 mL of Milli-Q H_2O and then added to the pelleted peptides. The samples were incubated for 1 h with mild agitation and centrifuged at 14000*g* for 15 min and washed with Milli-Q H_2O × 2. Then, 30 μL of the sample was added to glass slides and air-dried overnight. Images were collected on a Leica Epifluorescence widefield microscope, with a polarizer.

Dot Blot Assay. Aβ40 or p3 fibrils (20 μM) were prepared as described above and kept at 37 °C. At each time point over the course of 7 days, 2 μL of sample was spotted on nitrocellulose. After the blots dried, they were blocked with 5% nonfat milk in TBST for 1 h at 25 °C. The samples were then washed with TBST for 5 min × 3 and incubated with OC antibody (1:1000 in 5% nonfat milk in TBST) overnight at 4 °C, followed by washing with TBST for 5 min × 3. The membrane was then incubated with the secondary antibody (1:10000 in 5% nonfat dry milk in TBST) for 1 h at 25 °C, washed with TBST for 5 min × 3, and then developed with the Opti-4CN Substrate kit (Bio-Rad, cat no. 1708235).

Oligomer Growth and Imaging. To trap the intermediate oligomers, lyophilized Aβ40 or p3 was dissolved in cold 20 mM NaOH and sonicated in an ice bath for 30 s. Samples were diluted to 20 μM in PBS and incubated at 4 °C for 6 h without agitation. TEM samples were prepared and imaged as described above.

ThT Assay and TAMRA Quenching Assays. The ThT and TAMRA quenching assays were conducted as described previously.[57,58]

Photochemically Induced Cross-Linking of Peptides. 4 μL of 1 mM $[Ru(bipy)_3]^{2+}$ and 4 μL of 20 mM ammonium persulfate were added to 32 μL aliquots of 20 μM Aβ40, p3, $p3_{F19Y}$, and $p3_{F20Y}$ in PBS. The samples were irradiated for 1.2 s with white light using our previously described setup.[55] Following irradiation, the samples were immediately quenched with 40 μL of loading buffer containing 5% 2-mercaptoethanol and separated by SDS-PAGE gel electrophoresis (12% tris-tricine polyacrylamide) at 100 V for 2 h. The gels were developed by silver staining.

■ ASSOCIATED CONTENT

Supporting Information

The Supporting Information is available free of charge at https://pubs.acs.org/doi/10.1021/acschemneuro.0c00160.

General experimental procedures; histogram of Aβ publication trends; sample characterization and purity; additional TEM images; ThT kinetics; cellular viability; SDS-PAGE gel of non-cross-linked peptides (PDF)

■ AUTHOR INFORMATION

Corresponding Author

Jevgenij A. Raskatov − *Department of Chemistry and Biochemistry, University of California, Santa Cruz, Santa Cruz, California 95064, United States*; orcid.org/0000-0002-0082-9113; Email: jraskato@ucsc.edu

Authors

Ariel J. Kuhn − *Department of Chemistry and Biochemistry, University of California, Santa Cruz, Santa Cruz, California 95064, United States*

Benjamin S. Abrams − *Department of Biomolecular Engineering, Life Sciences Microscopy Center, University of California, Santa Cruz, Santa Cruz, California 95064, United States*

Stella Knowlton − *Department of Chemistry and Biochemistry, University of California, Santa Cruz, Santa Cruz, California 95064, United States*

Complete contact information is available at: https://pubs.acs.org/10.1021/acschemneuro.0c00160

Author Contributions

A.J.K. and J.A.R. designed the study and wrote the manuscript. A.J.K. collected the data. B.S.A. developed the algorithm for quantitating the size of the oligomers shown in Figures 3 and S10. S.K. synthesized the two singly mutated p3 peptides ($p3_{F19Y}$ and $p3_{F20Y}$) and assisted A.J.K. in the photochemical cross-linking experiments and subsequent SDS-PAGE. All authors interpreted the data, provided intellectual contributions, and critically revised the manuscript.

Notes

The authors declare no competing financial interest.

■ ACKNOWLEDGMENTS

J.A.R. thanks UC Santa Cruz for the flexible start-up funds, and NIH for funding (R21AG058074). A.J.K. thanks the NIH for funding (F31AG066377). J.A.R. and A.J.K. also thank Dr. James Nowick for helpful conversations and Kareem Bdeir for his help with peptide purification.

■ REFERENCES

(1) Prince, M., Wilmo, A., Guerchet, M., Ali, G.-C., Wu, Y.-T., and Prina, M. (2015) *World Alzheimer Report 2015: The Global Impact of Dementia.*

(2) Duong, D. M., Peng, J., Rees, H. D., Wang, J., Liao, L., Levey, A. I., Gearing, M., Lah, J. J., Cheng, D., and Losik, T. G. (2004) Proteomic Characterization of Postmortem Amyloid Plaques Isolated by Laser Capture Microdissection. *J. Biol. Chem. 279* (35), 37061−37068.

(3) Drummond, E., Nayak, S., Faustin, A., Pires, G., Hickman, R. A., Askenazi, M., Cohen, M., Haldiman, T., Kim, C., Han, X., Shao, Y., Safar, J. G., Ueberheide, B., and Wisniewski, T. (2017) Proteomic Differences in Amyloid Plaques in Rapidly Progressive and Sporadic Alzheimer's Disease. *Acta Neuropathol. 133* (6), 933−954.

(4) Cummings, J., Lee, G., Ritter, A., and Zhong, K. (2018) Alzheimer's Disease Drug Development Pipeline: 2018. *Alzheimer's Dement.: Transl. Res. Clin Interventions 4*, 195−214.

(5) Knopman, D. S. (2019) Lowering of Amyloid-Beta by β-Secretase Inhibitors — Some Informative Failures. *N. Engl. J. Med. 380*, 1476−1478.

(6) Karran, E., and De Strooper, B. (2016) The Amyloid Cascade Hypothesis: Are We Poised for Success or Failure? *J. Neurochem. 139* (2), 237−252.

(7) Egan, M. F., Kost, J., Voss, T., Mukai, Y., Aisen, P. S., Cummings, J. L., Tariot, P. N., Vellas, B., Van Dyck, C. H., Boada, M., Zhang, Y., Li, W., Furtek, C., Mahoney, E., Mozley, L. H., Mo, Y., Sur, C., and Michelson, D. (2019) Randomized Trial of Verubecestat for Prodromal Alzheimer's Disease. *N. Engl. J. Med. 380* (15), 1408−1420.

(8) Egan, M. F., Kost, J., Tariot, P. N., Aisen, P. S., Cummings, J. L., Vellas, B., Sur, C., Mukai, Y., Voss, T., Furtek, C., Mahoney, E., Mozley, L. H., Vandenberghe, R., Mo, Y., and Michelson, D. (2018) Randomized Trial of Verubecestat for Mild-to-Moderate Alzheimer's Disease. *N. Engl. J. Med. 378* (18), 1691−1703.

(9) Henley, D., Raghavan, N., Sperling, R., Aisen, P., Raman, R., and Romano, G. (2019) Preliminary Results of a Trial of Atabecestat in Preclinical Alzheimer's Disease. *N. Engl. J. Med. 380* (15), 1483−1485.

(10) Wulff, M., Baumann, M., Thümmler, A., Yadav, J. K., Heinrich, L., Knüpfer, U., Schlenzig, D., Schierhorn, A., Rahfeld, J. U., Horn, U., Balbach, J., Demuth, H. U., and Fändrich, M. (2016) Enhanced Fibril

Fragmentation of N-Terminally Truncated and Pyroglutamyl-Modified Aβ Peptides. *Angew. Chem., Int. Ed.* 55 (16), 5081−5084.
(11) Barritt, J. D., Younan, N. D., and Viles, J. H. (2017) N-Terminally Truncated Amyloid-β(11−40/42) Cofibrillizes with Its Full-Length Counterpart: Implications for Alzheimer's Disease. *Angew. Chem., Int. Ed.* 56 (33), 9816−9819.
(12) Moghekar, A., Rao, S., Li, M., Ruben, D., Mammen, A., Tang, X., and O'Brien, R. J. (2011) Large Quantities of Aβ Peptide Are Constitutively Released during Amyloid Precursor Protein Metabolism in Vivo and in Vitro. *J. Biol. Chem.* 286 (18), 15989−15997.
(13) Kuhn, A. J., and Raskatov, J. A. (2020) Is the P3 (Aβ17−40, Aβ17−42) Peptide Relevant to the Pathology of Alzheimer's Disease? *J. Alzheimer's Dis.* 74 (1), 43−53.
(14) Han, W., Ji, T., Mei, B., and Su, J. (2011) Peptide P3May Play a Neuroprotective Role in the Brain. *Med. Hypotheses* 76 (4), 543−546.
(15) Wei, W., Norton, D. D., Wang, X., and Kusiak, J. W. (2002) Aβ 17−42 in Alzheimer's Disease Activates JNK and Caspase-8 Leading to Neuronal Apoptosis. *Brain* 125, 2036−2043.
(16) Jang, H., Arce, F. T., Ramachandran, S., Capone, R., Azimova, R., Kagan, B. L., Nussinov, R., and Lal, R. (2010) Truncated β-Amyloid Peptide Channels Provide an Alternative Mechanism for Alzheimer's Disease and Down Syndrome. *Proc. Natl. Acad. Sci. U. S. A.* 107 (14), 6538−6543.
(17) Querfurth, H. W., and LaFerla, F. M. (2010) Alzheimer's Disease. *N. Engl. J. Med.* 362 (4), 329−344.
(18) Naslund, J., Jensen, M., Tjernberg, L. O., Thyberg, J., Terenius, L., and Nordstedt, C. (1994) The Metabolic Pathway Generating P3, an Aβ Peptide Fragment, Is Probably Non-Amyloidogenic. *Biochem. Biophys. Res. Commun.* 204 (2), 780−787.
(19) Lalowski, M., Golabek, A., Lemere, C. A., Selkoe, D. J., Wisniewski, H. M., Beavis, R. C., Frangione, B., and Wisniewski, T. (1996) The "Nonamyloidogenic" P3 Fragment (Amyloid Beta 17−42) Is a Major Constituent of Down's Syndrome Cerebellar Preamyloid. *J. Biol. Chem.* 271 (52), 33623−33631.
(20) Pinheiro, L., and Faustino, C. (2019) Therapeutic Strategies Targeting Amyloid-Beta in Alzheimer's Disease. *Curr. Alzheimer Res.* 16, 418−452.
(21) Coronel, R., Bernabeu-Zornoza, A., Palmer, C., Muñiz-Moreno, M., Zambrano, A., Cano, E., and Liste, I. (2018) Role of Amyloid Precursor Protein (APP) and Its Derivatives in the Biology and Cell Fate Specification of Neural Stem Cells. *Mol. Neurobiol.* 55 (9), 7107−7117.
(22) Mañucat-Tan, N. B., Saadipour, K., Wang, Y. J., Bobrovskaya, L., and Zhou, X. F. (2019) Cellular Trafficking of Amyloid Precursor Protein in Amyloidogenesis Physiological and Pathological Significance. *Mol. Neurobiol.* 56 (2), 812−830.
(23) Pike, C. J., Overman, M. J., and Cotman, C. W. (1995) Amino-Terminal Deletions Enhance Aggregation of β-Amyloid Peptides in Vitro. *J. Biol. Chem.* 270 (41), 23895−23898.
(24) Schmechel, A., Zentgraf, H., Scheuermann, S., Fritz, G., Pipkorn, R., Reed, J., Beyreuther, K., Bayer, T. A., and Multhaup, G. (2003) Alzheimer β-Amyloid Homodimers Facilitate Aβ Fibrillization and the Generation of Conformational Antibodies. *J. Biol. Chem.* 278 (37), 35317−35324.
(25) Vandersteen, A., Hubin, E., Sarroukh, R., De Baets, G., Schymkowitz, J., Rousseau, F., Subramaniam, V., Raussens, V., Wenschuh, H., Wildemann, D., and Broersen, K. (2012) A Comparative Analysis of the Aggregation Behavior of Amyloid-β Peptide Variants. *FEBS Lett.* 586 (23), 4088−4093.
(26) Dutta, S., Foley, A. R., Warner, C. J. A., Zhang, X., Rolandi, M., Abrams, B., and Raskatov, J. A. (2017) Suppression of Oligomer Formation and Formation of Non-Toxic Fibrils upon Addition of Mirror-Image Aβ42 to the Natural l-Enantiomer. *Angew. Chem., Int. Ed.* 56 (38), 11506−11510.
(27) Petkova, A. T., Leapman, R. D., Guo, Z., Yau, W.-M., Mattson, M. P., and Tycko, R. (2005) Self-Propagating, Molecular-Level Polymorphism in Alzheimer's β-Amyloid Fibrils. *Science* 307, 262−266.
(28) Wolman, M., and Bubis, J. J. (1965) The Cause of the Green Polarization Color of Amyloid Stained with Congo Red. *Histochem. Cell Biol.* 4 (5), 351−356.
(29) Espargaró, A., Llabrés, S., Saupe, S. J., Curutchet, C., Luque, F. J., and Sabaté, R. (2020) On the Binding of Congo Red to Amyloid Fibrils. *Angew. Chem., Int. Ed.* 59, 1−5.
(30) Ali, F., Thompson, A. J., and Barrow, C. J. (2000) The P3 Peptide, a Naturally Occurring Fragment of the Amyloid-β Peptide (Aβ) Found in Alzheimer's Disease, Has a Greater Aggregation Propensity in Vitro than Full-Length Aβ, but Does Notbind Cu2+. *Aust. J. Chem.* 53, 321−326.
(31) Sawaya, M. R., Sambashivan, S., Nelson, R., Ivanova, M. I., Sievers, S. A., Apostol, M. I., Thompson, M. J., Balbirnie, M., Wiltzius, J. J. W., Mcfarlane, H. T., Madsen, A. Ø., Riekel, C., and Eisenberg, D. (2007) Atomic Structures of Amyloid Cross-β Spines Reveal Varied Steric Zippers. *Nature* 447, 453−457.
(32) Kayed, R., Head, E., Sarsoza, F., Saing, T., Cotman, C. W., Necula, M., Margol, L., Wu, J., Breydo, L., Thompson, J. L., Rasool, S., Gurlo, T., Butler, P., and Glabe, C. G. (2007) Fibril Specific, Conformation Dependent Antibodies Recognize a Generic Epitope Common to Amyloid Fibrils and Fibrillar Oligomers That Is Absent in Prefibrillar Oligomers. *Mol. Neurodegener.* 2 (1), 18.
(33) Westermark, P., Benson, M. D, Buxbaum, J. N, Cohen, A. S, Frangione, B., Ikeda, S.-I., Masters, C. L, Merlini, G., Saraiva, M. J, and Sipe, J. D (2005) Amyloid: Toward Terminology Clarification Report from the Nomenclature Committee of the International Society of Amyloidosis. *Amyloid* 12, 1−4.
(34) Benson, M. D., Buxbaum, J. N., Eisenberg, D. S., Merlini, G., Saraiva, M. J. M., Sekijima, Y., Sipe, J. D., and Westermark, P. (2018) Amyloid Nomenclature 2018: Recommendations by the International Society of Amyloidosis (ISA) Nomenclature Committee. *Amyloid* 25 (4), 215−219.
(35) Lu, J., Qiang, W., Yau, W., Schwieters, C. D., Meredith, S. C., and Tycko, R. (2013) Molecular Structure of β-Amyloid Fibrils in Alzheimer's Disease Brain Tissue. *Cell* 154 (6), 1257−1268.
(36) Garai, K., and Frieden, C. (2013) Quantitative Analysis of the Time Course of Aβ Oligomerization and Subsequent Growth Steps Using Tetramethylrhodamine-Labeled Aβ. *Proc. Natl. Acad. Sci. U. S. A.* 110 (9), 3321−3326.
(37) Hardy, J., and Selkoe, D. J. (2002) The Amyloid Hypothesis of Alzheimer's Disease: Progress and Problems on the Road to Therapeutics. *Science* 297, 353−356.
(38) Mclean, C. A., Cherny, R. A., Fraser, F. W., Fuller, S. J., Smith, M. J., Beyreuther, K., Bush, A. I., and Masters, C. L. (1999) Soluble Pool of Aβ Amyloid as a Determinant of Severity of Neurodegeneration in Alzheimer's Disease. *Ann. Neurol.* 46 (6), 860−866.
(39) Walsh, D. M., Klyubin, I., Fadeeva, J. V., Cullen, W. K., Anwyl, R., Wolfe, M. S., Rowan, M. J., and Selkoe, D. J. (2002) Naturally Secreted Oligomers of Amyloid-β Protein Potently Inhibit Hippocampal Long-Term Potentiation in Vivo. *Nature* 416 (6880), 535−539.
(40) Li, J. J., Dolios, G., Wang, R., and Liao, F. F. (2014) Soluble Beta-Amyloid Peptides, but Not Insoluble Fibrils, Have Specific Effect on Neuronal MicroRNA Expression. *PLoS One* 9 (3), No. e90770.
(41) Lesné, S., Koh, M. T., Kotilinek, L., Kayed, R., Glabe, C. G., Yang, A., Gallagher, M., and Ashe, K. H. (2006) A Specific Amyloid-β Protein Assembly in the Brain Impairs Memory. *Nature* 440 (7082), 352−357.
(42) Brouillette, J., Caillierez, R., Zommer, N., Alves-Pires, C., Benilova, I., Blum, D., de Strooper, B., and Buée, L. (2012) Neurotoxicity and Memory Deficits Induced by Soluble Low-Molecular-Weight Amyloid-β 1−42 Oligomers Are Revealed in Vivo by Using a Novel Animal Model. *J. Neurosci.* 32 (23), 7852−7861.
(43) Ahmed, M., Davis, J., Aucoin, D., Sato, T., Ahuja, S., Aimoto, S., Elliott, J. I., Van Nostrand, W. E., and Smith, S. O. (2010) Structural Conversion of Neurotoxic Amyloid-Beta(1−42) Oligomers to Fibrils. *Nat. Struct. Mol. Biol.* 17 (5), 561−567.

https://dx.doi.org/10.1021/acschemneuro.0c00160
ACS Chem. Neurosci. 2020, 11, 1539−1544

(44) Soreghan, B., Kosmoski, J., and Glabe, C. (1994) Surfactant Properties of Alzheimer's Aβ Peptides and the Mechanism of Amyloid Aggregation. *J. Biol. Chem. 269* (46), 28551−28554.
(45) Dulin, F., Léveillé, F., Ortega, J. B., Momon, J. P., Buisson, A., Callebaut, L, and Colloc'h, N. (2008) P3 Peptide, a Truncated Form of Aβ Devoid of Synaptotoxic Effect, Does Not Assemble into Soluble Oligomers. *FEBS Lett. 582* (13), 1865−1870.
(46) Miller, Y., Ma, B., and Nussinov, R. (2009) Polymorphism of Alzheimer's Aβ17−42 (P3) Oligomers: The Importance of the Turn Location and Its Conformation. *Biophys. J. 97* (4), 1168−1177.
(47) Liu, R., McAllister, C., Lyubchenko, Y., and Sierks, M. R. (2004) Residues 17−20 and 30−35 of β-Amyloid Play Critical Roles in Aggregation. *J. Neurosci. Res. 75* (2), 162−171.
(48) Fancy, D. A., and Kodadek, T. (1999) Chemistry for the Analysis of Protein−Protein Interactions: Rapid and Efficient Cross-Linking Triggered by Long Wavelength Light. *Proc. Natl. Acad. Sci. U. S. A. 96* (3), 6020−6024.
(49) Bitan, G., Vollers, S. S., and Teplow, D. B. (2003) Elucidation of Primary Structure Elements Controlling Early Amyloid Beta Protein Oligomerization. *J. Biol. Chem. 278* (37), 34882−34889.
(50) Bolognesi, B., Kumita, J. R., Barros, T. P., Esbjorner, E. K., Luheshi, L. M., Crowther, D. C., Wilson, M. R., Dobson, C. M., Favrin, G., and Yerbury, J. J. (2010) ANS Binding Reveals Common Features of Cytotoxic Amyloid Species. *ACS Chem. Biol. 5* (8), 735−740.
(51) Spencer, R. K., Li, H., and Nowick, J. S. (2014) X-Ray Crystallographic Structures of Trimers and Higher-Order Oligomeric Assemblies of a Peptide Derived from Aβ17−36. *J. Am. Chem. Soc. 136* (15), 5595−5598.
(52) Salveson, P. J., Haerianardakani, S., Thuy-Boun, A., Kreutzer, A. G., and Nowick, J. S. (2018) Controlling the Oligomerization State of Aβ-Derived Peptides with Light. *J. Am. Chem. Soc. 140* (17), 5842−5852.
(53) Streltsov, V. A., Varghese, J. N., Masters, C. L., and Nuttall, S. D. (2011) Crystal Structure of the Amyloid-β P3 Fragment Provides a Model for Oligomer Formation in Alzheimer's Disease. *J. Neurosci. 31* (4), 1419−1426.
(54) Honda, R. (2018) Amyloid-β Peptide Induces Prion Protein Amyloid Formation: Evidence for Its Widespread Amyloidogenic Effect. *Angew. Chem., Int. Ed. 57* (21), 6086−6089.
(55) Warner, C. J. A., Dutta, S., Foley, A. R., and Raskatov, J. A. (2016) Introduction of D-Glutamate at a Critical Residue of Aβ42 Stabilizes a Pre-Fibrillary Aggregate with Enhanced Toxicity. *Chem. - Eur. J. 22* (34), 11967−11970.
(56) Nakka, P. P., Li, K., and Forciniti, D. (2018) Effect of Differences in the Primary Structure of the A-Chain on the Aggregation of Insulin Fragments. *ACS OMEGA 3*, 9636−9647.
(57) Dutta, S., Foley, A. R., Warner, C. J. A., Zhang, X., Rolandi, M., Abrams, B., and Raskatov, J. A. (2017) Suppression of Oligomer Formation and Formation of Non-Toxic Fibrils upon Addition of Mirror-Image Aβ42 to the Natural L-Enantiomer. *Angew. Chem., Int. Ed. 56* (38), 11506−11510.
(58) Dutta, S., Finn, T. S., Kuhn, A. J., Abrams, B., and Raskatov, J. A. (2019) Chirality Dependence of Amyloid β Cellular Uptake and a New Mechanistic Perspective. *ChemBioChem 20*, 1023−1026.

https://dx.doi.org/10.1021/acschemneuro.0c00160
ACS Chem. Neurosci. 2020, 11, 1539−1544

Chapter 3. Biophysical and biological properties of heterogenous mixtures of p3 and Aβ

This chapter contains text and figures from the following manuscript: Kuhn, A. J.; Chan, K.; Rad, B.; Raskatov. J. A. **In preparation.**

Mixing of Aβ and p3 Results in Fibrilization Enhancement, Unique Intermediate Formation, and Suppression of Toxicity

Ariel J. Kuhn[a], Ka Chan[a], Behzad Rad[b], Jevgenij A. Raskatov[a]*

[a] Dept. of Chemistry and Biochemistry, University of California Santa Cruz, CA 95064, United States

[b] Molecular Foundry Division, Lawrence Berkeley National Laboratory, 1 Cyclotron Road, Berkeley, CA 94720, USA

* Corresponding author

INTRODUCTION

Alzheimer's Disease (AD) is a progressive neurodegenerative disease characterized by a rapid loss of cognitive function and memory. The cost of AD, and other related forms of dementia, is expected to be $1.1 trillion by as early as 2050.[36] AD is characterized by two major pathological features, dense amyloid plaques and neurofibrillary tau tangles. Amyloid plaques are primarily comprised of the Amyloid-β (Aβ) peptide, a predominantly 40-42 residue intrinsically disordered, aggregation-prone peptide with unknown healthy physiological function. Until 2019, Aβ was the primary target of disease-modifying AD therapeutics.[37,38] All of these amyloid-targeting drugs have failed clinical trials, barring the controversial Aducanumab approval, with some even making patients cognitively worse.[39–41] Explanations for this

barrage of failures have ranged from the suggestion that intervention took place too late in disease progression to an outright rejection of Aβ as the causative agent of AD.[39–42] Interestingly, plaques isolated from the brains of Alzheimer's patients contain a variety of Aβ peptides and over 900 unique proteins (approximately 200 of which are found consistently across many patient samples).[12,13] What is often not discussed is the role of alternative proteolytic fragments of Aβ in AD, many of which exhibit amyloidogenic properties as well. Aβ fragments, such as pyroglutamate-truncated-Aβ (AβpE3-40/42 and AβpE11-40/42)[17,18] and Aβ4-40/42,[19,20] exhibit enhanced aggregation propensity,[19,21–23] cellular toxicity,[21] and can even stimulate rapid fibril formation of Aβ.[43] Similarly, our lab's recent work on p3 has revealed that p3 rapidly forms oligomers and fibrils morphologically, and likely conformationally, indistinguishable from those formed by Aβ.[8,26] As outlined in our recent review article, these findings were in direct opposition with the previous claims that p3 was non-amyloidogenic.[8] In fact, in 2020, p3 received over 60x less publications as compared to Aβ, despite being the more prominent proteolytic product of Amyloid-β Precursor Protein (AβPP) (**Fig. 2**).

Despite this historical "non-amyloidogenic" designation from a relatively small body of literature (**Fig. 2**), p3 easily forms amyloidogenic fibrils.[26] These fibrils, which form more rapidly than those formed by Aβ, also share conformational similarities with Aβ, as evidenced by assays such as Thioflavin T (ThT), OC antibody binding, and Congo Red.[26] p3 can also form low-molecular weight (LMW) and high-molecular weight (HMW) oligomers as demonstrated by photo-induced crosslinking of

unmodified proteins (PICUP) and low-temperature isolation.[26] p3 has also exhibits cell toxicity, comparable to that of Aβ, although studies on this are conflicting.[26,44–47] Despite shared biophysical and biological properties with Aβ, p3 has been frequently described as neuroprotective and potentially therapeutic.[8] However, there is no scientific evidence that we are aware of supporting the claims that p3 is neuroprotective, only that its production precludes Aβ formation. This is an important distinction, and one that has not been made clearly enough. This dogma conflicts with the finding that p3 is the major component of preamyloid plaques in those with Down Syndrome, 50-77% of whom develop Alzheimer's Disease by the age of 60.[15]

While physiologically relevant ratios of Aβ42:Aβ40 have been extensively studied by a wide range of biophysical and biological methods,[48–51] little is known how Aβ interacts with other AβPP proteolytic processing products. To our knowledge, nothing is currently known about the relationship between p3 and Aβ, whether they can cooperatively aggregate, and the resultant neurological consequences of such aggregates. We hypothesized that p3 and Aβ could form heterogenous amyloids based on the shared amyloidogenic segments, spanning residues Aβ17-22 and Aβ30-42, highlighted in green (**Fig. 7A**).[25,26] Interestingly, the amyloidogenic segments of p3 and Aβ overlap with the hydrophobic residues, according to the hydropathy index developed by Kyte and coworkers.[52] This, combined with the finding that scrambled and reversed (42-1) Aβ also form oligomers and fibers,[53] offers insights into the mechanism of amyloidogenicity. We sought to investigate the molecular and cellular effects of interactions between Aβ and p3.

A

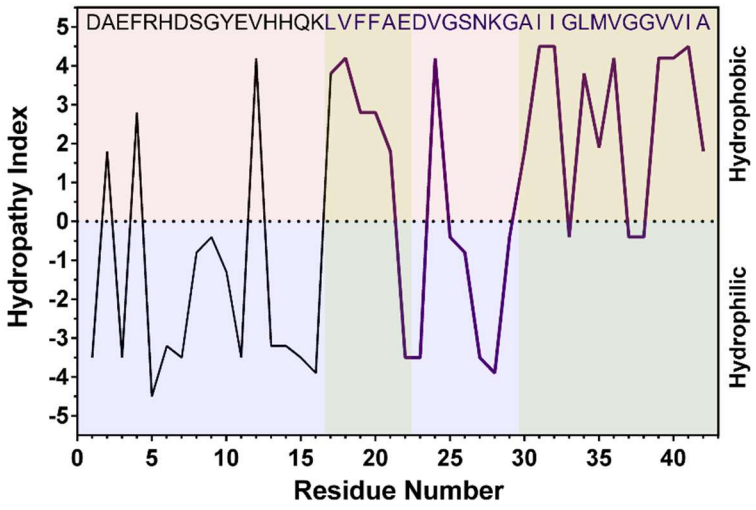

B

Peptide	GRAVVY Value
Aβ42	0.205
Aβ40	0.058
p3(17-42)	1.455
p3(17-40)	1.313

Figure 7. A) Hydropathy Profile of Aβ42 and p3. Hydropathy Index[52] values of each residue within Aβ42, including the p3 peptide. The p3 portion of the hydropathy plot is bold purple. Hydrophobic residues (HI > 0) are highlighted red. Hydrophilic residues (HI < 0) are highlighted in blue. Segments highlighted in green (Aβ17-22 and Aβ30-40) designate amyloidogenic regions, calculated by AGGRESCAN.[25,26] B) Grand Average of Hydropathy (GRAVVY) for different isoforms of Aβ and p3.[52] Heat map denotes hydrophobicity: dark red values are highly hydrophobic and light pink values are slightly hydrophobic

RESULTS & DISCUSSION

Herein, we report a biophysical and biological analysis of the relationship between p3 and Aβ, in an effort to deconvolute the role of p3 in AD. p3(17-40) was selected over p3(17-42) as p3(17-42) is too hydrophobic (see GRAVVY value

comparisons in **Fig. 7B**) compared to Aβ, making it difficult to use the same preparation protocols. In addition, even upon dissolution, p3(17-42) precipitates out of solution (data not shown), making it challenging to study its aggregation kinetics. Aβ42 was selected over Aβ40 given its known cellular toxicity to various cell lines.[54,55]

To first determine if p3 and Aβ could co-assemble to form heterogenous aggregates, fluorescent peptide analogs were synthesized. Aβ was N-terminally labeled with 5(6)-carboxyfluorescein (denoted as FAM-Aβ) and p3 was N-terminally labeled with 5(6)-carboxytetramethylrhodamine (denoted as TAMRA-p3). The fluorescent peptides were co-incubated at 37 °C for 7 days, alongside homogenous controls, and nonfibrillar aggregates were removed from solution by centrifugation. This methodology was adapted by work previously conducted in our lab.[55] The resultant aggregates were imaged with confocal microscopy on two channels (channel 1, FAM: λ_{ex} = 476 nm, λ_{em} = 484-514 nm; channel 2, TAMRA: λ_{ex} = 543 nm, λ_{em} = 630-690 nm) to afford the images displayed in **Fig. 8**. The heterogenous mixture of TAMRA-p3 and FAM-Aβ was easily detectable on both fluorescent channels, indicating significant colocalization (lower panels). In contrast, FAM-Aβ was only detectable on channel 1, while TAMRA-p3 was only detectable on channel 2. We have previously demonstrated that neither FAM conjugation to Aβ, nor TAMRA conjugation to p3, affects the biophysical properties of the unmodified peptides.[26,56,57]

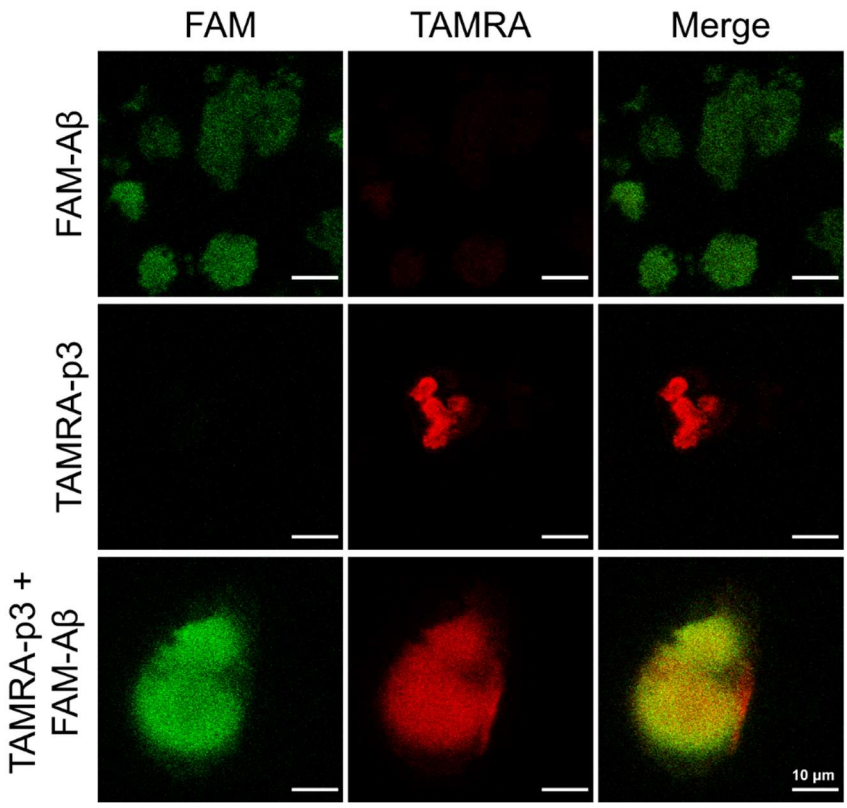

Figure 8. Confocal microscopy images (channel 1, left panel: FAM: λ_{ex} = 476 nm, λ_{em} = 484-514 nm; channel 2, middle panel: TAMRA: λ_{ex} = 543 nm, λ_{em} = 630-690 nm; right panel: merged channels 1 and 2 to assess colocalization). FAM-Aβ fibrils were active on channel 1, but not channel 2. TAMRA-p3 fibrils were active on channel 2, but not channel 1. Fibrils grown from an equimolar mixture of FAM-Aβ and TAMRA-p3 were active on both channels 1 and 2, with robust fluorescent colocalization. Scale bars: 20 µm.

Our finding that TAMRA-p3 and FAM-Aβ could co-assemble motivated us to probe the biophysics of this heterogenous fibril formation process. Our previous study demonstrated that p3 could form ThT-, Congo Red-, and OC antibody-positive fibrils more rapidly than Aβ, and that the resultant fibrils were morphologically indistinguishable from those formed by Aβ.[26] We also found that pre-aggregated p3 seeds enhanced Aβ fibril formation.[26] To measure the effect p3 exerts on Aβ fibril formation, we conducted several ThT experiments in which different Aβ:p3 ratios were employed (**Fig. 9A**). The ThT fibril formation assay is typically characterized by a sigmoidal growth curve, delineated by A) a nucleation phase, also known as a lag phase in which the amount of ThT-positive aggregates are below the detection limit, B) an elongation phase, the steep enhancement of fluorescence upon fibril growth, and C) a plateau phase, in which monomer to fibril equilibrium is reached.[58] This classical growth curve was observed for Aβ, but not for p3 or the various mixtures (1:1, 2:1, 4:1, and 8:1). All mixtures of Aβ and p3, as well as p3 alone, exhibited curves devoid of lag phases, instead beginning with the elongation phase. The 1:1 mixtures of Aβ and p3 aggregated more rapidly than 10 μM Aβ alone, at both concentrations (10:10 μM and 5:5 μM). However, 1 equivalent of p3 was not necessary for this effect, as when only 1.25 μM p3 was added to 10 μM Aβ (8:1 ratio), aggregation was significantly enhanced, and a lag phase was not observed. Thus, even at low concentrations, p3 sequesters Aβ and promotes fibril formation.

Since our previous study revealed that Aβ and p3 formed morphologically indistinguishable fibrils (both with and without agitation),[26] unique morphologies in

heterogenous fibrils were not anticipated. As expected, heterogenous fibrils were morphologically identical to the homogenous fibrils, as shown by SEM (**Fig. 9B-E, 9B-C, S4-8**). This observation held true regardless of fibril preparation method: under agitation (**Fig. 9, S4-5, S7-8**), analogous to the ThT experiment, or under quiescent conditions, as seen in **Fig. 9B-C (and Fig. S6)**, and in our previous study.[26]

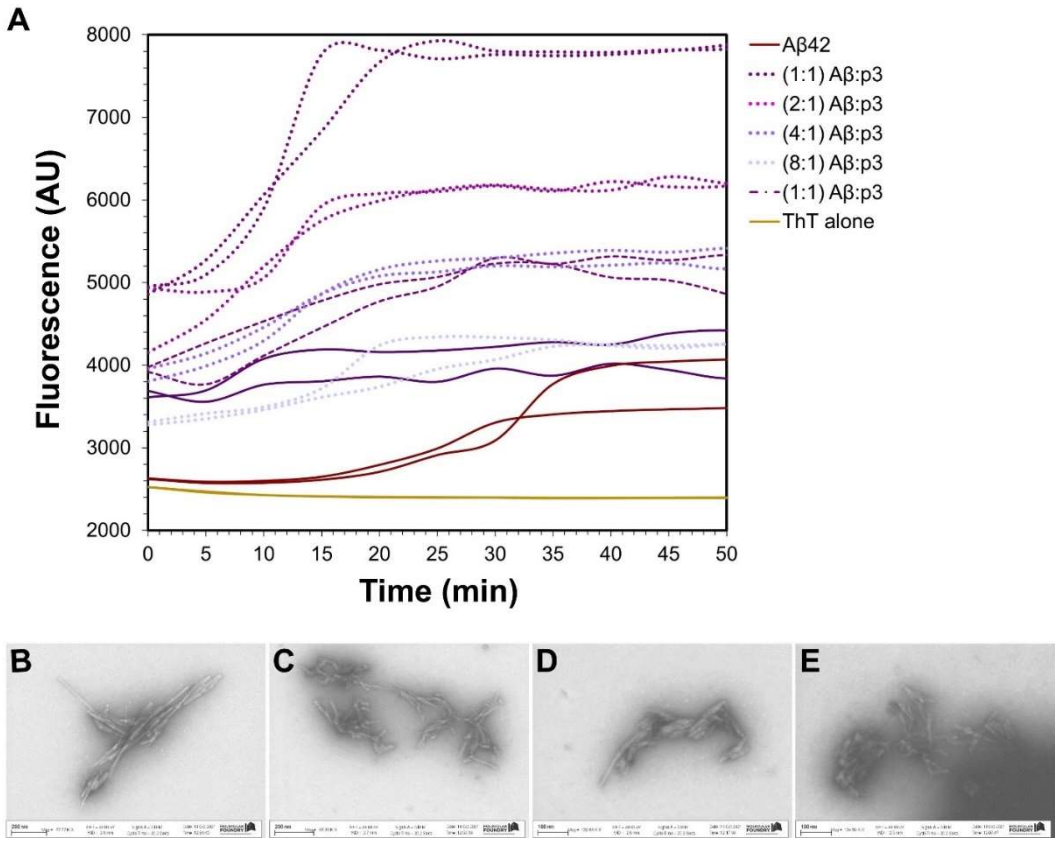

Figure 9. A) ThT-monitored aggregation kinetics of Aβ, p3, the following mixtures: 1:1, 2:1, 4:1 and 8:1 Aβ:p3. SEM images of agitated fibrils formed by B) p3, C) Aβ, D) 1:1 Aβ:p3, and E) 2:1 Aβ:p3. Scale bars are as shown.

The acceleration of fibril formation of Aβ by addition of p3 motivated us to investigate earlier stages of self-assembly, specifically soluble oligomer formation. Our

previous study found that since p3 lacked the essential tyrosine for effective photo-induced crosslinking of unmodified proteins (PICUP), p3 with Phe → Tyr ($p3_{F19Y}$ and $p3_{F20Y}$) mutations allowed for crosslinked oligomer isolation. We also found that these modifications did not dramatically affect aggregation kinetics.[26] $p3_{F20Y}$ was selected for use in this study because, of the two p3 mutations, $p3_{F19Y}$ and $p3_{F20Y}$, we found $p3_{F20Y}$ to exhibit the most closely related ThT curve to wild-type p3 (Figure S14 from Kuhn, A.J.; *et. al. ACS. Chem Neuro*. **2020**).[26] Upon exposing 1:1 Aβ and $p3_{F20Y}$ to PICUP, we found that compared to Aβ or $p3_{F20Y}$ alone, additional oligomers were formed between 10-30 kDa (**Fig. 10A**). In fact, nearly double the number of bands is formed from the mixture of Aβ and $p3_{F20Y}$, indicating the presence of unique oligomers not formed by either individual peptide. Additionally, there was increased accumulation of high-molecular-weight aggregates at the top of the gel from the mixture (black arrow in lane #4, **Fig. 10A**), supporting the immediate formation of fibrils observed in the ThT experiments. Thus, oligomer formation is slightly bypassed upon introducing p3 into Aβ. The same result was observed upon crosslinking a mixture of Aβ with $p3_{F19Y}$ (**Fig. S13**). Moreover, the increased presence of high molecular weight bands was qualitatively consistent with a previous study in which mixtures of L- and D-Aβ were mixed and subsequently crosslinked.[56]

To characterize the morphology of heterogenous oligomers formed by p3 and Aβ, a low temperature trapping protocol developed by Ahmed and coworkers[59] and later adapted by our lab,[26,55] was employed (**Fig.10D-G, S9-12**). The images of the 1:1 mixtures (10 μM each, 20 μM total) displayed a heterogenous mixture of round

oligomers and elongated fibrils (**Fig. 10D-E, S9-10**). No, fibrils were previously encountered in the individual images of p3 or Aβ,[26,55] further suggesting that p3 enhances rapid fibril formation of Aβ (**Fig. S11**). At a higher concentration (50 μM each, 100 μM total), we observed a heterogenous mixture of round oligomers, elongated fibrils, and what appear to be protofibrils (**Fig. 10F-G, S12**).These protofibrillar species are morphologically similar to what we previously found in a different Aβ-related study.[60]

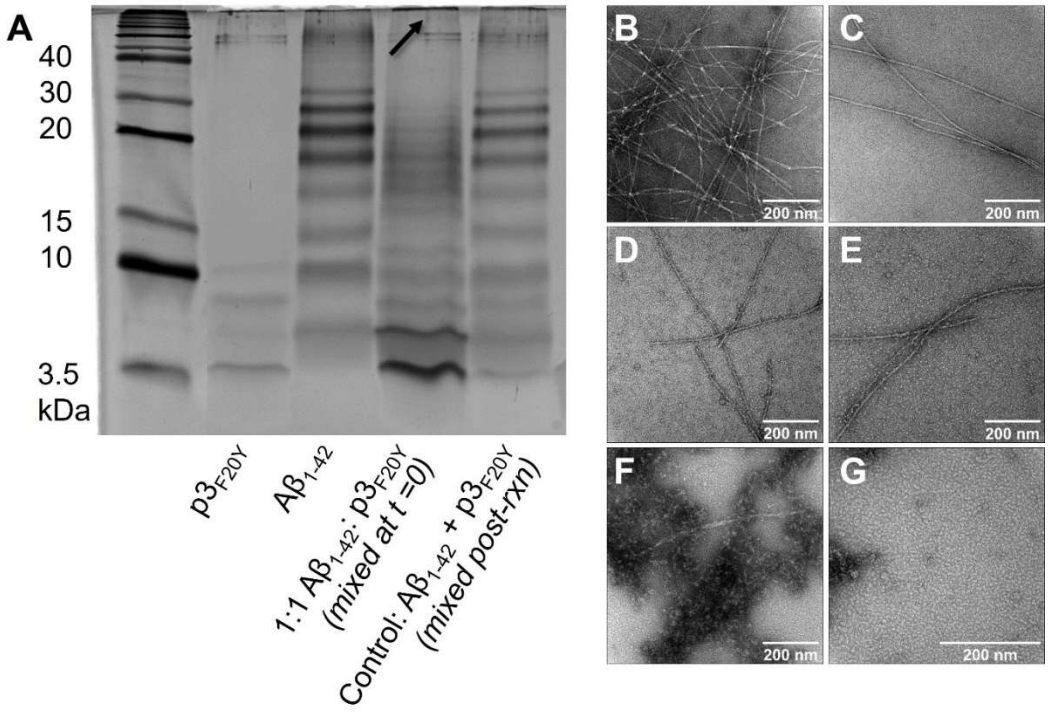

Figure 10. A) PICUP SDS-PAGE gel of $p3_{F20Y}$, Aβ, 1:1 Aβ:$p3_{F20Y}$ (mixed immediately, prior to PICUP), and a control 1:1 Aβ:$p3_{F20Y}$ (mixed after PICUP and quenching). B-G) TEM images of B-C) quiescently grown fibrils of 1:1 Aβ:p3, D-E) kinetically trapped intermediates of 1:1 Aβ:p3 (10 μM each, 20 μM total), and F-G)

kinetically trapped intermediates of 1:1 Aβ:p3 (50 μM each, 100 μM total). Scale bars: 200 nm.

Recent data suggest that transient Aβ oligomers are more toxic than stable fibrils.[61,62] To investigate whether the enhancement of fibril formation and consequential reduction in soluble intermediate oligomer formation observed upon mixing p3 with Aβ influenced the biological activity of Aβ, we probed the cytotoxicity of various peptidic mixtures after 72h incubations. Treatment of two neuron-like cell lines, PC12 and SH-SY5Y, with 50 μM Aβ reduced the cell viability by > 70% and 90% respectively (**Fig. 11A**), consistent with our previous reports.[55] This concentration was selected for this study as lower concentrations produce only modest cytotoxicity in these cell lines.[56] We found that 50 μM p3 was significantly less toxic to both cell lines when compared with Aβ. We observed that 50 μM p3 was mildly toxic to SH-SY5Y cells and non-toxic to PC12 cells, reducing viability by 35% and 0%, respectively. This was consistent with our previous finding that the 17-40 isoform of p3 was less toxic to SH-SY5Y cells.[26] Previous reports on cytotoxicity of p3 (17-40 and 17-42) have been conflicting.[44–47,63,64]

Interestingly, the addition of 1 equivalent of p3 (50μM) to Aβ (50μM) prior to dosing (100 μM total peptide concentration), resulted in significant cytotoxicity neutralization compared with Aβ (50μM) alone: viability of PC12 and SH-SY5Y cells after 72h was enhanced by over 50% and 30%, respectively (**Fig. 11B**), in agreement with our previous findings.[56,60] We observed that cytotoxicity of Aβ to both cell lines could be reduced, even at relatively low concentrations of p3 (12.5 μM p3, in the 4:1

Aβ:p3 mixture). Given that the addition of p3 into Aβ, even in small amounts, accelerates fibril formation, we attribute the reduced toxicity during long incubation periods to rapid fibril formation, similar to the cellular toxicity suppression observed in our previous work with racemic-Aβ.[56] To ensure robustness and reproducibility of our results, the WST-1 assay on Aβ, p3 and a 1:1 mixture was repeated in both cell lines three additional times, which produced consistent outcomes (**Fig. S14-15**).

We next aimed to understand the mechanisms by which these peptides exert toxic effects, specifically at earlier timepoints. Several studies have reported that Aβ inhibits healthy mitochondrial activity by increasing the formation of reactive oxygen species (ROS), leading to cell death.[65–68] The differential ROS production can be monitored within minutes,[69] as opposed to traditional viability assays in which detection can take days. To investigate an early mechanism of the protective effects of p3 against Aβ-induced cytotoxicity, we probed ROS production in SH-SY5Y cells with CM-H2DCFDA, an ROS-sensitive dye. We found that as early as 5 mins, both Aβ and p3 elicited a 30% higher production of ROS species as compared to untreated vehicle, at 50μM each (**Fig. 11C**). A significant difference in ROS production between Aβ and p3 emerges after 30 mins, when Aβ increased ROS production by 100%, while p3 increased ROS production by 150% (**Fig. 11C**). We observed that ROS production induced by Aβ could be neutralized by addition of p3 as early as 90 mins. This effect was noted even at lower concentrations of p3 relative to Aβ (4:1 Aβ:p3, in the 4:1 Aβ:p3 mixture). H2O2 (100mM) was used as a positive control (**Fig. S16**).

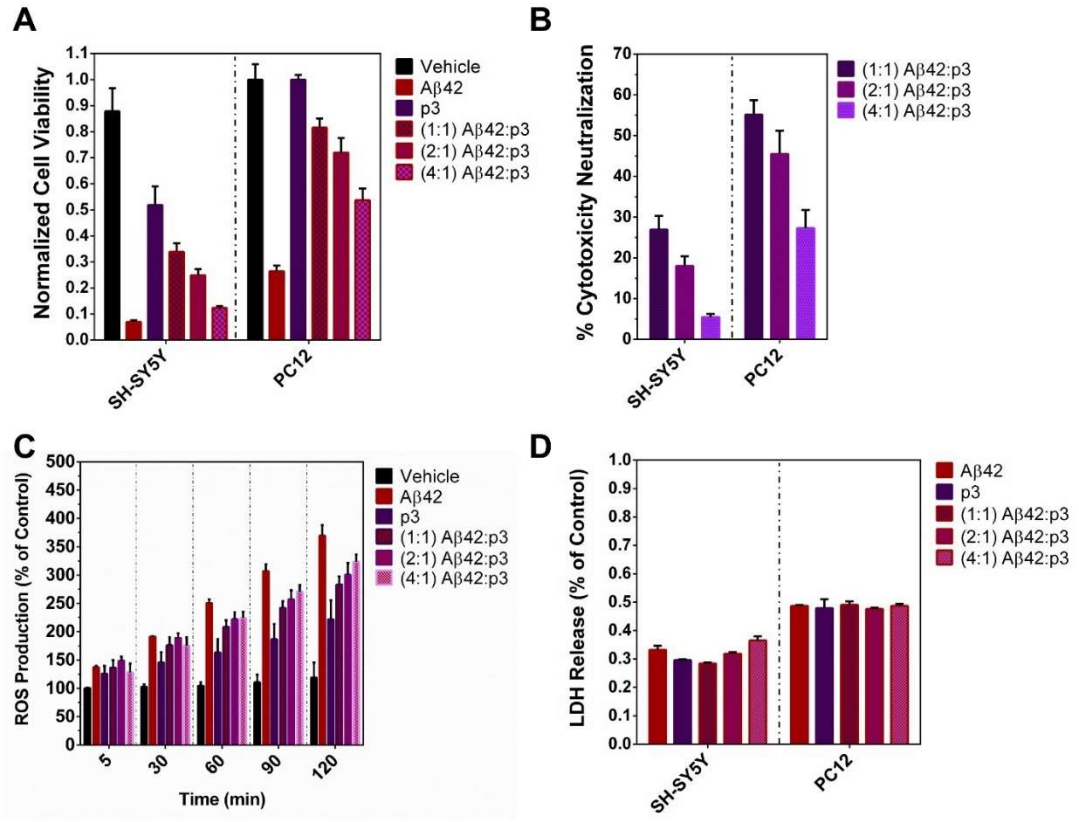

Figure 11. A) Cellular viability (SH-SY5Y or PC12) in response to treatment with either p3 (50 μM), Aβ (50 μM), 1:1 Aβ:p3 (50:50 μM), 2:1 Aβ:p3 (50:25 μM), or 4:1 Aβ:p3 (50:12.5 μM) using WST-1 cell proliferation reagent. PC12 cells were plated at 5,000 cells/well and SH-SY5Y cells were plated at 50,000 cells/well, and allowed to adhere for 24h. Biological triplicates are shown in the S.I. B) % Cytotoxicity neutralization calculated from A). C) ROS activity in SH-SY5Y cells in response to treatment with either p3 (50 μM), Aβ (50 μM), 1:1 Aβ:p3 (50:50 μM), 2:1 Aβ:p3 (50:25 μM), or 4:1 Aβ:p3 (50:12.5 μM). Fluorescent measurements were taken at 5, 30, 60, 90, and 120 mins. Cells were plated at a density of 50,000 cells/well and allowed to adhere for 24h. All data (A-D) are represented as mean ± s.d., performed in technical triplicate. D) LDH release from PC12 and SH-SY5Y cells in response to treatment with either p3 (50 μM), Aβ (50 μM), 1:1 Aβ:p3 (50:50 μM) 2:1 Aβ:p3 (50:25 μM), or 4:1 Aβ:p3 (50:12.5 μM). Cells were plated at a density of 50,000 cells/well and allowed to adhere for 24h.

Several recent studies have demonstrated that cellular internalization is inextricably linked with toxicity.[70,71] Recent work from our lab, and others, suggests that this uptake process is primarily receptor-mediated with only minor contributions from non-specific, passive processes.[57,72] Both Aβ and p3 were N-terminally conjugated to TAMRA, and flow cytometry experiments were performed. SH-SY5Y cells were incubated with either TAMRA-Aβ or TAMRA-p3 at 5 μM for 1h (**Fig. 12A**), 5 μM for 12h (**Fig. 12B**), or 10 μM for 12h (**Fig. 12C**). Methods adapted from our previous report.[57] Interestingly, for longer timepoints, a significant difference in uptake was observed between TAMRA-Aβ and TAMRA-p3, over a 5-fold difference in mean fluorescence for both 5 μM for 12h and 10 μM for 12h (**Fig. 12B-C**). Conversely, for the early timepoint, only a minimal difference in uptake was observed, 1.2-fold difference in mean fluorescence (**Fig. 12A**). This may indicate that during passive uptake at early time-points, TAMRA-Aβ and TAMRA-p3 are equally permeable, but when dependent mechanisms, such as receptor-mediated endocytosis, predominate, TAMRA-Aβ shows a significant enhancement in internalization over TAMRA-p3. A previous study demonstrated that p3 could form calcium-permeable ion channels in membranes, eliciting cell death in human cortical neurons. They were able to reverse the effect with zinc treatment, a known blocker of amyloid-related ion channel activity.[45] To probe this theory, we utilized a membrane disruption assay, which detects extracellular Lactate Dehydrogenase (LDH), a stable enzyme released upon cellular plasma membrane damage. We observed no significant difference in LDH release upon treatment with Aβ, p3, or any of the mixtures (1:1, 2:1, 4:1) (**Fig. 11D**). This may

indicate that p3 and Aβ can passively interact with and enter cell membranes via a similar mechanism.

We next probed how the addition of p3 influenced the uptake of Aβ under varying conditions. We treated SH-SY5Y cells with different ratios of TAMRA-Aβ42 to unlabeled p3 (1:1, 2:1, 4:1, 8:1, and 16:1 TAMRA-Aβ:p3) (**Fig. 12D-F**). Despite the enhancement in fibril formation of Aβ upon addition of p3, no significant effect on cellular uptake was observed at any of the timepoints or concentrations tested.

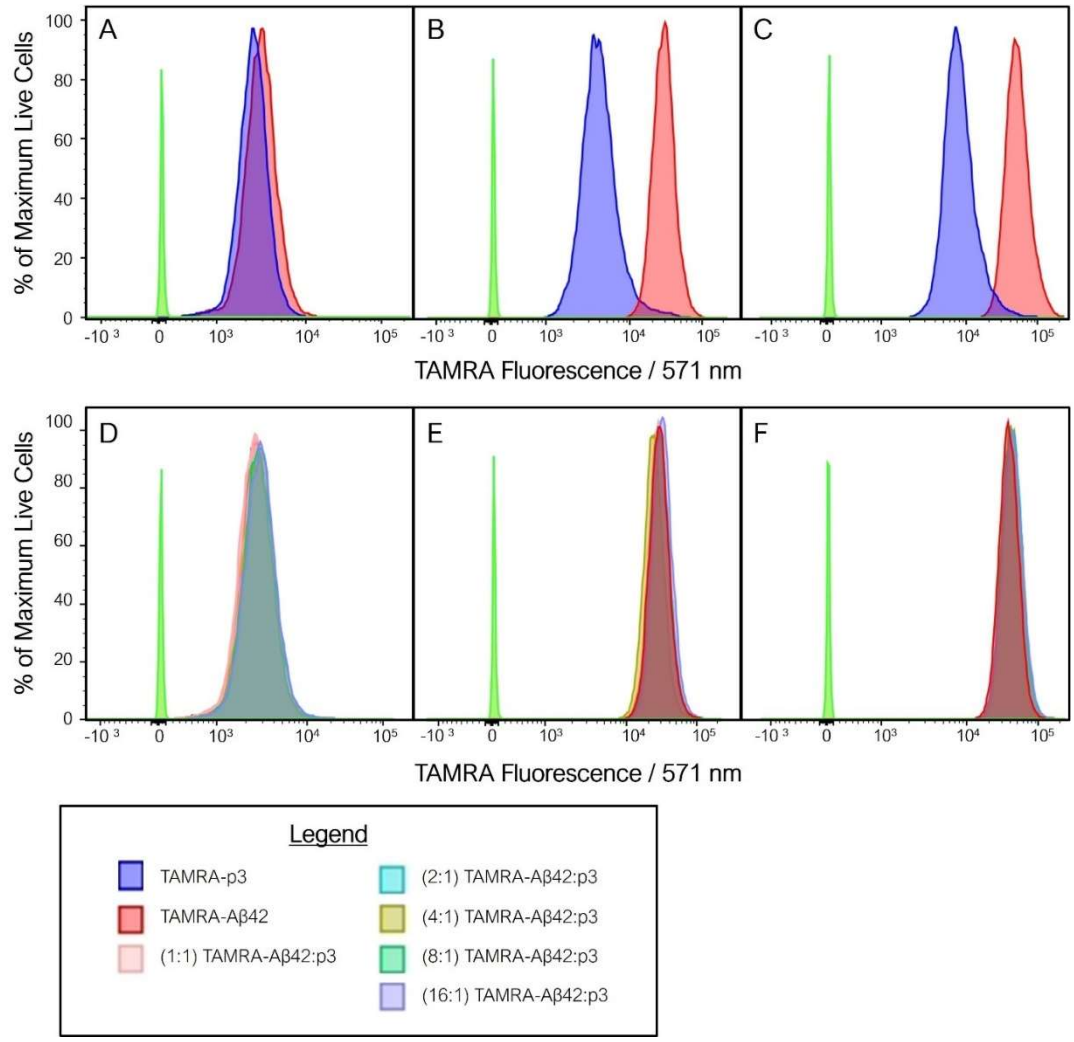

Figure 12. Flow cytometry quantitation of TAMRA-labeled peptide uptake by SH-SY5Y cells as indicated. Cells were exposed to A) TAMRA-Aβ (5 μM) or TAMRA-p3 (5 μM) for 1h. B) TAMRA-Aβ (5 μM) or TAMRA-p3 (5 μM) for 12h. C) TAMRA-Aβ (10 μM) or TAMRA-p3 (10 μM) for 1h. D) TAMRA-Aβ (5 μM), 1:1 TAMRA-Aβ: unlabeled p3 (5:5 μM), 2:1 TAMRA-Aβ: unlabeled p3 (5:2.5 μM), 4:1 TAMRA-Aβ: unlabeled p3 (5:1.25 μM), 8:1 TAMRA-Aβ: unlabeled p3 (5:0.625 μM) or 16:1 TAMRA-Aβ: unlabeled p3 (5:0.3125 μM) for 1h. E) TAMRA-Aβ (5 μM), 1:1 TAMRA-Aβ: unlabeled p3 (5:5 μM), 2:1 TAMRA-Aβ: unlabeled p3 (5:2.5 μM), 4:1 TAMRA-Aβ: unlabeled p3 (5:1.25 μM), 8:1 TAMRA-Aβ: unlabeled p3 (5:0.625 μM) or 16:1 TAMRA-Aβ: unlabeled p3 (5:0.3125 μM) for 12h. F) TAMRA-Aβ (10 μM), 1:1 TAMRA-Aβ: unlabeled p3 (10:10 μM), 2:1 TAMRA-Aβ: unlabeled p3 (10:5 μM), 4:1 TAMRA-Aβ: labeled p3 (10:2.5 μM), 8:1 TAMRA-Aβ: unlabeled p3 (10:1.25 μM) or 16:1 TAMRA-Aβ: unlabeled p3 (5:0.625 μM) for 12h.

In summary, we have shown that p3 expedites Aβ fibril formation, producing morphologically indistinguishable fibrils. We also found that fluorescently labeled derivatives of Aβ and p3 colocalized in heterogenous aggregates. The accelerated fibril formation formed unique oligomers not observed for either Aβ or $p3_{F20Y}$ independently. In addition, fibril formation is favorable in the heterogenous mixtures, even under oligomer-forming conditions. The enhanced fibril formation resulted in suppression of toxicity and ROS production in both PC12 and SH-SY5Y cells. Additionally, we found that at an early timepoint, TAMRA-Aβ and TAMRA-p3 uptake was comparable, while at a later timepoint, internalization of peptide was nearly 6x higher for the TAMRA-Aβ treated cells. However, no augmentation of uptake was observed upon addition of unlabeled p3 into TAMRA-Aβ treated cells.

CONCLUSION

This report is, to the best of our knowledge, the first evidence that p3 can interact with Aβ, and alter its biological effects *in vitro*, even at relatively low concentrations. In light of these findings, we call for an urgent revision of the role of p3 Amyloid Cascade Hypothesis.

METHODS

Additional experimental methods can be found in the Supporting Information.

Peptide Synthesis. All peptides were synthesized by SPPS using Fmoc chemistry, following our previously published protocols[73] on Tentagel® S PHB resin (Rapp Polymere GmbH, cat no. RA1327).

Peptide Purification and Preparation. Purification of Aβ40 was done as previously published.[26,74] For p3, solid, lyophilized peptide was dissolved in 8:2 0.1% NH_4OH H_2O/acetonitrile and purified using PLRP-S columns (8 μm, 300 Å) under basic conditions. All peptide purities range from 95-99%. The concentration of p3 was determined by the absorbance of the peptide backbone at 205 nm via Nanodrop (ε = 83,370 M^{-1} cm^{-1}) using the protein parameter calculator (http://nickanthis.com/tools/a205.html).[75] The concentration of Aβ40 was determined at 280 nm (ε = 1490 M^{-1} cm^{-1}).

Fibril growth. Lyophilized peptide (Aβ and/or p3) was dissolved in 20 mM NaOH and sonicated for 30 s, then diluted to 20 μM in PBS. The samples were incubated either (1) at 37 °C for 24 hours with mild agitation, or (2) at 37 °C quiescently for 7 days. For TEM imaging, 3 μL of sample aliquots were spotted onto freshly glow-discharged carbon-coated electron microscopy grids (Ted Pella, Catalog No. 01701-F). The grids were rinsed with milliQ water after 1 min incubation, followed by staining with 30 μL 1% uranyl acetate.

Colocalization. FAM-Aβ or TAMRA-p3 fibrils were grown quiescently as described above at 20 μM each. For the 1:1 mixture, FAM-Aβ and TAMRA-p3 fibrils

were grown quiescently at 40 μM total (20 μM each) for 7 days at 37 °C. Fibrils were centrifuged at 14000 g for 15 min and washed with MilliQ H_2O x2 to remove soluble aggregates, reducing background fluorescence.

Confocal Microscopy. 5 μL of each solution was added to a cover slide and imaged on a Leica SP5 confocal microscope using a 63x/1.2 HCX PL APO water immersion objective. Images were collected on two fluorescent channels (channel 1, FAM: λ_{ex} = 476 nm, λ_{em} = 484-514 nm; channel 2, TAMRA: λ_{ex} = 543 nm, λ_{em} = 630-690 nm). Zoom, frame size, gain, and offset values were held constant for all experiments.

Oligomer Growth and Imaging. To trap the intermediate oligomers, lyophilized Aβ or p3 was dissolved in cold 20mM NaOH and sonicated in an ice bath for 30 s. Peptides were individually diluted to either 10 or 50 μM in PBS and incubated at 4 °C for 6 h without agitation. TEM samples were prepared and imaged as described above.

ThT Assay and TAMRA Quenching Assays. The ThT assay was conducted as described previously.[26,56,76] ThT (Acros Organics, 2390-54-7) was dissolved in 10 mL of PBS buffer containing 0.02% (w/v) NaN_3 and filtered through a 0.22 μm filter. The concentration was determined by Nanodrop at 412 nm (ε = 36000$M^{-1}cm^{-1}$). Lyophilized samples of peptide were prepared as described above at 10 μM, with 20 μM ThT in PBS. 200 μL of sample was added to each well, in triplicate, of a black, clear bottom 96-well plate. Absorbance readings were measured every 5 min with 295

s of shaking between readings at 37 °C with a Biotek synergy HTX fluorescence plate reader (λ_{ex} = 444 nm λ_{em} = 485 nm).

Photochemically induced crosslinking of peptides. 4 μL of 1 mM $[Ru(bipy)_3]^{2+}$ and 4 μL of 20 mM ammonium persulfate were added to 32 μL aliquots of 20 μM Aβ, p3, $p3_{F20Y}$ in PBS. The samples were irradiated for 1.2 s with white light using our previously described setup.[73] Following irradiation, the samples were immediately quenched with 40 μL of loading buffer containing 5% 2-mercaptoethanol, and separated by SDS-PAGE gel electrophoresis (12% tris-tricine polyacrylamide) at 100 V for 2 h. The gels were developed by silver staining.

Cell Culture. Human neuroblastoma SH-SY5Y cells were cultured in 1:1 DMEM: F12 K media supplemented with 10% fetal bovine serum and 1% penicillin-streptomycin. PC12 cells were cultured in F12K media supplemented with 2.5% fetal bovine serum, 12.5 % horse serum and 1% penicillin-streptomycin. Cells were incubated at 37 °C with 5% CO_2.

Cell Viability (WST-1 Assay). SH-SY5Y cells were plated in a 96-well plate at a density of 50,000 cells/well (100 μL total volume/well) and allowed to adhere for 24 h before dosing. PC12 cells were plated in a 96-well plate at a density of 5,000 cells/well (100 μL total volume/well) and allowed to adhere for 24 h before dosing. Lyophilized peptides were dissolved in 30 μL of 20 mM NaOH and the solutions were diluted to a final concentration of 50 μM with culture media and added to cells. After dosing, cells were incubated for 72 h at 37 °C. Then, 10 μL aliquots of WST-1 (Roche) were added to each well and incubated for 3 h. Absorbance was measured at λ = 450nm.

Each bar represents an average of three technical replicates, normalized against the vehicle (cells and media only).

LDH Release. For the LDH release assay (Cayman Chemical, catalog number 601170), adhesive PC12 or SH-SY5Y cells were plated in a 96-well plate at a density of 50000 cells/well and allowed to adhere for 24 h before dosing. Each well contained 100 µL total volume. For control experiments, 10 µl of Triton X-100 (10%) was added (positive control, 100% cell death) and 10 µL of assay buffer was added (vehicle control). Lyophilized peptides were dissolved in 30 µL of 20 mM NaOH and the solutions were diluted to a final concentration of 50 µM with culture media and added to cells. Following a 24 h incubation, 50 µL of cell supernatant was transferred to a new 96-well plate and 50 µL of LDH reaction solution (Mixture of NAD+, Lactic acid, INT and Diaphorase) was added. The plate was incubated for 30 min at 37˚C and the absorbance at 450 nm was used to determine the LDH release. Each bar represents an average of three technical replicates, normalized against the positive control cells (Triton-X-treated cells).

ROS Production. SH-SY5Y cells were plated in a 96-well plate at a density of 50,000 cells/well (100 µL total volume/well) in a black 96-well plate, and allowed to adhere for 24 h before dosing. Cell media was removed, and cells were washed 2x with HBSS (w/ supplemented Mg^{2+} and Ca^{2+}). Next, cells were treated with 10 µM 5-(and-6)-chloromethyl-2', 7'-dichlorodihydro- fluorescein diacetate, acetyl ester (CM-H2DCFDA) (Invitrogen by Thermo Fisher, Catalog #: C6827) in HBSS (w/ Mg^{2+} and Ca^{2+}) for 20 min in complete darkness. Cells were washed 2x with HBSS (w/

supplemented Mg^{2+} and Ca^{2+}). Lyophilized peptides were dissolved in 30 μL of 20 mM NaOH and the solutions were diluted to a final concentration of 50 μM with HBSS (w/ Mg^{2+} and Ca^{2+}) and added to cells. After dosing, cells were incubated for 5 min at 37 °C. Absorbance was measured at λ = 450nm. Each bar represents an average of three technical replicates, normalized against the vehicle (cells and media only).

SUPPORTING INFORMATION

Sample characterization and purity; additional TEM and SEM images; PICUP gel; biological replicates of cellular viability; and ROS assay with H2O2 control.

REFERENCES

(1) Deiana, A.; Forcelloni, S.; Porrello, A.; Giansanti, A. Intrinsically Disordered Proteins and Structured Proteins with Intrinsically Disordered Regions Have Different Functional Roles in the Cell. *PLoS One* **2019**, *14* (8), 1–16. https://doi.org/10.1371/journal.pone.0217889.

(2) Morris, O. M.; Torpey, J. H.; Isaacson, R. L. Intrinsically Disordered Proteins: Modes of Binding with Emphasis on Disordered Domains. *Open Biol.* **2021**, *11* (10). https://doi.org/10.1098/rsob.210222.

(3) Uversky, V. N.; Gillespie, J. R.; Fink, A. L. Why Are "natively Unfolded" Proteins Unstructured under Physiologic Conditions? *Proteins Struct. Funct. Genet.* **2000**, *41* (3), 415–427. https://doi.org/10.1002/1097-

0134(20001115)41:3<415::AID-PROT130>3.0.CO;2-7.

(4) Olsen, J. G.; Teilum, K.; Kragelund, B. B. Behaviour of Intrinsically Disordered Proteins in Protein–Protein Complexes with an Emphasis on Fuzziness. *Cell Mol Life Sci* **2017**, *74* (17), 3175–3183. https://doi.org/10.1007/s00018-017-2560-7.

(5) Wright, P. E.; Dyson, H. J. Linking Folding and Binding. *Cur. Opin Struct Biol* **2009**, *19* (1), 31–38. https://doi.org/10.1016/j.sbi.2008.12.003.

(6) THAMBISETTY, M.; Howard, R.; Glymour, M. M.; Schneider, L. S. Alzheimer's Drugs: Does Reducing Amyloid Work? *Science* **2021**, *374* (6567), 544–545. https://doi.org/10.1126/science.abm1680.REF.

(7) Selkoe, D. J. Alzheimer's Drugs: Does Reducing Amyloid Work?-Response. *Science* **2021**, *374* (6567), 545–546. https://doi.org/10.1126/science.abm1680.REF.

(8) Kuhn, A. J.; Raskatov, J. Is the P3 Peptide (Aβ17-40, Aβ17-42) Relevant to the Pathology of Alzheimer's Disease? *J Alzheimer's Dis* **2020**, *74* (1), 43–53. https://doi.org/10.3233/JAD-191201.

(9) Willem, M.; Tahirovic, S.; Busche, M. A.; Ovsepian, S. V; Chafai, M.; Kootar, S.; Hornburg, D.; Evans, L. D. B.; Moore, S.; Daria, A.; Hampel, H.; et al. η-Secretase Processing of APP Inhibits Neuronal Activity in the Hippocampus. *Nature* **2015**, *526* (7573), 443–447. https://doi.org/10.1038/nature14864.

(10) Coronel, R.; Bernabeu-Zornoza, A.; Palmer, C.; Muñiz-Moreno, M.; Zambrano, A.; Cano, E.; Liste, I. Role of Amyloid Precursor Protein (APP)

and Its Derivatives in the Biology and Cell Fate Specification of Neural Stem Cells. *Mol Neurobiol* **2018**, *55* (9), 7107–7117. https://doi.org/10.1007/s12035-018-0914-2.

(11) Lichtenthaler, S. F. Alpha-Secretase in Alzheimer's Disease: Molecular Identity, Regulation and Therapeutic Potential. *J Neurochem* **2011**, *116* (1), 10–21. https://doi.org/10.1111/j.1471-4159.2010.07081.x.

(12) Duong, D. M.; Peng, J.; Rees, H. D.; Wang, J.; Liao, L.; Levey, A. I.; Gearing, M.; Lah, J. J.; Cheng, D.; Losik, T. G. Proteomic Characterization of Postmortem Amyloid Plaques Isolated by Laser Capture Microdissection. *J Biol Chem* **2004**, *279* (35), 37061–37068. https://doi.org/10.1074/jbc.m403672200.

(13) Drummond, E.; Nayak, S.; Faustin, A.; Pires, G.; Hickman, R. A.; Askenazi, M.; Cohen, M.; Haldiman, T.; Kim, C.; Han, X.; Shao, Y.; Safar, J. G.; Ueberheide, B.; Wisniewski, T. Proteomic Differences in Amyloid Plaques in Rapidly Progressive and Sporadic Alzheimer's Disease. *Acta Neuropathol* **2017**, *133* (6), 933–954. https://doi.org/10.1007/s00401-017-1691-0.

(14) Gowing, E.; Roher, A. E.; Woods, A. S.; Cotter, R. J.; Chaney, M.; Little, S. P.; Ball, M. J. Chemical Characterization of Abeta 17-42 Peptide, a Component of Diffuse Amyloid Deposits of Alzheimer Disease. *J Biol Chem* **1994**, *269* (15), 10987–10990.

(15) Lalowski, M.; Golabek, A.; Lemere, C. A.; Selkoe, D. J.; Wisniewski, H. M.; Beavis, R. C.; Frangione, B.; Wisniewski, T. The "Nonamyloidogenic" P3

Fragment (Amyloid Beta 17-42) Is a Major Constituent of Down's Syndrome Cerebellar Preamyloid. *J Biol Chem* **1996**, *271* (52), 33623–33631. https://doi.org/10.1074/jbc.271.52.33623.

(16) Warner, C. J. A.; Dutta, S.; Foley, A. R.; Raskatov, J. A. A Tailored HPLC Purification Protocol That Yields High-Purity Amyloid Beta 42 and Amyloid Beta 40 Peptides, Capable of Oligomer Formation. *JoVE* **2017**, No. 121, e55482. https://doi.org/doi:10.3791/55482.

(17) Perez-Garmendia, R.; Gevorkian, G. Pyroglutamate-Modified Amyloid Beta Peptides: Emerging Targets for Alzheimer´s Disease Immunotherapy. *Curr Neuropharmacol* **2013**, *11* (5), 491–498. https://doi.org/10.2174/1570159X11311050004.

(18) Jawhar, S.; Wirths, O.; Bayer, T. A. Pyroglutamate Amyloid-Beta (Abeta): A Hatchet Man in Alzheimer Disease. *J Biol Chem* **2011**, *286* (45), 38825–38832. https://doi.org/10.1074/jbc.R111.288308.

(19) Bouter, Y.; Dietrich, K.; Wittnam, J. L.; Rezaei-Ghaleh, N.; Pillot, T.; Papot-Couturier, S.; Lefebvre, T.; Sprenger, F.; Wirths, O.; Zweckstetter, M.; Bayer, T. A. N-Truncated Amyloid β (Aβ) 4-42 Forms Stable Aggregates and Induces Acute and Long-Lasting Behavioral Deficits. *Acta Neuropathol* **2013**, *126* (2), 189–205. https://doi.org/10.1007/s00401-013-1129-2.

(20) Antonios, G.; Saiepour, N.; Bouter, Y.; Richard, B. C.; Paetau, A.; Verkkoniemi-Ahola, A.; Lannfelt, L.; Ingelsson, M.; Kovacs, G. G.; Pillot, T.; Wirths, O.; Bayer, T. A. N-Truncated Abeta Starting with Position Four: Early

Intraneuronal Accumulation and Rescue of Toxicity Using NT4X-167, a Novel Monoclonal Antibody. *Acta Neuropathol. Commun.* **2014**, *2* (1), 1. https://doi.org/10.1186/2051-5960-1-56.

(21) Scheidt, H. A.; Adler, J.; Zeitschel, U.; Höfling, C.; Korn, A.; Krueger, M.; Roßner, S.; Huster, D. Pyroglutamate-Modified Amyloid β (11- 40) Fibrils Are More Toxic than Wildtype Fibrils but Structurally Very Similar. *Chem - A Eur J* **2017**, *23* (62), 15834–15838. https://doi.org/10.1002/chem.201703909.

(22) Dammers, C.; Reiss, K.; Gremer, L.; Lecher, J.; Ziehm, T.; Stoldt, M.; Schwarten, M.; Willbold, D. Pyroglutamate-Modified Amyloid-β(3–42) Shows α-Helical Intermediates before Amyloid Formation. *Biophys J* **2017**, *112* (8), 1621–1633. https://doi.org/10.1016/j.bpj.2017.03.007.

(23) Dammers, C.; Schwarten, M.; Buell, A. K.; Willbold, D. Pyroglutamate-Modified Aβ(3-42) Affects Aggregation Kinetics of Aβ(1-42) by Accelerating Primary and Secondary Pathways. *Chem. Sci.* **2017**, *8* (7), 4996–5004. https://doi.org/10.1039/c6sc04797a.

(24) Dammers, C.; Schwarten, M.; Buell, A. K.; Willbold, D. Pyroglutamate-Modified Aβ(3-42) Affects Aggregation Kinetics of Aβ(1-42) by Accelerating Primary and Secondary Pathways. *Chem Sci* **2017**, *8* (7), 4996–5004. https://doi.org/10.1039/C6SC04797A.

(25) Conchillo-Solé, O.; de Groot, N. S.; Avilés, F. X.; Vendrell, J.; Daura, X.; Ventura, S. AGGRESCAN: A Server for the Prediction and Evaluation of "Hot Spots" of Aggregation in Polypeptides. *BMC Bioinformatics* **2007**, *8* (65), 1–

17. https://doi.org/10.1186/1471-2105-8-65.

(26) Kuhn, A. J.; Abrams, B. S.; Knowlton, S.; Raskatov, J. A. Alzheimer's Disease "Non-Amyloidogenic" P3 Peptide Revisited: A Case for Amyloid-α. *ACS Chem Neurosci* **2020**, *11* (11), 1539–1544. https://doi.org/10.1021/acschemneuro.0c00160.

(27) Krysmann, M. J.; Castelletto, V.; Kelarakis, A.; Hamley, I. W.; Hule, R. A.; Pochan, D. J. Self-Assembly and Hydrogelation of an Amyloid Peptide Fragment. *Biochemistry* **2008**, *47*, 4597–4605.

(28) Bortolini, C.; Klausen, L. H.; Hoffmann, S. V.; Jones, N. C.; Saadeh, D.; Wang, Z.; Knowles, T. P. J.; Dong, M. Rapid Growth of Acetylated Aβ(16-20) into Macroscopic Crystals. *ACS Nano* **2018**, *12* (6), 5408–5416. https://doi.org/10.1021/acsnano.8b00448.

(29) Arai, T.; Sasaki, D.; Araya, T.; Sato, T.; Sohma, Y. A Cyclic KLVFF-Derived Peptide Aggregation Inhibitor Induces the Formation of Less-Toxic off-Pathway Amyloid-β Oligomers. *ChemBioChem* **2014**, *15*, 2577–2583. https://doi.org/10.1002/cbic.201402430.

(30) Brahmachari, S.; Arnon, Z. A.; Frydman-Marom, A.; Gazit, E.; Adler-Abramovich, L. Diphenylalanine as a Reductionist Model for the Mechanistic Characterization of β-Amyloid Modulators. *ACS Nano* **2017**, *11* (6), 5960–5969. https://doi.org/10.1021/acsnano.7b01662.

(31) Reches, M.; Gazit, E. Casting Metal Nanowires within Discrete Self-Assembled Peptide Nanotubes. *Science* **2003**, *300* (5619), 625–627.

https://doi.org/10.1126/science.1082387.

(32) Reches, M.; Gazit, E. Self-Assembly of Peptide Nanotubes and Amyloid-like Structures by Charged-Termini-Capped Diphenylalanine Peptide Analogues. *Isr J Chem* **2005**, *45* (3), 363–371. https://doi.org/10.1560/5mc0-v3dx-ke0b-yf3j.

(33) Lu, J.; Qiang, W.; Yau, W.; Schwieters, C. D.; Meredith, S. C.; Tycko, R. Molecular Structure of β-Amyloid Fibrils in Alzheimer's Disease Brain Tissue. *Cell* **2013**, *154* (6), 1257–1268. https://doi.org/10.1016/j.cell.2013.08.035.

(34) Westermark, P.; Benson, M. D.; Buxbaum, J. N.; Cohen, A. S.; Ikeda, S.; Masters, C. L.; Merlini, G.; Maria, J.; Sipe, J. D. Amyloid: Toward Terminology Clarification Report from the Nomenclature Committee of the International Society of Amyloidosis. *Amyloid* **2005**, *12*, 1–4. https://doi.org/10.1080/13506120500032196.

(35) Benson, M. D.; Buxbaum, J. N.; Eisenberg, D. S.; Merlini, G.; Saraiva, M. J. M.; Sekijima, Y.; Sipe, J. D.; Westermark, P. Amyloid Nomenclature 2018: Recommendations by the International Society of Amyloidosis (ISA) Nomenclature Committee. *Amyloid* **2018**, *25* (4), 215–219. https://doi.org/10.1080/13506129.2018.1549825.

(36) Alzheimer's Association. *2021 Alzheimer's Disease Facts and Figures*; 2021; Vol. 17.

(37) Cummings, J.; Reiber, C.; Kumar, P. The Price of Progress: Funding and Financing Alzheimer's Disease Drug Development. *Alzheimer's Dement.*

Transl. Res. Clin. Interv. **2018**, *4*, 330–343. https://doi.org/10.1016/j.trci.2018.04.008.

(38) Cummings, J.; Lee, G.; Ritter, A.; Sabbagh, M.; Zhong, K. Alzheimer's Disease Drug Development Pipeline: 2020. *Alzheimer's Dement. Transl. Res. Clin. Interv.* **2020**, *6* (1), 1–29. https://doi.org/10.1002/trc2.12050.

(39) Knopman, D. S. Lowering of Amyloid-Beta by β-Secretase Inhibitors — Some Informative Failures. *N Engl J Med* **2019**, *380*, 11–13. https://doi.org/10.1056/NEJMe1903193.

(40) Karran, E.; Mercken, M.; Strooper, B. De. The Amyloid Cascade Hypothesis for Alzheimer's Disease: An Appraisal for the Development of Therapeutics. *Nat Rev Drug Discov* **2011**, *10* (9), 698–712. https://doi.org/10.1038/nrd3505.

(41) Karran, E.; Strooper, B. De. The Amyloid Cascade Hypothesis: Are We Poised for Success or Failure? *J Neurochem* **2016**, *139* (2), 237–252. https://doi.org/10.1111/jnc.13632.

(42) Cummings, J.; Lee, G.; Ritter, A.; Zhong, K. Alzheimer's Disease Drug Development Pipeline: 2018. *Alzheimer's Dement Transl Res Clin Interv* **2018**, *4*, 195–214. https://doi.org/10.1016/j.trci.2018.03.009.

(43) Barritt, J. D.; Younan, N. D.; Viles, J. H. N-Terminally Truncated Amyloid-β(11–40/42) Cofibrillizes with Its Full-Length Counterpart: Implications for Alzheimer's Disease. *Angew. Chemie. - Int. Ed.* **2017**, *56* (33), 9816–9819. https://doi.org/10.1002/anie.201704618.

(44) Wei, W.; Norton, D. D.; Wang, X.; Kusiak, J. W. Aβ 17-42 in Alzheimer's

Disease Activates JNK and Caspase-8 Leading to Neuronal Apoptosis. *Brain* **2002**, *125*, 2036–2043. https://doi.org/10.1093/brain/awf205.

(45) Jang, H.; Arce, F. T.; Ramachandran, S.; Capone, R.; Azimova, R.; Kagan, B. L.; Nussinov, R.; Lal, R. Truncated β-Amyloid Peptide Channels Provide an Alternative Mechanism for Alzheimer's Disease and Down Syndrome. *Proc. Natl. Acad. Sci.* **2010**, *107* (14), 6538–6543. https://doi.org/10.1073/pnas.0914251107.

(46) Pike, C. J.; Overman, M. J.; Cotman, C. W. Amino-Terminal Deletions Enhance Aggregation of β-Amyloid Peptides in Vitro. *J Biol Chem* **1995**, *270* (41), 23895–23899.

(47) Liu, R.; McAllister, C.; Lyubchenko, Y.; Sierks, M. R. Residues 17-20 and 30-35 of β-Amyloid Play Critical Roles in Aggregation. *J Neurosci Res* **2004**, *75* (2), 162–171. https://doi.org/10.1002/jnr.10859.

(48) Pauwels, K.; Williams, T. L.; Morris, K. L.; Jonckheere, W.; Vandersteen, A.; Kelly, G.; Schymkowitz, J.; Rousseau, F.; Pastore, A.; Serpell, L. C.; Broersen, K. Structural Basis for Increased Toxicity of Pathological Aβ42:Aβ40 Ratios in Alzheimer Disease. *J Biol Chem* **2012**, *287* (8), 5650–5660. https://doi.org/10.1074/jbc.M111.264473.

(49) Hasegawa, K.; Yamaguchi, I.; Omata, S.; Gejyo, F.; Naiki, H. Interaction between Aβ(1-42) and Aβ(1-40) in Alzheimer's β-Amyloid Fibril Formation in Vitro. *Biochemistry* **1999**, *38* (47), 15514–15521. https://doi.org/10.1021/bi991161m.

(50) Cukalevski, R.; Yang, X.; Meisl, G.; Weininger, U.; Bernfur, K.; Frohm, B.; Knowles, T. P. J.; Linse, S. The Aβ40 and Aβ42 Peptides Self-Assemble into Separate Homomolecular Fibrils in Binary Mixtures but Cross-React during Primary Nucleation. *Chem. Sci.* **2015**, *6* (7), 4215–4233. https://doi.org/10.1039/c4sc02517b.

(51) Jan, A.; Gokce, O.; Luthi-Carter, R.; Lashuel, H. A. The Ratio of Monomeric to Aggregated Forms of Aβ40 and Aβ42 Is an Important Determinant of Amyloid-β Aggregation, Fibrillogenesis, and Toxicity. *J Biol Chem* **2008**, *283* (42), 28176–28189. https://doi.org/10.1074/jbc.M803159200.

(52) Kyte, J.; Doolittle, R. F. A Simple Method for Displaying the Hydropathic Character of a Protein. *J. Mol. Biol.* **1982**, *157* (1), 105–132. https://doi.org/10.1016/0022-2836(82)90515-0.

(53) Vadukul, D. M.; Gbajumo, O.; Marshall, K. E.; Serpell, L. C. Amyloidogenicity and Toxicity of the Reverse and Scrambled Variants of Amyloid-β 1-42. *FEBS Lett* **2017**, *591* (5), 822–830. https://doi.org/10.1002/1873-3468.12590.

(54) Zou, K.; Kim, D.; Kakio, A.; Byun, K.; Gong, J. S.; Kim, J.; Kim, M.; Sawamura, N.; Nishimoto, S. I.; Matsuzaki, K.; Lee, B.; Yanagisawa, K.; Michikawa, M. Amyloid β-Protein Aβ1-40 Protects Neurons from Damage Induced by Aβ1-42 in Culture and in Rat Brain. *J Neurochem* **2003**, *87* (3), 609–619. https://doi.org/10.1046/j.1471-4159.2003.02018.x.

(55) Dutta, S.; Foley, A. R.; Warner, C. J. A.; Zhang, X.; Rolandi, M.; Abrams, B.;

Raskatov, J. A. Suppression of Oligomer Formation and Formation of Non-Toxic Fibrils upon Addition of Mirror-Image Aβ42 to the Natural L-Enantiomer. *Angew. Chemie. - Int. Ed.* **2017**, *56* (38), 11506–11510. https://doi.org/10.1002/anie.201706279.

(56) Dutta, S.; Foley, A. R.; Warner, C. J. A.; Zhang, X.; Rolandi, M.; Abrams, B.; Raskatov, J. A. Suppression of Oligomer Formation and Formation of Non-Toxic Fibrils upon Addition of Mirror-Image Aβ42 to the Natural L-Enantiomer. *Angew. Chemie. - Int. Ed.* **2017**, *56* (38), 11506–11510. https://doi.org/10.1002/anie.201706279.

(57) Dutta, S.; Finn, T. S.; Kuhn, A. J.; Abrams, B.; Raskatov, J. A. Chirality Dependence of Amyloid Beta Cellular Uptake and a New Mechanistic Perspective. *ChemBioChem* **2019**, *20*, 1023–1026. https://doi.org/10.1002/cbic.201800708.

(58) Malmos, K. G.; Blancas-mejia, L. M.; Weber, B.; Ramirez-alvarado, M.; Naiki, H.; Otzen, D.; Gade, K.; Blancas-mejia, L. M.; Weber, B.; Ramirez-alvarado, M.; Naiki, H.; Otzen, D. ThT 101: A Primer on the Use of Thioflavin T to Investigate Amyloid Formation. **2017**, *6129*. https://doi.org/10.1080/13506129.2017.1304905.

(59) Ahmed, M.; Davis, J.; Aucoin, D.; Sato, T.; Ahuja, S.; Aimoto, S.; Elliott, J. I.; Van Nostrand, W. E.; Smith, S. O. Structural Conversion of Neurotoxic Amyloid-Beta(1-42) Oligomers to Fibrils. *Nat Struct Mol Biol* **2010**, *17* (5), 561–567. https://doi.org/10.1038/nsmb.1799.

(60) Foley, A. R.; Finn, T. S.; Kung, T.; Hatami, A.; Lee, H. W.; Jia, M.; Rolandi, M.; Raskatov, J. A. Trapping and Characterization of Nontoxic Aβ42 Aggregation Intermediates. *ACS Chem Neurosci* **2019**, *10* (8), 3880–3887. https://doi.org/10.1021/acschemneuro.9b00340.

(61) Haass, C.; Selkoe, D. J. Soluble Protein Oligomers in Neurodegeneration: Lessons from the Alzheimer's Amyloid Beta-Peptide. *Nat Rev Mol Cell Biol* **2007**, *8* (2), 101–112. https://doi.org/10.1038/nrm2101.

(62) Gong, Y.; Chang, L.; Viola, K. L.; Lacor, P. N.; Lambert, M. P.; Finch, C. E.; Krafft, G. A.; Klein, W. L. Alzheimer's Disease-Affected Brain: Presence of Oligomeric A Beta Ligands (ADDLs) Suggests a Molecular Basis for Reversible Memory Loss. *Proc. Natl. Acad. Sci. U.S.A.* **2003**, *100* (18), 10417–10422. https://doi.org/10.1073/pnas.1834302100.

(63) Szczepanik, A. M.; Rampe, D.; Ringheim, G. E. Amyloid-Beta Peptide Fragments P3 and P4 Induce pro-Inflammatory Cytokine and Chemokine Production in Vitro and in Vivo. *J Neurochem* **2001**, *77* (1), 304–317. https://doi.org/10.1046/j.1471-4159.2001.00240.x.

(64) Walsh, D. M.; Klyubin, I.; Fadeeva, J. V.; Cullen, W. K.; Anwyl, R.; Wolfe, M. S.; Rowan, M. J.; Selkoe, D. J. Naturally Secreted Oligomers of Amyloid-β Protein Potently Inhibit Hippocampal Long-Term Potentiation in Vivo. *Nature* **2002**, *416* (6880), 535–539. https://doi.org/10.1038/416535a.

(65) Hensley, K.; Carney, J. M.; Mattson, M. P.; Aksenova, M.; Harris, M.; Wu, J. F.; Floyd, R. A.; Butterfield, D. A. A Model for β-Amyloid Aggregation and

Neurotoxicity Based on Free Radical Generation by the Peptide: Relevance to Alzheimer Disease. *Proc. Natl. Acad. Sci. U.S.A.* **1994**, *91* (8), 3270–3274. https://doi.org/10.1073/pnas.91.8.3270.

(66) Shearman, M. S.; Ragan, C. I.; Iversen, L. L. Inhibition of PC12 Cell Redox Activity Is a Specific, Early Indicator of the Mechanism of β-Amyloid-Mediated Cell Death. *Proc. Natl. Acad. Sci. U.S.A.* **1994**, *91* (4), 1470–1474. https://doi.org/10.1073/pnas.91.4.1470.

(67) Behl, C.; Davis, J. B.; Lesley, R.; Schubert, D. Hydrogen Peroxide Mediates Amyloid β Protein Toxicity. *Cell* **1994**, *77* (6), 817–827. https://doi.org/10.1016/0092-8674(94)90131-7.

(68) Mattson, M. P.; Goodman, Y. Different Amyloidogenic Peptides Share a Similar Mechanism of Neurotoxicity Involving Reactive Oxygen Species and Calcium. *Brain Res* **1995**, *676* (1), 219–224. https://doi.org/10.1016/0006-8993(95)00148-J.

(69) Oguchi, T.; Ono, R.; Tsuji, M.; Shozawa, H.; Somei, M.; Inagaki, M.; Mori, Y.; Yasumoto, T.; Ono, K.; Kiuchi, Y. Cilostazol Suppresses Aß-Induced Neurotoxicity in SH-SY5Y Cells through Inhibition of Oxidative Stress and MAPK Signaling Pathway. *Front. Aging Neurosci.* **2017**, *9* (OCT), 1–12. https://doi.org/10.3389/fnagi.2017.00337.

(70) Jin, S.; Kedia, N.; Illes-Toth, E.; Haralampiev, I.; Prisner, S.; Herrmann, A.; Wanker, E. E.; Bieschke, J. Amyloid-β(1- 42) Aggregation Initiates Its Cellular Uptake and Cytotoxicity. *J Biol Chem* **2016**, *291* (37), 19590–19606.

https://doi.org/10.1074/jbc.M115.691840.

(71) LaFerla, F. M.; Green, K. N.; Oddo, S. Intracellular Amyloid-β in Alzheimer's Disease. *Nat Rev Neurosci* **2007**, *8* (7), 499–509. https://doi.org/10.1038/nrn2168.

(72) Foley, A. R.; Roseman, G. P.; Chan, K.; Smart, A.; Finn, T. S.; Yang, K.; Scott Lokey, R.; Millhauser, G. L.; Raskatov, J. A. Evidence for Aggregation-Independent, PrPC-Mediated Aβ Cellular Internalization. *Proc. Natl. Acad. Sci. U.S.A.* **2020**, *117* (46), 28625–28631. https://doi.org/10.1073/pnas.2009238117.

(73) Warner, C. J. A.; Dutta, S.; Foley, A. R.; Raskatov, J. A. Introduction of D-Glutamate at a Critical Residue of Aβ42 Stabilizes a Pre-Fibrillary Aggregate with Enhanced Toxicity. *Chem - A Eur J* **2016**, *22* (34), 11967–11970.

(74) AU - Warner, C. J. A.; AU - Dutta, S.; AU - Foley, A. R.; AU - Raskatov, J. A. A Tailored HPLC Purification Protocol That Yields High-Purity Amyloid Beta 42 and Amyloid Beta 40 Peptides, Capable of Oligomer Formation. *JoVE* **2017**, No. 121, e55482. https://doi.org/doi:10.3791/55482.

(75) Anthis, N. J.; Clore, G. M. Sequence-Specific Determination of Protein and Peptide Concentrations by Absorbance at 205 Nm. *Protein Sci* **2013**, *22* (6), 851–858. https://doi.org/10.1002/pro.2253.

(76) Dutta, S.; Finn, T. S.; Kuhn, A. J.; Abrams, B.; Raskatov, J. A. Chirality Dependence of Amyloid β Cellular Uptake and a New Mechanistic Perspective. *ChemBioChem* **2019**, *20*, 1–5.

https://doi.org/10.1002/cbic.201800708.

(77) Pujadas, L.; Rossi, D.; Andrés, R.; Teixeira, C. M.; Serra-Vidal, B.; Parcerisas, A.; Maldonado, R.; Giralt, E.; Carulla, N.; Soriano, E. Reelin Delays Amyloid-Beta Fibril Formation and Rescues Cognitive Deficits in a Model of Alzheimer's Disease. *Nat Commun* **2014**, *5*. https://doi.org/10.1038/ncomms4443.

(78) Lurs, T.; Ritter, C.; Adrian, M.; Riek-loher, D.; Bohrmann, B.; Do, H.; Schubert, D.; Riek, R. 3D Structure of Alzheimer's Amyloid- Beta (1 – 42) Fibrils. *Proc. Natl. Acad. Sci.* **2005**, *102* (48), 17342–17347.

(79) Schmidt, M.; Rohou, A.; Lasker, K.; Yadav, J. K.; Schiene-Fischer, C.; Fändrich, M.; Grigorieff, N. Peptide Dimer Structure in an Aβ(1-42) Fibril Visualized with Cryo-EM. *Proc. Natl. Acad. Sci. U.S.A.* **2015**, *112* (38), 11858–11863. https://doi.org/10.1073/pnas.1503455112.

(80) Gremer, L.; Scholzel, D.; Schenk, C.; Reinartz, E.; Labahn, J.; Ravelli, R. B. G.; Tusche, M.; Lopez-Iglesias, C.; Hoyer, W.; Heise, H.; Willbold, D.; Schroder, G. F. Fibril Structure of Amyloid Beta 1-42 by Cryoelectron Microscopy. *Science* **2017**, *358* (6359), 116–119.

(81) Wälti, M. A.; Ravotti, F.; Arai, H.; Glabe, C. G.; Wall, J. S.; Böckmann, A.; Güntert, P.; Meier, B. H.; Riek, R. Atomic-Resolution Structure of a Disease-Relevant Aβ(1–42) Amyloid Fibril. *Proc. Natl. Acad. Sci.* **2016**, *113* (34), E4976–E4984. https://doi.org/10.1073/pnas.1600749113.

(82) Xiao, Y.; Ma, B.; McElheny, D.; Parthasarathy, S.; Long, F.; Hoshi, M.;

Nussinov, R.; Ishii, Y. Aβ(1-42) Fibril Structure Illuminates Self-Recognition and Replication of Amyloid in Alzheimer's Disease. *Nat Struct Mol Biol* **2015**, *22* (6), 499–505. https://doi.org/10.1038/nsmb.2991.

(83) Colvin, M. T.; Silvers, R.; Ni, Q. Z.; Can, T. V.; Sergeyev, I.; Rosay, M.; Donovan, K. J.; Michael, B.; Wall, J.; Linse, S.; Griffin, R. G. Atomic Resolution Structure of Monomorphic Aβ42 Amyloid Fibrils. *J Am Chem Soc* **2016**, *138* (30), 9663–9674. https://doi.org/10.1021/jacs.6b05129.

(84) Kuhn, A. J.; Raskatov, J. A. *Using Mirror-Image Peptides to Enhance Robustness and Reproducibility in Studying the Amyloid β-Protein*, 1st ed.; Elsevier Inc., 2019; Vol. 168. https://doi.org/10.1016/bs.pmbts.2019.05.010.

(85) Foley, A. R.; Raskatov, J. A. Assessing Reproducibility in Amyloid β Research: Impact of Aβ Sources on Experimental Outcomes. *ChemBioChem* **2020**, *21* (17), 2425–2430. https://doi.org/10.1002/cbic.202000125.

(86) Roychaudhuri, R.; Yang, M.; Hoshi, M. M.; Teplow, D. B. Amyloid-β Protein Assembly and Alzheimer Disease. *J Biol Chem* **2009**, *284* (8), 4749–4753. https://doi.org/10.1074/jbc.R800036200.

(87) Lesné, S.; Koh, M. T.; Kotilinek, L.; Kayed, R.; Glabe, C. G.; Yang, A.; Gallagher, M.; Ashe, K. H. A Specific Amyloid-β Protein Assembly in the Brain Impairs Memory. *Nature* **2006**, *440* (7082), 352–357. https://doi.org/10.1038/nature04533.

(88) Soto, C.; Pritzkow, S. Protein Misfolding, Aggregation, and Conformational Strains in Neurodegenerative Diseases. *Nat Neurosci* **2018**, *21* (10), 1332–

1340. https://doi.org/10.1038/s41593-018-0235-9.

(89) Schnabel, J. Little Proteins, Big Clues. *Nature* **2011**, *475*, S12–S14.

(90) Dutta, S.; Foley, A. R.; Kuhn, A. J.; Abrams, B.; Lee, H. W.; Raskatov, J. A. New Insights into Differential Aggregation of Enantiomerically Pure and Racemic Aβ40 Systems. *Pept. Sci.* **2019**, *111* (6), e24139. https://doi.org/10.1002/pep2.24139.

(91) Pauling, L.; Corey, R. B. Two Rippled-Sheet Confirgurations of Polypeptide Chains, and a Note about the Pleated Sheets. *Proc. Natl. Acad. Sci. U.S.A.* **1953**, *39* (4), 253–256.

(92) Guo, C.; Luo, Y.; Zhou, R.; Wei, G. Triphenylalanine Peptides Self-Assemble into Nanospheres and Nanorods That Are Different from the Nanovesicles and Nanotubes Formed by Diphenylalanine Peptides. *Nanoscale* **2014**, *6* (5), 2800–2811. https://doi.org/10.1039/c3nr02505e.

Chapter 4. Tools to evade the challenges of studying intrinsically disordered proteins

This chapter contains text and figures from the following manuscripts: Kuhn, A. J.; Raskatov. J. A. A tailored purification and treatment protocol for the hydrophobic, aggregation-prone, p3 peptide. **In preparation.;** Roychaudhuri, R.; Yang, M.; Hoshi, M. M.; Teplow, D. B. Amyloid-β Protein Assembly and Alzheimer Disease. *J Biol Chem* **2009.;** Kuhn, A. J.; Raskatov, J. A. *Prog. Mol. Biol. Transl. Sci.* **2019**.; Dutta, S.; Foley, A. R.; Kuhn, A. J.; Abrams, B.; Lee, H-W.; Raskatov, J. A. *Pep. Sci..* **2019**.; Dutta, S.; Finn, T. S.; Kuhn, A. J.; Abrams, B.; Raskatov, J. A. *ChemBioChem.* **2019**, 20, 1023-1026. See appendix for RightsLinks.

4.1 Introduction

Aggregation-prone IDPs, such as Aβ, are remarkably difficult to study in a methodical fashion, and consequently, findings across the literature differ widely. Aggregates formed by Aβ exhibit dramatic structural variability, and homogenous solutions are nearly impossible to maintain, even with careful filtration and pre-treatment methods. For example, the time-required for ~20μM Aβ42 to form fibrils, as indicated by the Thioflavin T (ThT) assay, has can range from minutes[56] to days.[77] Moreover, many of the high-resolution fibrillar structures of Aβ, such as 2beg,[78] 5aef,[79] 5oqv,[80] 2nao,[81] 2mxu,[82] and 5kk3,[83] reveal conformational inconsistencies, such as the presence or absence of the S-shaped fold, and the extent of involvement of the N-terminus in structural stability. The biophysical and biological properties of Aβ differ greatly upon small perturbations, expression of recombinant DNA vs solid-phase peptide synthesis, differences in purification protocols, pH and identity of pre-treatment agents, filtration methods, and presence of impurities.[84,85] Moreover, even under consistent preparation conditions, there is still heterogeneity of aggregates at any given timepoint along the aggregation profile. The broad term, “fibril” can refer to a

protofibril or mature fibril, Aβ*56, and "oligomer" can refer to annulus, dodecamer, amylospheroid, or paranucleus (Figure 13).[86–89]

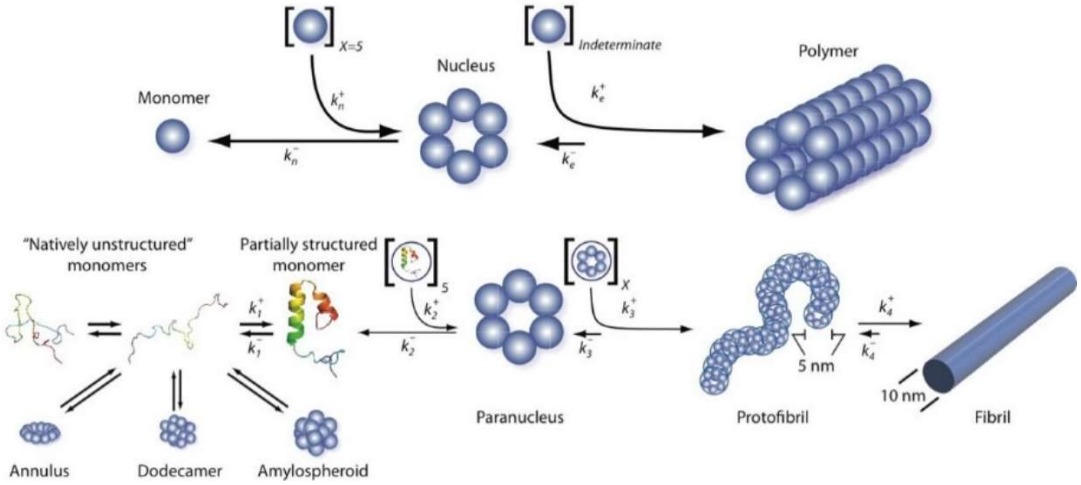

Figure 13. Nucleation-dependent, self-assembly of Aβ. *Reprinted from:* Roychaudhuri, R.; Yang, M.; Hoshi, M. M.; Teplow, D. B. Amyloid-β Protein Assembly and Alzheimer Disease. *J Biol Chem* **2009**.[86]

Another challenge in producing pure Aβ and related peptides is the significant hydrophobicity (Figure 7A). Aβ has two long hydrophobic sections, resulting in a net positive GRAVVY score (0.205 for Aβ42 and 0.058 for Aβ40) and p3 is almost entirely hydrophobic, with a GRAVVY score range of 1.313-1.455 (Figure 7B).

To improve reproducibility, and combat the specific challenges of working with hydrophobic, aggregation-prone, intrinsically disordered Aβ and p3, the Raskatov

laboratory has implemented a tailored HPLC purification protocol to yield >95% pure peptides.[16] I have revised this protocol for use with the p3 peptide (Figure 14).

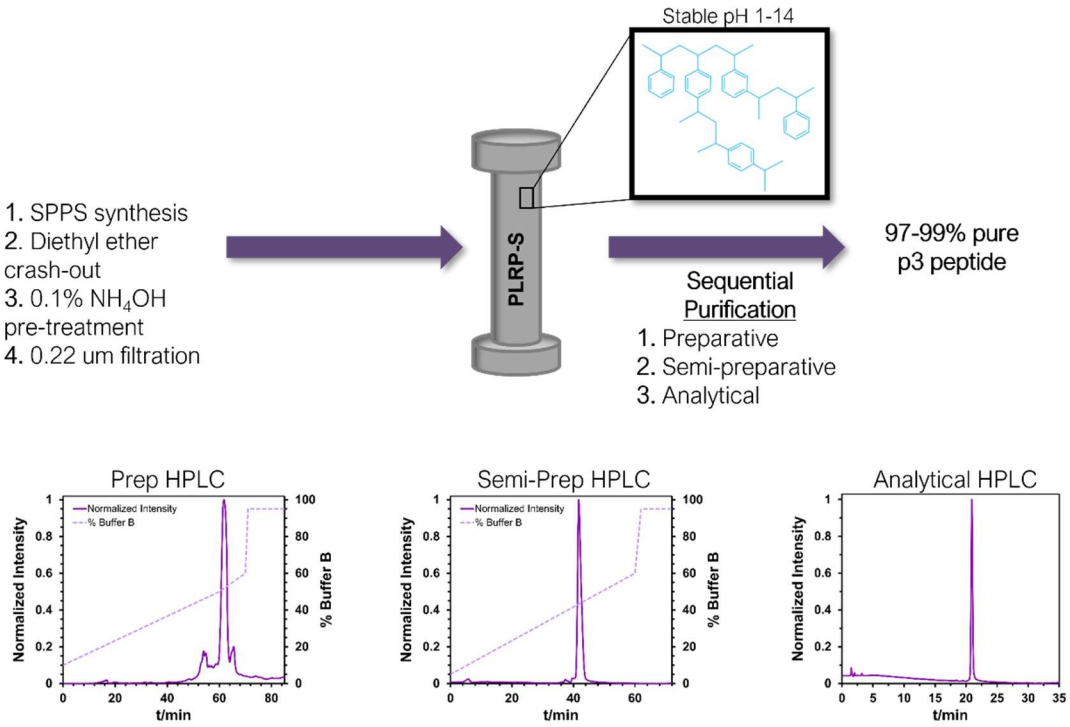

Figure 14. Multi-step purification protocol of the p3 peptide.

Another productive strategy for reducing batch-to-batch variation in Aβ and related peptides is to employ the all-D enantiomer of any given peptide as a control in biophysical and biological assays. Enantiomers have the same structure, bond lengths, bond angles, relative energies, etc…, but they are non-superimposable mirror images. Thus, biophysical assays such as ThT, TAMRA-quenching, and PICUP should all yield identical results for All-L- and All-D-Aβ, assuming that purities are matched. Should this not be the case, a reevaluation of peptide preparation, purification, and dissolution is necessary. Under these circumstances, the following protocols may be implemented:

peptides are repurified and reassessed for the presence of pre-aggregates, resin and amino acid qualities are assessed, and buffers are remade. This overall approach is more explicitly explained in the reprinted manuscript at the end of this chapter (Kuhn, A. J.; Raskatov, J. A. *Prog. Mol. Biol. Transl. Sci.* **2019**).

Beyond enhancing reproducibility, chirality also allowed us to probe the mechanism of cellular internalization of Aβ. By comparing the uptake of TAMRA-L-Aβ(40 and 42) vs. TAMRA-D-Aβ(40 and 42) in SH-SY5Y, PC12 and rat primary hippocampal neurons, we observed a 5-fold preference for the L stereoisomer over the D. Presumably, receptor binding is stereospecific. The finding that uptake is stereospecific may indicate that Aβ uptake is primarily receptor-mediated, with only minor contributions from passive, non-stereospecific mechanisms. This rationale is more explicitly detailed in the manuscript reprinted at the end of this chapter (Dutta, S.; Finn, T. S.; Kuhn, A. J.; Abrams, B.; Raskatov, R. A. *ChemBioChem.* **2019**).

All-D-enantiomers are also incredibly useful for what our lab has dubbed, "Chiral Inactivation", a method for bypassing toxic intermediates and expediting non-toxic fibril formation.[56,90] Specifically, we found that a racemic mixture of L- and D-Aβ40 accelerated fibril formation, bypassing the characteristic lag phase typically observed via ThT. The resultant racemic fibrils exhibited distinct differences, such as lack of twisting, shorter length, and larger width. We were able to observe this phenomenon by ^{1}H-NMR, in which immediate signal suppression and broadening was observed for racemic Aβ40, indicative of precipitation of fibrils out of aqueous solution. In contrast, signal intensity for enantiopure Aβ40 remained constant. Our

findings are explained in more detail in the manuscript reprinted at the end of this chapter (Dutta, S.; Foley, A. R.; Kuhn, A. J.; Lee, H-W.; Abrams, B.; Raskatov, J. A. *Pep. Sci.* **2019**).

In 1953, Pauling and Corey theorized that racemic peptide mixtures could form what they referred to as "rippled sheets".[91] Given the morphological differences we observed between racemic and enantiopure fibrils,[56,90] we suspected that racemic fibrils may have rippled sheet elements. Since ascertaining structural information from IDPs is exceptionally challenging, we first employed a relevant model system: the FFF and fff peptides. Previous work has demonstrated that FF is the smallest portion of Aβ capable of fibril formation,[30] but we were unable to grow sufficiently large FF crystals, and instead opted for the longer FFF peptide. FFF has been shown to spontaneously assemble into solid nanospheres and nanorods with substantial β-sheet character, making it an interesting candidate from the standpoint of rippled sheet design.[92] With this approach, we observed a high-resolution crystal structure, in which (L,L,L)-triphenylalanine and (D,D,D)-triphenylalanine formed dimeric antiparallel rippled sheets. The sheets packed into herringbone layer structures, which were in excellent agreement with the theoretical predictions by Pauling and Corey. A subsequent mining of the PDB identified three orphaned rippled sheets among racemic protein crystal structures, in which the authors did not recognize the structural element.

4.2 Reprint

Reprinted with permission from (*Prog. Mol. Biol. Transl. Sci.* **2019**, 168 (1), 57-67). Elsevier. License Number 5183211383213. RightsLink in Appendix.

Using mirror-image peptides to enhance robustness and reproducibility in studying the amyloid β-protein

Ariel J. Kuhn, Jevgenij A. Raskatov*
Department of Chemistry and Biochemistry, University of California, Santa Cruz, CA, United States
*Corresponding author: e-mail address: jraskato@ucsc.edu

Contents

1. Introduction 1
2. Intrinsically disordered proteins and the challenge in studying their kinetics 2
3. Biophysical characterization methods of the amyloid-β protein 3
4. Potential sources of deviations from trends in fibril formation assays 4
5. Mirror image Aβ to increase rigor in assessing quality of peptide preparations 5
6. Kinetic timescale inconsistencies: Aβ40 vs. Aβ42 8
7. Conclusion 9
References 9

Abstract

Alzheimer's disease, the most common form of dementia, is a devastating disease that affects over 44 million people worldwide. One etiological agent of Alzheimer's, the amyloid β-protein (Aβ), is an aggregation-prone, intrinsically disordered peptide that can form a wide variety of aggregates. The pathways by which Aβ aggregates in order to exert its toxicity, referred to as the Amyloid Cascade, remains largely elusive despite substantial deconvolution efforts. Preparing high-quality material that exhibits reproducible biophysical characteristics has proven challenging. Herein, we propose that mirror-image peptides can be used to rigorously control Aβ preparation quality.

1. Introduction

The pathology of Alzheimer's disease is characterized, in part, by extracellular Aβ deposits, commonly referred to as plaques, as well as intracellular tau protein tangles.[1,2] The inherently disordered, aggregation-prone Aβ peptide remains an extremely challenging system to work with. One of

Progress in Molecular Biology and Translational Science
ISSN 1877-1173
https://doi.org/10.1016/bs.pmbts.2019.05.010

© 2019 Elsevier Inc.
All rights reserved.

the substantial challenges is the peptide's propensity toward substantial variance of aggregation properties. Some of this variance is intrinsic to the synthetic history of the peptide synthesis.[3] In addition to that, small impurities, such as those present in buffers and reagents needed to conduct the various assays, may induce pronounced changes in aggregation.[4,5]

Here, we propose that using the natural ("all-L" or "L") stereoisomer side-by-side with its mirror-image ("all-D" or "D") counterpart can assist in controlling for the quality of Aβ preparations. As can be derived from basic stereochemical arguments, enantiomers are expected to display identical properties if studied in an otherwise achiral environment. Deviations in aggregation properties of the enantiomers can be considered a strong indication that there are issues somewhere in the synthesis ➔ purification ➔ biophysical characterization pipeline. Recommendations are made on how to use this approach and what parameters to troubleshoot.

2. Intrinsically disordered proteins and the challenge in studying their kinetics

The aggregation pathway of Aβ is often depicted as a simple linear schematic, in which monomeric Aβ forms soluble, intermediate oligomers, and eventually, insoluble fibrils with parallel β-sheet character (Fig. 1A).[6,7] In more detailed representations, other intermediate species, such as protofibrils, are depicted as additional species in the step-wise formation of fibrils. Aβ is an intrinsically disordered protein (IDP), and can, therefore, exist in a vast number of potentially aggregation-prone conformations.[8] The energy landscape of its folding exhibits a multitude of local minima that can act as kinetic traps for different intermediate folded states.[9,10] Thus, amyloid deposits often exist as mixtures of Aβ aggregates of varying structures and sizes.[11] Even the late stage fibrils can vary widely in width, length, branching, and twisting.[11–13] The remarkable ability of the peptide to adopt distinct foldameric states is exemplified by the structural variability observed between the six recently published structures of Aβ fibrils (2beg,[14] 5aef,[15] 5oqv,[16] 2nao,[17] 2mxu,[18] and 5kk3[19]). Certain aspects, such as the twist of individual Aβ peptides along the z-axis (which arises as a consequence of cross-β hydrogen bonding) and the structural disorder observed within the N-terminal flexible domain (residues 1–16) are observed in all of these structures.[14–19] However, large discrepancies are also noted, such as the existence of the S-shaped fold in some but not all structures,[16–19] as well as smaller topological differences. This variability continues to pose a challenge in studying the folding mechanism of such a peptide.

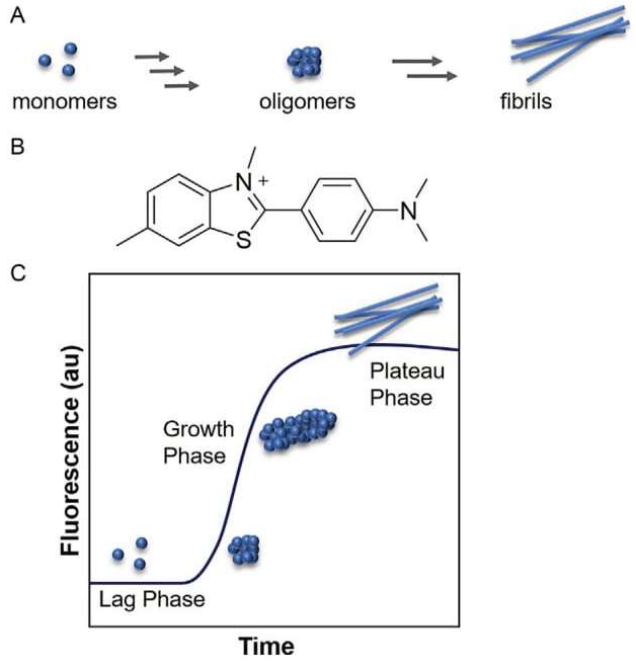

Fig. 1 (A) Simplified linear schematic of the Amyloid Cascade Pathway. (B) Molecular structure of Thioflavin t (ThT). (C) Schematic diagram of a representative curve one would expect to obtain from a ThT Fibril Formation Assay.

3. Biophysical characterization methods of the amyloid-β protein

To tackle the complex folding of Aβ, the field has adopted a collection of techniques, ranging from fluorescent probes and microscopy to gel electrophoresis. A frequently used probe for studying fibril formation kinetics of Aβ is the fluorophore, Thioflavin T (ThT) (Fig. 1B). Upon binding the cross-β sheets of Aβ fibrils, ThT exhibits a red shift of its fluorescence intensity that scales with concentration of fibrils in solution (Fig. 1C).[4,20,21] However, ThT has been suggested to have a multitude of binding modes for Aβ (for a detailed review, see Biancalana; Koide, 2010).[22] In fact, it is worth noting here that the existence of cross-β does not appear to be a strict pre-requisite. Landau and coworkers recently found that ThT can bind the cross-α structure of modulin PSMα3 and exhibit the characteristic fluorescence increase.[23] The length of the lag phase varies for different isoforms of Aβ and is considered to be the time required for nucleation and initial formation of β-sheets to occur, enabling the nucleated growth mechanism.[12,24,25]

Another amyloid-specific dye, Congo Red, which exhibits birefringence under polarized light when bound to the β-sheets of Aβ, is often implemented for studying the assembly states of Aβ.[26] However, this assay requires a polarized light microscope and is generally considered to be more laborious than the ThT assay.[22] For studying the intermediate species formed during aggregation, many have adopted photo-induced cross-linking of unmodified proteins (PICUP).[27,28] These chemical modifications allow for quantitation of transient, metastable species.

4. Potential sources of deviations from trends in fibril formation assays

When conducting biophysical studies on Aβ, it is crucial that one first assess peptide quality to ensure that results are consistent and reliable. Aβ can be either synthesized by solid phase peptide synthesis or with expressed via recombinant DNA. Peptides from different batches and sources have been reported to demonstrate differing biophysical characteristics.[29–31] When isolating pure peptide via either of these methods, extreme care must be taken because any impurity may affect the aggregation properties of Aβ. More importantly, impurities can affect different isoforms and other variants of the peptide in ways that are unique to those peptides and therefore cannot be analyzed in a systematic fashion. Thus, if Aβ is purchased, it is critical to validate peptide quality with mass spectrometry and HPLC.

When preparing peptides synthetically, common impurities that may arise include truncations, fragments, side products from cleaving reagents, amino acid epimerization (sometimes erroneously referred to as racemization), and methionine oxidation.[5] For example, the use of trifluoroacetic acid (TFA) for cleaving and/or purification can form TFA salts with Aβ, resulting in concentration calculation errors and overall effects on fibrilization.[32] The other aforementioned impurities, such as fragments or truncations from insufficient coupling procedures, may aggregate at a different rate or lose their aggregation propensity completely, affecting the overall kinetics.[33] In addition, since fibrilization is thought to be a nucleation-based process, amyloidogenic proteins are extremely sensitive to seeding effects.[24,34] It has been shown that oligomers, protofibrils and fibrils can promote Aβ fibrillization even at very low concentrations.[24,35] It is thus critical to eliminate preformed aggregates from solution prior to conducting the experiment; this can be done with base pre-treatment, ultrafiltration and preparing solutions at low temperature (4 °C).[3] Pretreatment with base

and/or de-aggregating agents, such as hexafluoroisopropanol (HFIP) and dimethylsulfoxide (DMSO), can also be used in low concentrations to reduce preformed species. However, it is important to note that low-weight oligomers can still exist under these described conditions. In addition, Leone and coworkers demonstrated that ThT promotes the fibrillization of Aβ40 by affecting solvent−peptide interactions and stabilizing more ordered β-sheet conformation.[36] Another example of this is the difference seen in ThT kinetics and morphology of Aβ allowed to aggregate quiescently vs. with shaking. Continuous shaking has been shown to dramatically speed up ThT binding, but also to create fibrils with qualitatively different morphology.[13] Fibril agitation can also promote shear effects, which alters the fibril formation kinetics and thus the morphology.[25]

ThT itself may also have impurities and which may affect kinetics of Aβ aggregation in ways that are hard to predict for different isoforms.[5] For this reason, recrystallization of commercial ThT is highly recommended, which leaves only 0.5% proton-containing impurities.[5,36,37] The TAMRA (tetramethylrhodamine) quenching assay, introduced by Garai and Frieden,[38] offers a simplified assay in terms of the number of reagents, as it does not require ThT. The N-terminus of Aβ is labeled with TAMRA, and upon aggregation, fluorescence is quenched. This assay offers an additional standard for comparison alongside the ThT assay.[38,39]

5. Mirror image Aβ to increase rigor in assessing quality of peptide preparations

We were introduced to the challenge of producing both enantiomers of Aβ with otherwise identical biophysical properties when we thought to use mirror-image Aβ to probe the mechanism of cellular uptake,[39] Enantiomers are (chiral) pairs of molecules that are non-superimposable mirror images of one another. Enantiomers are constitutionally identical, i.e., they have identical bond lengths and angles and relative energies on the chemical scale, but all of their dihedral angles are inverted. Because energy is a scalar and not a vector, this inversion produces potential energy surfaces that are exact mirror images of one another with both local minima and activation barriers connecting those minima exhibiting identical relative energies. This property is exemplified utilizing the protonated form of the amino acid histidine, as shown in Fig. 2. One can imagine that the imidazole ring of histidine is held in place while the dihedral angle (1-2-3-4) (Fig. 2B and D) is rotated incrementally by 1° per step for a total of 360° for each of the

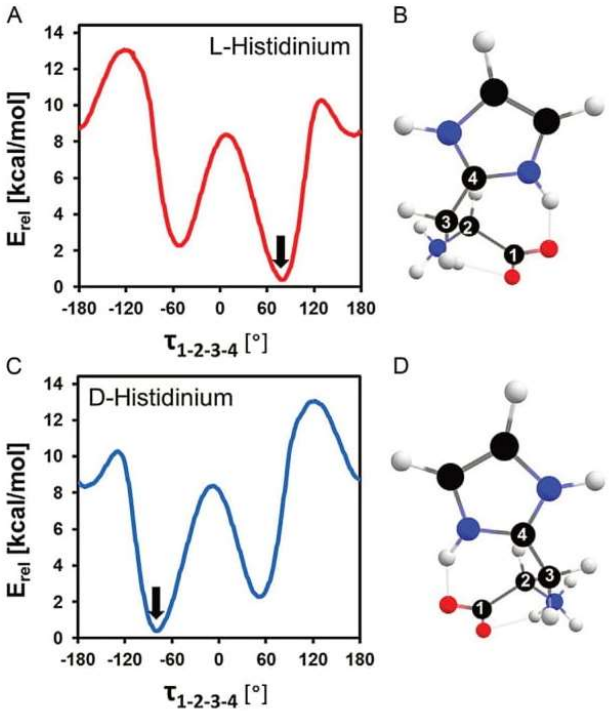

Fig. 2 L- or D-Histidinium (i.e., protonated Histidine) was subjected to a set of restricted geometry optimizations (Gaussian 09, M062X/6-31G*, solvent contribution (water)) modeled through the polarizable continuum model. For each enantiomer, 360 torsionally restricted calculations were conducted, in which the dihedral angle τ (1-2-3-4) was incremented by 1° per step and all other coordinates relaxed for 10 steps per increment, yielding a total of 3600 optimization steps per enantiomer. The mirror image nature of the torsional potential energy surfaces of L- and D-Histidinium has no impact on the relative energies of the three minima, while the absolute values of the dihedral angles are inverted between the two enantiomers. *Minima.* L-Histidine: 0.0 kcal/mol (+79.2°); +1.9 kcal/mol (−51.8°); +7.95 (+171.2°) D-Histidine: 0.0 kcal/mol (−79.2°); +1.9 kcal/mol (51.8°); +7.95 kcal/mol (−171.2°).

enantiomers. This rotation produces two exact mirror image relative energy plots (Fig. 2A and C) for both enantiomers of histidine. This phenomenon is universal for all chiral molecules and, as such, holds true for the L- and D- enantiomers of Aβ.

While exploring the differing cell uptake of the two enantiomers of Aβ, we were frequently confronted with drastically different ThT curves for the two enantiomers (Fig. 3). We expected to obtain the ThT fluorescence curves depicted in Fig. 3A and B, as the trends are consistent between the two mirror-image peptides and with previous experiments. However, when we collected the ThT fluorescence curve depicted in Fig. 3D, with an 18-h

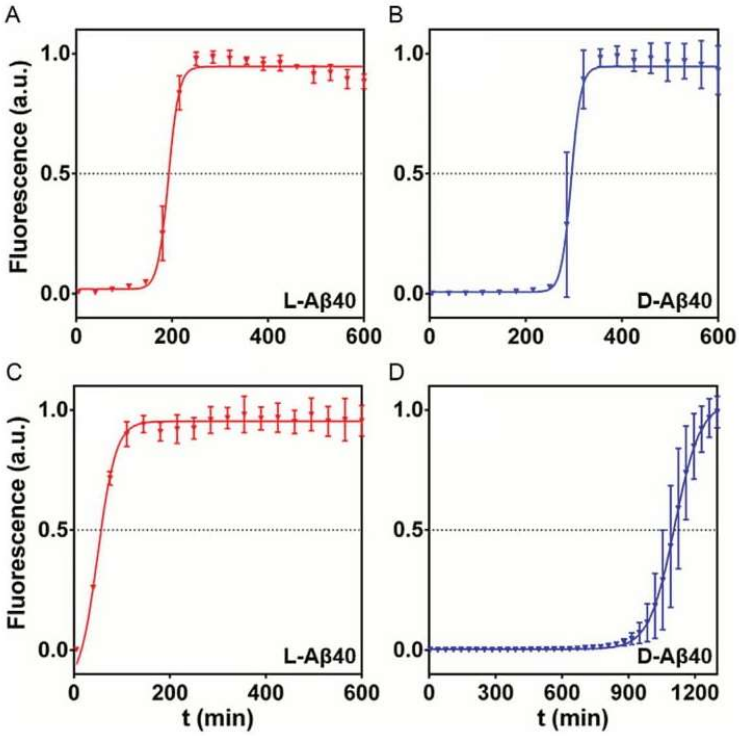

Fig. 3 ThT fibril formation assays of (A) L-Aβ40, (B) D-Aβ40 (top quality preparations), (C) L-Aβ40, and (D) D-Aβ40 (lower quality preparations). All peptides (20 μM) were freshly dissolved in 20 mM NaOH, and diluted in PBS (pH 7.4) containing ThT (20 μM). All peptides used were at purities above 97%. All ThT experiments were conducted in black, clear bottom 96-well plates with shaking in a Molecular Device Gemini EM fluorescence plate reader ($\lambda_{ex} = 444$ nm, $\lambda_{em} = 485$ nm) at 37 °C. Readings were collected every 5 min with 5 s shaking before reading and 295 s shaking in between readings. Each data point is an average of four replicates with error bars representing the standard deviations.

delay in fibrilization onset, it was clear that the corresponding batch of Aβ was not top quality, despite the 97% purity exhibited by HPLC and Mass Spectrometry. Similar conclusions were drawn upon observation of the curve depicted in Fig. 3C, with a shorter than expected lag time of approximately 52 min. When a deviation of this nature would arise, it would prompt us to reassess the synthetic, purification and dissolution steps for sources of potential impurities. This eventually led to the implementation of D-Aβ for our experiments as a standard for comparison. By conducting such experiments on Aβ alongside with its mirror image counterpart, we have been able to carefully assess peptide quality and identify the presence of minor impurities. If deviations arise, we would proceed by re-making buffers, changing the source of milliQ water (certain impurities are invisible

by standard spectroscopic techniques; metal ions and other salts, small particles, such as dust, as well as traces of organic solvent are some examples), amino acid provider and resin manufacturer. In our experience, double-purification by HPLC to a purity of >97% was found to enhance reproducibility of biophysical assays.

Given the above, through comparison with the chiral variant of Aβ, one can implement a new standard to ensure quality of preparations and evaluate the effectiveness of aggregation modulators. Aggregation modulators, those that alter or inhibit fibril formation of Aβ,[40] can be incubated with both L- and D-Aβ for comparison. It is expected that the $\Delta t_{1/2}$ (difference in $t_{1/2}$ between Aβ alone vs. Aβ with the inhibitor) should be identical for both enantiomers. If the modulators are chiral, both enantiomers will need to be produced and incubated with their corresponding Aβ-enantiomer. If the modulators are achiral, the same molecule can be introduced to both peptide enantiomers. Our approach may have a degree of generality, as other IDPs capable of binding ThT, such as familial mutants of Aβ, amylin, as well as some non-canonical ThT binders (e.g., PSMα3[23]), can also be studied alongside their respective enantiomers to produce higher rigor in assessing quality of preparations.

6. Kinetic timescale inconsistencies: Aβ40 vs. Aβ42

As previously mentioned, Aβ is an IDP, and thus has a complex and multifaceted energy landscape. Thus, while the folding trajectory depicted in Fig. 1A is often referred to as the "pathway" of Aβ folding, it simply does not account for the myriad of energetically accessible folded states of Aβ.[41] One could even say that there is no true "pathway," but rather, that there are a handful of commonly studied fibrillar structures of Aβ and their respective, proposed mechanisms of formation.

In our lab, we have obtained consistent ThT kinetic curves for Aβ42 with a $t_{1/2}$ of approximately 20 min.[39,42,43] However, the Aβ40 system has proved much more inconsistent. In fact, as shown in Fig. 3, two preparations of the same peptide can result in drastically different ThT fluorescence curves. We have obtained $t_{1/2}$ values ranging from 1 to 18 h with Aβ40 exhibiting >97% purity, while obtaining consistent lag times for Aβ42.[39,42,43] This is likely a direct consequence of the slower aggregation kinetics of Aβ40, allowing for the formation more off-pathway species that ThT may not readily bind. Other possible contributing factors are the suggested differences in mechanisms of fibrilization between Aβ40 and

Aβ42.[44] For example, it has been suggested that the aggregation of Aβ42 is seeded by dodecamer protofibrils, while Aβ40 is not.[45]

Mirror-image Aβ can be introduced as a standard when assessing Aβ40 fibrilization to address these inconsistencies. Aβ40 vs. Aβ42: $t_{1/2}$ values are trends in a certain direction. If $t_{1/2}$ (Aβ40) is divided by $t_{1/2}$ (Aβ42), the number obtained may and will likely vary between labs, preparations and systems employed to perform the assays. However, when L-Aβ40 is compared to D-Aβ40 (or L-Aβ42 vs. D-Aβ42), the $t_{1/2}$ of L-Aβ40 divided by that of D-Aβ40 must be 1. Absolute values will be representative of the instrumentation used for the experiment and will likely vary between labs as a consequence.

7. Conclusion

Care must be taken when characterizing the complex aggregation properties of the IDP, Aβ. To ensure reproducibility, it is important to assess peptide and reagent quality from synthesis to reconstitution. By analyzing the all-L stereoisomer side-by-side with its mirror-image D-counterpart, one can evaluate the quality of Aβ preparations. Deviations in kinetic trends indicate the presence of minor impurities from solid phase peptide synthesis, purification, and/or characterization protocols. Additionally, other methods, such as the TAMRA-quenching assay, can also be implemented in conjunction with traditional methods.

References

1. Querfurth HW, LaFerla FM. Alzheimer's disease. *N Engl J Med*. 2010;3628(4):329–344. https://doi.org/10.1136/bmj.b158.
2. Selkoe DJ. Alzheimer's disease: genes, proteins, and therapy. *Physiol Rev*. 2001; 81(2):741–766.
3. Teplow DB. Preparation of amyloid-β protein for structural and functional studies. In: *Amyloid, Prions, and Other Protein Aggregates*. 2006:20–33. vol 413. https://doi.org/10.1016/S0076-6879(06)13002-5.
4. Malmos KG, Blancas-mejia LM, Weber B, et al. ThT 101: a primer on the use of thioflavin T to investigate amyloid formation. 2017:6129:1–16. https://doi.org/10.1080/13506129.2017.1304905.
5. Groenning M. Binding mode of thioflavin T and other molecular probes in the context of amyloid fibrils-current status. *J Chem Biol*. 2010;3(1):1–18. https://doi.org/10.1007/s12154-009-0027-5.
6. Arosio P, Knowles TPJ, Linse S. On the lag phase in amyloid fibril formation. *Phys Chem Chem Phys*. 2015;17:7606–7618. https://doi.org/10.1039/c4cp05563b.
7. Karran E, Mercken M, De Strooper B. The amyloid cascade hypothesis for Alzheimer's disease: an appraisal for the development of therapeutics. *Nat Rev Drug Discov*. 2011;10(9):698–712. https://doi.org/10.1038/nrd3505.

8. Chiti F, Dobson CM. Protein misfolding, functional amyloid, and human disease. *Annu Rev Biochem.* 2006;75(1):333–366. https://doi.org/10.1146/annurev.biochem.75.101304.123901.
9. Jahn TR, Radford SE. The Yin and Yang of protein folding. *FEBS J.* 2005;272:5962–5970. https://doi.org/10.1111/j.1742-4658.2005.05021.x.
10. Burger VM, Gurry T, Stultz CM. Intrinsically disordered proteins: where computation meets experiment. *Polymers (Basel).* 2014;6:2684–2719. https://doi.org/10.3390/polym6102684.
11. Fändrich M, Meinhardt J, Grigorieff N. Structural polymorphism of Alzheimer Aβ and other amyloid fibrils. *Prion.* 2009;3(2):89–93. https://doi.org/10.4161/pri.3.2.8859.
12. Harper JD, Lieber CM, Lansbury PT. Atomic force microscopic imaging of seeded fibril formation and fibril branching by the Alzheimer's disease amyloid-β protein. *Chem Biol.* 1997;4(12):951–959.
13. Petkova AT, Leapman RD, Guo Z, Yau W-M, Mattson MP, Tycko R. Self-propagating, molecular-level polymorphism in Alzheimer's beta-amyloid fibrils. *Science.* 2005;307:262–266.
14. Lurs T, Ritter C, Adrian M, et al. 3D structure of Alzheimer's amyloid-beta (1-42) fibrils. *Proc Natl Acad Sci USA.* 2005;102(48):17342–17347.
15. Schmidt M, Rohou A, Lasker K, et al. Peptide dimer structure in an Aβ(1-42) fibril visualized with cryo-EM. *Proc Natl Acad Sci USA.* 2015;112(38):11858–11863. https://doi.org/10.1073/pnas.1503455112.
16. Gremer L, Scholzel D, Schenk C, et al. Fibril structure of amyloid beta 1-42 by cryoelectron microscopy. *Science.* 2017;358(6359):116–119.
17. Wälti MA, Ravotti F, Arai H, et al. Atomic-resolution structure of a disease-relevant Aβ (1–42) amyloid fibril. *Proc Natl Acad Sci USA.* 2016;113(34):E4976–E4984. https://doi.org/10.1073/pnas.1600749113.
18. Xiao Y, Ma B, McElheny D, et al. Aβ(1-42) fibril structure illuminates self-recognition and replication of amyloid in Alzheimer's disease. *Nat Struct Mol Biol.* 2015;22(6):499–505. https://doi.org/10.1038/nsmb.2991.
19. Colvin MT, Silvers R, Ni QZ, et al. Atomic resolution structure of monomorphic Aβ42 amyloid fibrils. *J Am Chem Soc.* 2016;138(30):9663–9674. https://doi.org/10.1021/jacs.6b05129.
20. Naiki H, Higuchi K, Hosokawa M, Takeda T. Fluorometric determination of amyloid fibrils in vitro using the fluorescent dye, thioflavine T. *Anal Biochem.* 1989;177:244–249.
21. Naiki H, Higuchi K, Nakakuki K, Takeda T. Kinetic analysis of amyloid fibril polymerization in vitro. *Lab Invest.* 1991;65(1):104–110.
22. Biancalana M, Koide S. Molecular mechanism of thioflavin-T binding to amyloid fibrils. *Biochim Biophys Acta.* 2010;1804(7):1405–1412. https://doi.org/10.1016/j.bbapap.2010.04.001.
23. Tayeb-Fligelman E, Tabachnikov O, Moshe A, et al. The cytotoxic Staphylococcus aureus PSMα3 reveals a cross-α amyloid-like fibril. *Science.* 2017;355(80):831–833.
24. Hayashi H, Kimura N, Yamaguchi H, et al. A seed for Alzheimer amyloid in the brain. *J Neurosci.* 2004;24(20):4894–4902. https://doi.org/10.1523/JNEUROSCI.0861-04.2004.
25. Cohen SIA, Linse S, Luheshi LM, et al. Proliferation of amyloid-β 42 aggregates occurs through a secondary nucleation mechanism. *Proc Natl Acad Sci USA.* 2013;110(24):9758–9763. https://doi.org/10.1073/pnas.1218402110.
26. Klunk WE, Jacob RF, Mason RP. Quantifying amyloid Beta -peptide aggregation using the Congo red spectrophotometric assay. *Anal Biochem.* 1999;266:66–76.
27. Fancy DA, Kodadek T. Chemistry for the analysis of protein–protein interactions: rapid and efficient cross-linking triggered by long wavelength light. *Proc Natl Acad Sci USA.* 1999;96(3):6020–6024. https://doi.org/10.1073/pnas.96.11.6020.

28. Bitan G, Lomakin A, Teplow DB. Amyloid β -protein oligomerization. *J Biol Chem*. 2001;276(37):35176–35184. https://doi.org/10.1074/jbc.M102223200.
29. Howlett DR, Jennings KH, Lee DC, et al. Aggregation state and neurotoxic properties of Alzheimer beta-amyloid peptide. *Neurodegeneration*. 1995;4(1):23–32.
30. Simmons LK, May PC, Tomaselli KJ, et al. Secondary structure of amyloid beta peptide correlates with neurotoxic activity in vitro. *Mol Pharmacol*. 1994;45(3):373 LP–379. http://molpharm.aspetjournals.org/content/45/3/373.abstract.
31. Soto C, Castano EM, Kumar A, Beavis RC, Frangione B. Fibrillogenesis of synthetic amyloid-Beta peptides is dependent on their initial secondary structure. *Neurosci Lett*. 1995;200:105–108.
32. Shen C, Murphy RM. Solvent effects on self-assembly of β-amyloid peptide. *Biophys J*. 1995;69:640–651.
33. Adams DJ, Nemkov TG, Mayer JP, Old WM, Stowell MHB. Identification of the primary peptide contaminant that inhibits fibrillation and toxicity in synthetic amyloid-β 42. *PLoS One*. 2017;12(8):1–17.
34. Come JH, Fraser PE, Lansbury PT. A kinetic model for amyloid formation in the prion diseases: importance of seeding. *Proc Natl Acad Sci USA*. 1993;90:5959–5963.
35. Hu X, Crick SL, Bu G, Frieden C, Pappu RV, Lee J-M. Amyloid seeds formed by cellular uptake, concentration, and aggregation of the amyloid-beta peptide. *Proc Natl Acad Sci USA*. 2009;106(48):20324–20329. https://doi.org/10.1073/pnas.0911281106.
36. Amico MD, Giovanna M, Carlo D, et al. Thioflavin T promotes Aβ (1 − 40) amyloid fibrils formation. *J Phys Chem Lett*. 2012;3:1596–1601. https://doi.org/10.1021/jz300412v.
37. De FGV, Mallender WD, Inestrosa NC, Rosenberry TL. Thioflavin T is a fluorescent probe of the acetylcholinesterase peripheral site that reveals conformational interactions between the peripheral and acylation sites. *J Biol Chem*. 2001;276(26):23282–23287. https://doi.org/10.1074/jbc.M009596200.
38. Garai K, Frieden C. Quantitative analysis of the time course of Aβ oligomerization and subsequent growth steps using tetramethylrhodamine-labeled Aβ. *Proc Natl Acad Sci USA*. 2013;110(9):3321–3326. https://doi.org/10.1073/pnas.1222478110.
39. Dutta S, Finn TS, Kuhn AJ, Abrams B, Raskatov JA. Chirality dependence of amyloid β cellular uptake and a new mechanistic perspective. *Chembiochem*. 2019;20:1–5. https://doi.org/10.1002/cbic.201800708.
40. Necula M, Kayed R, Milton S, Glabe CG. Small molecule inhibitors of aggregation indicate that amyloid beta oligomerization and fibrillization pathways are independent and distinct. *J Biol Chem*. 2007;282(14):10311–10324. https://doi.org/10.1074/jbc.M608207200.
41. Foley AR, Raskatov J. A DFT-assisted topological analysis of four polymorphic, S-shaped Aβ42 fibril structures. *Chembiochem*. 2019;1–4. Accepted. https://doi.org/10.1002/cbic.201900036.
42. Dutta S, Foley AR, Warner CJA, et al. Suppression of oligomer formation and formation of non-toxic fibrils upon addition of mirror-image Aβ42 to the natural L-enantiomer. *Angew Chem Int Ed Engl*. 2017;56(38):11506–11510. https://doi.org/10.1002/anie.201706279.
43. Warner CJA, Dutta S, Foley AR, Raskatov JA. Introduction of D-glutamate at a critical residue of Aβ42 stabilizes a pre-fibrillary aggregate with enhanced toxicity. *Chemistry*. 2016;22(34):11967–11970.
44. Bernstein SL, Dupuis NF, Lazo ND, et al. Amyloid-β protein oligomerization and the importance of tetramers and dodecamers in the aetiology of Alzheimer's disease. *Nat Chem*. 2009;1(4):326–331. https://doi.org/10.1038/nchem.247.
45. Economou NJ, Giammona MJ, Do TD, et al. Amyloid β-protein assembly and Alzheimer's disease: dodecamers of Aβ42, but not of Aβ40, seed fibril formation. *J Am Chem Soc*. 2016;138(6):1772–1775. https://doi.org/10.1021/jacs.5b11913.

4.3 Reprint: Reprinted with permission from (*Pep. Sci.*. **2019**, 111, e24139). John Wiley and Sons. License Number 5182250786198. RightsLink in Appendix.

Received: 2 August 2019 | Revised: 10 September 2019 | Accepted: 12 September 2019
DOI: 10.1002/pep2.24139

FULL PAPER

PeptideScience WILEY

New insights into differential aggregation of enantiomerically pure and racemic Aβ40 systems

Subrata Dutta[1] | Alejandro R. Foley[1] | Ariel J. Kuhn[1] | Benjamin Abrams[2] | Hsiau-Wei Lee[1] | Jevgenij A. Raskatov[1]

[1]Department of Chemistry and Biochemistry, University of California Santa Cruz, Santa Cruz, California

[2]Department of Biomolecular Engineering, Life Sciences Microscopy Center, University of California Santa Cruz, Santa Cruz, California

Correspondence
Jevgenij A. Raskatov, Department of Chemistry and Biochemistry, University of California Santa Cruz, Santa Cruz, CA 95064.
Email: jraskato@ucsc.edu

Funding information
National Institutes of Health, Grant/Award Numbers: S10OD016246-01A1, R21AG058074

Abstract

Racemic mixtures frequently display properties that are different from those associated with their enantiopure counterparts, and are often characterized by higher propensity to form aggregates. Our previous research established that mixing of the enantiomers of Alzheimer amyloid β (Aβ) 42 peptides is an effective strategy to induce an oligomer-to-fibril conversion, which puts Aβ42 into a substantially less toxic state. Here, new insights into this chiral inactivation effect are presented. In addition to the commonly used Thioflavin T fibril formation assays, the use of the less aggregation-prone Aβ40 system allowed us to monitor peptide aggregation by NMR. Whereas enantiopure peptide was well soluble under the chosen experimental conditions and showed no sign of precipitation, addition of one equivalent of the mirror-image peptide triggered an instant and rapid aggregation, observable through the attenuation of the NMR signal. The racemic Aβ40 fibrils were found by transmission electron microscopy to be distinct in morphology, exhibiting a ~2-fold narrowing as compared with their enantiopure counterparts.

KEYWORDS
amyloid beta, chiral inactivation, rippled beta-sheets

1 | INTRODUCTION

The aggregation-prone, intrinsically disordered amyloid β (Aβ) peptide was initially characterized in 1984, and has since continuously attracted widespread interest of the chemical, biological, and medicinal communities alike, due to its believed principal role in Alzheimer disease.[1–6] It has also served as an inspiration for reductionist studies, which established new design principles for amyloid-based materials.[7]

In 2017, we reported that the mixing of the two Aβ42 enantiomers led to acceleration in fibril formation with a concomitant removal of oligomeric aggregation intermediates from solution and toxicity suppression in two model neuron-like cell lines.[8,9] A striking feature observed in that study was the complete disappearance of the incubation phase that is the characteristic for enantiopure Aβ fibril formation kinetics (in Thioflavin T [ThT] assays) upon mixing of enantiomers. This pointed to a fundamentally different mechanism of assembly. We hypothesized this to be due to the formation of a new and unique type of cross-β configuration in the racemic Aβ mixture, which was termed rippled β-sheets by Pauling and Corey in 1953,[10] and is not available to the enantiopure peptide. Our hypothesis was further validated in 2019 by Nilsson and coworkers, who used the Aβ (16-22) segment, that is, the KLVFFAE peptide, which represents the key central hydrophobic domain of Aβ, and found, using IR-based structural analysis, that the racemic mixture of this peptide showed a signature consistent with the formation of rippled β-sheets.[11] The authors also noted a substantial solubility reduction upon mixing of enantiomers, in agreement with our study on the full-length system. Other short hydrogel-forming peptides with propensity to form

Subrata Dutta, Alejandro R. Foley, and Ariel J. Kuhn contributed equally to this study.

 © 2019 Wiley Periodicals, Inc.

rippled β-sheet networks with enhanced stability and mechanical rigidity upon mixing of enantiomers have also been reported.[12,13]

2 | MATERIALS AND METHODS

2.1 | Solid phases Aβ40 synthesis

Peptides were synthesized by Fmoc HOBt//DIC/Piperidine chemistry on a Liberty One CEM peptide synthesizer equipped with a CEM discovery microwave, as previously described.[8] All syntheses were performed at a 0.1-mmol scale. Resins were cleaved by using a cocktail solution of trifluoroacetic acid (10 mL), 1, 2-diethanethiol (0.5 mL), triisopropylsilane (1 mL), and liquefied phenol (0.5 mL). The cocktail solution was added to the resins, mixtures agitated for 2 h, cocktail solution then evaporated to 2 mL under nitrogen gas, and peptides precipitated with cold diethyl ether and centrifuged at 6000 rpm. The peptide pellet was washed with cold diethyl ether, dried, dissolved in 1:1 acetonitrile:water, flash frozen in liquid nitrogen, and lyophilized. Peptides were than purified by HPLC as before to afford 95% purity or greater Aβ40 peptides.

2.2 | Circular dichroism experiments

L-Aβ40 or D-Aβ40 peptide of 0.1 mg was dissolved in 20 μL of 20-mM NaOH and sonicated for 30 s; 440 μL of 20-mM phosphate buffer solution (pH 7.4) was added to yield 50-μM final concentration of L-Aβ40 or D-Aβ40 peptide. For the racemic mixture, 0.1 mg of L-Aβ40 and 0.1 mg of D-Aβ40 were dissolved separately in 20 μL of 20-mM NaOH solution each, and then mixed to yield racemic Aβ40. Subsequently, 880 μL of freshly prepared 20-mM phosphate buffer solution (pH 7.4) were added to yield a final concentration of 50-μM rac-Aβ40 in a final volume of 920 μL. Spectra were recorded using a Jasco 1500 circular dichroism (CD) spectrophotometer at room temperature, set to a scan range of 180 to 280 nm, a DIT of 4 s, and a scan speed of 50 nm per minute.

2.3 | Thioflavin T assay

Lyophillized L- or D-Aβ40 was dissolved in 20-mM NaOH (~15 μL of 20-mM NaOH per 0.1 mg of peptide) and sonicated for 30 s and concentration was measured by nanodrop (ε = 1490 M^{-1} cm^{-1} at 280 nm). Enantiomers were mixed in a 1:1 ratio for rac-Aβ40. L-and D-Aβ40 were then diluted with PBS containing 0.02% (w/v) NaN_3 and 20 μM ThT, yielding 20 μM L- or D-Aβ40 solutions. For rac-Aβ40, two solutions were made (20 μM L and 20 μM D-Aβ40, 40 μM total; 10 μM L- and 10 μM D-Aβ40, 20 μM total). ThT experiments were conducted in black, clear bottom 96-well plates using a Molecular Device Gemini EM fluorescence plate reader (λ_{em} = 444 nm, λ_{ex} = 485 nm). Each well contained 200 μL of peptide solution and was sealed with optically clear adhesive film. Three replicates were obtained per condition. Each ThT assay was conducted for 24 h at 37 °C. Readings were collected every 5 min with 5 s shaking before reading and 295 s shaking in between readings.

2.4 | ^{1}H NMR experiments

For the enantiopure samples in aqueous conditions, NH_4OH-treated, lyophilized Aβ40 (L- or D-) was dissolved in 0.6 mL of 50 mM phosphate buffer containing the internal standard 4,4-dimethyl-4-silapentane-1-sulfonic acid (DSS) with 10% D_2O (pH 7.4), yielding 160-μM peptide solutions. For the racemic samples, the two peptides (L- and D-Aβ40) were prepared as described above and then mixed at a 1:1 M ratio prior to spectra acquisition. For the experiments conducted in DMSO, NH_4OH-treated, lyophilized Aβ (L-, D-, or rac-) was dissolved in 0.6 mL of d_6-DMSO containing the internal standard DSS to give a 160-μM peptide solution. The exact concentration of the peptide solutions was determined with a Nanodrop by absorbance at 280 nm (ε = 1490 M^{-1} cm^{-1}). Time points were collected every minute for a total of ~40 min. The NMR data were processed using MestreNova.

2.5 | TEM experiments

The samples of Aβ40 (L-, D-, or racemic) for transmission electron microscopy (TEM) were taken directly from ThT assays (20 μM total concentration of Aβ40) after 24 h. For specimen preparation, 3 μL of sample was spotted onto a freshly glow-discharge carbon-coated electron microscopy grid (Ted Pella, Catalog No. 01701-F). Grids were rinsed with 30 μL of milliQ water after 1 min incubation, followed by staining with 30 μL 1% uranyl acetate. All fibrils were imaged by using a Tecnai 12 microscope at an accelerating voltage of 120 kV. Images taken at 23000× were quantitatively analyzed as follows. The fibril width was measured at the thickest point where the fibril appeared to be a single fiber rather than a bundle using the FIJI/ImageJ software (https://fiji.sc/). Between 18 and 36 fibrils were measured per chiral form and pairwise two-sample *t* tests with unequal variance were performed between each condition using Microsoft Excel.

2.6 | Structural DFT-computational analysis

The peptidic backbone for the heterochiral, parallel, "rippled" dimeric interface was generated using the distances and symmetry operations published by Pauling and Corey.[10] Substituents of the LVFFA sequence were positioned using the standard geometric parameters defined in the Molden program package, the peptide N-terminally acetylated and C-terminally amidated. The resultant structure was imported into the SPARTAN program package, the backbone heavy atoms (C,N,O) are frozen, and the side chains are optimized using the SPARTAN MM/MD search engine. The lowest energy structure thus obtained was optimized for ~20 cycles using Gaussian 09 at the M062X/6-31G* level of theory, with solvent modeled via PCM.[14–17] The resultant structure was exported back into SPARTAN, backbone atoms frozen again, and sidechains reoptimized by MM/MD, and the lowest energy structure was imported back into Gaussian to repeat the DFT optimization cycle. The SPARTAN-Gaussian iteration was then repeated once more, yielding a total of three MM/MD-DFT back-and-forth iterations. The thus obtained refined structural guess

was then fully optimized at the M062X/6-31G* level of theory, with water contribution included via PCM (same as above), using an ultrafine integration grid and tight SCF convergence criteria, as defined in Gaussian 09.[14] Cartesian force constants were calculated explicitly via frequency calculation and used in structural optimization to facilitate energy minimization. A structure was considered converged based on negligible forces (10-fold below the standard threshold defined in Gaussian 09) and energy changes ΔE < 0.01 kcal/mol over 10 consecutive geometry optimization cycles. Cartesian coordinates have been deposited as part of the Supporting Information.

3 | RESULTS AND DISCUSSION

In continuation of our research efforts on the racemic aggregating Aβ system, we performed experiments with the two enantiopure Aβ40 peptides and their racemic mixture. The two Aβ40 enantiomers were synthesized and purified, using our previously published protocols and procedures.[8] The two peptides displayed reciprocal CD bands of comparable intensity, as expected for mirror-image peptides, and mixing of the enantiomers in a 1:1 ratio led to disappearance of that band (Figure 1A). The aggregation $t_{1/2}$ values were measured for the two enantiopure peptide in ThT fibril formation assays as $t_{1/2,\text{L-Aβ40}}$ = 104 ± 15 min and $t_{1/2,\text{D-Aβ40}}$ = 116 ± 13 min at 20-μM peptide concentration (Figure 1B,C). Mixing of the two enantiomers resulted in an acceleration of fibril formation to $t_{1/2,\text{rac-Aβ40}}$ = 19.1 ± 0.5 min when 20 μM each L- and 20 μM D-peptide (40 μM total racemic Aβ40) were used (Figure 1D). It was slightly higher at 20 μM total racemic Aβ40, with $t_{1/2,\text{rac-Aβ40}}$ = 26.2 ± 0.3 min (Figure 1E). Consistent with our previously reported findings, the racemic aggregating Aβ40 system was characterized by a lack of lag phase, much smaller error bars, and a lower final fluorescence output than the two enantiopure counterparts, all indicating that the fibrils formed were of a distinctly different polymorph for the racemic Aβ40 mixture.

To probe further the acceleration of fibril formation upon enantiomer mixing, ^{1}H NMR experiments were conducted. It was anticipated that the relatively high solubility of Aβ40, as compared with Aβ42, which had been the subject of the majority of our experiments in the past,[8] would be an asset for these experiments. An enantiopure aqueous solution of L-Aβ40 displayed a well-defined ^{1}H NMR spectrum, and showed no evidence of precipitation (298 K; 160 μM L-Aβ40; 9:1 H_2O/D_2O mixture, phosphate-buffered to pH 7.4; Figure 2A). Mixing of L- and D-Aβ40 in a 1:1 ratio initiated rapid precipitation, which could be readily monitored via loss of ^{1}H NMR signal intensity (Figure 2B), and was found to be consistent with the enhanced precipitation tendency of *rac*-Aβ40 observed by ThT (Figure 1). Within 40 min of incubation, the ^{1}H NMR signal intensity was reduced to ~39% with the Aβ40 racemate, corresponding to a loss of 61% of soluble species due to precipitation. Conversely, signal intensity remained invariant over the same time window with

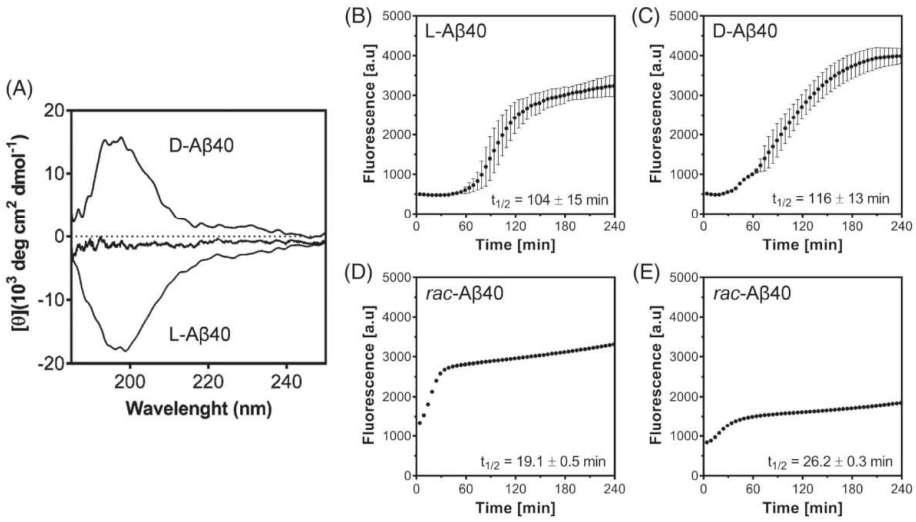

FIGURE 1 A, CD spectra of enantiopure (L- or D-) Aβ40, and the racemic mixture of the two peptides; spectra were obtained immediately upon reconstitution. Samples were dissolved in 20-mM NaOH and diluted to 50 μM in 20-mM phosphate buffer (pH 7.4). For rac-Aβ40, the mixture was composed of 25 μM L- and 25 μM D-Aβ40 (total peptide concentration of 50 μM). All CD spectra were obtained at room temperature. B, ThT fibril formation assay performed for L-Aβ40 (20 μM). L-Aβ40 was dissolved in 20-mM NaOH and diluted to 20 μM in 1xPBS (pH 7.4) along with 20-μM ThT. Samples were monitored by ThT fluorescence (λ_{em} = 444 nm, λ_{ex} = 485 nm) under shaking at 37 °C with data acquisition every 5 min. Curves show an average of three technical replicates with error bars as SD. C, ThT assay with D-Aβ40 (same conditions). D, ThT assay with rac-Aβ40 (20-μM L- and 20-μM D-Aβ40, otherwise the same conditions). E, ThT assay with rac-Aβ40 (10-μM L- and 10-μM D-Aβ40, otherwise the same conditions)

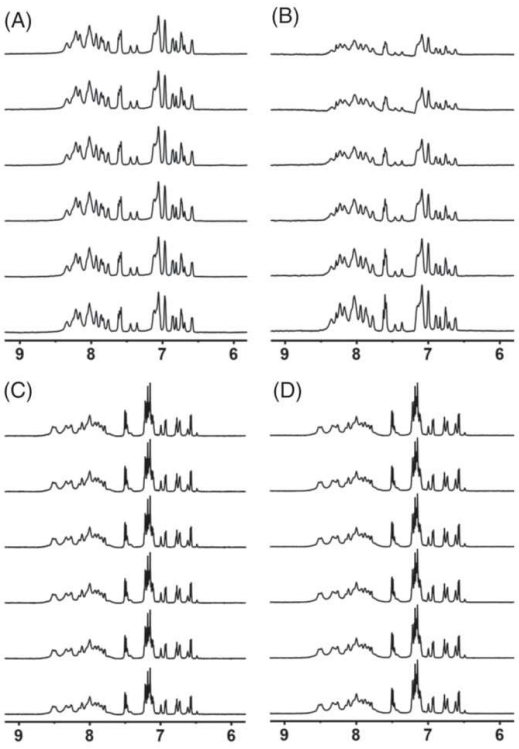

FIGURE 2 A, Enantiopure (L-)Aβ40 in a 9:1 H_2O/D_2O mixture, phosphate-buffered to pH 7.4. B, rac-Aβ40 in a 9:1 H_2O/D_2O mixture, phosphate-buffered to pH 7.4. C, L-Aβ40 in d_6-DMSO. D, rac-Aβ40 in d_6-DMSO. All ^{1}H NMR experiments were performed at 298 K with 160 μM total Aβ40 in all cases. The stacked spectra correspond, from lowest up, to t = 1, 9, 17, 25, 33, and 41 min. Racemic Aβ40 loses 61% signal in water over that time period, whereas signal intensity is invariant in all other cases. Aromatic ^{1}H NMR spectral regions are shown; full spectra can be found in the Supporting Information (Supporting Information Figure S1)

enantiopure L-Aβ40. To test for solvent influence, analogous experiments were also performed in DMSO. In stark contrast to the observations made with aqueous Aβ40 solutions, mixing of Aβ40 enantiomers did not trigger precipitation in DMSO, highlighting the importance of solvent for the effect (Figure 2C,D).

Because the findings made via ThT fibril formation assays (Figure 1) and ^{1}H NMR (Figure 2) indicated a significant mechanistic difference between fibril formation from enantiopure and racemic Aβ40 in aqueous solution, TEM imaging experiments were conducted. Mimicking conditions of ThT fibril formation assays, L-, D-, or *rac*-Aβ40 was incubated for 24 h with shaking at 37 °C. Samples were subsequently transferred onto TEM grids, stained with uranyl acetate and imaged, following previously published protocols and procedures.[8] Fibrils obtained from L- or D-Aβ40 had an appearance that was distinct from those derived from racemic Aβ40. As such, fibrils

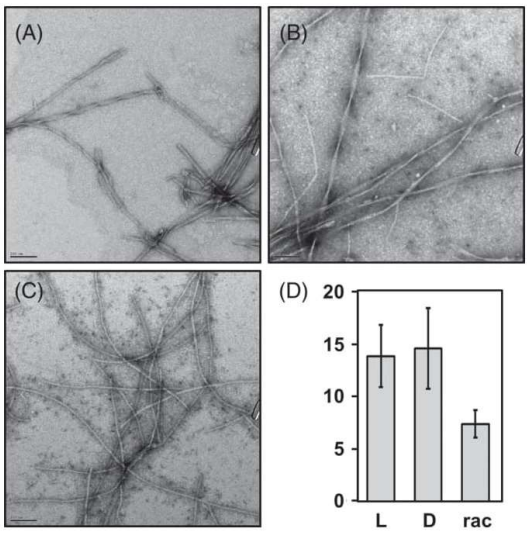

FIGURE 3 A, Fibrils grown from L-Aβ40. B, Fibrils grown from D-Aβ40. C, Fibrils grown from rac-Aβ40. Fibrils were obtained by incubating 20-μM Aβ40 with 20-μM ThT in phosphate buffer (pH 7.4) for 24 h at 37 °C, transferred to TEM grids, stained with uranyl acetate, and imaged (magnification: 23 k; scale bar corresponds to 100 nm). D, Statistical analysis of fibril widths. Fibrils used in the analysis are shown in Supporting Information Figures S2-S4

derived from enantiopure material were wider than the ones formed from the racemate and also often displayed a twist, whereas the racemic ones did not (Figure 3A-C).

To determine whether there was in fact a statistically significant difference in width, measurements were made using FIJI/ImageJ. Six fibril TEM images were selected per condition. Representative images are shown in Figure 3; the full collection images used for the analysis can be found in the Supporting Information. Fibrils derived from enantiopure Aβ40 were measured to have a width of 13.9 ± 3.0 nm (L-Aβ40; 37 datapoints) and 14.6 ± 3.8 nm (D-Aβ40; 18 datapoints). Because the mature fibrils made from enantiopure Aβ40 frequently displayed a periodic twisting, care was taken to take measurements at their widest points. Fibril widths were found to be comparable and statistically indistinguishable (P > 0.05, two-tailed t test with unequal variance), as expected for the two mirror-image systems.[18] A notable difference in width was apparent between fibrils formed from enantiopure Aβ40 and those formed from the racemate. The width of rac-Aβ40 fibrils was determined as 7.4 ± 1.3 nm (30 datapoints), and the difference with fibrils formed from both L- and D-Aβ40 was statistically significant (P < 0.05, two-tailed t test with unequal variance).

Because racemic Aβ40 fibrils were clearly different and because mixing of enantiomers of the much smaller peptidic segment KLVFFAE that comprises the central hydrophobic domain of Aβ recapitulated the key trends,[11] the hydrophobic rippled interface LVFFA was constructed using the parallel rippled Pauling-Corey cross-β coordinates,[10] and analyzed through the combination of MM/MD

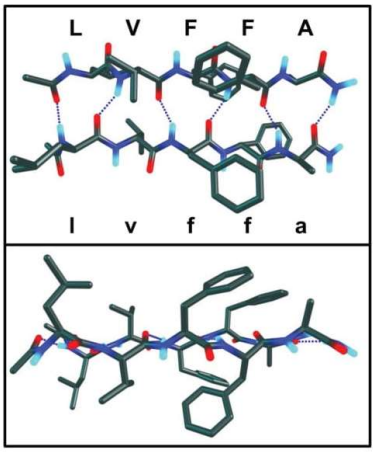

FIGURE 4 A DFT-optimized low-energy structure of the rippled parallel cross-β interface formed in the racemic LVFFA:lvffa dimer peptide (two orthogonal projections). See Section 2 for details on how the structure has been obtained. Cartesian coordinates for the structure have been provided as part of the Supporting Information

and DFT computational methods (see Section 2 for further technical details). The LVFFA segment is well suited for DFT analysis because of the lack of charges, which can complicate DFT calculations that model solvent contributions as a continuum.

A low-energy structure of the dimeric-rippled parallel LVFFA:lvffa cross-β structure is shown in Figure 4. The opposite chirality sense of the two layers projects the bulky hydrophobic sidechains onto opposing sides, thus minimizing steric clashes between residues and yielding a stable structure. The LVFFA:lvff interface qualitatively recapitulates the rippled cross-β backbone topology found by Urban *et al.*[11] It should be noted that Urban *et al.* reported an antiparallel arrangement of KLVFFAE:klvffae in the racemic mixture, which is reasonable to assume due to the better positioning of the opposite charges (K close to E as opposed to K close to K and E close to E). We believe that the parallel arrangement chosen in our study, on the other hand, would allow for better rippled cross-β interactions for the long, hydrophobic C-terminal domain IIGLMVGGVVIA, as found in full-length enantiopure Aβ40 fibrils,[19] and is, therefore, more relevant here.

4 | CONCLUSIONS

Taken together, findings presented here corroborate our initial observations made with the Aβ42 system,[8] further supporting the notion that the racemic Aβ system is fundamentally different from the enantiopure one. The morphological differences determined for the Aβ40 isoform using TEM were more pronounced and well defined than those observed with Aβ42.[8] This allowed for a quantitative fibril analysis, revealing an approximately 2-fold narrowing of *rac*-Aβ40 fibrils along with the disappearance of the helical twisting that was often present with enantiopure Aβ40. DFT calculations supported the viability of rippled cross-β interactions as a likely underlying driving force for accelerated fibril formation upon Aβ40 enantiomer mixing. Future experimental structural work on *rac*-Aβ40 would be of interest as it may give insights into packing and molecular-level interactions of the Aβ40 enantiomers in racemic fibrils.

Whereas strong experimental evidence has been provided by the Schneider and the Nillson laboratories that racemic mixtures of short peptides likely assemble to form rippled cross-β configurations,[11–13,20,21] there is, to the best of our knowledge, not a single high-resolution rippled cross-β structure available yet. The *rac*-Aβ40 system may offer a unique opportunity to obtain the first such structure in the future. There is a broad significance in the heterochiral molecular recognition phenomena that underlie the formation of rippled cross-β structures, ranging from materials,[11–13,20] as well as biomedical applications,[8] to phenomena related to origins of life and chirality of biospheres.[9,22,23]

ACKNOWLEDGMENTS

J.A.R. thanks UCSC for flexible start-up funds and the National Institutes of Health for funding (R21AG058074). UCSC and Dr. Nikolaos Sgourakis are gratefully acknowledged for access to computational facilities. Mr. Stephen Hauskins and the UCSC computing team are acknowledged for help and support. We also acknowledge the National Institutes of Health S10OD016246-01A1 award for the purchase of the JASCO J1500 CD.

ORCID

Alejandro R. Foley https://orcid.org/0000-0002-8644-0546
Jevgenij A. Raskatov https://orcid.org/0000-0002-0082-9113

REFERENCES

[1] G. G. Glenner, C. W. Wong, *Biochem. Biophys. Res. Commun.* **1984**, *120*, 885.
[2] D. J. Selkoe, J. Hardy, *EMBO Mol. Med.* **2016**, *8*, 595.
[3] J. Hardy, D. J. Selkoe, *Science* **2002**, *297*, 353.
[4] G. Bitan, M. D. Kirkitadze, A. Lomakin, S. S. Vollers, G. B. Benedek, D. B. Teplow, *Proc. Natl. Acad. Sci. U.S.A.* **2003**, *100*, 330.
[5] C. L. Masters, G. Simms, N. A. Weinman, G. Multhaup, B. L. McDonald, K. Beyreuther, *Proc. Nat. Acad. Sci. U.S.A.* **1985**, *82*, 4245.
[6] J. Hardy, G. Higgins, *Science* **1992**, *256*, 184.
[7] I. Cherny, E. Gazit, *Angew. Chem. Int. Ed.* **2008**, *47*, 4062.
[8] S. Dutta, A. R. Foley, C. J. A. Warner, X. Zhang, M. Rolandi, B. Abrams, J. A. Raskatov, *Angew. Chem. Int. Ed.* **2017**, *56*, 11506.
[9] J. A. Raskatov, *Chem. Eur. J.* **2017**, *23*, 16920.
[10] L. Pauling, R. B. Corey, *Proc. Natl. Acad. Sci. U.S.A.* **1953**, *39*, 253.
[11] J. M. Urban, J. Ho, G. Piester, R. Fu, B. L. Nilsson, *Molecules* **2019**, *24*, 1983.
[12] R. J. Swanekamp, J. T. M. DiMaio, C. J. Bowerman, B. L. Nilsson, *J. Am. Chem. Soc.* **2012**, *134*, 5556.
[13] K. J. Nagy, M. C. Giano, A. Jin, D. J. Pochan, J. P. Schneider, *J. Am. Chem. Soc.* **2011**, *133*, 14975.
[14] M. J. Frisch, G. W. Trucks, H. B. Schlegel, G. E. Scuseria, M. A. Robb, J. R. Cheeseman, G. Scalmani, V. Barone, B. Mennucci, G. A. Petersson, H. Nakatsuji, M. Caricato, X. Li, H. P. Hratchian,

A. F. Izmaylov, J. Bloino, G. Zheng, J. L. Sonnenberg, M. Hada, M. Ehara, K. Toyota, R. Fukuda, J. Hasegawa, M. Ishida, T. Nakajima, Y. Honda, O. Kitao, H. Nakai, T. Vreven Jr., J. E. Peralta, F. Ogliaro, M. Bearpark, J. J. Heyd, E. Brothers, K. N. Kudin, V. N. Staroverov, R. Kobayashi, J. Normand, K. Raghavachari, A. Rendell, J. C. Burant, S. S. Iyengar, J. Tomasi, M. Cossi, N. Rega, J. M. Millam, M. Klene, J. E. Knox, J. B. Cross, V. Bakken, C. Adamo, J. Jaramillo, R. Gomperts, R. E. Stratmann, O. Yazyev, A. J. Austin, R. Cammi, C. Pomelli, J. W. Ochterski, R. L. Martin, K. Morokuma, V. G. Zakrzewski, G. A. Voth, P. Salvador, J. J. Dannenberg, S. Dapprich, A. D. Daniels, J. B. Farkas, J. V. Foresman, J. Ortiz, Cioslowski, D. J. Fox, *Gaussian 09 Revision A.02*, Gaussian Inc, Wallingford, CT **2009**.

[15] W. J. Hehre, R. Ditchfield, J. A. Pople, *J. Chem. Phys.* **1972**, *56*, 2257.

[16] R. Ditchfield, W. J. Hehre, J. A. Pople, *J. Chem. Phys.* **1971**, *54*, 724.

[17] Y. Zhao, D. G. Truhlar, *Theor. Chem. Acc.* **2008**, *120*, 215.

[18] A. J. Kuhn, J. A. Raskatov, *Prog. Mol. Biol. Transl. Sci.* **2019** *In print*.

[19] R. Tycko, *Neuron* **2015**, *86*, 632.

[20] K. Nagy-Smith, P. J. Beltramo, E. Moore, R. Tycko, E. M. Furst, J. P. Schneider, *ACS Cent. Sci.* **2017**, *3*, 586.

[21] D. M. Raymond, B. L. Nilsson, *Chem. Soc. Rev.* **2018**, *47*, 3659.

[22] I. Weissbuch, R. A. Illos, G. Bolbach, M. Lahav, *Acc. Chem. Res.* **2009**, *42*, 1128.

[23] I. Weissbuch, M. Lahav, L. Leiserowitz, *Cryst. Growth Des.* **2003**, *3*, 125.

SUPPORTING INFORMATION

Additional supporting information may be found online in the Supporting Information section at the end of this article.

How to cite this article: Dutta S, Foley AR, Kuhn AJ, Abrams B, Lee H-W, Raskatov JA. New insights into differential aggregation of enantiomerically pure and racemic Aβ40 systems. *Peptide Science*. 2019;111:e24139. https://doi.org/10.1002/pep2.24139

4.4 Reprint

Reprinted with permission from (*ChemBioChem.* **2019**, 20, 1023-1026). John Wiley and Sons. License Number 518225144510. RightsLink in Appendix.

ChemPubSoc Europe

DOI: 10.1002/cbic.201800708

CHEMBIOCHEM Communications

Chirality Dependence of Amyloid β Cellular Uptake and a New Mechanistic Perspective

Subrata Dutta,[a] Thomas S. Finn[+],[a] Ariel J. Kuhn[+],[a] Benjamin Abrams,[b] and Jevgenij A. Raskatov*[a]

Amyloid β is an inherently disordered peptide that can form diverse neurotoxic aggregates, and its 42-amino-acid isoform is believed to be the agent responsible for Alzheimer's disease (AD). Cellular uptake of the peptide is a pivotal step for it to be able to exert many of its toxic actions. The cellular uptake process is complex, and numerous competing internalization pathways have been proposed. To date, it remains unclear which of the uptake mechanisms are particularly important for the overall process, and improvement of this understanding is needed, so that better molecular AD therapeutics can be designed. Chirality can be used as a unique tool to study this process, because some of the proposed mechanisms are expected to proceed in stereoselective fashion, whereas others are not. To shed light on this important issue, we synthesized fluorescently labeled enantiomers of amyloid β and quantified their cellular uptake, finding that uptake occurs in stereoselective fashion, with a typical preference for the L stereoisomer of ≈5:1. This suggests that the process is predominantly receptor-mediated, with likely minor contributions of non-stereoselective mechanisms.

Amyloid β (Aβ) is an aggregation-prone, inherently disordered peptide that is produced by neurons through two sequential cleavage events from its transmembrane protein precursor, amyloid precursor protein (APP), and can vary in length. The 40-amino-acid variant (Aβ40) is produced predominantly, but the 42-amino-acid isoform (Aβ42) is substantially more aggregation-prone and neurotoxic, and is believed to be responsible for some of the key actions that lead to synaptic dysfunction and neuronal death that is observed in Alzheimer's disease (AD).[1]

Although recent studies strongly suggest that intracellular accumulation of Aβ is required for the peptide to exert some of its key toxic actions,[2] there are substantial gaps in our knowledge of the mechanism of Aβ cellular uptake. Advances in our understanding of the phenomenon are urgently needed so that molecular AD therapeutics targeting cellular uptake of Aβ can be rationally designed. Diverse biomolecules that might act as Aβ cellular binding partners and lead to its internalization (i.e., receptors) have been proposed; they include transmembrane proteins, lipids, and other biomacromolecules.[3] However, receptor binding is not a strict prerequisite for cellular uptake. Cells employ, for example, the macropinocytosis process to internalize molecules without any requirement to provide discrete molecular binding sites for them.[4] Membrane pore assembly is another mechanism through which antimicrobial, aggregation-prone peptides can enter cells in a receptor-independent fashion.[5] All of the above have been proposed to contribute to Aβ cellular uptake to some degree, yet it remains unclear which of the many postulated mechanisms are the dominant ones.

Chirality can be employed as a unique tool with which to distinguish between the two classes of peptide internalization mechanisms: receptor-mediated cell-uptake events are likely to occur with a certain degree of stereoselectivity (these are referred to as uptake mechanism class I or the chirality-dependent uptake component), whereas receptor-independent processes lack the chiral interactions between the molecule that is being taken up and the cell and are not expected to proceed in a stereoselective fashion (these are referred to as uptake mechanism class II or the chirality-independent uptake component). Aβ42 cellular toxicity has been found to depend on chirality by us and others, with the natural L-Aβ42 stereoisomer being significantly more toxic than the mirror-image D-peptide.[6] This led us to hypothesize that Aβ cellular uptake is a stereoselective process. To test this hypothesis, we synthesized fluorescently tagged Aβ enantiomers and used them as tools to study the stereoselectivity of the Aβ cellular uptake process.

Using microwave-assisted, Fmoc-based solid-phase peptide synthesis, we made the two L and D enantiomers of Aβ(40/42). The peptides were labeled with 5(6)-carboxytetramethylrhodamine (TAMRA) according to our published methods (see also the Experimental Procedures in the Supporting Information, as well as Figures S1–S4).[6a] Thioflavin T (ThT) fibril formation assays were conducted and showed L- and D-Aβ42 to form fibrils with $t_{1/2}$ values that were consistent with our previous studies our previous studies (and, as expected, within experimental error) of the two enantiomers [Figure 1, $t_{1/2;\text{L-A}\beta42} = (21.0 \pm 0.7)$ min, $t_{1/2;\text{D-A}\beta42} = (20.2 \pm 0.2)$ min].

We found that the N-terminal TAMRA derivatization did not affect fibril formation properties in any significant fashion [Figure 1, $t_{1/2;\text{L-A}\beta42\text{-TAMRA}} = (22.6 \pm 0.7)$ min, $t_{1/2;\text{D-A}\beta42\text{-TAMRA}} = (21.8 \pm$

[a] Dr. S. Dutta, T. S. Finn,[+] A. J. Kuhn,[+] Prof. Dr. J. A. Raskatov
Department of Chemistry and Biochemistry
University of California, Santa Cruz
1156 High Street, Santa Cruz, CA 95064 (USA)
E-mail: jraskato@ucsc.edu

[b] Dr. B. Abrams
Department of Biomolecular Engineering, Life Sciences Microscopy Center, University of California, Santa Cruz
1156 High Street, Santa Cruz, CA 95064 (USA)

[+] These authors contributed equally to this work.

Supporting information and the ORCID identification numbers for the authors of this article can be found under https://doi.org/10.1002/cbic.201800708.

© 2019 Wiley-VCH Verlag GmbH & Co. KGaA, Weinheim

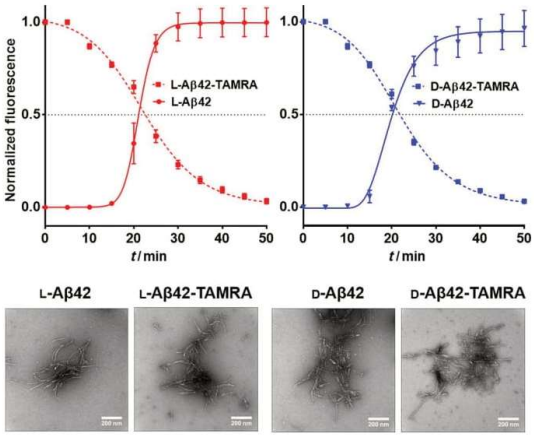

Figure 1. Fibril formation kinetics for L-/D-Aβ42, monitored by ThT (20 μM) fluorescence, and L-/D-Aβ42-TAMRA, monitored by TAMRA self-quenching, at 37 °C in PBS (pH 7.4, Aβ at 20 μM in all cases). Each data point is an average of five replicates with error bars representing the standard deviations.

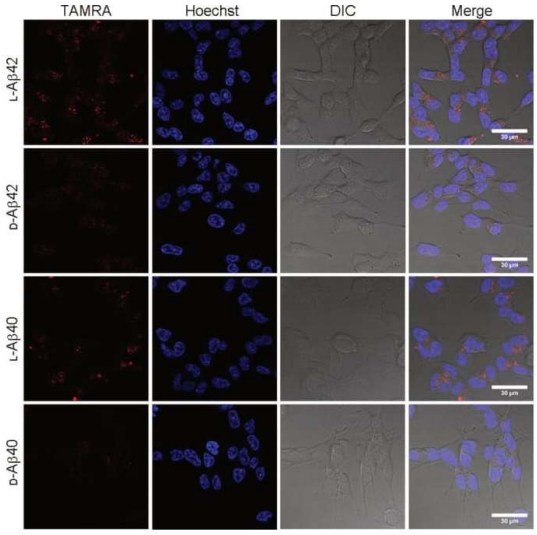

Figure 2. Confocal microscopy imaging of SH-SY5Y cells incubated with L-/D-Aβ(40/42), as indicated, at 5 μM for 2 h and rinsed with DPBS prior to imaging. TAMRA (TAMRA-Aβ uptake): λ_{ex} = 543 nm, λ_{em} = 590–720 nm. Hoechst (nuclear staining): λ_{ex} = 405 nm, λ_{em} = 415–485 nm. Scale bar: 30 μm.

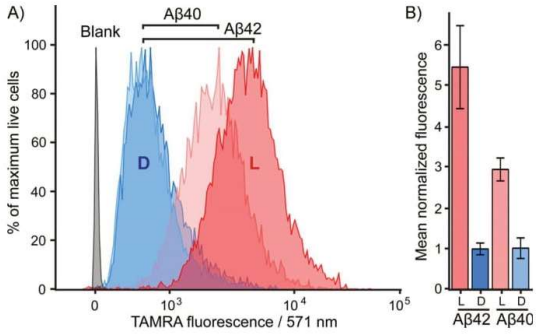

Figure 3. A) Flow cytometry quantitation of TAMRA-labeled L-/D-Aβ(40/42) uptake by SH-SY5Y cells as indicated; representative biological replicate shown. Cells were exposed to 5 μM Aβ for 2 h and then analyzed by flow cytometry (10 000 cells sampled per set of conditions; only live cells selected for analysis; data analyzed by using the FlowJo software package). B) Relative uptake levels of L-/D-Aβ(40/42)-TAMRA, obtained through averaging of three biological replicates (D-Aβ42 uptake was normalized to 1). Live cells were selected through LIVE/DEAD Fixable Violet Dead Cell Staining (see the Supporting Information for descriptive protocols and individual biological replicates of the experiments).

0.4) min], consistently with previous reports.[7] Fibril formation of TAMRA-labeled Aβ (i.e., L-/D-Aβ42-TAMRA) was monitored through TAMRA fluorescence quenching upon fibril assembly.[7a] Fibril formation was confirmed through TEM (Figure S5).[1] We found that this modification did not influence cellular toxicity to any significant degree (Figure S6).

To determine the dependence of cellular uptake on Aβ chirality, confocal imaging experiments were conducted. SH-SY5Y human neuroblastoma cells were incubated with TAMRA-labeled peptide solutions (5 μM, 2 h), counterstained with the Hoechst nuclear stain, washed with Dulbecco's phosphate-buffered saline (DPBS; i.e., PBS containing calcium and magnesium), and imaged (see the Supporting Information for a detailed procedure). A significant and consistent difference in uptake quantity between L- and D-Aβ, observable for both the 40- and the 42-residue isoforms, was noted (Figure 2). Bright intracellular puncta were clearly visible, consistently with a recent study that probed intracellular localization of L-Aβ42 to SH-SY5Y and reported that the majority of it localized to cell lysosomes.[8] We confirmed this further by conducting lysotracker co-staining experiments for both Aβ stereoisomers and isoforms (Figure S7). Prolonged incubation of SH-SY5Y cells with L-/D-Aβ42-TAMRA (15 h instead of 2 h) revealed a consistent preference for the internalization of the L stereoisomer (Figure S8), which was also recapitulated in PC12 cells (Figure S9).

To examine Aβ cellular uptake differences further, in a more quantitative, unbiased fashion, flow cytometry experiments were performed (Figure 3). Cells were incubated with 5 μM L-/D-Aβ(40/42) peptide for 2 h, under conditions identical to those employed in the confocal imaging experiments (Figure 2). After this incubation, cells were rinsed with PBS, trypsinized, pelleted, resuspended in PBS, and subjected to flow cytometry analysis (see the Supporting Information for a more detailed description). A 5.45-fold difference ($p < 0.01$) between L-Aβ42 and D-Aβ42 in terms of SH-SY5Y cellular peptide was observed. Stereodifferentiation was still highly significant, albeit less pronounced, for the Aβ40 isoform, with L-Aβ40 localizing to SH-SY5Y cells 2.9 times more efficiently ($p < 0.001$)

[1] *Analogous ThT fibril formation assays were also performed with L-/D-Aβ40 and L-/D-Aβ40-TAMRA, but the $t_{1/2}$ variance between experiments was too large, thus rendering the outcome of those measurements inconclusive.*

© 2019 Wiley-VCH Verlag GmbH & Co. KGaA, Weinheim

than D-Aβ40. The signal measured for L-Aβ42 was 1.85 times stronger ($p < 0.05$) than that measured for L-Aβ40, in good agreement with a previously reported approximately twofold difference.[9] We also found this trend to hold true over a range of L-/D-Aβ42 concentrations (Figure S10). In further support for stereoselectivity in the cellular uptake process, a comparable preference for the L stereoisomer was observed through flow cytometry for the Aβ42 isoform in PC12 cells and in rat primary hippocampal neurons (Figure S11). In a separate experiment, SH-SY5Y cells were incubated with L-/D-Aβ42-TAMRA for 2 h at 4 °C (Figure S12) and, in agreement with a previous study,[9] showed low fluorescence, indicating limited membrane binding. This further corroborates our interpretation that the fluorescence measured by flow cytometry for cells incubated with Aβ at 37 °C (Figures 3, S10 and S11) stems from intracellular and not membrane-bound peptide, and is also consistent with the confocal microscopy experiments (Figures 2 and S7).

The experiments presented above demonstrate that molecular chirality is an important determinant of cellular uptake of Aβ. Consistent trends were observed for both the Aβ40 and the Aβ42 peptide isoforms by confocal microscopy and flow cytometry in two model cell lines (SH-SY5Y cells and PC12 cells) at various incubation times (2 and 15 h) over a range of concentrations (0.1 to 5 μM). The trend was also found to hold true with primary neurons. The observed level of generality suggests that intracellular (e.g., lysosomal) peptide degradation, which might occur at different rates for the two Aβ40/42 enantiomers, is unlikely to contribute to more than a minor degree to the overall picture that has emerged from our study. Because chiral interactions between the cell and the peptide are a prerequisite for stereodifferentiation, our findings strongly suggest that cellular uptake of Aβ is receptor-mediated to a substantial degree. Cellular uptake of the D enantiomer, although significantly less pronounced, was still clearly and consistently detectable in all experiments, pointing towards the complexity of the process and suggestive of multiple mechanisms of intracellular localization being in play simultaneously. The ≈5:1 ratio, which is a representative stereoselectivity ratio for cellular uptake of the two Aβ42 enantiomers, can be interpreted as follows: approximately 80% of L-Aβ42 is taken up by cells through chirality-dependent mechanisms (i.e., uptake mechanism class I), whereas the residual ≈20% enters the cells by a chirality-independent—that is, class II—mechanism. Some likely contributors are discussed below.

Class I

The stereoselective component of Aβ cellular uptake has to arise as a consequence of interactions between the peptide and cell-associated chiral binding partners. It has been proposed that diverse biomolecules contribute to intracellular Aβ localization, including the transmembrane proteins PrP and RAGE, as well as the soluble protein APOE, inter alia.[3a,b,10] The head groups of certain lipids, such as the GM1 ganglioside and phosphatidylserine, have also been found to play roles in physiologically relevant interactions between Aβ and cellular membranes.[3c,d,11] Because binding of Aβ to membranes can affect its aggregation properties and cellular internalization capacity, interactions between Aβ and chiral lipid head groups might also make contributions to the stereoselectivity of Aβ cellular uptake by providing chiral binding sites on cell membranes.

Class II

The non-stereoselective component of Aβ uptake likely arises through mechanisms of action that do not involve the establishment of chiral interactions between the peptide and the cell. Macropinocytosis, for example, can be expected to operate with no chiral preference, and has been suggested to play a role in cellular uptake of Aβ.[9] Membrane poration constitutes another mechanism that has been discussed as a potential contributor to Aβ uptake and toxicity.[12] This mechanism of action is perhaps best-established in the context of antimicrobial peptides. In the seminal study published by Merrifield and co-workers in 1990, it was found that L and D enantiomers of three α-helical peptides (cecropin, magainin, and melittin) were equally potent as pore-forming antibacterial peptides.[5b] It should be noted that there is evidence of Aβ having antimicrobial activity,[13] which is likely related to its ability to permeabilize membranes of pathogens.

In summary, we made fluorescently tagged amyloid β enantiomers of the 40- and 42-amino-acid isoforms and were able to use them as mechanistic tools to gain unique insights into the cellular uptake process, which is believed to be a critical step for various toxic actions of the peptide to become manifest.[2] A conundrum for the field for over two decades, innumerable uptake mechanisms, often with contradictory implications, have been proposed.[6b,14] We have found that Aβ uptake depends on the chirality of the peptide, with a typical preference of ≈5:1 in favor of the L stereoisomer. Consistent observations have been made for both Aβ40 and Aβ42 in SH-SY5Y and PC12 cells by using flow cytometry and confocal microscopy. Our results provide a new perspective on the cellular Aβ uptake process, through which it emerges as a multi-mechanism process that is dominated by a stereoselective, receptor-mediated component.

Acknowledgements

J.A.R. thanks UCSC for the flexible start-up funds and the NIH for the award of the grant R21AG058074. We are grateful to The Institute for the Biology of Stem Cells (IBSC) Shared FACS Facility for assistance with flow cytometry experiments.

Conflict of Interest

The authors declare no conflict of interest.

Keywords: amyloid beta-peptides · cellular uptake mechanism · chirality · fluorescent probes · mirror-image peptides

© 2019 Wiley-VCH Verlag GmbH & Co. KGaA, Weinheim

[1] a) D. J. Selkoe, J. Hardy, *EMBO Mol. Med.* **2016**, *8*, 595 – 608; b) H. W. Querfurth, F. M. LaFerla, *N. Engl. J. Med.* **2010**, *362*, 329 – 344; c) C. Haass, D. J. Selkoe, *Nat. Rev. Mol. Cell Biol.* **2007**, *8*, 101 – 112; d) G. Bitan, M. D. Kirkitadze, A. Lomakin, S. S. Vollers, G. B. Benedek, D. B. Teplow, *Proc. Natl. Acad. Sci. USA* **2003**, *100*, 330 – 335.

[2] a) S. Jin, N. Kedia, E. Illes-Toth, I. Haralampiev, S. Prisner, A. Herrmann, E. E. Wanker, J. Bieschke, *J. Biol. Chem.* **2016**, *291*, 19590 – 19606; b) F. M. LaFerla, K. M. Green, S. Oddo, *Nat. Rev. Neurosci.* **2007**, *8*, 499 – 509.

[3] a) H. H. Jarosz-Griffiths, E. Noble, J. V. Rushworth, N. M. Hooper, *J. Biol. Chem.* **2016**, *291*, 3174 – 3183; b) B. V. Zlokovich, *Nat. Rev. Neurosci.* **2011**, *12*, 723 – 738; c) W. Gibson Wood, G. P. Eckert, U. Igbavboa, W. E. Müller, *Biochim. Biophys. Acta Biomembr.* **2003**, *1610*, 281 – 290; d) E. Terzi, G. Hölzemann, J. Seelig, *Biochemistry* **1997**, *36*, 14845 – 14852.

[4] J. P. Lim, P. A. Gleeson, *Immunol. Cell Biol.* **2011**, *89*, 836 – 843.

[5] a) C. K. Wang, G. J. King, A. C. Conibear, M. C. Ramos, S. Chaousis, S. T. Henriques, D. J. Craik, *J. Am. Chem. Soc.* **2016**, *138*, 5706 – 5713; b) D. Wade, A. Boman, B. Wåhlin, C. M. Drain, D. Andreu, H. G. Boman, R. B. Merrifield, *Proc. Natl. Acad. Sci. USA* **1990**, *87*, 4761 – 4765.

[6] a) S. Dutta, A. R. Foley, C. J. A. Warner, X. Zhang, M. Rolandi, B. Abrams, J. A. Raskatov, *Angew. Chem. Int. Ed.* **2017**, *56*, 11506 – 11510; *Angew. Chem.* **2017**, *129*, 11664 – 11668; b) G. D. Ciccotosto, D. J. Tew, S. C. Drew, D. G. Smith, T. Johanssen, V. Lal, T. L. Lau, K. Perez, C. C. Curtain, J. D. Wade, F. Separovic, C. L. Masters, J. P. Smith, K. J. Barnham, R. Cappai, *Neurobiol. Aging* **2011**, *32*, 235 – 248.

[7] a) K. Garai, C. Frieden, *Proc. Natl. Acad. Sci. USA* **2013**, *110*, 3321 – 3326; b) D. M. Walsh, E. Thulin, A. M. Minogue, N. Gustavsson, E. Pang, D. B. Teplow, S. Linse, *FEBS J.* **2009**, *276*, 1266 – 1281.

[8] X. Hu, S. L. Crick, G. Bu, C. Frieden, R. V. Pappu, J.-M. Lee, *Proc. Natl. Acad. Sci. USA* **2009**, *106*, 20324 – 20329.

[9] E. Wesén, G. D. M. Jeffries, M. M. Dzebo, E. K. Esbjörner, *Sci. Rep.* **2017**, *7*, 2021.

[10] a) C.-C. Liu, T. Kanekiyo, H. Xu, G. Bu, *Nat. Rev. Neurol.* **2013**, *9*, 106 – 118; b) A. Sagare, R. Deane, R. D. Bell, B. Johnson, K. Hamm, R. Pendu, A. Marky, P. J. Lenting, Z. Wu, T. Zarcone, A. Goate, K. Mayo, D. Perlmutter, M. Coma, Z. Zhong, B. V. Zlokovic, *Nat. Med.* **2007**, *13*, 1029 – 1031; c) R. Deane, S. D. Yan, R. K. Submamaryan, B. LaRue, S. Jovanovic, E. Hogg, D. Welch, L. Manness, C. Lin, J. Yu, H. Zhu, J. Ghiso, B. Frangione, A. Stern, A. M. Schmidt, D. L. Armstrong, B. Arnold, B. Liliensiek, P. Nawroth, F. Hofman, M. Kindy, D. Stern, B. Zlokovic, *Nat. Med.* **2003**, *9*, 907 – 913.

[11] a) S. Hong, B. L. Ostaszewski, T. Yang, T. T. O'Malley, M. Jin, K. Yanagisawa, S. Li, T. Bartels, D. J. Selkoe, *Neuron* **2014**, *82*, 308 – 319; b) G. Lee, H. B. Pollard, N. Arispe, *Peptides* **2002**, *23*, 1249 – 1263; K. Yanagisawa, A. Odaka, N. Suzuki, Y. Ihara, *Nat. Med.* **1995**, 1062 – 1066.

[12] a) C. DiScala, N. Yahi, S. Boutemeur, A. Flores, L. Rodriguez, H. Chahinian, J. Fantini, *Sci. Rep.* **2016**, *6*, 28781; b) M. Serra-Batiste, M. Ninot-Pedrosa, M. Bayoumi, M. Gairi, G. Maglia, N. Carulla, *Proc. Natl. Acad. Sci. USA* **2016**, *113*, 10866 – 10871; c) A. G. Kreutzer, I. L. Hamza, R. K. Spencer, J. S. Nowick, *J. Am. Chem. Soc.* **2016**, *138*, 4634 – 4642.

[13] D. K. Kumar, S. H. Choi, K. J. Washicosky, W. A. Eimer, S. Tucker, J. Ghofrani, A. Lefkowitz, G. McColl, L. E. Goldstein, R. E. Tanzi, R. D. Moir, *Sci. Transl. Med.* **2016**, *8*, 340ra72.

[14] D. H. Cribbs, C. J. Pike, S. L. Weinstein, P. Velazquez, C. W. Cotman, *J. Biol. Chem.* **1997**, *272*, 7431 – 7436.

Manuscript received: November 17, 2018
Accepted manuscript online: December 14, 2018
Version of record online: February 27, 2019

© 2019 Wiley-VCH Verlag GmbH & Co. KGaA, Weinheim

4.5 Reprint

The following text and figures are from the manuscript:

Kuhn, A.J.*; Ehlke, B.*; Johnstone, T. C.; Oliver, S. R. J.; Raskatov, J. A. *Chemical Science. In Review.* **2021**.

View Article Online
DOI: 10.1039/D1SC05731F

Open Access Article. Published on 08 December 2021. Downloaded on 12/8/2021 8:00:24 PM.
This article is licensed under a Creative Commons Attribution 3.0 Unported Licence.

A Crystal-Structural Study of Pauling-Corey Rippled Sheets

Ariel J. Kuhn,[a,♪] Beatriz Ehlke,[a,♪] Timothy C. Johnstone,[a]
Scott R. J. Oliver,[a] Jevgenij A. Raskatov[a,*]

* corresponding author; ♪ denotes equal contribution

[a] Dept. of Chemistry and Biochemistry, UCSC, 1156 High Street, Santa Cruz, California, USA.
E-mail: jraskato@ucsc.edu

Dedicated to the memory of John W. Phillips: a great scientist and a great friend

Chemical Science Accepted Manuscript

View Article Online
DOI: 10.1039/D1SC05731F

ABSTRACT

Following on their seminal theoretical work on the pleated β-sheet published by Pauling and Corey in 1951, the rippled β-sheet was hypothesized by the same authors in 1953. In the pleated β-sheet the interacting β-strands have the same chirality, whereas in the rippled β-sheet the interacting β-strands are mirror-images. Unlike with the pleated β-sheet that is now common textbook knowledge, the rippled β-sheet has been much slower to evolve. Much of the experimental work on rippled sheets came from groups that study aggregating racemic peptide systems over the course of the past decade. This includes MAX1/DMAX hydrogels (Schneider), L/D-KFE8 aggregating systems (Nilsson), and racemic Amyloid β mixtures (Raskatov). Whether a racemic peptide mixture is "ripple-genic" (*i.e.*, whether it forms a rippled sheet) or "pleat-genic" (*i.e.*, whether it forms a pleated sheet) is likely governed by a complex interplay of thermodynamic and kinetic effects. Structural insights into rippled sheets remain limited to only a very few studies that combined sparse experimental structural constraints with molecular modeling. Crystal structures of rippled sheets are needed so we can rationally design rippled sheet architectures. Here we report a high-resolution crystal structure, in which (L,L,L)-triphenylalanine and (D,D,D)-triphenylalanine form dimeric antiparallel rippled sheets, which pack into herringbone layer structures. The arrangement of the tripeptides and their mirror-images in the individual dimers were in excellent agreement with the theoretical predictions by Pauling and Corey. A subsequent mining of the PDB identified three orphaned rippled sheets among racemic protein crystal structures.

SIGNIFICANCE

The rippled sheet is a structural motif hypothesized by Pauling and Corey in 1953, in which extended peptidic β-strands associate with their mirror-images. Reflecting the growing interest in D-peptides and the need for new materials, the rippled sheet has been attracting increasing attention in the last decade. However, for the rational design of rippled sheet nanomaterials to become tractable, crystal structures are urgently needed. Here we report that a racemic mixture of (L,L,L)- and (D,D,D)-triphenylalanine, yields crystals that are built from periodically repeating rippled sheet dimers. Mining of the PDB reveals three further rippled sheet-containing crystal structures that had escaped the attention of the field thus far.

Chemical Science Accepted Manuscript

View Article Online
DOI: 10.1039/D1SC05731F

INTRODUCTION

Peptides with mixed chirality may be used to access frameworks with unique properties, including protease-resistant peptide drugs,[1,2] hydrogels with enhanced rigidity,[3,4] aggregation blockers,[5,6] amyloid oligomer-to-fibril converters,[7,8] and mechanistic tools.[9,10] Mirror-image proteins may also be used to enhance crystallization of proteins that are hard to crystallize, sometimes by creating unique interactions between the protein enantiomers.[11–14] A systematic incorporation of D-amino acids into proteins and peptides is expected to give access to a huge structure-function space that cannot be accessed in any other way.

In 1951, Pauling and Corey introduced the pleated β-sheet as a two-dimensional periodic layer configuration built from extended homochiral peptide strands.[15] The pleated β-sheet rapidly established itself as a key protein structural motif that is commonly known in textbooks as the β-sheet. Thousands of protein structures have been published that contain β-sheets. This includes structures that may be as huge as a periodic, fibrillary β-sheet network on the one side and as small as a β-sheet dimer in the context of a globular protein on the other side. In 1953, Pauling and Corey introduced the rippled β-sheet as a configuration closely related to the pleated β-sheet, but with every alternate peptide chain mirrored, thus giving rise to unique structures.[16] Some of the key structural differences between pleated and rippled β-sheets, including differences in hydrogen bonding and relative side-chain disposition in the β-sheet frameworks, have been discussed very recently.[17] As illustrated in **Fig. 1**., in an antiparallel pleated sheet, amino acid side chains are aligned in a vertical line orthogonal to the peptide backbones (**Fig. 1, left panel**). In contrast, in an antiparallel rippled sheet, to reduce steric repulsion between the alternating enantiomeric peptides, the side chains are oriented diagonally across the peptidic network (**Fig. 1, right panel**).

Unlike with the pleated β-sheet (now known as the β-sheet), the growth of our body of knowledge on the rippled β-sheet has been extremely sluggish. The first experimental observation of an (antiparallel) rippled sheet was made in the 1970s by Lotz, Moore and Krimm, on polyglycine I.[18–20] The authors used space group considerations to conclude that polyglycine I crystals contained rippled rather than pleated antiparallel sheets (monoclinic rather than orthorhombic unit cell geometry). Some three decades later, Lahav and co-workers used clever labeling strategies in conjunction with mass-spectrometry, to produce evidence for rippled sheet formation, based on templated peptide replication.[21,22] Conversely, Chung and Nowick noted in their solution-phase NMR studies a thermodynamic preference for a dimeric pleated β-sheet, with the alternative rippled sheet observed as a minor diastereomer.[23] A more recent study by Liu and Gellman is broadly consistent with Chung and Nowick.[24] Our understanding of the interplay of thermodynamics and kinetics that underlie the formation of pleated vs rippled sheets remains extremely limited. Experiments performed in the laboratories of Schneider,[3,4] Nilsson,[25,26] Raskatov,[7,8] and Torbeev,[27] showed that mirror-image peptide strands may assemble into rippled sheets, but there is also evidence that some sequences may favor homochiral association.[28] The structural insights available for the MAX1/DMAX systems,[3] a short Amyloid-β (Aβ) segment,[25] and, most recently, racemic full-length Aβ40[29] were obtained from theoretical calculations constrained by a fairly limited number of experimental data. These studies provide valuable insights into rippled sheets, but not experimental high-resolution structures.

It is interesting to note that not all racemic peptide mixtures form rippled sheets,[23,24,30] as self-sorting into pleated sheets may also occur.[30] We are just beginning to learn why some racemic peptide mixtures form rippled sheets (*i.e.*, are “ripple-genic”), whereas others prefer to form pleated sheets instead (*i.e.*, are “pleat-genic”). To systematically map out the structure-function space and to close this major knowledge gap, the field urgently needs high-resolution structures of rippled sheets. Here we report the X-ray crystal structure of (L,L,L)-triphenylalanine that is hydrogen-bonded to (D,D,D-)-triphenylalanine in a dimeric antiparallel rippled sheet. We

Chemical Science Accepted Manuscript

View Article Online
DOI: 10.1039/D1SC05731F

then draw comparisons with hitherto orphaned rippled sheet crystal structures that we discovered by searching the PDB for racemic proteins.

RESULTS

Choice of system. The significance of the oligomeric phenylalanine motif for amyloid formation is well-established. For example, it is known that the hydrophobic LVFFA segment that spans the amino acid residues 17-21 of the Amyloid β (*i.e.*, Aβ17-21) peptide is crucial for Aβ fibrillization.[31] Furthermore, Kiessling and coworkers have taken advantage of this by using the KLVFF segment for molecular recognition studies with Aβ.[31,32] Reductionist studies of Aβ by Gazit and co-workers demonstrated that the short diphenylalanine peptide is itself capable of forming amyloid nanostructures.[33] Unlike the dipeptide, FF, which has been shown to form water-filled nanovesicles and hollow tubes, the tripeptide, FFF, spontaneously assembles into a diverse set of supramolecular assemblies depending on conditions, such as solid nanospheres, nanorods, helical-ribbons, plates, dendrimers, and doughnuts,[34–36] similar to what has been reported for Aβ,[37] making it an interesting candidate from the standpoint of rippled sheet design. Additionally, Gazit and coworkers found that FFF demonstrated improved stability and peptide-network propensity over FF.[36] The authors also reported Thioflavin T (ThT) positivity for the FFF assemblies, indicative of ordered β-sheet content.[36]

More recently, Nilsson and co-workers demonstrated that the Aβ16-22 segment, KLVFFAE, rapidly formed precipitates when mixed with its mirror-image counterpart klvffae, which the authors ascribed to rippled sheet formation based on isotope-edited FT-ICR mass spectrometric and solid state NMR spectroscopic experiments.[25]

Peptides containing bulky, hydrophobic amino acids Phe (F), Val (V), Ile (I) and Leu (L) are believed to be particularly prone to forming rippled sheets.[17] Phenylalanine stands out because of its relative rigidity, which should favor crystallization.[38] We chose a racemic mixture of (L,L,L)-triphenylalanine and (D,D,D)-triphenylalanine (*i.e.*, FFF:fff), as our model. The N- and C-termini of FFF and fff were kept as free amines and free carboxylates, respectively, to afford peptides that (a) are water-soluble and (b) favor a defined antiparallel arrangement due to Coulombic attraction. Peptides were made on solid support and purified using a procedure similar to one we previously developed for Aβ purification (**Fig. S1** and **Fig. S2**).[39]

The FFF:fff dimer structure. Combination of concentrated solutions of FFF and fff led to rapid formation of a fine precipitate. Optimization of conditions led to a protocol, in which controlled cooling of a solution saturated with a racemic mixture of FFF and fff from 75 to 25 °C at a rate of 0.1 °C min^{-1} afforded single-crystal needles with length exceeding 3 mm. A short needle, suitable for single crystal X-ray diffraction was selected and the metric symmetry and Laue symmetry of the diffraction pattern obtained with Cu K_α radiation revealed that the crystal belonged to the monoclinic crystal system. Strict observance of Friedel's Law and the $\langle E^2 - 1 \rangle$ value of 1.008 indicate that the crystal is centrosymmetric, suggesting that the molecules had crystallized as the racemic compound. Centrosymmetry was confirmed by analysis of the systematic absences, which unambiguously confirmed the space group to be $P2_1/c$. The structure was solved using intrinsic phasing and refined against 0.84 Å-resolution data (Table S1). The resolution and quality of the data permitted anisotropic refinement of all non-H atoms and semi-free refinement of H-atom positions.

The asymmetric unit contains a single tripeptide in its zwitterionic form (**Fig. S3**). Both amides assume the expected *trans* configuration. The ψ angles of 114.6(2)° and 132.3(1)° and the φ angles of –124.7(4)° and –155.1(1)° for FFF fall within the range typically observed for β-pleated sheets. The side chains of the three residues assume, from N to C terminus, the *gauche*$^+$ (χ_1 = –63.2(2)°), *trans* (χ_1 = –175.1(1)°), and *gauche*$^-$ (χ_1 = 70.7(2)°) configurations.

The dimer resides on a crystallographic inversion center, across which FFF and fff form two symmetry-related pairs of hydrogen bonds (**Fig. 2**). The terminal ammonium and carboxylate

Chemical Science Accepted Manuscript

View Article Online
DOI: 10.1039/D1SC05731F

groups form a salt bridge with a N···O distance of 2.7660(18) Å and a N–H···O angle of 152.8(19)°. The hydrogen bond formed between the neutral amide units features an expectedly longer N···O distance of 2.9097(18) Å and a N–H···O angle of 157.4(17)°. The hydrogen bonds comprise the only significant intermolecular contacts between the components of the dimer; the torsion angles assumed by each of the phenylalanine units allow them to effectively interleave given the inversion symmetry relating the two molecules. This arrangement of hydrogen bonds is in excellent agreement with the model put forward by Pauling and Corey (**Fig. 2** and **Fig. S4**). In that original work, they model the antiparallel rippled sheet using a translation of 7.00 Å, which agrees well with the $C_{\alpha,1}\cdots C_{\alpha,3}$ distance of 6.888(2) Å in the present crystal structure.

Crystal lattice analysis. The crystal is held together by a combination of interdimer hydrogen bonds, ionic interactions, and van der Waals interactions (**Fig. S5**). In addition to interacting with the terminal carboxylate of the inversion-generated dimer mate, the terminal ammonium also forms hydrogen bonds to a glide-generated carbonyl of an enantiomeric tripeptide molecule (N···O = 2.7244(17) Å) and to the screw-generated terminal carboxylate of a molecule of identical handedness (N···O = 2.6645(18) Å). The internal amide N–H unit that is not involved in the antiparallel cross-β FFF:fff dimer also hydrogen bonds to this same screw-generated terminal carboxylate (N···O = 3.0168(17) Å). The H-atom positions in the final model are consistent with this hydrogen bonding pattern.

These hydrogen bonds extend to form sheets parallel to the crystallographic *bc* plane (**Fig. 3**). These sheets feature a hydrophilic core bounded on both sides by hydrophobic layers. The layers stack on one another with an interlayer spacing corresponding to the crystallographic *a* lattice parameter of 11.3563(5) Å (**Fig. S6**). This nanoscale architecture, with clear alternation between hydrophobic and hydrophilic layers, is reminiscent of a phase separation. The dimeric rippled sheets do not assemble into extended "fibrillary" rippled sheets with long-range order, packing into a classic herringbone pattern instead (**Fig. 4**).

To confirm that an isolated FFF:fff rippled antiparallel cross-β dimer is in itself a stable arrangement, the dimer was subjected to full geometry optimization using Density Functional Theory (DFT) methods. The optimization produced only marginal local structural changes (**Fig. S7, Table S2**), confirming that the structural features of the dimer are inherent to the β-rippled-sheet hydrogen bonding pattern and not crystal packing forces. This result stands in good agreement with our previous computational work on related rippled interfaces.[8,17,40,41]

DISCUSSION

Above we presented a range of structural features we were able to glean from a crystal-structural analysis of the FFF:fff lattice. To the best of our knowledge, this is the first time that a rippled sheet crystal structure is being discussed in the literature. However, owing to the efforts of racemic protein crystallography, many crystal structures that contain potentially interacting mirror-image protein pairs are now available. It seemed plausible that the enantiomers in some of those structures might interact *via* rippled sheets. We interrogated this possibility by searching the Cambridge Structural Database (CSD) and the Protein Data Bank (PDB), as described in the Materials and Methods section. The CSD search revealed no rippled sheet structures. The PDB search identified three racemic protein crystal structures with a qualitative appearance suggesting the presence of antiparallel rippled sheets. We analyzed the three structures and validated that dimeric rippled sheets were indeed present in all three cases (**Fig. 5**). As such, we found that in the racemic crystal structure of the Rv1738 protein, the protein enantiomers interact through an antiparallel rippled sheet formed by the Lys-Glu-Leu triad and its enantiomer (**Fig. 5A**).[42] We also found that, in the racemic ester insulin crystal structure, the enantiomers are bridged by a rippled sheet formed between the Phe-Phe-Tyr triad and its enantiomer (**Fig. 5B**).[43] Finally, we observed a very short rippled sheet segment of only one Phe residue and its enantiomer in the racemic crystal structure of kaliotoxin (**Fig. 5C**).[44] Whereas in those three structural studies, the authors

Chemical Science Accepted Manuscript

View Article Online
DOI: 10.1039/D1SC05731F

did recognize there were mirror-image interactions between their protein pairs, none of them identified those interactions as rippled sheets, which may be why those important structural insights appear to have escaped the attention of the rippled sheet community thus far. To gain deeper insights into the backbone conformations associated with the four rippled antiparallel sheet structures, we analyzed their Ramachandran angles (**Fig. 6**). We noted that three of the rippled sheets contain internal L-Phe:D-Phe pairs, i.e., (F:::f). Their Ramachandran angles range from φ = -127.6° and ψ = 132.4 ° with FFF:fff (**Fig. 6A**) to φ = -161.0° and ψ = 162.3° with racemic ester insulin (**Fig. 6B**). This means that there is significant flexibility that is available to the (F:::f) pair in the context of the antiparallel rippled sheet, which may become a useful design element if the interest of the materials community to the rippled sheet motif continues to grow.

Pleated β-sheets are often observed in fibrils formed by aggregating enantiopure peptides, where they tend to display a one-dimensional long-range order. Numerous structures are available through the work of the Eisenberg lab on steric zippers and related systems.[45–50] Some examples are shown in **Fig. S8**. In contrast to the long-range packing noted in the Eisenberg systems, we observed dimeric antiparallel rippled sheets with FFF:fff (**Fig. 2**), but those dimers did not form extended rippled sheets (**Figs. 3 and 4**). The lack of extended sheets may also be rooted in the hydrophobicity of the FFF:fff dimer that leads it to precipitate from water before it can mature into an extended fibrillary rippled sheet. Systematic optimization of crystallization parameters, including concentration, solvent identity, temperature, as well as variations in sequence, may allow the synthesis of extended fibrillary rippled sheet networks in the future. In that context it is interesting to compare our FFF:fff dimer structure with (a) the racemic Aβ40 structure, published in a recent collaborative study by the Raskatov and Tycko labs,[29] and (b) the hydrophobic Aβ16-22 segment in its interactions with its mirror-image, studied by the Nilsson lab. All three systems contain rippled antiparallel dimers, which is likely due, at least in part, to Coulombic attractions. However, there are important differences. Racemic Aβ40 forms fibrils with three Aβ40 units per layer and a fibril thickness of 7 ± 1 nm.[8] The crystalline Aβ16-22 aggregates, on the other hand, are micron-wide, which is consistent with the presence of thousands of peptides per layer.[25] Future X-ray structural studies of racemic Aβ16-22 should determine whether it (a) forms extended rippled sheets, (b) aggregates into rippled antiparallel cross-β dimers that then pack in ways similar to FFF:fff, or (c) packs in a way that is completely different.

Our findings have to be put in context with the recent paper by Liu and Gellman, where peptides designed to form two-stranded β-hairpins, composed of half L and half D residues did not exhibit any heterochiral stand pairing detectable by solution NMR.[24] It is noteworthy that one of the systems studied by the authors contained the VFF motif that is present in Aβ and is believed to be important for racemic Aβ fibrillization (*i.e.*, Aβ Chiral Inactivation, Aβ-CI).[7,25,29] The VFF motif is also very similar in terms of its size and hydrophobicity to the FFF motif studied here. A possible reason for the apparent discrepancy is that in Gellman's work, the L- and D- sequences were linked together, which may have induced a preference for homochiral strand pairing. Possibly more significantly, FFF:fff crystallization (similarly to Aβ-CI and the racemic Aβ16-22 model system studied by Nilsson) appears to occur under kinetic control, whereas the foldamers of the Gellman hairpin were monitored under thermodynamic equilibrium conditions. Similarly (albeit in the non-polar solvent $CDCl_3$), Chung and Nowick found that hydrophobic β-turn peptide mimics preferentially form homochiral (pleated) dimers.[23] Another important difference between our work and the two solution NMR studies is that, in our study, the rippled antiparallel FFF:fff dimers are packed into a three-dimensional crystal lattice that may, in itself, be a ripple-genic factor. In contrast, the solution NMR studies lacked evidence for the formation of higher order aggregates, and instead highlighted interactions between dimerizing peptide strands as isolated entities.

It may be tempting to ascribe the difference between the solution NMR experiments discussed above and our findings to the fact that solution NMR work studied systems as pure dimers, whereas our work produced extended layers, in which the individual dimers were stabilized through interactions with the crystal lattice. However, we are aware of a crystal structure

Chemical Science Accepted Manuscript

View Article Online
DOI: 10.1039/D1SC05731F

of the GSTSTA peptide in a racemic mixture with its enantiomer, in which self-sorting into pleated fibrillary structures was observed, showing that racemic aggregating peptide mixtures are not ripple-genic *per se* either.[30] In this specific case, it may have been because GSTSTA lacks bulky, hydrophobic groups that appear to promote rippled sheet formation.[17] Yet it seems that the presence of bulky residues is not obligate either, as the first rippled sheet structure was reported for polyglycine I, which does not have sidechains.[18,19] It should also be noted that, in addition to sequence, aggregation conditions are important. As such, it was noted with the MAX1:DMAX system developed by the Schneider lab, that the rigidity of the hydrogels formed depended on whether peptides were aggregated under kinetic or thermodynamic control, with thermodynamically controlled assembly producing the most rigid hydrogel systems.[3,4,17] These are all conditions that should be explored in future research.

CONCLUSIONS

We presented crystal-structural insights into a rippled sheet-based nanostructure that we obtained by temperature-controlled crystallization of FFF:fff. The structure consists of arrays of dimeric antiparallel rippled sheet, whose internal structural parameters agree well with the predictions by Pauling and Corey. The rippled dimers are arranged in a herringbone-pattern, into networks that are held together by in-plane salt bridges and hydrogen bonds and display lateral long-range segregation into hydrophobic and hydrophilic domains. Comparison of FFF:fff with the three orphaned rippled sheets identified by analyzing the racemic protein crystallography PDB supports the notion of Phe as a ripple-genic residue. Systematic exploration of Phe-containing racemic peptide mixtures may provide a rational framework on how to devise functional rippled sheet materials in the future.

MATERIALS AND METHODS

Peptide Synthesis. The (L,L,L)-triphenylalanine (*i.e.*, FFF) and (D,D,D)-triphenylalanine (*i.e.*, fff) peptides were synthesized by standard Fmoc-based, solid-phase peptide chemistry, following our previously reported protocols.[39,51] Both peptides were synthesized using preloaded, Fmoc-phenylalanine 4-alkoxybenzyl alcohol Wang resin: Fmoc-L-Phe-Wang (Sigma) or Fmoc-D-Phe-Wang (Fisher). All syntheses were performed manually at 0.2 mM scale relative to resin loading. An orbital shaker was used for mixing in both the deprotection and coupling steps. The resin was swelled in 3 mL of dimethylformamide (DMF) in a filter tube, housing 250 mg Fmoc-Phe Wang resin (0.796 mmol/g loading) for 20 min. For Fmoc-deprotection, 30% piperidine (Spectrum) in DMF was added to the resin, and allowed to shake on an orbital shaker for 20 min. The deprotection solution was rinsed with DMF (3x) and dichloromethane (DCM, 2x) and the deprotection step was repeated. Coupling reagents used were 4 eq. *N*,*N*-diisopropylethylamine (Fisher), 3 eq. *N*,*N*,*N*',*N*'-tetramethyl-O-(1*H*-benzotriazol-1-yl)uronium hexafluorophosphate (Fisher) and 3 eq. hydroxybenzotriazole hydrate (Oakwood Products). For amino acid coupling, 3 eq. of either Fmoc-L-Phe-OH (Fisher) or Fmoc-D-Phe-OH (ChemPep) with coupling reagents listed above were dissolved in 3 mL DMF and added to the reaction vessel, and allowed to shake for 30 min. The coupling step was repeated for each amino acid addition to improve yield. The aforementioned steps were repeated to produce the resin-bound tripeptides, NH_2-L-FFF-COOH and NH_2-D-fff-COOH. The peptides were cleaved and deprotected with a mixture consisting of trifluoroacetic acid (10 mL, Fisher), tri-isopropylsilane (1 mL, Fisher), and liquefied phenol (0.5 mL, Sigma). The peptide identities were confirmed with mass spectrometry (Fig. S1-S2). Peptides were purified by reverse-phase high-performance liquid chromatography (HPLC) with PLRP-S columns (Agilent), as previously described,[39,51] yielding peptides with purities exceeding 95% (Figure S1-S2). HPLC was conducted under basic conditions (0.1% NH_4OH), to reduce aggregation and/or precipitation. Samples were lyophilized and stored as solid powders at –40 °C.

Chemical Science Accepted Manuscript

View Article Online
DOI: 10.1039/D1SC05731F

Crystallization. Solutions of L-FFF and D-fff peptides were prepared separately by dissolving 7 mg of each individual peptide in 4 mL of nanopure water. The resulting solutions were sonicated and transferred to an oil bath at 90 °C and kept under stirring for one hour. To enhance dissolution of the cloudy slurries, 80 µL of hexafluoroisopropanol (HFIP; Fisher) was added to the solutions (2% of total volume), but significant cloudiness was still observed. After an additional 1 h of heating in the oil bath, the two individual peptide solutions were combined by adding D-fff to the L-FFF solution, dropwise. The resulting cloudy solution was rapidly transferred to a Teflon lined stainless steel autoclave, which was sealed and placed on an oven at 75 °C for 10 d followed by a slow colling process at a rate of 0.1°C/min, leading to the formation of colorless, needle-like crystals.

Single-Crystal X-ray Diffraction. A suitable colorless needle with dimensions of 0.1 x 0.09 x 0.03 mm^3 was used for single-crystal X-ray diffraction data collection at 100 K on a Rigaku XtaLAB Synergy-S diffractometer using Cu K_α radiation (λ = 1.54 Å). Data collection, processing and reduction were performed with $CrysAlis^{Pro}$.[52] After face indexing, numerical absorption correction was applied using gaussian integration. Empirical absorption correction using spherical harmonics was applied using SCALE3 ABSPACK scaling algorithm. The structure was solved by intrinsic phasing using ShelXT and refined with ShelXL via Olex2.[53–55] All non-hydrogen atoms were refined anisotropically using standard procedures.[56] Atomic displacement parameters for hydrogen atoms in the terminal amine group were fixed to 1.5(U_{iso}) of the attached nitrogen atom. For all other hydrogen atoms, the values were fixed to 1.2(U_{iso}) of the atoms to which they are attached. The N-H distances in the amine and amide groups were restrained to 0.91(2) Å and 0.88(2) Å, respectively. All other hydrogen atoms were placed at geometrically calculated positions and refined using a riding model.

Computational Chemistry. The input geometry for the optimization of FFF:fff was generated using the crystallographic data. The optimization was performed using ORCA 4.2.1, using Becke's 1988 exchange functional and Perdew's 1986 correlation functional (*i.e.*, BP86)[57,58] and the resolution of the identity approximation. Ahlrichs' def2-SVP basis set and the def2/J auxiliary basis set were used.[59,60] An atom-pairwise dispersion correction with the Becke-Johnson damping scheme was applied (D3BJ).[61,62] Implicit aqueous solvation was achieved using a conductor-like polarizable continuum model (CPCM=water).[63]

CSD Search. A systematic search of the CSD (version 5.41) was performed using ConQuest (version 2.0.4). Two queries were submitted simultaneously. The first searched for a C(C)C(O)NHC(C)C(O)NHC(C)C(O)NH fragment with all bond types set to "any", with both φ torsion angles from -180–0°, and with both ψ torsion angles within the range 0–180°. The second query required the presence of a distinct C(C)C(O)NHC(C)C(O)NHC(C)C(O)NH fragment with all bond types set to "any", with both φ torsion angles from 0–180°, and with both ψ torsion angles within the range -180–0°. The hits from this search were inspected manually and none featured a rippled sheet motif.

PDB Structural Database Mining. The PDB database was searched for the term "Racemic", and the results were narrowed by selecting "protein" as the polymer entity type, producing a total of 387 hits. The majority of those hits were, however, not truly racemic protein structures, but rather, enantiomerically pure proteins complexed with racemic molecules or simply included racemic compounds used during synthesis. These were excluded from our search. From the remaining hits, we manually selected those, in which the mirror-image proteins had β-strands oriented in ways that made them potentially capable of forming rippled sheets. This eventually produced three structures that can be accessed through the PDB via reference codes 4WPY[42], 4IUZ[43], and 3ODV.[44]

Chemical Science Accepted Manuscript

View Article Online
DOI: 10.1039/D1SC05731F

Considerations Regarding Nomenclature. In the original theory papers Pauling and Corey introduced the concepts of the pleated sheet that since became textbook knowledge as the β-sheet, and the closely related, but understudied rippled sheet[16]. Those seminal papers discussed periodic layer structures, and the original definition of sheets originated from there. However, this nomenclature since evolved: it is now common to refer to adequately paired peptide strands of the same handedness as pleated β-sheets. In this paper we follow analogy and refer to adequately paired peptide strands of opposite chirality as rippled β-sheets. The periodic β-sheets are discussed in the context of fibril structures, which is specified where necessary.

ACKNOWLEDGEMENTS

This work was supported by the NIH awards R21AG058074 and R21AG070888 to J.A.R., as well as the NIH pre-doctoral fellowship F31AG066377 to A.J.K.; The single-crystal X-ray diffractometer housed in UCSC X-ray Diffraction Facility was funded by NSF MRI grant 2018501.

AUTHOR CONTRIBUTIONS

The author contributions are defined below according to the CRediT contributor roles taxonomy. Conceptualization: J.A.R. Investigation, formal analysis, and methodology: A.J.K., B.E., J.A.R., and T.C.J. Supervision, resources, and funding acquisition: J.A.R., S.R.J.O., and T.C.J. Writing – original draft: A.J.K. and J.A.R. Writing – review and editing: All authors.

Chemical Science Accepted Manuscript

View Article Online
DOI: 10.1039/D1SC05731F

REFERENCES

1 T. N. M. Schumacher, L. M. Mayr, D. L. Minor Jr., M. A. Milhollen, M. W. Burgess and P. S. Kim, Identification of D-Peptide Ligands Through Mirror-Image Phage Display, *Science*, 1996, **271**, 1854–1857.

2 D. M. Eckert, V. N. Malashkevich, L. H. Hong, P. A. Carr and P. S. Kim, Inhibiting HIV-1 entry: Discovery of D-peptide inhibitors that target the gp41 coiled-coil pocket, *Cell*, 1999, **99**, 103–115.

3 K. Nagy-Smith, P. J. Beltramo, E. Moore, R. Tycko, E. M. Furst and J. P. Schneider, Molecular, Local, and Network-Level Basis for the Enhanced Stiffness of Hydrogel Networks Formed from Coassembled Racemic Peptides: Predictions from Pauling and Corey, *ACS Cent. Sci.*, 2017, **3**, 586–597.

4 K. J. Nagy, M. C. Giano, A. Jin, D. J. Pochan and J. P. Schneider, Enhanced mechanical rigidity of hydrogels formed from enantiomeric peptide assemblies, *J. Am. Chem. Soc.*, 2011, **133**, 14975–14977.

5 D. Willbold and J. Kutzsche, Do we need anti-prion compounds to treat Alzheimer's disease?, *Molecules*, 2019, **24**, 2237.

6 T. Van Groen, S. Schemmert, O. Brener, L. Gremer, T. Ziehm, M. Tusche, L. Nagel-Steger, I. Kadish, E. Schartmann, A. Elfgen, D. Jürgens, A. Willuweit, J. Kutzsche and D. Willbold, The Aβ oligomer eliminating D-enantiomeric peptide RD2 improves cognition without changing plaque pathology, *Sci. Rep.*, 2017, **7**, 16275.

7 S. Dutta, A. R. Foley, C. J. A. Warner, X. Zhang, M. Rolandi, B. Abrams and J. A. Raskatov, Suppression of Oligomer Formation and Formation of Non-Toxic Fibrils upon Addition of Mirror-Image Aβ42 to the Natural L-Enantiomer, *Angew. Chemie. - Int. Ed.*, 2017, **56**, 11506–11510.

8 S. Dutta, A. R. Foley, A. J. Kuhn, B. Abrams, H. W. Lee and J. A. Raskatov, New insights into differential aggregation of enantiomerically pure and racemic Aβ40 systems, *Pept. Sci.*, 2019, **111**, e24139.

9 A. R. Foley, G. P. Roseman, K. Chan, A. Smart, T. S. Finn, K. Yang, R. Scott Lokey, G. L. Millhauser and J. A. Raskatov, Evidence for aggregation-independent, PrPC-mediated Aβ cellular internalization, *Proc. Natl. Acad. Sci. U.S.A.*, 2020, **117**, 28625–28631.

10 A. R. Foley and J. A. Raskatov, Understanding and controlling amyloid aggregation with chirality, *Curr. Opin. Chem. Biol.*, 2021, **64**, 1–9.

11 T. O. Yeates and S. B. H. Kent, Racemic protein crystallography, *Annu. Rev. Biophys.*, 2012, **41**, 41–61.

12 K. W. Kurgan, A. F. Kleman, C. A. Bingman, D. F. Kreitler, B. Weisblum, K. T. Forest and S. H. Gellman, Retention of Native Quaternary Structure in Racemic Melittin Crystals, *J. Am. Chem. Soc.*, 2019, **141**, 7704–7708.

13 L. E. Zawadzke and J. M. Berg, The structure of a centrosymmetric protein crystal, *Proteins Struct. Funct. Bioinforma.*, 1993, **16**, 301–305.

14 B. L. Pentelute, Z. P. Gates, V. Tereshko, J. L. Dashnau, J. M. Vanderkooi, A. A. Kossiakoff and S. B. H. Kent, X-ray structure of snow flea antifreeze protein determined by racemic crystallization of synthetic protein enantiomers, *J. Am. Chem. Soc.*, 2008, **130**, 9695–9701.

15 L. Pauling and R. B. Corey, The pleated sheet, a new layer configuration of polypeptide chains, *Proc. Natl. Acad. Sci. U.S.A.*, 1951, **37**, 251–256.

16 L. Pauling and R. B. Corey, Two Rippled-Sheet Confirgurations of Polypeptide Chains, and a Note about the Pleated Sheets, *Proc. Natl. Acad. Sci. U.S.A.*, 1953, **39**, 253–256.

17 J. A. Raskatov, J. P. Schneider and B. L. Nilsson, Defining the Landscape of the Pauling-Corey Rippled Sheet: An Orphaned Motif Finding New Homes, *Acc. Chem. Res.*, 2021, **54**, 2488–2501.

18 B. Lotz, Crystal structure of polyglycine I, *J. Mol. Biol.*, 1974, **87**, 169–180.

19 F. Colonna-Cesari, S. Premilat and B. Lotz, Structure of polyglycine I: A comparison of the antiparallel pleated and antiparallel rippled sheets, *J. Mol. Biol.*, 1974, **87**, 181–191.

20 W. H. Moore and S. Krimm, Vibrational analysis of peptides, polypeptides, and proteins. I. Polygylcine I, *Biopolymers*, 1976, **15**, 2439–2464.

21 I. Weissbuch, R. A. Illos, G. Bolbach and M. Lahav, Racemic β-sheets as templates of relevance to the origin of homochirality of peptides: Lessons from crystal chemistry, *Acc. Chem. Res.*, 2009, **42**, 1128–1140.

22 I. Rubinstein, R. Eliash, G. Bolbach, I. Weissbuch and M. Lahav, Racemic β sheets in

Chemical Science Accepted Manuscript

View Article Online
DOI: 10.1039/D1SC05731F

biochirogenesis, *Angew. Chemie. - Int. Ed.*, 2007, **46**, 3710–3713.
23 D. M. Chung and J. S. Nowick, Enantioselective Molecular Recognition between β-Sheets, *J. Am. Chem. Soc.*, 2004, **126**, 3062–3063.
24 X. Liu and S. H. Gellman, Comparisons of β-Hairpin Propensity Among Peptides with Homochiral or Heterochiral Strands, *ChemBioChem*, 2021, **22**, 2772–2776.
25 J. M. Urban, J. Ho, G. Piester, R. Fu and B. L. Nilsson, Rippled β-sheet formation by an amyloid-β fragment indicates expanded scope of sequence space for enantiomeric β-sheet peptide coassembly, *Molecules*, 2019, **24**, 1983.
26 R. J. Swanekamp, J. T. M. Dimaio, C. J. Bowerman and B. L. Nilsson, Coassembly of enantiomeric amphipathic peptides into amyloid-inspired rippled β-sheet fibrils, *J. Am. Chem. Soc.*, 2012, **134**, 5556–5559.
27 A. M. Garcia, C. Giorgiutti, Y. El Khoury, V. Bauer, C. Spiegelhalter, E. Leize-Wagner, P. Hellwig, N. Potier and V. Torbeev, Aggregation and Amyloidogenicity of the Nuclear Coactivator Binding Domain of CREB-Binding Protein, *Chem. – A. Eur. J.*, 2020, **26**, 9889–9899.
28 V. Torbeev, M. Grogg, J. Ruiz, R. Boehringer, A. Schirer, P. Hellwig, G. Jeschke and D. Hilvert, Chiral recognition in amyloid fiber growth, *J. Pept. Sci.*, 2016, **22**, 290–304.
29 J. A. Raskatov, A. R. Foley, J. M. Louis, W.-M. Yau and R. Tycko, Constraints on the Structure of Fibrils Formed by a Racemic Mixture of Amyloid-β Peptides from Solid-State NMR, Electron Microscopy, and Theory, *J. Am. Chem. Soc.*, 2021, **143**, 13299–13313.
30 C.-T. Zee, C. Glynn, M. Gallagher-Jones, J. Miao, C. G. Santiago, D. Cascio, T. Gonen, M. R. Sawaya and J. A. Rodriguez, Homochiral and racemic MicroED structures of a peptide repeat from the ice-nucleation protein InaZ, *IUCrJ*, 2019, **6**, 197–205.
31 J. Ghanta, C. L. Shen, L. L. Kiessling and R. M. Murphy, A strategy for designing inhibitors of β-amyloid toxicity, *J Biol Chem*, 1996, **271**, 29525–29528.
32 T. L. Lowe, A. Strzelec, L. L. Kiessling and R. M. Murphy, Structure - Function relationships for inhibitors of β-Amyloid toxicity containing the recognition sequence KLVFF, *Biochemistry*, 2001, **40**, 7882–7889.
33 S. Brahmachari, Z. A. Arnon, A. Frydman-Marom, E. Gazit and L. Adler-Abramovich, Diphenylalanine as a Reductionist Model for the Mechanistic Characterization of β-Amyloid Modulators, *ACS Nano.*, 2017, **11**, 5960–5969.
34 C. Guo, Y. Luo, R. Zhou and G. Wei, Triphenylalanine peptides self-assemble into nanospheres and nanorods that are different from the nanovesicles and nanotubes formed by diphenylalanine peptides, *Nanoscale*, 2014, **6**, 2800–2811.
35 E. Mayans, J. Casanovas, A. M. Gil, A. I. Jiménez, C. Cativiela, J. Puiggalí and C. Alemán, Diversity and Hierarchy in Supramolecular Assemblies of Triphenylalanine: From Laminated Helical Ribbons to Toroids, *Langmuir*, 2017, **33**, 4036–4048.
36 P. Tamamis, L. Adler-Abramovich, M. Reches, K. Marshall, P. Sikorski, L. Serpell, E. Gazit and G. Archontis, Self-assembly of phenylalanine oligopeptides: Insights from experiments and simulations, *Biophys. J.*, 2009, **96**, 5020–5029.
37 R. Roychaudhuri, M. Yang, M. M. Hoshi and D. B. Teplow, Amyloid-β protein assembly and Alzheimer disease, *J. Biol. Chem.*, 2009, **284**, 4749–4753.
38 J. Jaques, A. A. Collet and S. H. Wilen, *Enantiomers, Racemates, and Resolutions*, John Wiley & Sons, Ltd, 1991.
39 C. J. A. Warner, S. Dutta, A. R. Foley and J. A. Raskatov, A Tailored HPLC Purification Protocol That Yields High-purity Amyloid Beta 42 and Amyloid Beta 40 Peptides, Capable of Oligomer Formation, *JoVE*, 2017, e55482.
40 J. A. Raskatov, Conformational Selection as the Driving Force of Amyloid β Chiral Inactivation, *ChemBioChem*, 2020, **21**, 2945–2949.
41 J. A. Raskatov, A DFT study of structure and stability of pleated and rippled cross-β sheets with hydrophobic sidechains, *Biopolymers*, 2021, **112**, e23391.
42 R. D. Bunker, K. Mandal, G. Bashiri, J. J. Chaston, B. L. Pentelute, J. S. Lott, S. B. H. Kent and E. N. Baker, A functional role of Rv1738 in Mycobacterium tuberculosis persistence suggested by racemic protein crystallography, *Proc. Natl. Acad. Sci. U.S.A.*, 2015, **112**, 4310–4315.
43 M. Avital-Shmilovici, K. Mandal, Z. P. Gates, N. B. Phillips, M. A. Weiss and S. B. H. Kent, Fully convergent chemical synthesis of ester insulin: Determination of the high resolution X-ray structure by racemic protein crystallography, *J. Am. Chem. Soc.*, 2013, **135**, 3173–3185.

Chemical Science Accepted Manuscript

View Article Online
DOI: 10.1039/D1SC05731F

44 B. L. Pentelute, K. Mandal, Z. P. Gates, M. R. Sawaya, T. O. Yeates and S. B. H. Kent, Total chemical synthesis and X-ray structure of kaliotoxin by racemic protein crystallography, *Chem. Commun.*, 2010, **46**, 8174–8176.

45 M. R. Sawaya, S. Sambashivan, R. Nelson, M. I. Ivanova, S. A. Sievers, M. I. Apostol, M. J. Thompson, M. Balbirnie, J. J. W. Wiltzius, H. T. Mcfarlane, A. Ø. Madsen, C. Riekel and D. Eisenberg, Atomic structures of amyloid cross-β spines reveal varied steric zippers, *Nature*, 2007, **447**, 453–457.

46 M. P. Hughes, M. R. Sawaya, D. R. Boyer, L. Goldschmidt, J. A. Rodriguez, D. Cascio, L. Chong, T. Gonen and D. S. Eisenberg, Atomic structures of low-complexity protein segments reveal kinked β sheets that assemble networks, *Science*, 2018, **359**, 698–701.

47 E. L. Guenther, Q. Cao, H. Trinh, J. Lu, M. R. Sawaya, D. Cascio, D. R. Boyer, J. A. Rodriguez, M. P. Hughes and D. S. Eisenberg, Atomic structures of TDP-43 LCD segments and insights into reversible or pathogenic aggregation, *Nat. Struct. Mol. Biol.*, 2018, **25**, 463–471.

48 D. Li, E. M. Jones, M. R. Sawaya, H. Furukawa, F. Luo, M. Ivanova, S. A. Sievers, W. Wang, O. M. Yaghi, C. Liu and D. S. Eisenberg, Structure-based design of functional amyloid materials, *J. Am. Chem. Soc.*, 2014, **136**, 18044–18051.

49 J. A. Rodriguez, M. I. Ivanova, M. R. Sawaya, D. Cascio, F. E. Reyes, D. Shi, S. Sangwan, E. L. Guenther, L. M. Johnson, M. Zhang, L. Jiang, M. A. Arbing, B. L. Nannenga, J. Hattne, J. Whitelegge, A. S. Brewster, M. Messerschmidt, S. Boutet, N. K. Sauter, T. Gonen and D. S. Eisenberg, Structure of the toxic core of α-synuclein from invisible crystals., *Nature*, 2015, **525**, 486–490.

50 L. Saelices, L. M. Johnson, W. Y. Liang, M. R. Sawaya, D. Cascio, P. Ruchala, J. Whitelegge, L. Jiang, R. Riek and D. S. Eisenberg, Uncovering the mechanism of aggregation of human transthyretin, *J. Biol. Chem.*, 2015, **290**, 28932–28943.

51 A. J. Kuhn, B. S. Abrams, S. Knowlton and J. A. Raskatov, Alzheimer's Disease 'non-amyloidogenic' p3 Peptide Revisited: A Case for Amyloid-α, *ACS Chem. Neurosci.*, 2020, **11**, 1539–1544.

52 Rigaku, 2020, CrysAlisPro 1.171.41.110a.

53 G. M. Sheldrick, SHELXT - Integrated space-group and crystal-structure determination, *Acta Crystallogr. Sect. A Found. Crystallogr.*, 2015, **71**, 3–8.

54 G. M. Sheldrick, Crystal structure refinement with SHELXL, *Acta Crystallogr. Sect. C*, 2015, **71**, 3–8.

55 O. V. Dolomanov, L. J. Bourhis, R. J. Gildea, J. A. K. Howard and H. Puschmann, OLEX2: A complete structure solution, refinement and analysis program, *J. Appl. Crystallogr.*, 2009, **42**, 339–341.

56 P. Muller, Practical suggestions for better crystal structures, *Crystallogr. Rev.*, 2009, **15**, 57–83.

57 A. D. Becke, Density-functional exchange-energy approximation with correct asymptotic behavior, *Phys. Rev. A*, 1988, **38**, 3098–3100.

58 J. P. Perdew, Density-functional approximation for the correlation energy of the inhomogeneous electron gas, *Phys. Rev. B*, 1986, **33**, 8822–8824.

59 F. Weigend and R. Ahlrichs, Balanced basis sets of split valence, triple zeta valence and quadruple zeta valence quality for H to Rn: Design and assessment of accuracy, *Phys. Chem. Chem. Phys.*, 2005, **7**, 3297–3305.

60 F. Weigend, Accurate Coulomb-fitting basis sets for H to Rn, *Phys. Chem. Chem. Phys.*, 2006, **8**, 1057–1065.

61 S. Grimme, J. Antony, S. Ehrlich and H. Krieg, A consistent and accurate ab initio parametrization of density functional dispersion correction (DFT-D) for the 94 elements H-Pu, *J. Chem. Phys.*, 2010, **132**, 1–19.

62 S. Grimme, S. Ehrlich and L. Goerigk, Effect of the Damping Function in Dispersion Corrected Density Functional Theory, *J. Comput. Chem.*, 2011, **32**, 1456–1465.

63 M. Garcia-Ratés and F. Neese, Efficient implementation of the analytical second derivatives of hartree–fock and hybrid DFT energies within the framework of the conductor-like polarizable continuum model, *J. Comput. Chem.*, 2019, **40**, 1816–1828.

Chemical Science Accepted Manuscript

View Article Online
DOI: 10.1039/D1SC05731F

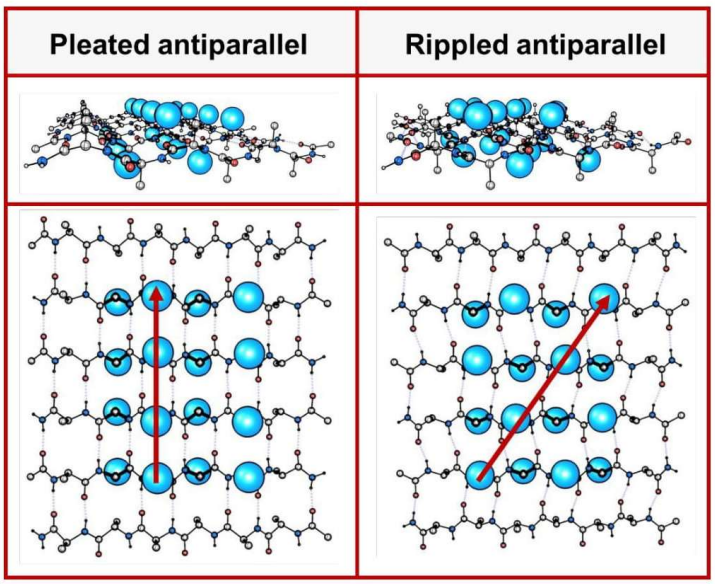

Figure 1. Left panel: Antiparallel pleated sheet in different projections. Right panel: Antiparallel rippled sheet in different projections. A selected number of amino acid side chains are depicted as blue spheres on the left panel (pleated, along red vertical line) and on the right (rippled, along red diagonal), to reduce steric repulsion in each case.

Chemical Science Accepted Manuscript

View Article Online
DOI: 10.1039/D1SC05731F

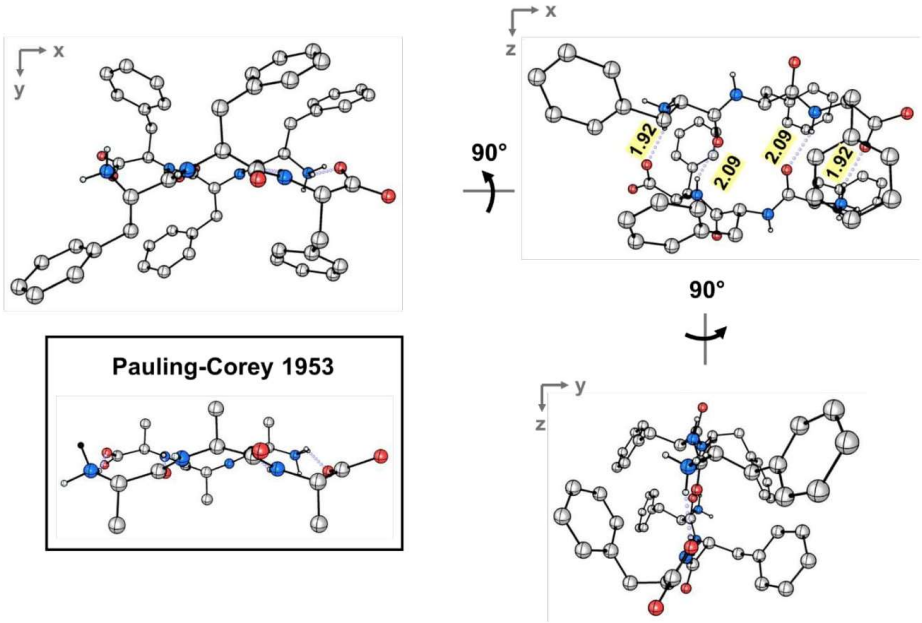

Figure 2. Ball-and-stick depiction of the experimental rippled antiparallel FFF:fff cross-β dimer, shown in three orthogonal projections. The Pauling-Corey rippled antiparallel backbone dimer is shown in the inset, with apical carbon atoms added geometrically to facilitate comparison; (color code: C, gray; O, red; N, blue).

Chemical Science Accepted Manuscript

View Article Online
DOI: 10.1039/D1SC05731F

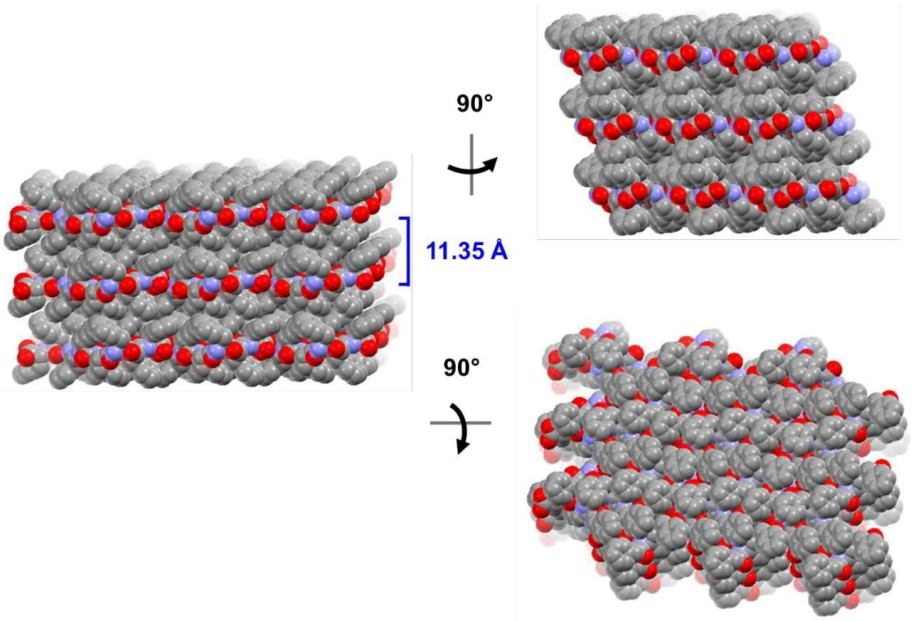

Figure 3. Long-range packing of the FFF:fff lattice, shown in three orthogonal projections. The layer-to-layer distance is indicated in blue.

Chemical Science Accepted Manuscript

View Article Online
DOI: 10.1039/D1SC05731F

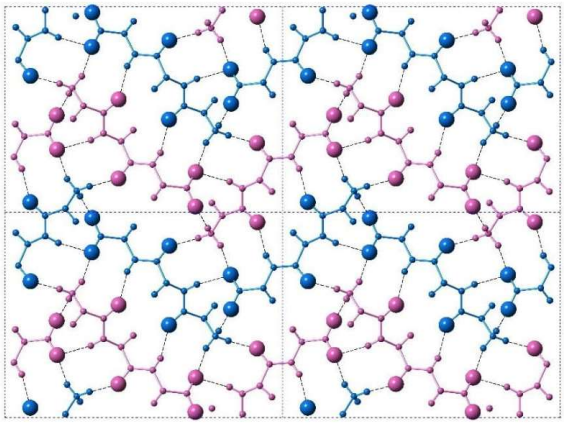

Figure 4. A top-on view of a single layer containing the peptidic backbones. Individual rippled antiparallel FFF:fff cross-β dimers are centered about the unit cell corners and center. L-peptides are shown in purple, and D-peptides are shown in blue.

Chemical Science Accepted Manuscript

View Article Online
DOI: 10.1039/D1SC05731F

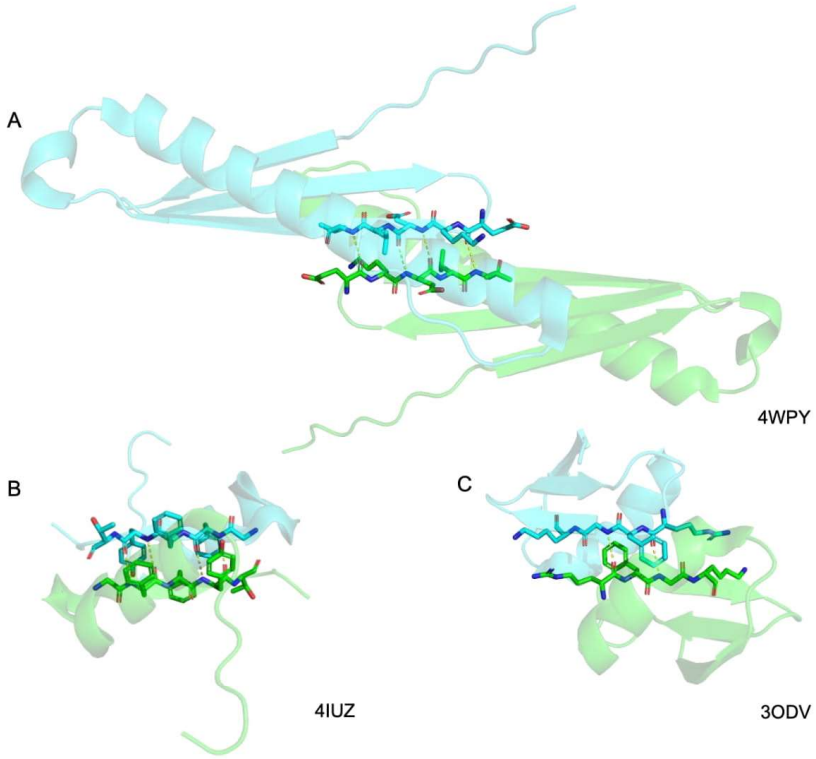

Fig. 5. Detail of the antiparallel rippled motifs in the proteins selected by the PDB structural database mining. (*A)* glu-lys-glu-leu-val sequence in RV1738.[42] (*B*) phe-phe-tyr sequence in ester insulin.[43] (*C*) lys-gly-phe-arg sequence in Kaliotoxin.[44] PDB codes are displayed on the bottom right.

Chemical Science Accepted Manuscript

View Article Online
DOI: 10.1039/D1SC05731F

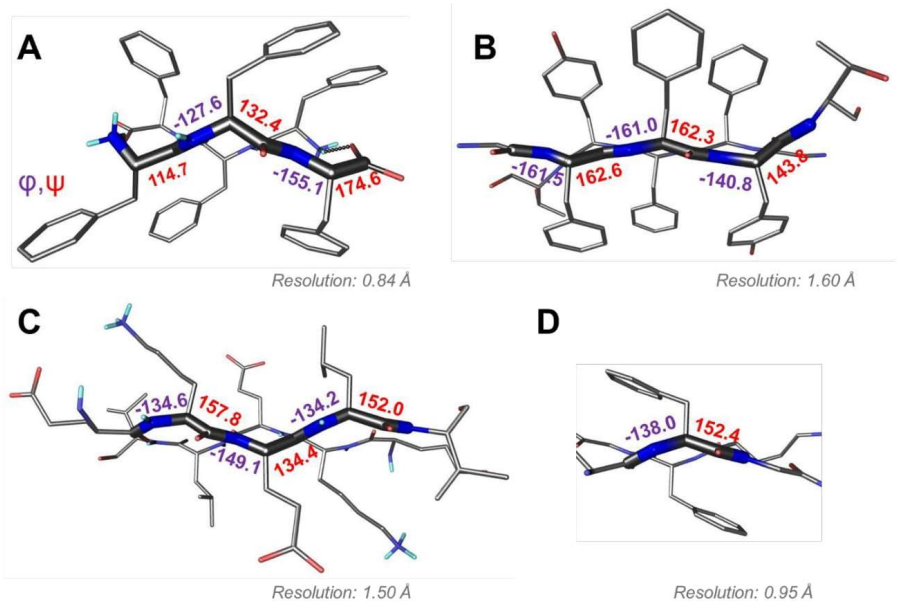

Fig. 6. Ramachandran angle analysis for the rippled sheets noted with A) the FFF:fff system; B) racemic Ester Insulin (4IUZ)[43]; C) racemic RV1738 (4WPY)[42]; D) racemic Kaliotoxin (3ODV).[44]

Chemical Science Accepted Manuscript

REFERENCES

(1) Deiana, A.; Forcelloni, S.; Porrello, A.; Giansanti, A. Intrinsically Disordered Proteins and Structured Proteins with Intrinsically Disordered Regions Have Different Functional Roles in the Cell. *PLoS One* **2019**, *14* (8), 1–16. https://doi.org/10.1371/journal.pone.0217889.

(2) Morris, O. M.; Torpey, J. H.; Isaacson, R. L. Intrinsically Disordered Proteins: Modes of Binding with Emphasis on Disordered Domains. *Open Biol.* **2021**, *11* (10). https://doi.org/10.1098/rsob.210222.

(3) Uversky, V. N.; Gillespie, J. R.; Fink, A. L. Why Are "natively Unfolded" Proteins Unstructured under Physiologic Conditions? *Proteins Struct. Funct. Genet.* **2000**, *41* (3), 415–427. https://doi.org/10.1002/1097-0134(20001115)41:3<415::AID-PROT130>3.0.CO;2-7.

(4) Olsen, J. G.; Teilum, K.; Kragelund, B. B. Behaviour of Intrinsically Disordered Proteins in Protein–Protein Complexes with an Emphasis on Fuzziness. *Cell Mol Life Sci* **2017**, *74* (17), 3175–3183. https://doi.org/10.1007/s00018-017-2560-7.

(5) Wright, P. E.; Dyson, H. J. Linking Folding and Binding. *Cur. Opin Struct Biol* **2009**, *19* (1), 31–38. https://doi.org/10.1016/j.sbi.2008.12.003.

(6) THAMBISETTY, M.; Howard, R.; Glymour, M. M.; Schneider, L. S. Alzheimer's Drugs: Does Reducing Amyloid Work? *Science* **2021**, *374* (6567),

544–545. https://doi.org/10.1126/science.abm1680.REF.

(7) Selkoe, D. J. Alzheimer's Drugs: Does Reducing Amyloid Work?-Response. *Science* **2021**, *374* (6567), 545–546. https://doi.org/10.1126/science.abm1680.REF.

(8) Kuhn, A. J.; Raskatov, J. Is the P3 Peptide (Aβ17-40, Aβ17-42) Relevant to the Pathology of Alzheimer's Disease? *J Alzheimer's Dis* **2020**, *74* (1), 43–53. https://doi.org/10.3233/JAD-191201.

(9) Willem, M.; Tahirovic, S.; Busche, M. A.; Ovsepian, S. V; Chafai, M.; Kootar, S.; Hornburg, D.; Evans, L. D. B.; Moore, S.; Daria, A.; Hampel, H.; et al. η-Secretase Processing of APP Inhibits Neuronal Activity in the Hippocampus. *Nature* **2015**, *526* (7573), 443–447. https://doi.org/10.1038/nature14864.

(10) Coronel, R.; Bernabeu-Zornoza, A.; Palmer, C.; Muñiz-Moreno, M.; Zambrano, A.; Cano, E.; Liste, I. Role of Amyloid Precursor Protein (APP) and Its Derivatives in the Biology and Cell Fate Specification of Neural Stem Cells. *Mol Neurobiol* **2018**, *55* (9), 7107–7117. https://doi.org/10.1007/s12035-018-0914-2.

(11) Lichtenthaler, S. F. Alpha-Secretase in Alzheimer's Disease: Molecular Identity, Regulation and Therapeutic Potential. *J Neurochem* **2011**, *116* (1), 10–21. https://doi.org/10.1111/j.1471-4159.2010.07081.x.

(12) Duong, D. M.; Peng, J.; Rees, H. D.; Wang, J.; Liao, L.; Levey, A. I.; Gearing, M.; Lah, J. J.; Cheng, D.; Losik, T. G. Proteomic Characterization of Postmortem Amyloid Plaques Isolated by Laser Capture Microdissection. *J*

Biol Chem **2004**, *279* (35), 37061–37068. https://doi.org/10.1074/jbc.m403672200.

(13) Drummond, E.; Nayak, S.; Faustin, A.; Pires, G.; Hickman, R. A.; Askenazi, M.; Cohen, M.; Haldiman, T.; Kim, C.; Han, X.; Shao, Y.; Safar, J. G.; Ueberheide, B.; Wisniewski, T. Proteomic Differences in Amyloid Plaques in Rapidly Progressive and Sporadic Alzheimer's Disease. *Acta Neuropathol* **2017**, *133* (6), 933–954. https://doi.org/10.1007/s00401-017-1691-0.

(14) Gowing, E.; Roher, A. E.; Woods, A. S.; Cotter, R. J.; Chaney, M.; Little, S. P.; Ball, M. J. Chemical Characterization of Abeta 17-42 Peptide, a Component of Diffuse Amyloid Deposits of Alzheimer Disease. *J Biol Chem* **1994**, *269* (15), 10987–10990.

(15) Lalowski, M.; Golabek, A.; Lemere, C. A.; Selkoe, D. J.; Wisniewski, H. M.; Beavis, R. C.; Frangione, B.; Wisniewski, T. The "Nonamyloidogenic" P3 Fragment (Amyloid Beta 17-42) Is a Major Constituent of Down's Syndrome Cerebellar Preamyloid. *J Biol Chem* **1996**, *271* (52), 33623–33631. https://doi.org/10.1074/jbc.271.52.33623.

(16) Warner, C. J. A.; Dutta, S.; Foley, A. R.; Raskatov, J. A. A Tailored HPLC Purification Protocol That Yields High-Purity Amyloid Beta 42 and Amyloid Beta 40 Peptides, Capable of Oligomer Formation. *JoVE* **2017**, No. 121, e55482. https://doi.org/doi:10.3791/55482.

(17) Perez-Garmendia, R.; Gevorkian, G. Pyroglutamate-Modified Amyloid Beta Peptides: Emerging Targets for Alzheimer´s Disease Immunotherapy. *Curr*

Neuropharmacol **2013**, *11* (5), 491–498. https://doi.org/10.2174/1570159X11311050004.

(18) Jawhar, S.; Wirths, O.; Bayer, T. A. Pyroglutamate Amyloid-Beta (Abeta): A Hatchet Man in Alzheimer Disease. *J Biol Chem* **2011**, *286* (45), 38825–38832. https://doi.org/10.1074/jbc.R111.288308.

(19) Bouter, Y.; Dietrich, K.; Wittnam, J. L.; Rezaei-Ghaleh, N.; Pillot, T.; Papot-Couturier, S.; Lefebvre, T.; Sprenger, F.; Wirths, O.; Zweckstetter, M.; Bayer, T. A. N-Truncated Amyloid β (Aβ) 4-42 Forms Stable Aggregates and Induces Acute and Long-Lasting Behavioral Deficits. *Acta Neuropathol* **2013**, *126* (2), 189–205. https://doi.org/10.1007/s00401-013-1129-2.

(20) Antonios, G.; Saiepour, N.; Bouter, Y.; Richard, B. C.; Paetau, A.; Verkkoniemi-Ahola, A.; Lannfelt, L.; Ingelsson, M.; Kovacs, G. G.; Pillot, T.; Wirths, O.; Bayer, T. A. N-Truncated Abeta Starting with Position Four: Early Intraneuronal Accumulation and Rescue of Toxicity Using NT4X-167, a Novel Monoclonal Antibody. *Acta Neuropathol. Commun.* **2014**, *2* (1), 1. https://doi.org/10.1186/2051-5960-1-56.

(21) Scheidt, H. A.; Adler, J.; Zeitschel, U.; Höfling, C.; Korn, A.; Krueger, M.; Roßner, S.; Huster, D. Pyroglutamate-Modified Amyloid β (11- 40) Fibrils Are More Toxic than Wildtype Fibrils but Structurally Very Similar. *Chem - A Eur J* **2017**, *23* (62), 15834–15838. https://doi.org/10.1002/chem.201703909.

(22) Dammers, C.; Reiss, K.; Gremer, L.; Lecher, J.; Ziehm, T.; Stoldt, M.; Schwarten, M.; Willbold, D. Pyroglutamate-Modified Amyloid-β(3–42) Shows

α-Helical Intermediates before Amyloid Formation. *Biophys J* **2017**, *112* (8), 1621–1633. https://doi.org/10.1016/j.bpj.2017.03.007.

(23) Dammers, C.; Schwarten, M.; Buell, A. K.; Willbold, D. Pyroglutamate-Modified Aβ(3-42) Affects Aggregation Kinetics of Aβ(1-42) by Accelerating Primary and Secondary Pathways. *Chem. Sci.* **2017**, *8* (7), 4996–5004. https://doi.org/10.1039/c6sc04797a.

(24) Dammers, C.; Schwarten, M.; Buell, A. K.; Willbold, D. Pyroglutamate-Modified Aβ(3-42) Affects Aggregation Kinetics of Aβ(1-42) by Accelerating Primary and Secondary Pathways. *Chem Sci* **2017**, *8* (7), 4996–5004. https://doi.org/10.1039/C6SC04797A.

(25) Conchillo-Solé, O.; de Groot, N. S.; Avilés, F. X.; Vendrell, J.; Daura, X.; Ventura, S. AGGRESCAN: A Server for the Prediction and Evaluation of "Hot Spots" of Aggregation in Polypeptides. *BMC Bioinformatics* **2007**, *8* (65), 1–17. https://doi.org/10.1186/1471-2105-8-65.

(26) Kuhn, A. J.; Abrams, B. S.; Knowlton, S.; Raskatov, J. A. Alzheimer's Disease "Non-Amyloidogenic" P3 Peptide Revisited: A Case for Amyloid-α. *ACS Chem Neurosci* **2020**, *11* (11), 1539–1544. https://doi.org/10.1021/acschemneuro.0c00160.

(27) Krysmann, M. J.; Castelletto, V.; Kelarakis, A.; Hamley, I. W.; Hule, R. A.; Pochan, D. J. Self-Assembly and Hydrogelation of an Amyloid Peptide Fragment. *Biochemistry* **2008**, *47*, 4597–4605.

(28) Bortolini, C.; Klausen, L. H.; Hoffmann, S. V.; Jones, N. C.; Saadeh, D.;

Wang, Z.; Knowles, T. P. J.; Dong, M. Rapid Growth of Acetylated Aβ(16-20) into Macroscopic Crystals. *ACS Nano* **2018**, *12* (6), 5408–5416. https://doi.org/10.1021/acsnano.8b00448.

(29) Arai, T.; Sasaki, D.; Araya, T.; Sato, T.; Sohma, Y. A Cyclic KLVFF-Derived Peptide Aggregation Inhibitor Induces the Formation of Less-Toxic off-Pathway Amyloid-β Oligomers. *ChemBioChem* **2014**, *15*, 2577–2583. https://doi.org/10.1002/cbic.201402430.

(30) Brahmachari, S.; Arnon, Z. A.; Frydman-Marom, A.; Gazit, E.; Adler-Abramovich, L. Diphenylalanine as a Reductionist Model for the Mechanistic Characterization of β-Amyloid Modulators. *ACS Nano* **2017**, *11* (6), 5960–5969. https://doi.org/10.1021/acsnano.7b01662.

(31) Reches, M.; Gazit, E. Casting Metal Nanowires within Discrete Self-Assembled Peptide Nanotubes. *Science* **2003**, *300* (5619), 625–627. https://doi.org/10.1126/science.1082387.

(32) Reches, M.; Gazit, E. Self-Assembly of Peptide Nanotubes and Amyloid-like Structures by Charged-Termini-Capped Diphenylalanine Peptide Analogues. *Isr J Chem* **2005**, *45* (3), 363–371. https://doi.org/10.1560/5mc0-v3dx-ke0b-yf3j.

(33) Lu, J.; Qiang, W.; Yau, W.; Schwieters, C. D.; Meredith, S. C.; Tycko, R. Molecular Structure of β-Amyloid Fibrils in Alzheimer's Disease Brain Tissue. *Cell* **2013**, *154* (6), 1257–1268. https://doi.org/10.1016/j.cell.2013.08.035.

(34) Westermark, P.; Benson, M. D.; Buxbaum, J. N.; Cohen, A. S.; Ikeda, S.;

Masters, C. L.; Merlini, G.; Maria, J.; Sipe, J. D. Amyloid: Toward Terminology Clarification Report from the Nomenclature Committee of the International Society of Amyloidosis. *Amyloid* **2005**, *12*, 1–4. https://doi.org/10.1080/13506120500032196.

(35) Benson, M. D.; Buxbaum, J. N.; Eisenberg, D. S.; Merlini, G.; Saraiva, M. J. M.; Sekijima, Y.; Sipe, J. D.; Westermark, P. Amyloid Nomenclature 2018: Recommendations by the International Society of Amyloidosis (ISA) Nomenclature Committee. *Amyloid* **2018**, *25* (4), 215–219. https://doi.org/10.1080/13506129.2018.1549825.

(36) Alzheimer's Association. *2021 Alzheimer's Disease Facts and Figures*; 2021; Vol. 17.

(37) Cummings, J.; Reiber, C.; Kumar, P. The Price of Progress: Funding and Financing Alzheimer's Disease Drug Development. *Alzheimer's Dement. Transl. Res. Clin. Interv.* **2018**, *4*, 330–343. https://doi.org/10.1016/j.trci.2018.04.008.

(38) Cummings, J.; Lee, G.; Ritter, A.; Sabbagh, M.; Zhong, K. Alzheimer's Disease Drug Development Pipeline: 2020. *Alzheimer's Dement. Transl. Res. Clin. Interv.* **2020**, *6* (1), 1–29. https://doi.org/10.1002/trc2.12050.

(39) Knopman, D. S. Lowering of Amyloid-Beta by β-Secretase Inhibitors — Some Informative Failures. *N Engl J Med* **2019**, *380*, 11–13. https://doi.org/10.1056/NEJMe1903193.

(40) Karran, E.; Mercken, M.; Strooper, B. De. The Amyloid Cascade Hypothesis

for Alzheimer's Disease: An Appraisal for the Development of Therapeutics. *Nat Rev Drug Discov* **2011**, *10* (9), 698–712. https://doi.org/10.1038/nrd3505.

(41) Karran, E.; Strooper, B. De. The Amyloid Cascade Hypothesis: Are We Poised for Success or Failure? *J Neurochem* **2016**, *139* (2), 237–252. https://doi.org/10.1111/jnc.13632.

(42) Cummings, J.; Lee, G.; Ritter, A.; Zhong, K. Alzheimer's Disease Drug Development Pipeline: 2018. *Alzheimer's Dement Transl Res Clin Interv* **2018**, *4*, 195–214. https://doi.org/10.1016/j.trci.2018.03.009.

(43) Barritt, J. D.; Younan, N. D.; Viles, J. H. N-Terminally Truncated Amyloid-β(11–40/42) Cofibrillizes with Its Full-Length Counterpart: Implications for Alzheimer's Disease. *Angew. Chemie. - Int. Ed.* **2017**, *56* (33), 9816–9819. https://doi.org/10.1002/anie.201704618.

(44) Wei, W.; Norton, D. D.; Wang, X.; Kusiak, J. W. Aβ 17-42 in Alzheimer's Disease Activates JNK and Caspase-8 Leading to Neuronal Apoptosis. *Brain* **2002**, *125*, 2036–2043. https://doi.org/10.1093/brain/awf205.

(45) Jang, H.; Arce, F. T.; Ramachandran, S.; Capone, R.; Azimova, R.; Kagan, B. L.; Nussinov, R.; Lal, R. Truncated β-Amyloid Peptide Channels Provide an Alternative Mechanism for Alzheimer's Disease and Down Syndrome. *Proc. Natl. Acad. Sci.* **2010**, *107* (14), 6538–6543. https://doi.org/10.1073/pnas.0914251107.

(46) Pike, C. J.; Overman, M. J.; Cotman, C. W. Amino-Terminal Deletions Enhance Aggregation of β-Amyloid Peptides in Vitro. *J Biol Chem* **1995**, *270*

(41), 23895–23899.

(47) Liu, R.; McAllister, C.; Lyubchenko, Y.; Sierks, M. R. Residues 17-20 and 30-35 of β-Amyloid Play Critical Roles in Aggregation. *J Neurosci Res* **2004**, *75* (2), 162–171. https://doi.org/10.1002/jnr.10859.

(48) Pauwels, K.; Williams, T. L.; Morris, K. L.; Jonckheere, W.; Vandersteen, A.; Kelly, G.; Schymkowitz, J.; Rousseau, F.; Pastore, A.; Serpell, L. C.; Broersen, K. Structural Basis for Increased Toxicity of Pathological Aβ42:Aβ40 Ratios in Alzheimer Disease. *J Biol Chem* **2012**, *287* (8), 5650–5660. https://doi.org/10.1074/jbc.M111.264473.

(49) Hasegawa, K.; Yamaguchi, I.; Omata, S.; Gejyo, F.; Naiki, H. Interaction between Aβ(1-42) and Aβ(1-40) in Alzheimer's β-Amyloid Fibril Formation in Vitro. *Biochemistry* **1999**, *38* (47), 15514–15521. https://doi.org/10.1021/bi991161m.

(50) Cukalevski, R.; Yang, X.; Meisl, G.; Weininger, U.; Bernfur, K.; Frohm, B.; Knowles, T. P. J.; Linse, S. The Aβ40 and Aβ42 Peptides Self-Assemble into Separate Homomolecular Fibrils in Binary Mixtures but Cross-React during Primary Nucleation. *Chem. Sci.* **2015**, *6* (7), 4215–4233. https://doi.org/10.1039/c4sc02517b.

(51) Jan, A.; Gokce, O.; Luthi-Carter, R.; Lashuel, H. A. The Ratio of Monomeric to Aggregated Forms of Aβ40 and Aβ42 Is an Important Determinant of Amyloid-β Aggregation, Fibrillogenesis, and Toxicity. *J Biol Chem* **2008**, *283* (42), 28176–28189. https://doi.org/10.1074/jbc.M803159200.

(52) Kyte, J.; Doolittle, R. F. A Simple Method for Displaying the Hydropathic Character of a Protein. *J. Mol. Biol.* **1982**, *157* (1), 105–132. https://doi.org/10.1016/0022-2836(82)90515-0.

(53) Vadukul, D. M.; Gbajumo, O.; Marshall, K. E.; Serpell, L. C. Amyloidogenicity and Toxicity of the Reverse and Scrambled Variants of Amyloid-β 1-42. *FEBS Lett* **2017**, *591* (5), 822–830. https://doi.org/10.1002/1873-3468.12590.

(54) Zou, K.; Kim, D.; Kakio, A.; Byun, K.; Gong, J. S.; Kim, J.; Kim, M.; Sawamura, N.; Nishimoto, S. I.; Matsuzaki, K.; Lee, B.; Yanagisawa, K.; Michikawa, M. Amyloid β-Protein Aβ1-40 Protects Neurons from Damage Induced by Aβ1-42 in Culture and in Rat Brain. *J Neurochem* **2003**, *87* (3), 609–619. https://doi.org/10.1046/j.1471-4159.2003.02018.x.

(55) Dutta, S.; Foley, A. R.; Warner, C. J. A.; Zhang, X.; Rolandi, M.; Abrams, B.; Raskatov, J. A. Suppression of Oligomer Formation and Formation of Non-Toxic Fibrils upon Addition of Mirror-Image Aβ42 to the Natural L-Enantiomer. *Angew. Chemie. - Int. Ed.* **2017**, *56* (38), 11506–11510. https://doi.org/10.1002/anie.201706279.

(56) Dutta, S.; Foley, A. R.; Warner, C. J. A.; Zhang, X.; Rolandi, M.; Abrams, B.; Raskatov, J. A. Suppression of Oligomer Formation and Formation of Non-Toxic Fibrils upon Addition of Mirror-Image Aβ42 to the Natural L-Enantiomer. *Angew. Chemie. - Int. Ed.* **2017**, *56* (38), 11506–11510. https://doi.org/10.1002/anie.201706279.

(57) Dutta, S.; Finn, T. S.; Kuhn, A. J.; Abrams, B.; Raskatov, J. A. Chirality Dependence of Amyloid Beta Cellular Uptake and a New Mechanistic Perspective. *ChemBioChem* **2019**, *20*, 1023–1026. https://doi.org/10.1002/cbic.201800708.

(58) Malmos, K. G.; Blancas-mejia, L. M.; Weber, B.; Ramirez-alvarado, M.; Naiki, H.; Otzen, D.; Gade, K.; Blancas-mejia, L. M.; Weber, B.; Ramirez-alvarado, M.; Naiki, H.; Otzen, D. ThT 101: A Primer on the Use of Thioflavin T to Investigate Amyloid Formation. **2017**, *6129*. https://doi.org/10.1080/13506129.2017.1304905.

(59) Ahmed, M.; Davis, J.; Aucoin, D.; Sato, T.; Ahuja, S.; Aimoto, S.; Elliott, J. I.; Van Nostrand, W. E.; Smith, S. O. Structural Conversion of Neurotoxic Amyloid-Beta(1-42) Oligomers to Fibrils. *Nat Struct Mol Biol* **2010**, *17* (5), 561–567. https://doi.org/10.1038/nsmb.1799.

(60) Foley, A. R.; Finn, T. S.; Kung, T.; Hatami, A.; Lee, H. W.; Jia, M.; Rolandi, M.; Raskatov, J. A. Trapping and Characterization of Nontoxic Aβ42 Aggregation Intermediates. *ACS Chem Neurosci* **2019**, *10* (8), 3880–3887. https://doi.org/10.1021/acschemneuro.9b00340.

(61) Haass, C.; Selkoe, D. J. Soluble Protein Oligomers in Neurodegeneration: Lessons from the Alzheimer's Amyloid Beta-Peptide. *Nat Rev Mol Cell Biol* **2007**, *8* (2), 101–112. https://doi.org/10.1038/nrm2101.

(62) Gong, Y.; Chang, L.; Viola, K. L.; Lacor, P. N.; Lambert, M. P.; Finch, C. E.; Krafft, G. A.; Klein, W. L. Alzheimer's Disease-Affected Brain: Presence of

Oligomeric A Beta Ligands (ADDLs) Suggests a Molecular Basis for Reversible Memory Loss. *Proc. Natl. Acad. Sci. U.S.A.* **2003**, *100* (18), 10417–10422. https://doi.org/10.1073/pnas.1834302100.

(63) Szczepanik, A. M.; Rampe, D.; Ringheim, G. E. Amyloid-Beta Peptide Fragments P3 and P4 Induce pro-Inflammatory Cytokine and Chemokine Production in Vitro and in Vivo. *J Neurochem* **2001**, *77* (1), 304–317. https://doi.org/10.1046/j.1471-4159.2001.00240.x.

(64) Walsh, D. M.; Klyubin, I.; Fadeeva, J. V.; Cullen, W. K.; Anwyl, R.; Wolfe, M. S.; Rowan, M. J.; Selkoe, D. J. Naturally Secreted Oligomers of Amyloid-β Protein Potently Inhibit Hippocampal Long-Term Potentiation in Vivo. *Nature* **2002**, *416* (6880), 535–539. https://doi.org/10.1038/416535a.

(65) Hensley, K.; Carney, J. M.; Mattson, M. P.; Aksenova, M.; Harris, M.; Wu, J. F.; Floyd, R. A.; Butterfield, D. A. A Model for β-Amyloid Aggregation and Neurotoxicity Based on Free Radical Generation by the Peptide: Relevance to Alzheimer Disease. *Proc. Natl. Acad. Sci. U.S.A.* **1994**, *91* (8), 3270–3274. https://doi.org/10.1073/pnas.91.8.3270.

(66) Shearman, M. S.; Ragan, C. I.; Iversen, L. L. Inhibition of PC12 Cell Redox Activity Is a Specific, Early Indicator of the Mechanism of β-Amyloid-Mediated Cell Death. *Proc. Natl. Acad. Sci. U.S.A.* **1994**, *91* (4), 1470–1474. https://doi.org/10.1073/pnas.91.4.1470.

(67) Behl, C.; Davis, J. B.; Lesley, R.; Schubert, D. Hydrogen Peroxide Mediates Amyloid β Protein Toxicity. *Cell* **1994**, *77* (6), 817–827.

https://doi.org/10.1016/0092-8674(94)90131-7.

(68) Mattson, M. P.; Goodman, Y. Different Amyloidogenic Peptides Share a Similar Mechanism of Neurotoxicity Involving Reactive Oxygen Species and Calcium. *Brain Res* **1995**, *676* (1), 219–224. https://doi.org/10.1016/0006-8993(95)00148-J.

(69) Oguchi, T.; Ono, R.; Tsuji, M.; Shozawa, H.; Somei, M.; Inagaki, M.; Mori, Y.; Yasumoto, T.; Ono, K.; Kiuchi, Y. Cilostazol Suppresses Aß-Induced Neurotoxicity in SH-SY5Y Cells through Inhibition of Oxidative Stress and MAPK Signaling Pathway. *Front. Aging Neurosci.* **2017**, *9* (OCT), 1–12. https://doi.org/10.3389/fnagi.2017.00337.

(70) Jin, S.; Kedia, N.; Illes-Toth, E.; Haralampiev, I.; Prisner, S.; Herrmann, A.; Wanker, E. E.; Bieschke, J. Amyloid-β(1- 42) Aggregation Initiates Its Cellular Uptake and Cytotoxicity. *J Biol Chem* **2016**, *291* (37), 19590–19606. https://doi.org/10.1074/jbc.M115.691840.

(71) LaFerla, F. M.; Green, K. N.; Oddo, S. Intracellular Amyloid-β in Alzheimer's Disease. *Nat Rev Neurosci* **2007**, *8* (7), 499–509. https://doi.org/10.1038/nrn2168.

(72) Foley, A. R.; Roseman, G. P.; Chan, K.; Smart, A.; Finn, T. S.; Yang, K.; Scott Lokey, R.; Millhauser, G. L.; Raskatov, J. A. Evidence for Aggregation-Independent, PrPC-Mediated Aβ Cellular Internalization. *Proc. Natl. Acad. Sci. U.S.A.* **2020**, *117* (46), 28625–28631. https://doi.org/10.1073/pnas.2009238117.

(73) Warner, C. J. A.; Dutta, S.; Foley, A. R.; Raskatov, J. A. Introduction of D-Glutamate at a Critical Residue of Aβ42 Stabilizes a Pre-Fibrillary Aggregate with Enhanced Toxicity. *Chem - A Eur J* **2016**, *22* (34), 11967–11970.

(74) AU - Warner, C. J. A.; AU - Dutta, S.; AU - Foley, A. R.; AU - Raskatov, J. A. A Tailored HPLC Purification Protocol That Yields High-Purity Amyloid Beta 42 and Amyloid Beta 40 Peptides, Capable of Oligomer Formation. *JoVE* **2017**, No. 121, e55482. https://doi.org/doi:10.3791/55482.

(75) Anthis, N. J.; Clore, G. M. Sequence-Specific Determination of Protein and Peptide Concentrations by Absorbance at 205 Nm. *Protein Sci* **2013**, *22* (6), 851–858. https://doi.org/10.1002/pro.2253.

(76) Dutta, S.; Finn, T. S.; Kuhn, A. J.; Abrams, B.; Raskatov, J. A. Chirality Dependence of Amyloid β Cellular Uptake and a New Mechanistic Perspective. *ChemBioChem* **2019**, *20*, 1–5. https://doi.org/10.1002/cbic.201800708.

(77) Pujadas, L.; Rossi, D.; Andrés, R.; Teixeira, C. M.; Serra-Vidal, B.; Parcerisas, A.; Maldonado, R.; Giralt, E.; Carulla, N.; Soriano, E. Reelin Delays Amyloid-Beta Fibril Formation and Rescues Cognitive Deficits in a Model of Alzheimer's Disease. *Nat Commun* **2014**, *5*. https://doi.org/10.1038/ncomms4443.

(78) Lurs, T.; Ritter, C.; Adrian, M.; Riek-loher, D.; Bohrmann, B.; Do, H.; Schubert, D.; Riek, R. 3D Structure of Alzheimer's Amyloid- Beta (1 – 42) Fibrils. *Proc. Natl. Acad. Sci.* **2005**, *102* (48), 17342–17347.

(79) Schmidt, M.; Rohou, A.; Lasker, K.; Yadav, J. K.; Schiene-Fischer, C.; Fändrich, M.; Grigorieff, N. Peptide Dimer Structure in an Aβ(1-42) Fibril Visualized with Cryo-EM. *Proc. Natl. Acad. Sci. U.S.A.* **2015**, *112* (38), 11858–11863. https://doi.org/10.1073/pnas.1503455112.

(80) Gremer, L.; Scholzel, D.; Schenk, C.; Reinartz, E.; Labahn, J.; Ravelli, R. B. G.; Tusche, M.; Lopez-Iglesias, C.; Hoyer, W.; Heise, H.; Willbold, D.; Schroder, G. F. Fibril Structure of Amyloid Beta 1-42 by Cryoelectron Microscopy. *Science* **2017**, *358* (6359), 116–119.

(81) Wälti, M. A.; Ravotti, F.; Arai, H.; Glabe, C. G.; Wall, J. S.; Böckmann, A.; Güntert, P.; Meier, B. H.; Riek, R. Atomic-Resolution Structure of a Disease-Relevant Aβ(1–42) Amyloid Fibril. *Proc. Natl. Acad. Sci.* **2016**, *113* (34), E4976–E4984. https://doi.org/10.1073/pnas.1600749113.

(82) Xiao, Y.; Ma, B.; McElheny, D.; Parthasarathy, S.; Long, F.; Hoshi, M.; Nussinov, R.; Ishii, Y. Aβ(1-42) Fibril Structure Illuminates Self-Recognition and Replication of Amyloid in Alzheimer's Disease. *Nat Struct Mol Biol* **2015**, *22* (6), 499–505. https://doi.org/10.1038/nsmb.2991.

(83) Colvin, M. T.; Silvers, R.; Ni, Q. Z.; Can, T. V.; Sergeyev, I.; Rosay, M.; Donovan, K. J.; Michael, B.; Wall, J.; Linse, S.; Griffin, R. G. Atomic Resolution Structure of Monomorphic Aβ42 Amyloid Fibrils. *J Am Chem Soc* **2016**, *138* (30), 9663–9674. https://doi.org/10.1021/jacs.6b05129.

(84) Kuhn, A. J.; Raskatov, J. A. *Using Mirror-Image Peptides to Enhance Robustness and Reproducibility in Studying the Amyloid β-Protein*, 1st ed.;

Elsevier Inc., 2019; Vol. 168. https://doi.org/10.1016/bs.pmbts.2019.05.010.

(85) Foley, A. R.; Raskatov, J. A. Assessing Reproducibility in Amyloid β Research: Impact of Aβ Sources on Experimental Outcomes. *ChemBioChem* **2020**, *21* (17), 2425–2430. https://doi.org/10.1002/cbic.202000125.

(86) Roychaudhuri, R.; Yang, M.; Hoshi, M. M.; Teplow, D. B. Amyloid-β Protein Assembly and Alzheimer Disease. *J Biol Chem* **2009**, *284* (8), 4749–4753. https://doi.org/10.1074/jbc.R800036200.

(87) Lesné, S.; Koh, M. T.; Kotilinek, L.; Kayed, R.; Glabe, C. G.; Yang, A.; Gallagher, M.; Ashe, K. H. A Specific Amyloid-β Protein Assembly in the Brain Impairs Memory. *Nature* **2006**, *440* (7082), 352–357. https://doi.org/10.1038/nature04533.

(88) Soto, C.; Pritzkow, S. Protein Misfolding, Aggregation, and Conformational Strains in Neurodegenerative Diseases. *Nat Neurosci* **2018**, *21* (10), 1332–1340. https://doi.org/10.1038/s41593-018-0235-9.

(89) Schnabel, J. Little Proteins, Big Clues. *Nature* **2011**, *475*, S12–S14.

(90) Dutta, S.; Foley, A. R.; Kuhn, A. J.; Abrams, B.; Lee, H. W.; Raskatov, J. A. New Insights into Differential Aggregation of Enantiomerically Pure and Racemic Aβ40 Systems. *Pept. Sci.* **2019**, *111* (6), e24139. https://doi.org/10.1002/pep2.24139.

(91) Pauling, L.; Corey, R. B. Two Rippled-Sheet Confirgurations of Polypeptide Chains, and a Note about the Pleated Sheets. *Proc. Natl. Acad. Sci. U.S.A.* **1953**, *39* (4), 253–256.

(92) Guo, C.; Luo, Y.; Zhou, R.; Wei, G. Triphenylalanine Peptides Self-Assemble into Nanospheres and Nanorods That Are Different from the Nanovesicles and Nanotubes Formed by Diphenylalanine Peptides. *Nanoscale* **2014**, *6* (5), 2800–2811. https://doi.org/10.1039/c3nr02505e.

Appendix

A. RightsLinks

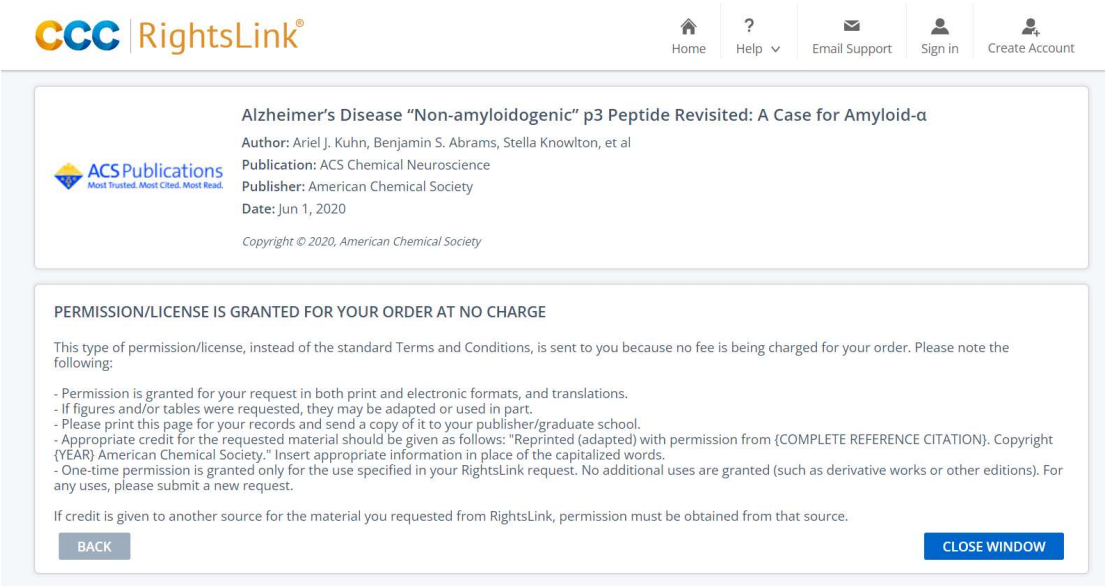

Permissions for: Kuhn, A. J. Raskatov, R. A. Is the p3 (Aβ17-40, Aβ17-42) peptide relevant to the pathology of Alzheimer's Disease? *J. Alz. Dis.* **2020**, 74 (1), 43-53. PMID: 32176648. doi: 10.3233/JAD-191201

Carry Koolbergen 6:05 AM (4 hours ago)
to me

Dear Ariel Kuhn,

We hereby grant you permission to reproduce the below mentioned material in **print and electronic format** at no charge subject to the following conditions:

1. If any part of the material to be used (for example, figures) has appeared in our publication with credit or acknowledgement to another source, permission must also be sought from that source. If such permission is not obtained then that material may not be included in your publication/copies.

2. Suitable acknowledgement to the source must be made, either as a footnote or in a reference list at the end of your publication, as follows:

"Reprinted from Publication title, Vol number, Author(s), Title of article, Pages No., Copyright (Year), with permission from IOS Press".
"The publication is available at IOS Press through http://dx.doi.org/[insert DOI]"

3. This permission is granted for non-exclusive world **English** rights only. For other languages please reapply separately for each one required.

4. Reproduction of this material is confined to the purpose for which permission is hereby given.

Yours sincerely

Carry Koolbergen (Mrs.)
Contracts, Rights & Permissions Coordinator
Not in the office on Wednesdays

IOS Press | Nieuwe Hemweg 6B, 1013 BG Amsterdam, The Netherlands
Tel.: +31 (0)20 688 3355/ +31 (0) 687 0022 | c.koolbergen@iospress.nl | www.iospress.nl
Twitter: @IOSPress_STM | Facebook: publisheriospress
View the latest IOS Press newsletter here
Confidentiality note: This e-mail may contain confidential information from IOS Press. If that is the case any disclosure, copying, distribution or use of the contents of this e-mail is strictly prohibited. If you are not the intended recipient, please delete this e-mail and notify the sender immediately.

CCC | RightsLink®

My Orders | My Library | My Profile | Welcome ajkuhn@ucsc.edu | Log out | Help | FAQ

My Orders > Orders > All Orders

License Details

This Agreement between Ariel J. Kuhn ("You") and John Wiley and Sons ("John Wiley and Sons") consists of your license details and the terms and conditions provided by John Wiley and Sons and Copyright Clearance Center.

Print Copy

License Number	5182250786198
License date	Nov 04, 2021
Licensed Content Publisher	John Wiley and Sons
Licensed Content Publication	PEPTIDE SCIENCE
Licensed Content Title	New insights into differential aggregation of enantiomerically pure and racemic Aß40 systems
Licensed Content Author	Jevgenij A. Raskatov, Hsiau-Wei Lee, Benjamin Abrams, et al
Licensed Content Date	Oct 6, 2019
Licensed Content Volume	111
Licensed Content Issue	6
Licensed Content Pages	6
Type of Use	Dissertation/Thesis
Requestor type	Author of this Wiley article
Format	Electronic
Portion	Full article
Will you be translating?	No
Title	Using mirror-image peptides to enhance robustness and reproducibility in studying the amyloid β-protein
Institution name	University of California, Santa Cruz
Expected presentation date	Dec 2021
Order reference number	45678
Requestor Location	Ariel J. Kuhn

CCC | RightsLink®

My Orders | My Library | My Profile | Welcome ajkuhn@ucsc.edu | Log out | Help | FAQ

My Orders > Orders > All Orders

License Details

This Agreement between Ariel J. Kuhn ("You") and John Wiley and Sons ("John Wiley and Sons") consists of your license details and the terms and conditions provided by John Wiley and Sons and Copyright Clearance Center.

Print Copy

License Number	5182251445108
License date	Nov 04, 2021
Licensed Content Publisher	John Wiley and Sons
Licensed Content Publication	ChemBioChem
Licensed Content Title	Chirality Dependence of Amyloid β Cellular Uptake and a New Mechanistic Perspective
Licensed Content Author	Jevgenij A. Raskatov, Benjamin Abrams, Ariel J. Kuhn, et al
Licensed Content Date	Feb 27, 2019
Licensed Content Volume	20
Licensed Content Issue	8
Licensed Content Pages	4
Type of Use	Dissertation/Thesis
Requestor type	Author of this Wiley article
Format	Electronic
Portion	Full article
Will you be translating?	No
Title	Using mirror-image peptides to enhance robustness and reproducibility in studying the amyloid β-protein
Institution name	University of California, Santa Cruz
Expected presentation date	Dec 2021
Order reference number	45678
Requestor Location	Ariel J. Kuhn

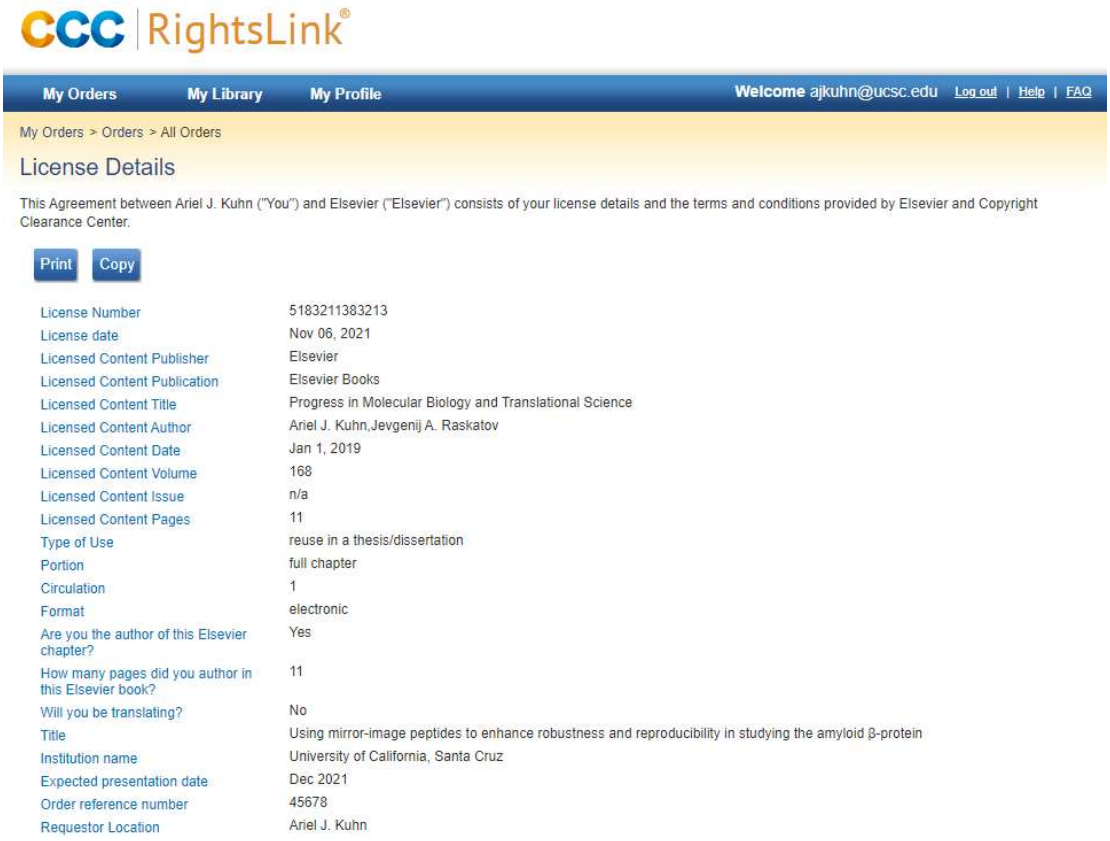

CCC RightsLink®

My Orders | My Library | My Profile | Welcome ajkuhn@ucsc.edu | Log out | Help | FAQ

My Orders > Orders > All Orders

License Details

This Agreement between Ariel J. Kuhn ("You") and Elsevier ("Elsevier") consists of your license details and the terms and conditions provided by Elsevier and Copyright Clearance Center.

Print Copy

License Number	5183211383213
License date	Nov 06, 2021
Licensed Content Publisher	Elsevier
Licensed Content Publication	Elsevier Books
Licensed Content Title	Progress in Molecular Biology and Translational Science
Licensed Content Author	Ariel J. Kuhn,Jevgenij A. Raskatov
Licensed Content Date	Jan 1, 2019
Licensed Content Volume	168
Licensed Content Issue	n/a
Licensed Content Pages	11
Type of Use	reuse in a thesis/dissertation
Portion	full chapter
Circulation	1
Format	electronic
Are you the author of this Elsevier chapter?	Yes
How many pages did you author in this Elsevier book?	11
Will you be translating?	No
Title	Using mirror-image peptides to enhance robustness and reproducibility in studying the amyloid β-protein
Institution name	University of California, Santa Cruz
Expected presentation date	Dec 2021
Order reference number	45678
Requestor Location	Ariel J. Kuhn

RightsLink for Figure 13: Roychaudhuri, R.; Yang, M.; Hoshi, M. M.; Teplow, D. B. Amyloid-β Protein Assembly and Alzheimer Disease. *J Biol Chem* **2009**, *284* (8), 4749–4753.

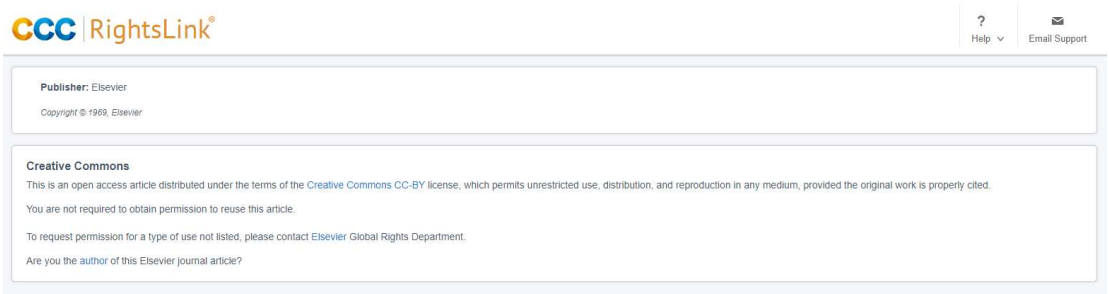

CCC RightsLink®

Help | Email Support

Publisher: Elsevier

Copyright © 1969, Elsevier

Creative Commons

This is an open access article distributed under the terms of the Creative Commons CC-BY license, which permits unrestricted use, distribution, and reproduction in any medium, provided the original work is properly cited.

You are not required to obtain permission to reuse this article.

To request permission for a type of use not listed, please contact Elsevier Global Rights Department.

Are you the author of this Elsevier journal article?

Permissions for Figure 5: Gowing, E.; Ball, M. J.; et. al. *J. Biol. Chem.* **1994.**

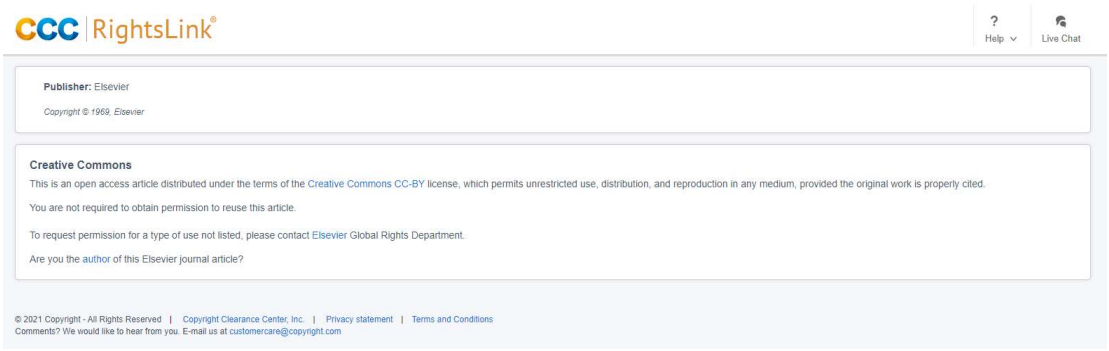

Permissions for Figure 5: Lalowski, M.; Wisniewski, T.; et. al. *J. Biol. Chem.* 1996.

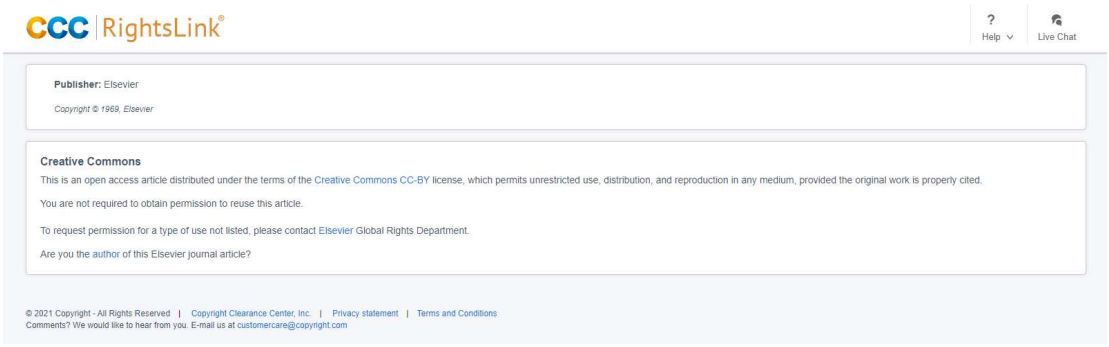

B. Supporting Information (SI) for reprinted publications

B.1

Alzheimer's Disease "non-amyloidogenic" p3 peptide revisited: a case for Amyloid-α

Ariel J. Kuhn[a], Benjamin S. Abrams[b], Stella Knowlton[a], Jevgenij A. Raskatov[a]*

[a] Dept. of Chemistry and Biochemistry, University of California Santa Cruz, CA 95064, United States

[b] Dept. of Biomolecular Engineering, Life Sciences Microscopy Center, University of California Santa Cruz, CA 95064, United States

SUPPORTING INFORMATION

Table of Contents

	Page #
General Experimental Procedures	3
Figure S1. Histogram revealing number of annual publications on Aβ from 1955 until February 2020, according to PubMed.	4
Table S1. Literature analysis of conflicting findings characterizing the p3 peptide	5
Figure S2. Mass spectrometry and analytical HPLC characterization of a representative synthetic batch of $p3_{17-40}$.	6
Figure S3. Mass spectrometry and analytical HPLC characterization of a representative synthetic batch of $Aβ_{1-40}$.	6
Figure S4. Mass spectrometry and analytical HPLC characterization of a representative synthetic batch of $p3_{F19Y}$.	7
Figure S5. Mass spectrometry and analytical HPLC characterization of a representative synthetic batch of $p3_{F20Y}$.	7
Figure S6. Mass spectrometry and analytical HPLC characterization of a representative synthetic batch of TAMRA-labelled $Aβ_{1-40}$.	8
Figure S7. Mass spectrometry and analytical HPLC characterization of a representative synthetic batch of TAMRA-labelled $p3_{17-40}$.	8
Figure S8. TEM images of $Aβ_{1-40}$ prepared quiescently or under agitation.	9
Figure S9. TEM images of $p3_{17-40}$ prepared quiescently or under agitation as well as TEM images of TAMRA-labelled-$p3_{17-40}$ prepared quiescently or under agitation.	10
Figure S10. ThT – monitored aggregation kinetics of Aβ seeded with p3 fibrils.	11
Figure S11. TEM images of kinetically trapped, intermediate oligomers of $Aβ_{1-40}$ and $p3_{17-40}$.	12
Figure S12. SH-SY5Y Cellular Viability of Oligomeric p3 and Aβ	12
Figure S13. Sequences of p3 singly substituted peptides and SDS-PAGE gel of photo-induced crosslinked samples of Aβ, p3, $p3_{F19Y}$, and $p3_{F20Y}$ with non-crosslinked controls included.	13
Figure S14. ThT- monitored aggregation kinetics and biological activity of $Aβ_{1-40}$, $p3_{17-40}$, $p3_{F19Y}$, and $p3_{F20Y}$.	13

General Experimental Procedures

Peptide Preparation. Purification of Aβ40 was done as previously published.[2] For p3, solid, lyophilized peptide was dissolved in 8:2 0.1% NH_4OH H_2O/acetonitrile and purified using PLRP-S columns (8 μm, 300 Å) under basic conditions. All peptide purities range from 95-99%. The concentration of p3 was determined by the absorbance of the peptide backbone at 205 nm via Nanodrop (ε = 83,370 M^{-1} cm^{-1}) using the protein parameter calculator (http://nickanthis.com/tools/a205.html).[3] The concentration of Aβ40 was determined at 280 nm (ε = 1490 M^{-1} cm^{-1}).

Microscopy. Samples were imaged on a JEOL 1230 microscope at University of California Santa Cruz or a Tecnai-12 microscope at University of California Berkeley.

Oligomer Image Analysis. The TEM images of oligomers were converted to 8-bit and the following filters were applied: 1) process → filters → median → radius = 4. 2) Image → Adjust → Auto Local Threshold → method = Phansalkar; radius = 15. 3) Process → Noise → Despeckle. 4) Process → Binary → Fill holes. 5) Process → Binary → Watershed. 6) Analyze → Set Measurements → Select Area, Limit to Threshold, Decimal places = 2. 7) Analyze → Analyze Particles → Set Size = 120 – infinity, Circularity = 0.35-1 → Add to Manager. The area values were then converted to diameters and displayed as a histogram.

ThT Assay. ThT (Acros Organics, 2390-54-7) was dissolved in 10 mL of PBS buffer containing 0.02% (w/v) NaN_3 and filtered through a 0.22 μm filter. The concentration was determined by Nanodrop at 412 nm (ε = 36000$M^{-1}cm^{-1}$). Lyophilized samples of peptide were prepared as described above at 20 μM, with 20 μM ThT in PBS. 200 μL of sample was added to each well, in triplicate, of a black, clear bottom 96-well plate. Absorbance readings were measured ever 5 min with 5 s of shaking before reading and 295 s of shaking between readings at 37 °C with a Biotek synergy HTX fluorescence plate reader (λ_{ex} = 444 nm λ_{em} = 485 nm).

TAMRA Quenching Assay. Lyophilized TAMRA-Aβ40 and TAMRA-p3 were each dissolved in 20 mM NaOH, and sonicated for 30 s. The samples were diluted in PBS and the corresponding concentrations were determined by Nanodrop (ε = 99000 M^{-1} cm^{-1}) at 555 nm. Readings were collected on a plate reader as described above (λ_{ex} = 550 nm λ_{em} = 580 nm).

Peptide structure images. Coordinates of peptide structures were downloaded from the pdb database (2M4J, 4NTR, 6CG4, and 3MOQ) and rendered using the freely available VMD software. Centroid-to-centroid distances were calculated using the ChemCraft program package.

Cellular viability. Lyophilized peptides were dissolved in 15 μL of 20 mM NaOH and the solutions were diluted to a final concentration of 50 μM with culture media. The samples were then incubated at 4 °C for 6 hours (consistent with method employed in Fig. 3 and S11, per published method by Ahmed *et. al.*[5]) The culture media intended for the vehicle cells as well as the blank samples was also incubated at 4 °C for 6 hours to account for any effects induced by low temperature. Human neuroblastoma SH-SY5Y cells were cultured in 1:1 DMEM: F12 K media supplemented with 10% fetal bovine serum and 1% penicillin-streptomycin. Cells were incubated at 37 °C with 5% CO_2. SH-SY5Y cells were plated in a 96-well plate at a density of 50,000 cells/well (100 μL total volume/well) and allowed to adhere for 24 h before dosing. After dosing, SH-SY5Y cells were incubated for 72 h at 37 °C. Then, 10 μL aliquots of WST-1 (Roche) were added to each well and incubated for 4 h. Then, absorbance was measured at λ = 490nm. Each bar represents an average of four replicates, normalized against the vehicle (cells and media only).

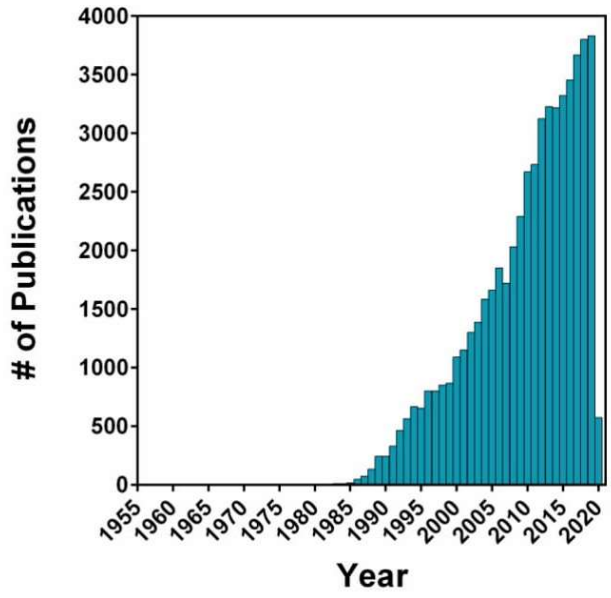

Figure S1. Histogram revealing number of annual publications on Aβ from 1955 until February 2020, according to PubMed.

Table S1. Literature analysis of conflicting findings characterizing the p3 peptide

CATEGORY	QUESTION	EVIDENCE TO SUPPORT	EVIDENCE TO CONTRADICT	AMBIGUOUS EVIDENCE
ISOLATION FROM AD PATIENTS	**From brains?**	1. p3 identified as major constituent of Down syndrome cerebellar preamyloid plaques[6] 2. major component of diffuse amyloid plaques[7]	1. No p3 isolated from sporadic AD brains[8]	1. p3 minor component of AD plaques[9] 2. p3 found in diffuse plaques and dystrophic neurites, but not in plaque cores[10]
	From cerebrospinal fluid (CSF)?	1. p3 levels in CSF correlates with mild cognitive impairment[11]		
AGGREGATION PROPENSITY	**Fibrilization possible?**	1. p3 formed irregular fibers[12] 2. fibril formation[13] 3. short fragments dissimilar to Aβ[14]	1. p3 formed intricate, dense lattices, unlike Aβ[15] 2. amorphous aggregates[6] 3. Small, granular particles[16]	1. Few p3 fibrils formed that were in dense networks shorter and narrower than Aβ[17]
	Theoretical simulations of fibrils	1. MD simulation of p3 fibrils[18]		
	ThT binding?	1. ThT positive[14,17]	1. ThT negative[15]	1. Very little ThT binding[6,12]
	Oligomerization possible?		1. Unable to trap oligomers[19]	
	Theoretical simulation of oligomerization	1. Molecular model of $A\beta_{18-41}$ oligomers[20] 2. MD simulations of theorized trimers and paranuclei[21] 3. MD simulations of theorized U- and S-shaped intermediates[22,23]	1. Simulations of p3 oligomers unstable[19]	
TOXICITY	**To cellular models?**	1. fresh and aged p3 found to be toxic to rat hippocampal neurons[17] 2. aged p3 toxic to SH-SY5Y cells[24] 3. toxicity to SH-SY5Y and IMR-32 cells[25] 3.p3 **formed** ion channels in cells, disrupting Ca^{2+} regulation, causing neuronal death[26] 4. p3 activated JNK and caspase-8[25]		
LONG-TERM POTENTIATION (LTP)	**Affected by p3?**		1. p3 found to not inhibit rat hippocampal LTP (11.5nM)[27]	
PRO-INFLAMMATORY CYTOKINE AND CHEMOKINE PRODUCTION	**Affected by p3?**	1. p3 stimulated production of IL-1α, IL-1β, IL-6, TNFα, MCP-1[28]		

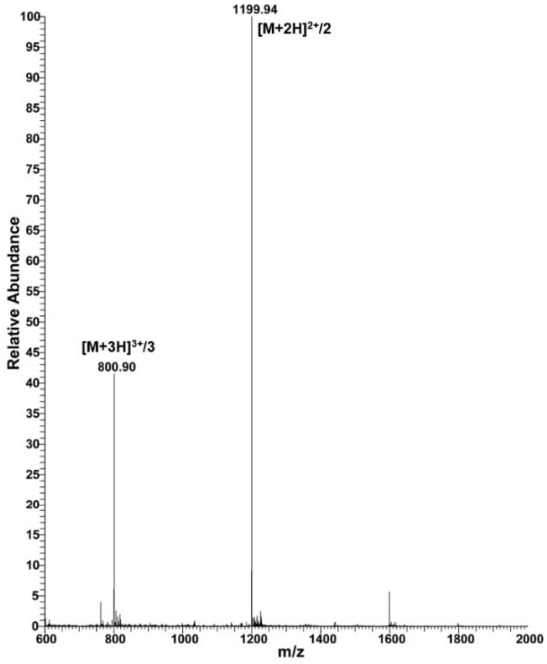

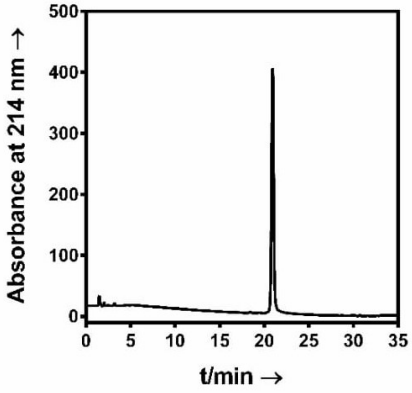

Peak #	Time (min)	Area	% Area
1	18.426	25.8	0.370
2	19.486	24.2	0.348
3	20.513	33.3	0.479
4	20.937	6876.5	98.803

Figure S2. Mass spectrometry and analytical HPLC characterization of a representative synthetic batch of $p3_{17-40}$.

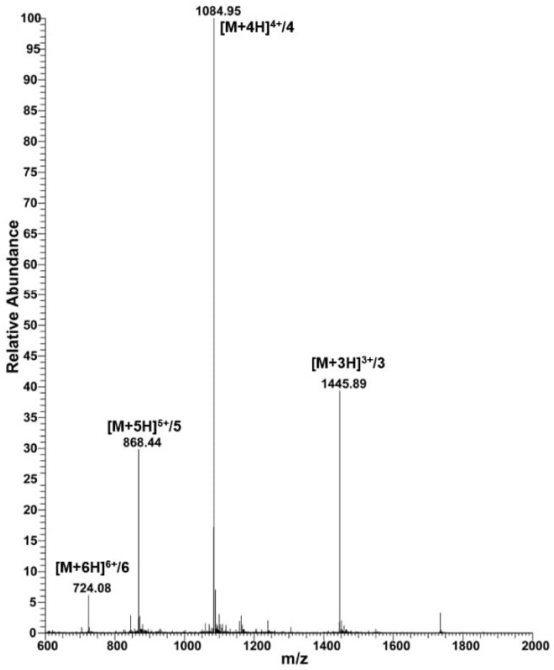

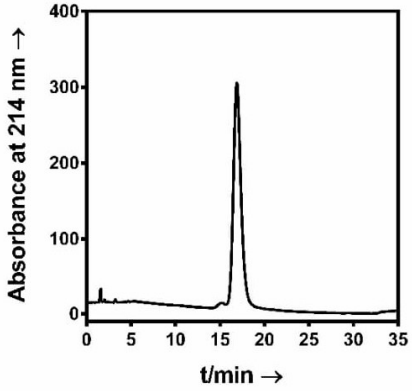

Peak #	Time (min)	Area	% Area
1	15.193	375.3	2.018
2	16.895	18187	97.786
3	19.121	36.4	0.196

Figure S3. Mass spectrometry and analytical HPLC characterization of a representative synthetic batch of $A\beta_{1-40}$.

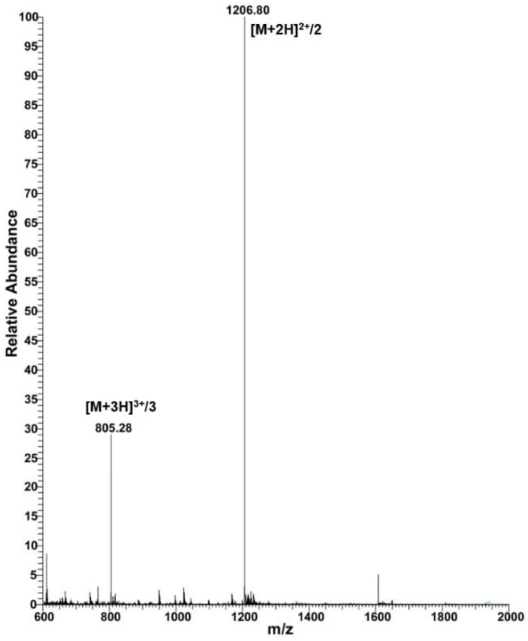

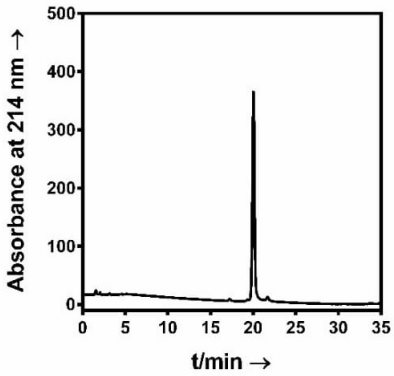

Peak #	Time (min)	Area	% Area
1	16.88	37.4	0.518
2	19.467	7210.8	98.672
3	20.972	59.2	0.810

Figure S4. Mass spectrometry and analytical HPLC characterization of a representative synthetic batch of $p3_{F19}$

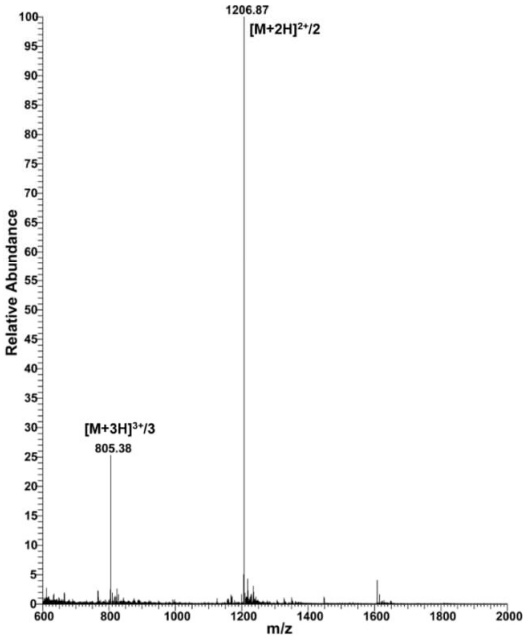

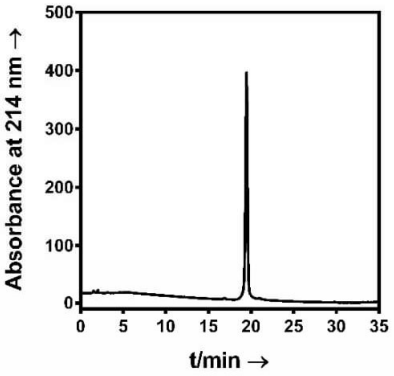

Peak #	Time (min)	Area	% Area
1	17.264	45.4	0.664
2	19.346	48.5	0.709
3	20.048	6572.9	96.176
4	21.705	167.5	2.451

Figure S5. Mass spectrometry and analytical HPLC characterization of a representative synthetic batch of $p3_{F20Y}$.

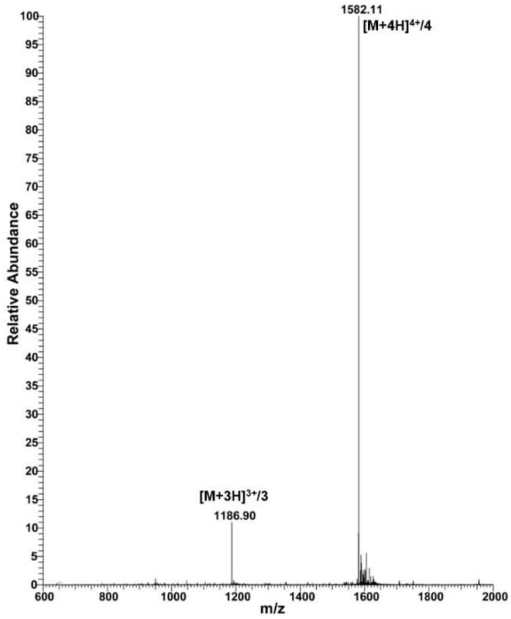

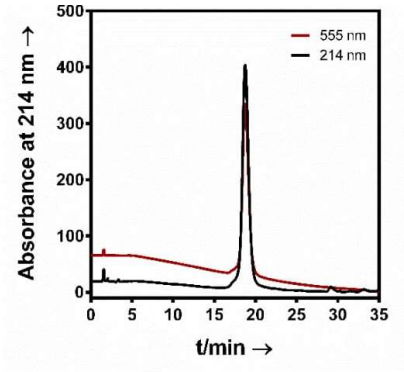

Peak #	Time (min)	Area	% Area
1	17.287	188	0.804
2	18.748	22674.3	96.960
3	29.136	334.1	1.429
4	33.154	188.9	0.808

Figure S6. Mass spectrometry and analytical HPLC characterization of a representative synthetic batch of TAMRA-labelled $A\beta_{1\text{-}40}$.

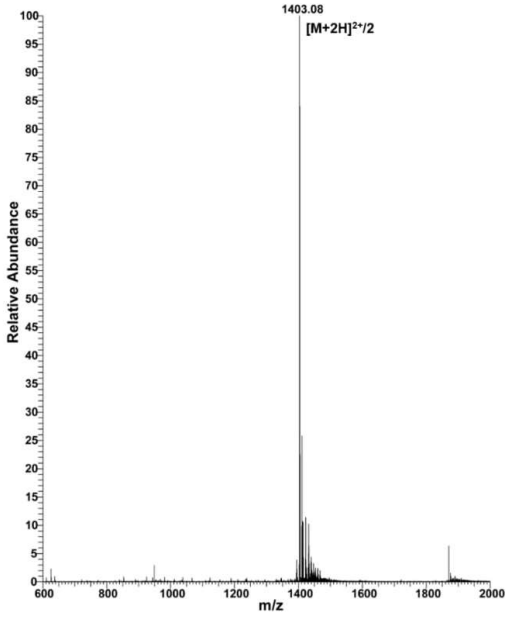

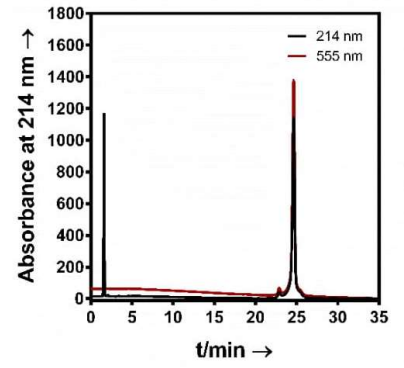

Peak #	Time (min)	Area	% Area
1	22.875	647.2	2.573
2	24.641	23772.7	94.517
3	25.231	732	2.910

Figure S7. Mass spectrometry and analytical HPLC characterization of a representative synthetic batch of TAMRA-labelled $p3_{17\text{-}40}$.

$A\beta_{1-40}$

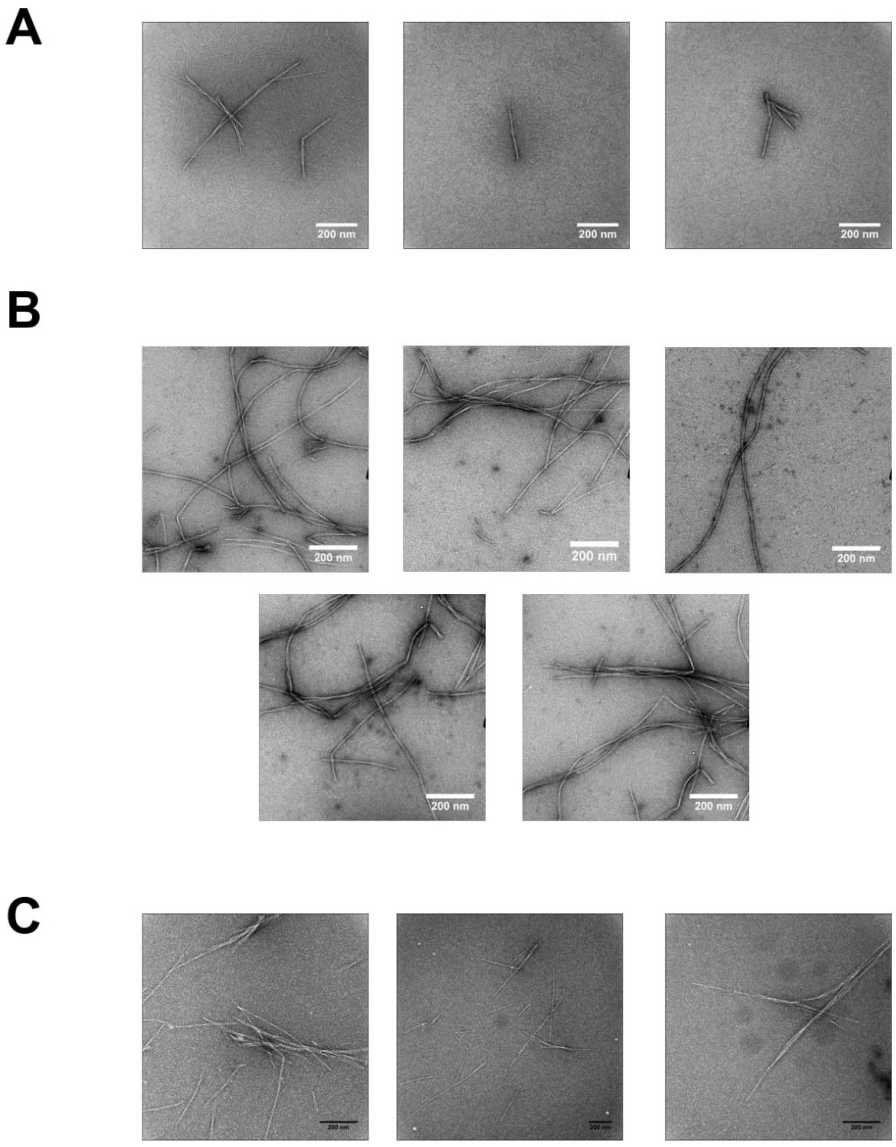

Figure S8. TEM images of $A\beta_{1-40}$ prepared A) quiescently (20 μM, 37 °C for 7 days) acquired at the University of California Santa Cruz Microscopy Center (JOEL 1230 Microscope), B) quiescently (20 μM, 37 °C for 7 days) acquired at the University of California Berkeley Electron Microscope Laboratory (Tecnai-12 Microscope), C) under agitation (20 μM, 37 °C for 24 hours with continuous shaking) acquired at the University of California Santa Cruz Microscopy Center (JOEL 1230 Microscope).

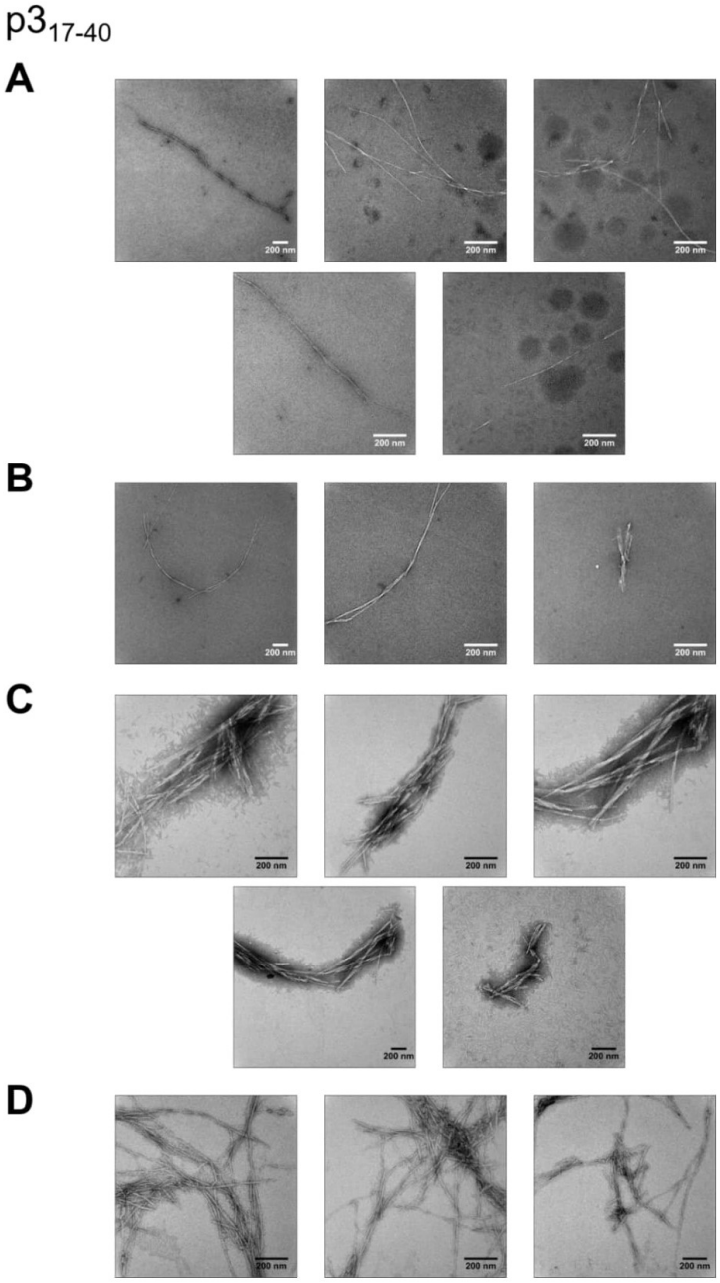

Figure S9. TEM images of $p3_{17-40}$ prepared A) quiescently (20 μM, 37 °C for 7 days), B) quiescently (40 μM, 37 C for 7 days), C) under agitation (20 μM, 37 °C for 24 hours with shaking every 5 minutes), D) TAMRA-labeled-$p3_{17-40}$ under agitation (20 μM, 37 °C for 24 hours with continuous shaking). A-D were acquired at the University of California Santa Cruz Microscopy Center (JOEL 1230 Microscope).

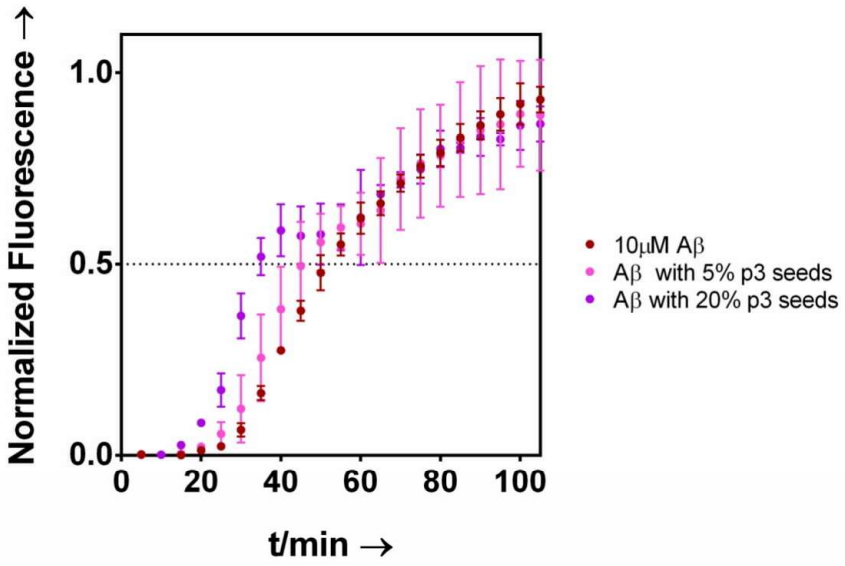

Figure S10. ThT- monitored aggregation kinetics of $A\beta_{1\text{-}40}$ alone, and amyloid beta with p3 fibrils added (at 5 or 20% of total concentration). p3 fibrils were formed at 37 °C under continuous shaking for 24 h, followed by centrifugation and washing x3.

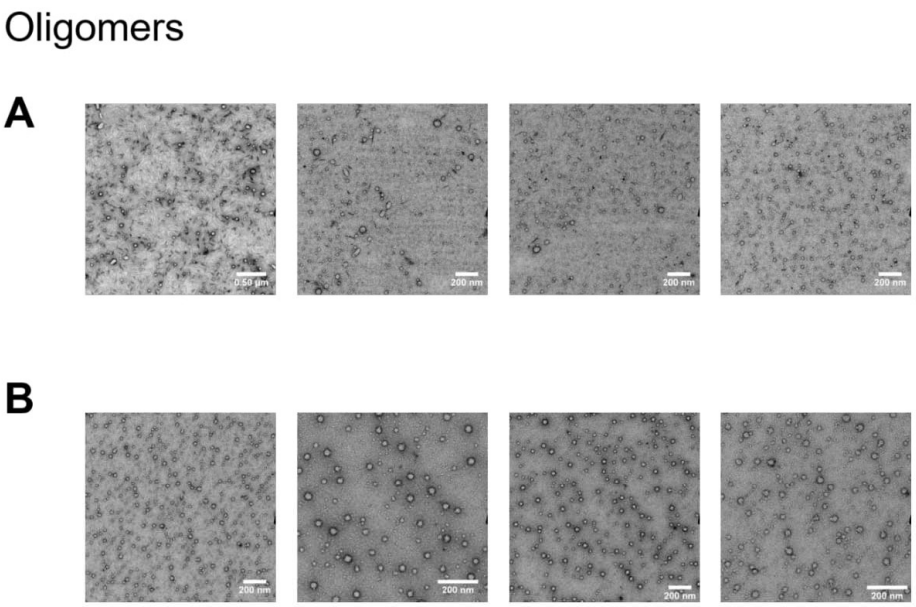

Figure S11. TEM images of kinetically trapped, intermediate oligomers of A) $A\beta_{1\text{-}40}$ (20 µM, 4 °C for 6 hours) and B) $p3_{17\text{-}40}$ (20 µM, 4 °C for 6 hours). These images were used to quantify the size distributions of spherical oligomers shown in Fig. 3C. Both A-B were acquired at the University of California Berkeley Electron Microscope Laboratory (Tecnai-12 Microscope).

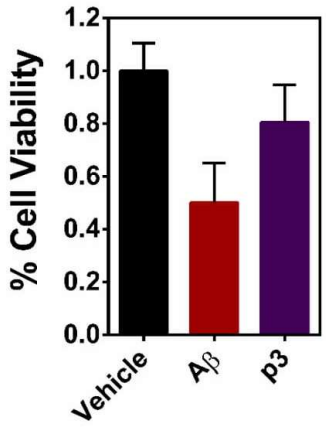

Figure S12. Cellular viability in SH-SY5Y cell lines following treatment with 50 µM oligomeric $A\beta_{1\text{-}40}$ or $p3_{17\text{-}40}$. Each sample, including controls, was incubated at 4 °C for 6 hours (consistent with method employed in Fig. 3 and S11, per published method by Ahmed *et. al.*[5])

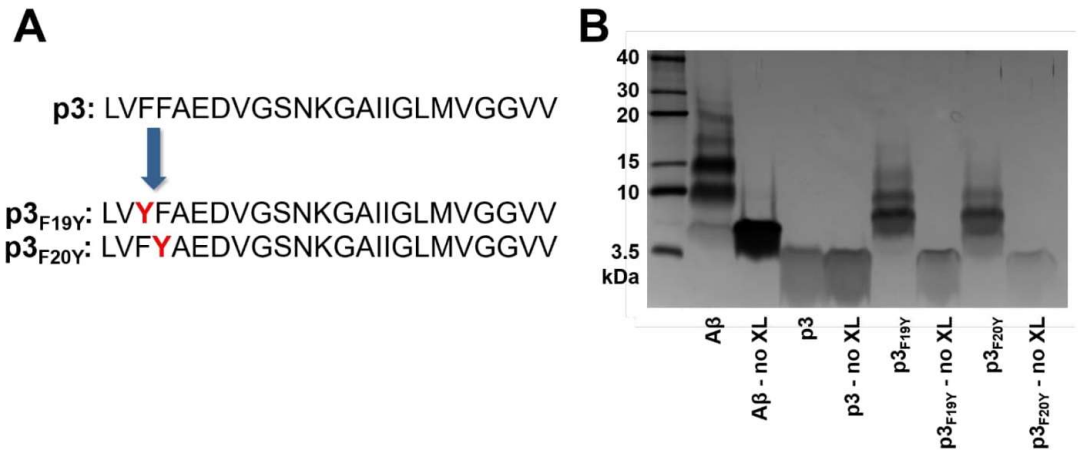

Figure S13. A) Sequence of p3 and 2 additional p3 peptides with Phe→ Tyr (F→ Y) substitutions at either the F19 or F20 position. B) SDS-PAGE gel of photo-induced crosslinked samples of Aβ, p3, $p3_{F19Y}$, and $p3_{F20Y}$. "No XL" denotes samples were not exposed to light.

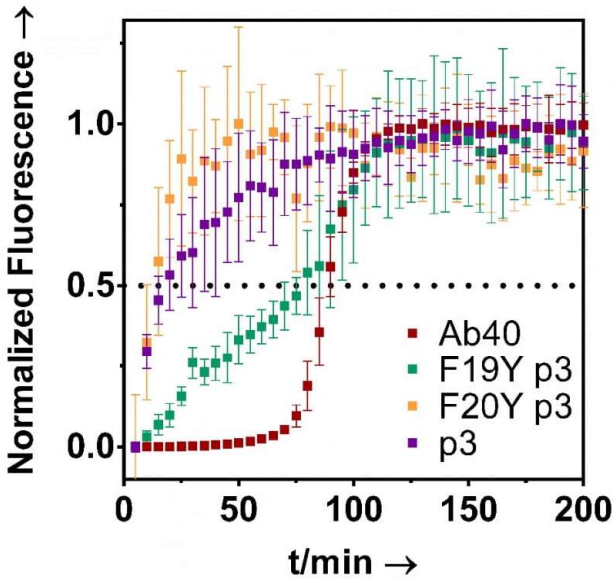

Figure S14. ThT- monitored aggregation kinetics of $Aβ_{1-40}$, $p3_{17-40}$, $p3_{F19Y}$, and $p3_{F20Y}$ (20 μM, 37 °C, with continuous shaking).

References

(1) Warner, C. J. A.; Dutta, S.; Foley, A. R.; Raskatov, J. A. Introduction of D-Glutamate at a Critical Residue of Aβ42 Stabilizes a Pre-Fibrillary Aggregate with Enhanced Toxicity. *Chem - A Eur J* **2016**, *22* (34), 11967–11970.

(2) AU - Warner, C. J. A.; AU - Dutta, S.; AU - Foley, A. R.; AU - Raskatov, J. A. A Tailored HPLC Purification Protocol That Yields High-Purity Amyloid Beta 42 and Amyloid Beta 40 Peptides, Capable of Oligomer Formation. *JoVE* **2017**, No. 121, e55482. https://doi.org/doi:10.3791/55482.

(3) Anthis, N. J.; Clore, G. M. Sequence-Specific Determination of Protein and Peptide Concentrations by Absorbance at 205 Nm. *Protein Sci* **2013**, *22* (6), 851–858. https://doi.org/10.1002/pro.2253.

(4) Nakka, P. P.; Li, K.; Forciniti, D. Effect of Differences in the Primary Structure of the A-Chain on the Aggregation of Insulin Fragments. *ACS OMEGA* **2018**, *3*, 9636–9647. https://doi.org/10.1021/acsomega.8b00500.

(5) Ahmed, M.; Davis, J.; Aucoin, D.; Sato, T.; Ahuja, S.; Aimoto, S.; Elliott, J. I.; Van Nostrand, W. E.; Smith, S. O. Structural Conversion of Neurotoxic Amyloid-Beta(1-42) Oligomers to Fibrils. *Nat Struct Mol Biol* **2010**, *17* (5), 561–567. https://doi.org/10.1038/nsmb.1799.

(6) Lalowski, M.; Golabek, A.; Lemere, C. A.; Selkoe, D. J.; Wisniewski, H. M.; Beavis, R. C.; Frangione, B.; Wisniewski, T. The "Nonamyloidogenic" P3 Fragment (Amyloid Beta 17-42) Is a Major Constituent of Down's Syndrome Cerebellar Preamyloid. *J Biol Chem* **1996**, *271* (52), 33623–33631. https://doi.org/10.1074/jbc.271.52.33623.

(7) Gowing, E.; Roher, A. E.; Woods, A. S.; Cotter, R. J.; Chaney, M.; Little, S. P.; Ball, M. J. Chemical Characterization of Abeta 17-42 Peptide, a Component of Diffuse Amyloid Deposits of Alzheimer Disease. *J Biol Chem* **1994**, *269* (15), 10987–10990.

(8) Näslund, J.; Schierhorn, A.; Hellman, U.; Lannfelt, L.; Roses, a D.; Tjernberg, L. O.; Silberring, J.; Gandy, S. E.; Winblad, B.; Greengard, P. Relative Abundance of Alzheimer A Beta Amyloid Peptide Variants in Alzheimer Disease and Normal Aging. *Proc Natl Acad Sci USA* **1994**, *91* (18), 8378–8382. https://doi.org/10.1073/pnas.91.18.8378.

(9) Saido, T. C.; Yamao-Harigaya, W.; Iwatsubo, T.; Kawashima, S. Amino- and Carboxyl-Terminal Heterogeneity of β-Amyloid Peptides Deposited in Human Brain. *Neurosci Lett* **1996**, *215* (3), 173–176. https://doi.org/10.1016/S0304-3940(96)12970-0.

(10) Higgins, L. S.; Murphy, G. M.; Forno, L. S.; Catalano, R.; Cordell, B. P3 Beta-Amyloid Peptide Has a Unique and Potentially Pathogenic Immunohistochemical Profile in Alzheimer's Disease Brain. *Am J Pathol* **1996**, *149* (2), 585–596.

(11) Abraham, J. D.; Prome, S.; Salvetat, N.; Rubrecht, L.; Cobo, S.; du Paty, E.; Galea, P.; Mathieu-Dupas, E.; Ranaldi, S.; Caillava, C.; Cremer, G. A.; Rieunuer, F.; Robert, P.; Molina, F.; Laune, D.; Checler, F.; Fareh, J. Cerebrospinal Aβ 11-x and 17-x Levels as Indicators of Mild Cognitive Impairment and Patients' Stratification in Alzheimer's Disease. *Transl Psychiatry* **2013**, *3* (e281), 1–8. https://doi.org/10.1038/tp.2013.58.

(12) Shi, J. M.; Zhang, L.; Liu, E. Q. Dissecting the Behaviour of β-Amyloid Peptide Variants during Oligomerization and Fibrillation. *J Pept Sci* **2017**, *23* (11), 810–817. https://doi.org/10.1002/psc.3028.

(13) Milton, N. G. N.; Harris, J. R. Polymorphism of Amyloid-β Fibrils and Its Effects on Human Erythrocyte Catalase Binding. *Micron* **2009**, *40* (8), 800–810. https://doi.org/10.1016/j.micron.2009.07.006.

(14) Vandersteen, A.; Hubin, E.; Sarroukh, R.; De Baets, G.; Schymkowitz, J.; Rousseau, F.; Subramaniam, V.; Raussens, V.; Wenschuh, H.; Wildemann, D.; Broersen, K. A Comparative Analysis of the Aggregation Behavior of Amyloid-β Peptide Variants. *FEBS Lett* **2012**, *586* (23), 4088–4093. https://doi.org/10.1016/j.febslet.2012.10.022.

(15) Naslund, J.; Jensen, M.; Tjernberg, L. O.; Thyberg, J.; Terenius, L.; Nordstedt, C. The Metabolic Pathway Generating P3, an Aβ Peptide Fragment, Is Probably Non-Amyloidogenic. *Biochem Biophys Res Commun* **1994**, *204* (2), 780–787. https://doi.org/10.1006/bbrc.1994.2527.

(16) Schmechel, A.; Zentgraf, H.; Scheuermann, S.; Fritz, G.; Reed, J.; Beyreuther, K.; Bayer, T. A.; Multhaup, G. Alzheimer β-Amyloid Homodimers Facilitate Aβ Fibrillization and the Generation of Conformational Antibodies*. *J Biol Chem* **2003**, *278* (37), 35317–35324. https://doi.org/10.1074/jbc.M303547200.

(17) Pike, C. J.; Overman, M. J.; Cotman, C. W. Amino-Terminal Deletions Enhance Aggregation of β-Amyloid Peptides in Vitro. *J Biol Chem* **1995**, *270* (41), 23895–23899.

(18) Zheng, J.; Jang, H.; Ma, B.; Tsai, C.-J.; Nussinov, R. Modeling the Alzheimer Aβ17-42 Fibril Architecture: Tight Intermolecular Sheet-Sheet Association and Intramolecular Hydrated Cavities. *Biophys J* **2007**, *93* (9), 3046–3057. https://doi.org/10.1529/biophysj.107.110700.

(19) Dulin, F.; Léveillé, F.; Ortega, J. B.; Mornon, J. P.; Buisson, A.; Callebaut, I.; Colloc'h, N. P3 Peptide, a Truncated Form of Aβ Devoid of Synaptotoxic Effect, Does Not Assemble into Soluble Oligomers. *FEBS Lett* **2008**, *582* (13), 1865–1870. https://doi.org/10.1016/j.febslet.2008.05.002.

(20) Streltsov, V. A.; Varghese, J. N.; Masters, C. L.; Nuttall, S. D. Crystal Structure of the Amyloid-β P3 Fragment Provides a Model for Oligomer Formation in Alzheimer's Disease. *J Neurosci* **2011**, *31* (4), 1419–1426. https://doi.org/10.1523/JNEUROSCI.4259-10.2011.

(21) Cheon, M.; Kang, M.; Chang, I. Polymorphism of Fibrillar Structures Depending on the Size of Assembled Aβ17-42 Peptides. *Sci Rep* **2016**, *6* (November), 38196. https://doi.org/10.1038/srep38196.

(22) Cheon, M.; Hall, C. K.; Chang, I. Structural Conversion of Aβ17–42 Peptides from Disordered Oligomers to U-Shape Protofilaments via Multiple Kinetic Pathways. *PLoS Comput Biol* **2015**, *11* (5), 1–23. https://doi.org/10.1371/journal.pcbi.1004258.

(23) Miller, Y.; Ma, B.; Nussinov, R. Polymorphism of Alzheimer's Aβ17-42 (P3) Oligomers: The Importance of the Turn Location and Its Conformation. *Biophys J* **2009**, *97* (4), 1168–1177. https://doi.org/10.1016/j.bpj.2009.05.042.

(24) Liu, R.; McAllister, C.; Lyubchenko, Y.; Sierks, M. R. Residues 17-20 and 30-35 of β-Amyloid Play Critical Roles in Aggregation. *J Neurosci Res* **2004**, *75* (2), 162–171. https://doi.org/10.1002/jnr.10859.

(25) Wei, W.; Norton, D. D.; Wang, X.; Kusiak, J. W. Aβ 17-42 in Alzheimer's Disease Activates JNK and Caspase-8 Leading to Neuronal Apoptosis. *Brain* **2002**, *125*, 2036–2043. https://doi.org/10.1093/brain/awf205.

(26) Jang, H.; Arce, F. T.; Ramachandran, S.; Capone, R.; Azimova, R.; Kagan, B. L.; Nussinov, R.; Lal, R. Truncated β-Amyloid Peptide Channels Provide an Alternative Mechanism for Alzheimer's Disease and Down Syndrome. *Proc Natl Acad Sci* **2010**, *107* (14), 6538–6543. https://doi.org/10.1073/pnas.0914251107.

(27) Walsh, D. M.; Klyubin, I.; Fadeeva, J. V.; Cullen, W. K.; Anwyl, R.; Wolfe, M. S.; Rowan, M. J.; Selkoe, D. J. Naturally Secreted Oligomers of Amyloid-β Protein Potently Inhibit Hippocampal Long-Term Potentiation in Vivo. *Nature* **2002**, *416* (6880), 535–539. https://doi.org/10.1038/416535a.

(28) Szczepanik, A. M.; Rampe, D.; Ringheim, G. E. Amyloid-Beta Peptide Fragments P3 and P4 Induce pro-Inflammatory Cytokine and Chemokine Production in Vitro and in Vivo. *J Neurochem* **2001**, *77* (1), 304–317. https://doi.org/10.1046/j.1471-4159.2001.00240.x.

B.2.

SUPPORTING INFORMATION

Mixing of Aβ and p3 Results in Fibrilization Enhancement, Unique Intermediate Formation, and Suppression of Toxicity

Ariel J. Kuhn[a], Ka Chan[a], Behzad Rad[b], Jevgenij A. Raskatov[a]*

[a] Dept. of Chemistry and Biochemistry, University of California Santa Cruz, CA 95064, United States

[b] Molecular Foundry Division, Lawrence Berkeley National Laboratory, 1 Cyclotron Road, Berkeley, CA 94720, USA

* Corresponding author

Table of Contents

Figure S1. Mass spectrometry and analytical HPLC characterization of a representative synthetic batch of $p3_{17-40}$ and $A\beta_{1-42}$.

Figure S2. Mass spectrometry and analytical HPLC characterization of a representative synthetic batch of TAMRA-$A\beta_{1-42}$ and TAMRA-$p3_{17-40}$.

Figure S3. Mass spectrometry and analytical HPLC characterization of a representative synthetic batch of FAM-labeled $A\beta_{1-42}$ and $p3_{F20Y}$ (17-40).

Figure S4. STEM Images of Aβ fibrils formed under agitation.

Figure S5. STEM Images of p3 fibrils formed under agitation.

Figure S6. TEM Images of 1:1 Aβ:p3 quiescent fibrils.

Figure S7. STEM Images of 1:1 Aβ:p3 fibrils formed under agitation.

Figure S8. STEM Images of 2:1 Aβ:p3 fibrils formed under agitation.

Figure S9. TEM Images of 1:1 Aβ:p3 trapped oligomers.

Figure S10. STEM Images of 1:1 Aβ:p3 trapped oligomers.

Figure S11. STEM Images of p3 trapped oligomers.

Figure S12. TEM Images of 1:1 Aβ:p3 trapped oligomers.

Figure S13. SDS-PAGE gel of photo-induced crosslinked samples**.**

Figure S14. WST-1 cell viability assays (3 additional biological replicates from main text **Fig. 7A**) in PC12 cells.

Figure S15. WST-1 cell viability assays (3 additional biological replicates from main text **Fig. 7A**) in SH-SY5Y cells.

Figure S16. ROS activity in SH-SY5Y cells from main text **Fig. 7C** (with H_2O_2 control shown).

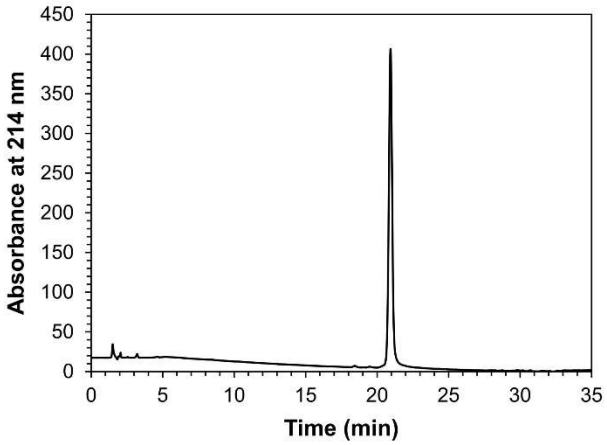

Peak #	Time (min)	Area %
1	18.425	0.388
2	19.486	0.360
3	20.493	0.474
4	20.937	98.778

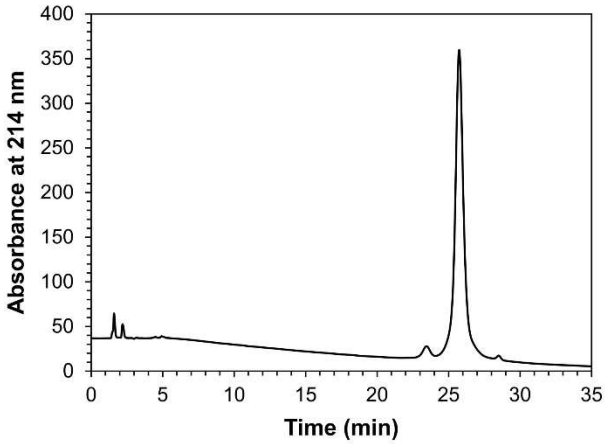

Peak #	Time (min)	Area %
1	23.463	2.793
2	25.745	96.521
3	28.515	0.686

Figure S1. TOP: Mass spectrometry and analytical HPLC characterization of a representative synthetic batch of p3 (17-40). BOTTOM: Mass spectrometry and analytical HPLC characterization of a representative synthetic batch of Aβ(1-42).

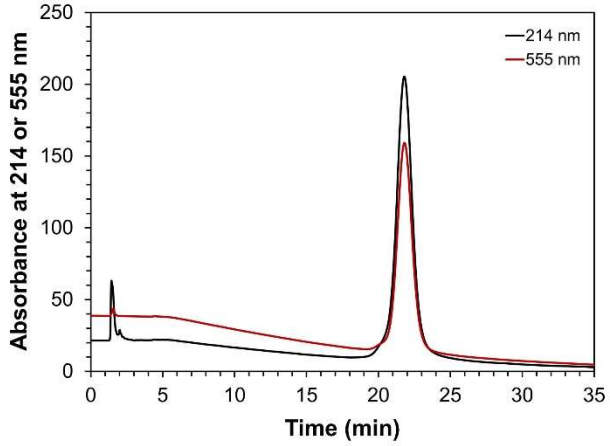

Peak #	Time (min)	Area %
1	20.319	1.764
2	21.797	98.236

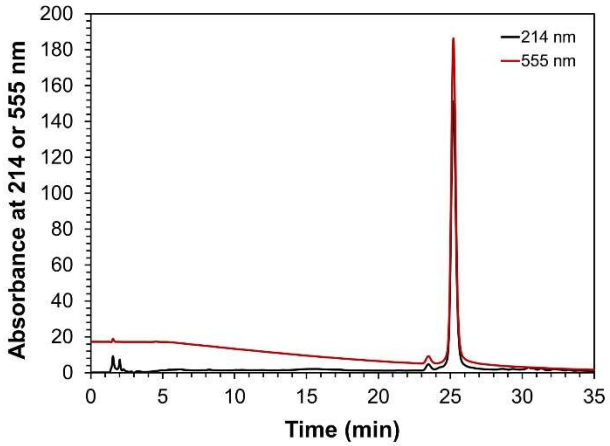

Peak #	Time (min)	Area %
1	23.469	1.741
2	24.503	0.782
3	25.212	97.477

Figure S2. TOP: Mass spectrometry and analytical HPLC characterization of a representative synthetic batch of TAMRA-Aβ42. BOTTOM: Mass spectrometry and analytical HPLC characterization of a representative synthetic batch of TAMRA-p3(17-40).

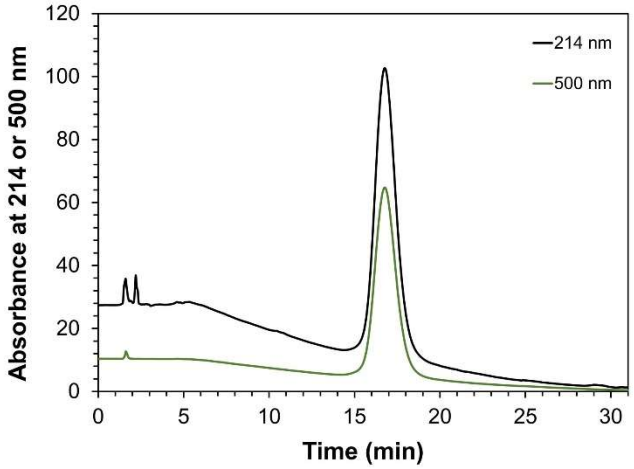

Peak #	Time (min)	Area %
1	15.502	0.542
2	16.768	99.458

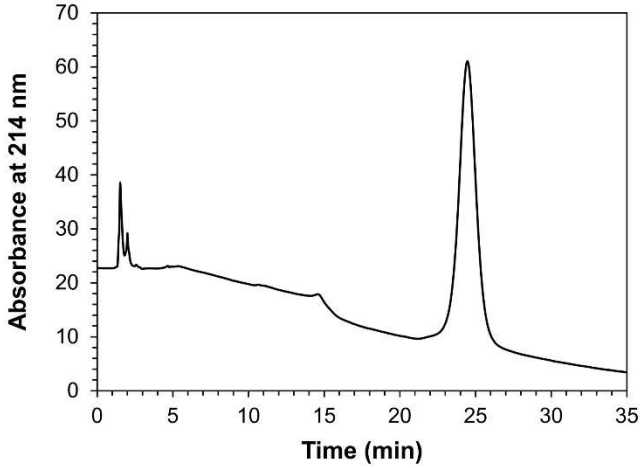

Peak #	Time (min)	Area %
1	14.65	2.409
2	24.464	97.591

Figure S3. TOP: Mass spectrometry and analytical HPLC characterization of a representative synthetic batch of FAM-Aβ42. BOTTOM: Mass spectrometry and analytical HPLC characterization of a representative synthetic batch of p3(F20Y mutant).

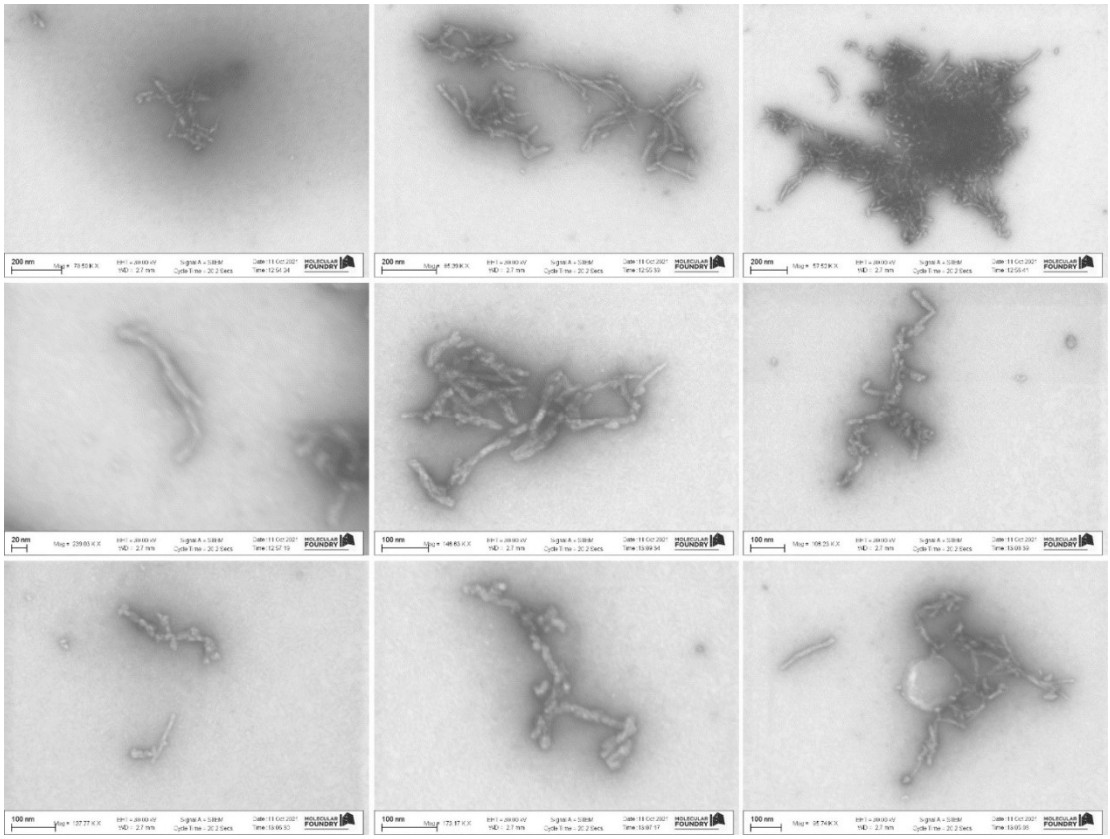

Figure S4. STEM Images of Aβ fibrils formed under agitation, in the presence of ThT (20 μM). Fibrils were formed by incubating Aβ (10 μM total) for 24 hours at 37 °C. Samples were negatively stained. Scalebars as marked.

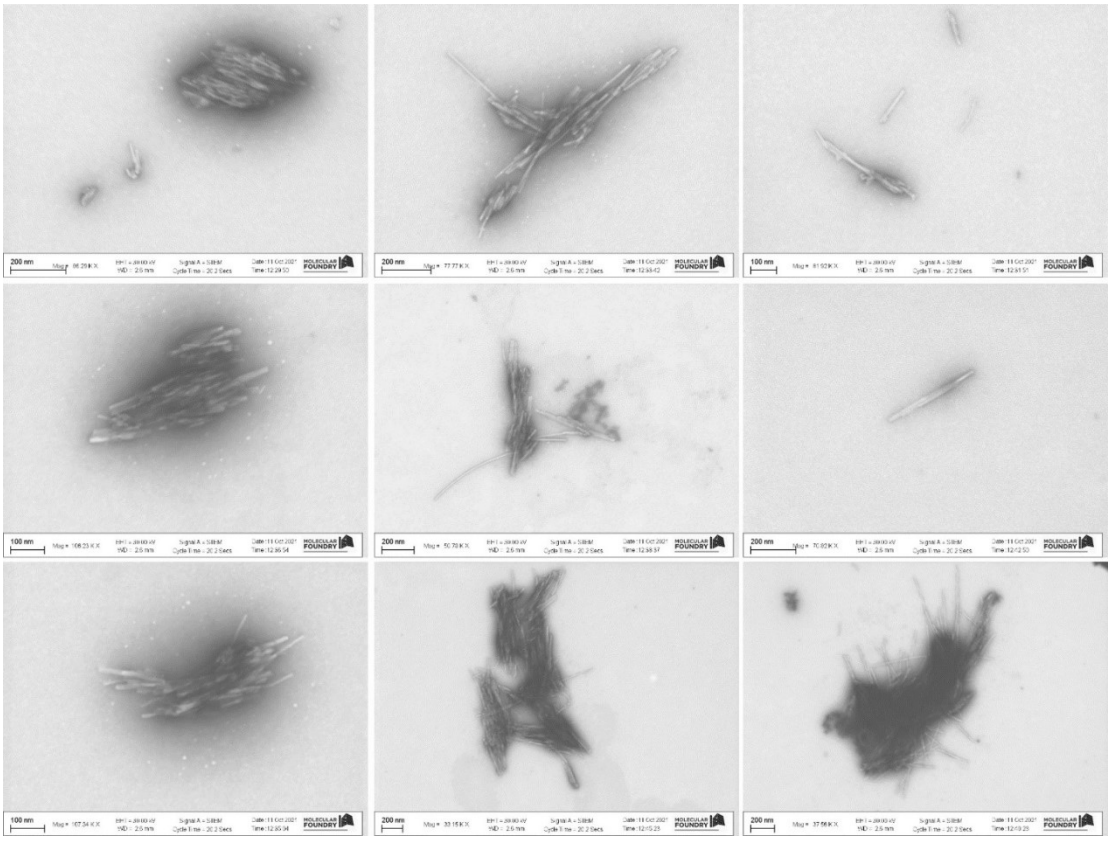

Figure S5. STEM Images of p3 fibrils formed under agitation, in the presence of ThT (20 μM). Fibrils were formed by incubating p3 (10 μM total) for 24 hours at 37 °C. Samples were negatively stained. Scalebars as marked.

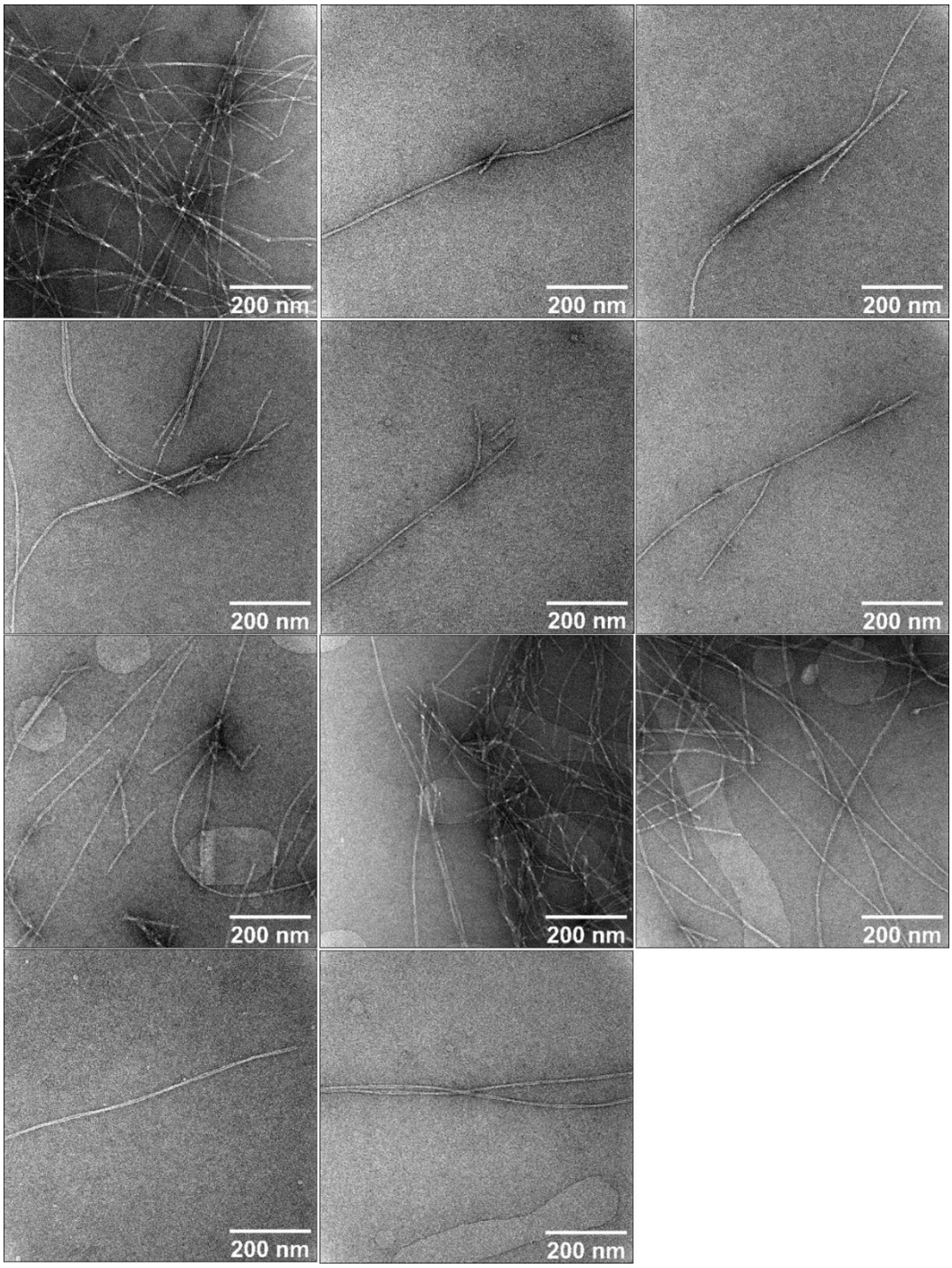

Figure S6. TEM Images of 1:1 Aβ:p3 quiescent fibrils. Fibrils were formed by incubating a 1:1 mixture of Aβ:p3 (20 μM each, 40 μM total) for 7 days at 37 °C. Samples were negatively stained. Scalebar = 200 nm.

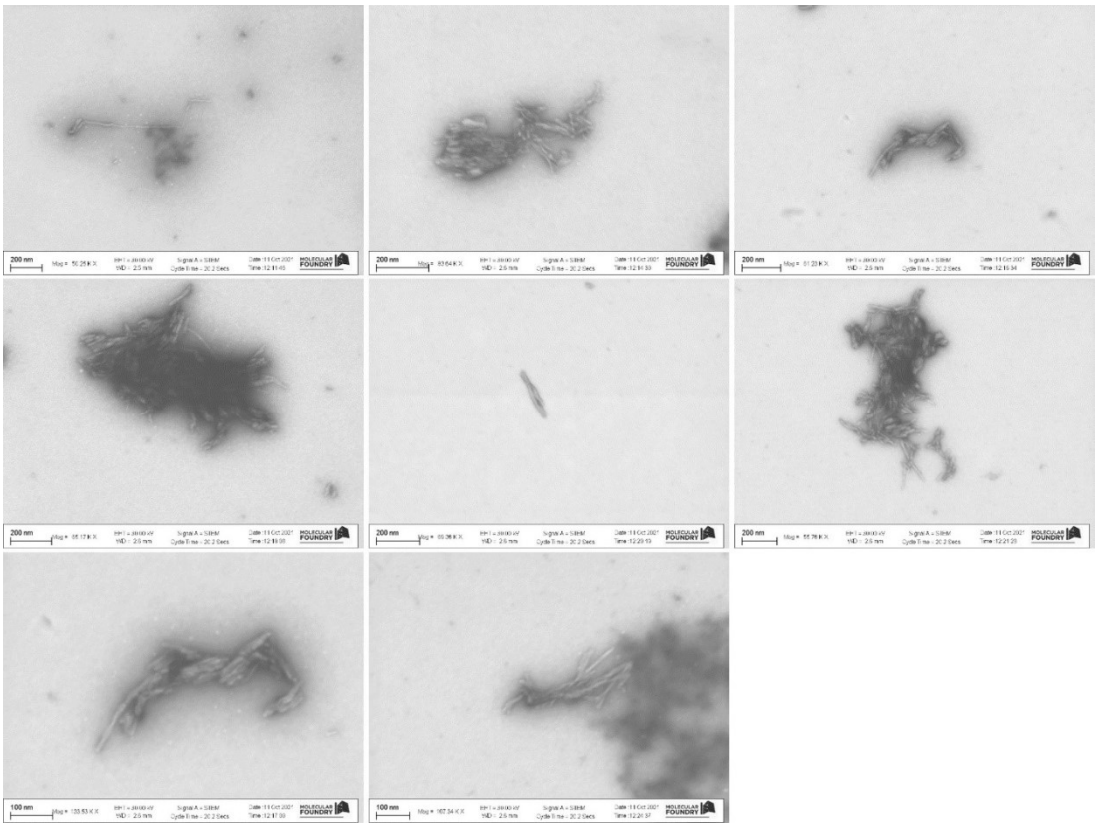

Figure S7. STEM Images of 1:1 Aβ:p3 fibrils formed under agitation, in the presence of ThT(20 μM). Fibrils were formed by incubating a 1:1 mixture of Aβ:p3 (10 μM each, 20 μM total) for 24 hours at 37 °C. Samples were negatively stained. Scalebars as marked.

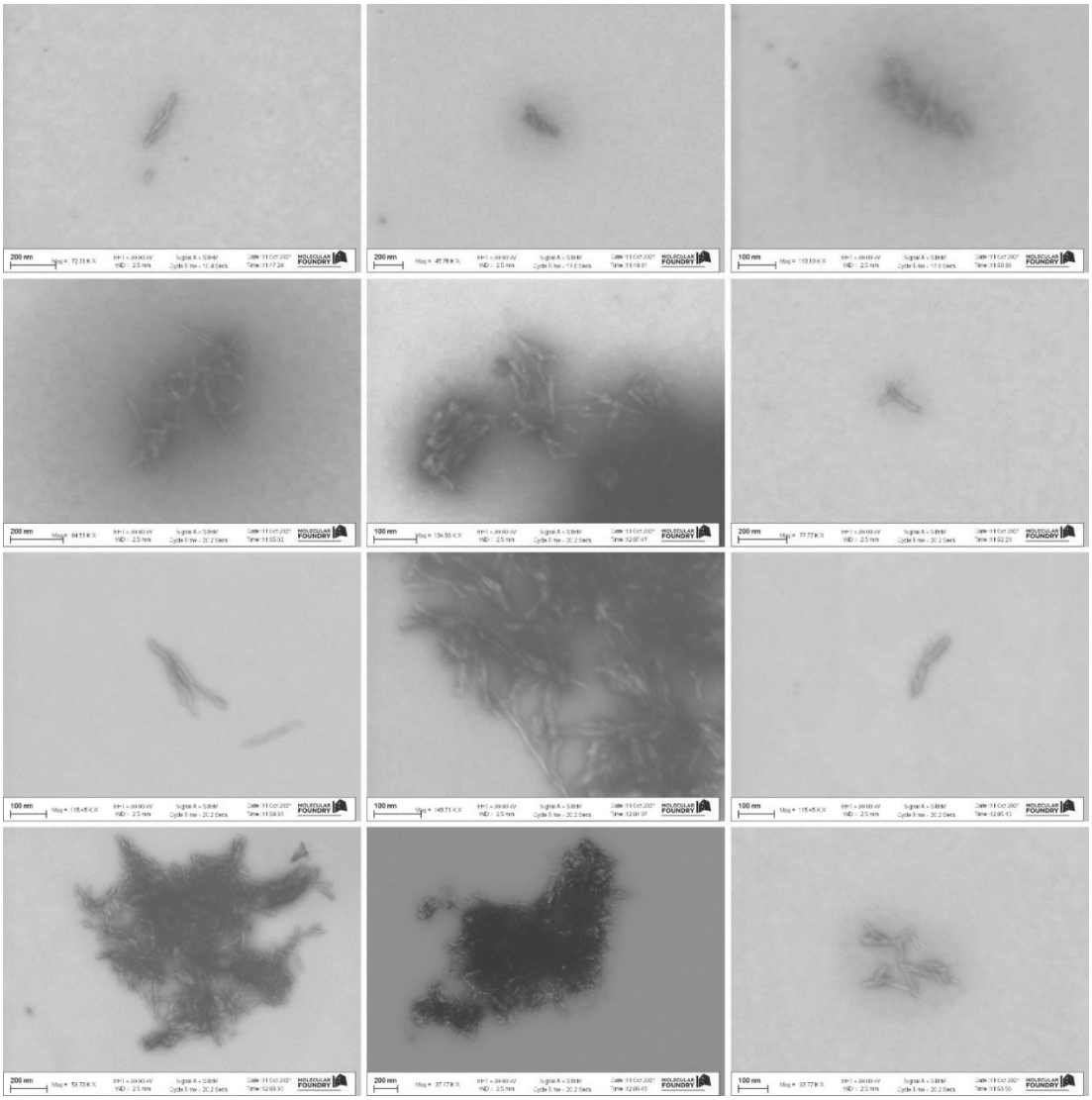

Figure S8. STEM Images of 2:1 Aβ:p3 fibrils formed under agitation, in the presence of ThT (20 μM). Fibrils were formed by incubating a 2:1 mixture of Aβ:p3 (10 μM Aβ, 5 μM p3, 15 μM total) for 24 hours at 37 °C. Samples were negatively stained. Scalebars as marked.

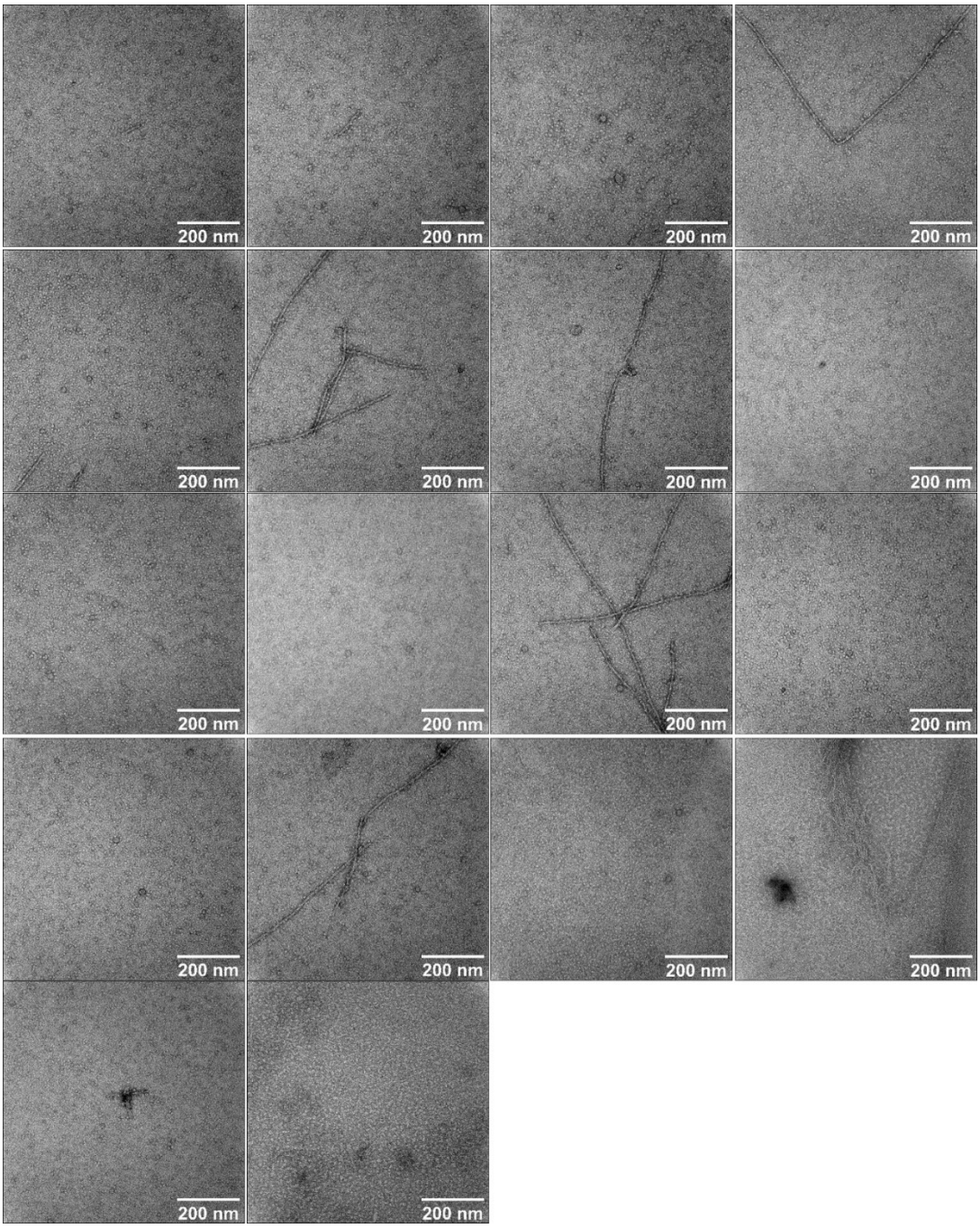

Figure S9. TEM Images of 1:1 Aβ:p3 trapped oligomers. Oligomers were formed by incubating a 1:1 mixture of Aβ:p3 (10 μM each, 20 μM total) for 6 hours at 4 °C. Samples were negatively stained. Scalebar = 200 nm.

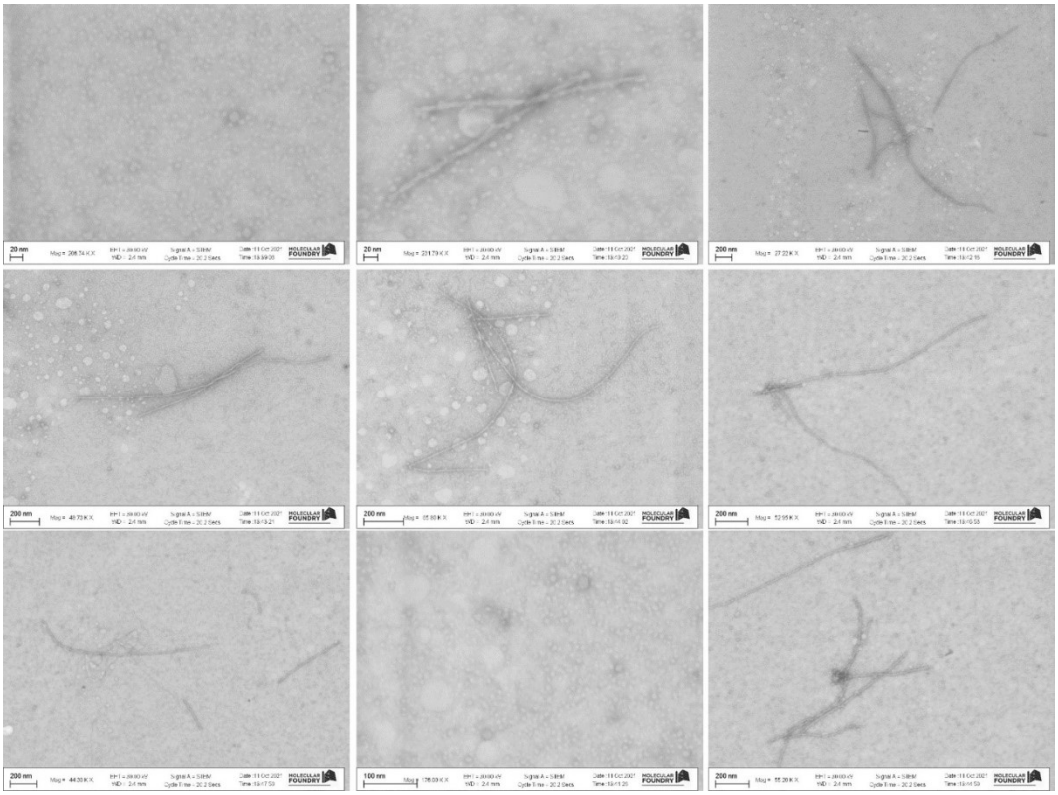

Figure S10. STEM Images of 1:1 Aβ:p3 trapped oligomers. Oligomers were formed by incubating a 1:1 mixture of Aβ:p3 (10 μM each, 20 μM total) for 6 hours at 4 °C. Samples were negatively stained. Scalebars as marked.

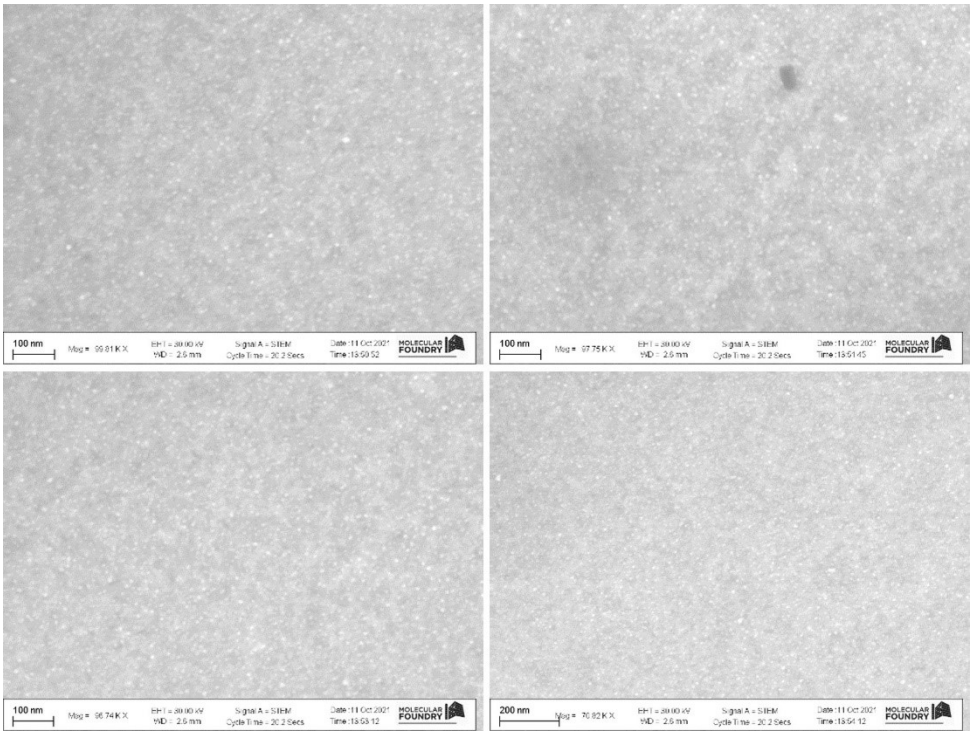

Figure S11. STEM Images of p3 trapped oligomers. Oligomers were formed by incubating p3 (10 μM) for 6 hours at 4 °C. Samples were negatively stained. Scalebars as marked.

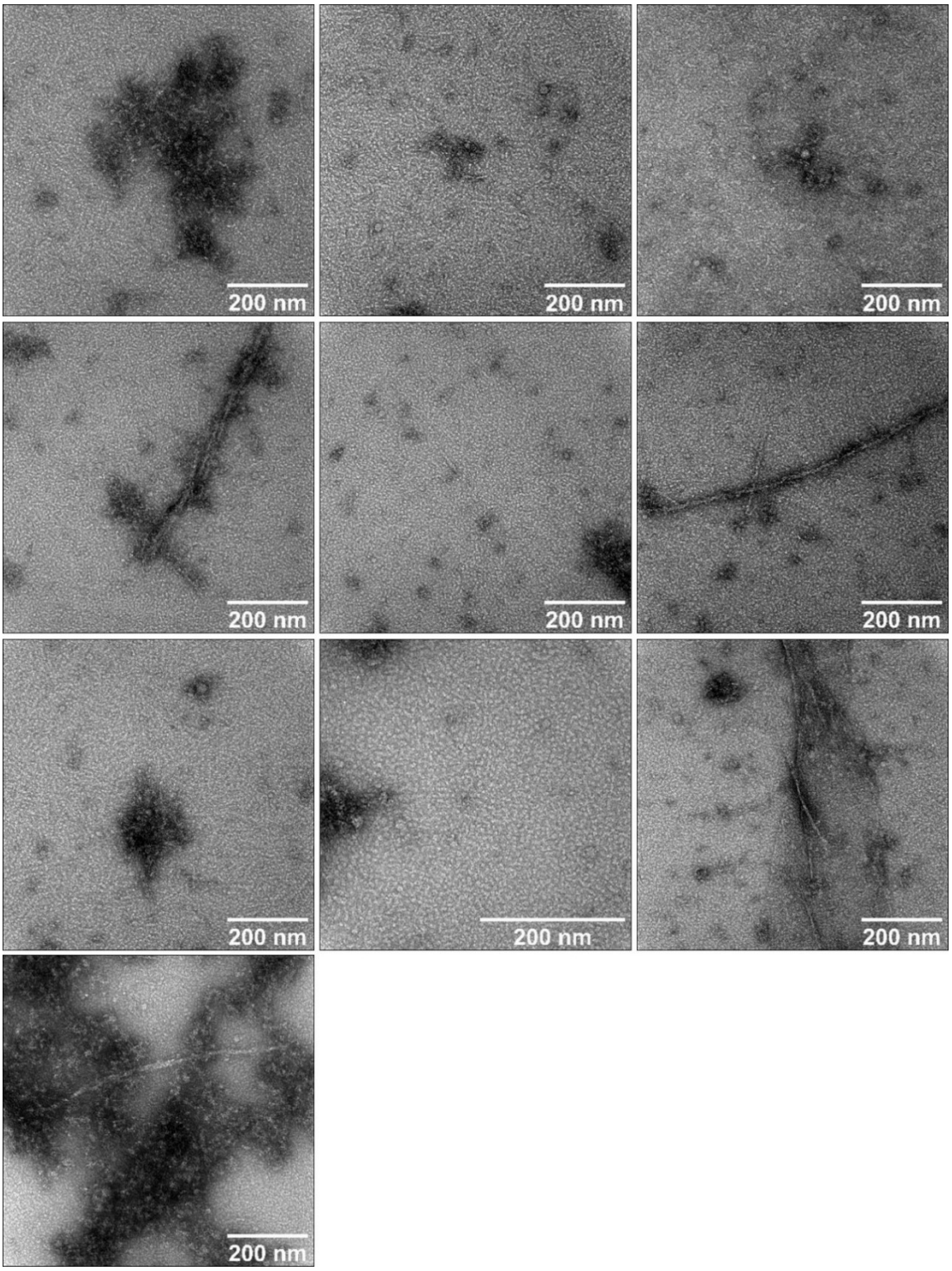

Figure S12. TEM Images of 1:1 Aβ:p3 trapped oligomers. Oligomers were formed by incubating a 1:1 mixture of Aβ:p3 (50 μM each, 100 μM total) for 6 hours at 4 °C. Samples were negatively stained. Scalebar = 200 nm.

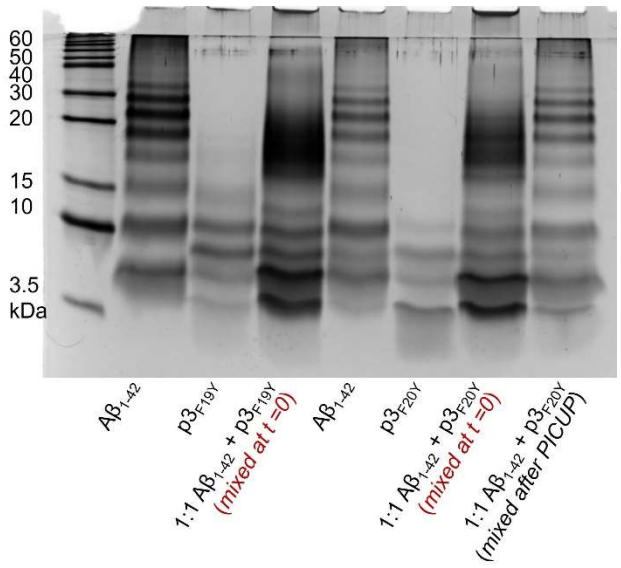

Figure S13. SDS-PAGE gel of photo-induced crosslinked samples: Aβ, $p3_{F19Y}$, 1:1 Aβ: $p3_{F19Y}$, control 1:1 Aβ: $p3_{F19Y}$ (mixed after PICUP reaction and quenching) and Aβ, $p3_{F20Y}$, 1:1 Aβ: $p3_{F20Y}$, control 1:1 Aβ: $p3_{F20Y}$ (mixed after PICUP reaction and quenching).

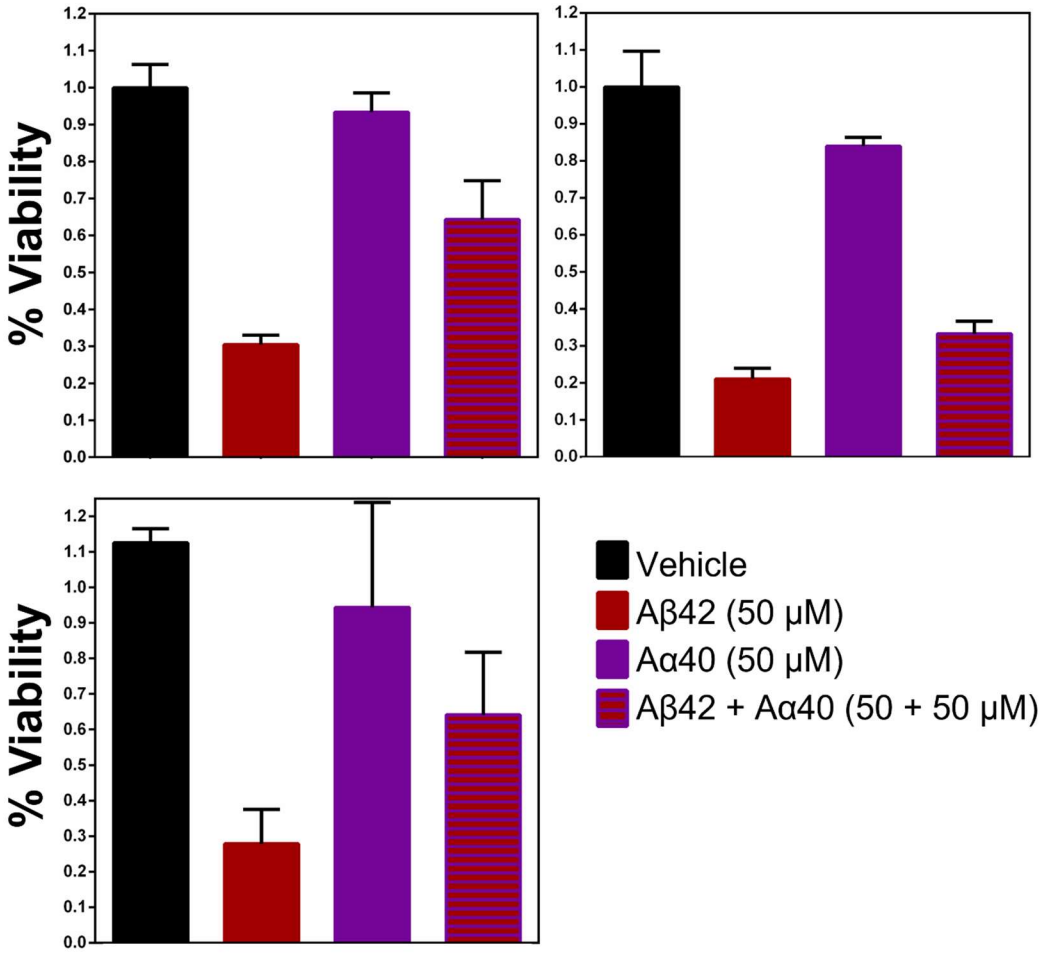

Figure S14. WST-1 cell viability assays (3 additional biological replicates from main text **Fig. 7A**) in PC12 cell line, comparing Aβ (50 μM), p3 (50 μM), vs 1:1 Aβ + p3 (50 + 50 μM). Cells were incubated with the peptides for 72 hours. Columns show mean and SD for three technical replicates. Colors represent peptides as indicated in the legend.

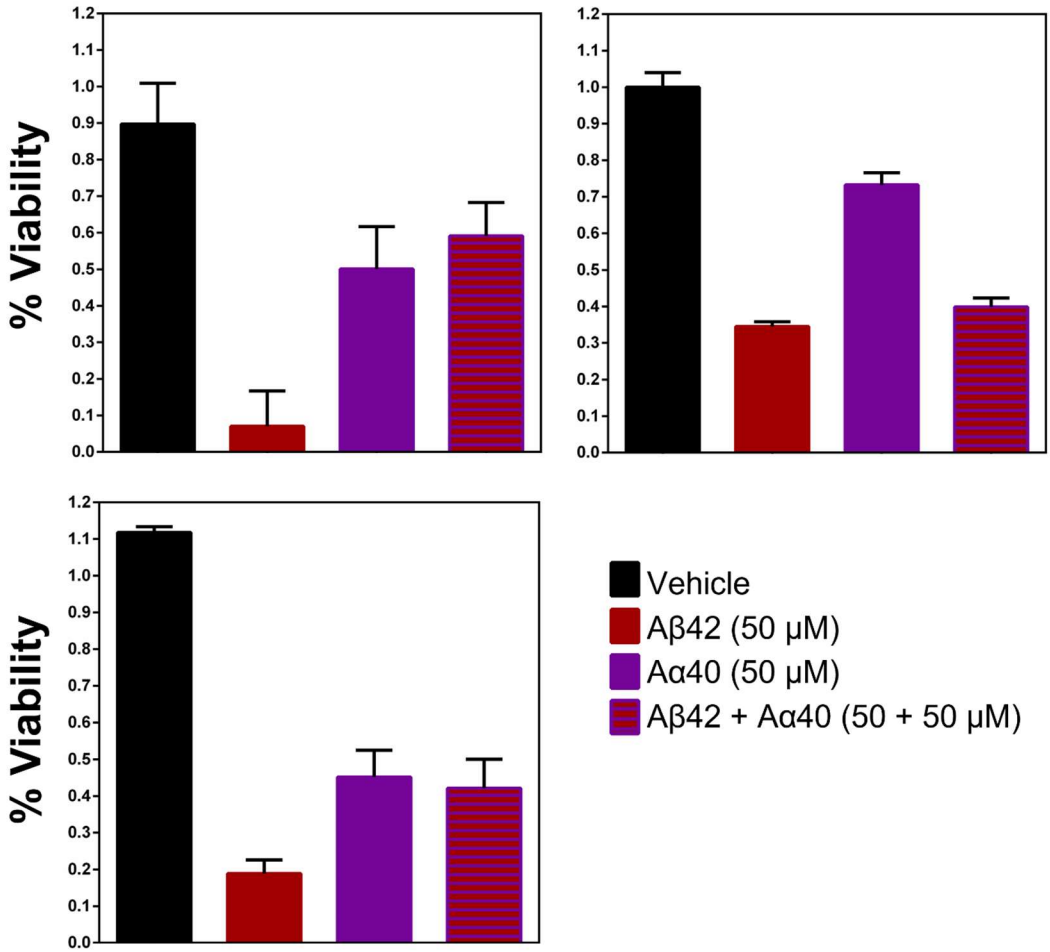

Figure S15. WST-1 cell viability assays (3 additional biological replicates from main text **Fig. 7A**) in SH-SY5Y cell line, comparing Aβ (50 μM), p3 (50 μM), vs 1:1 Aβ + p3 (50 + 50 μM). Cells were incubated with the peptides for 72 hours. Columns show mean and SD for three technical replicates.

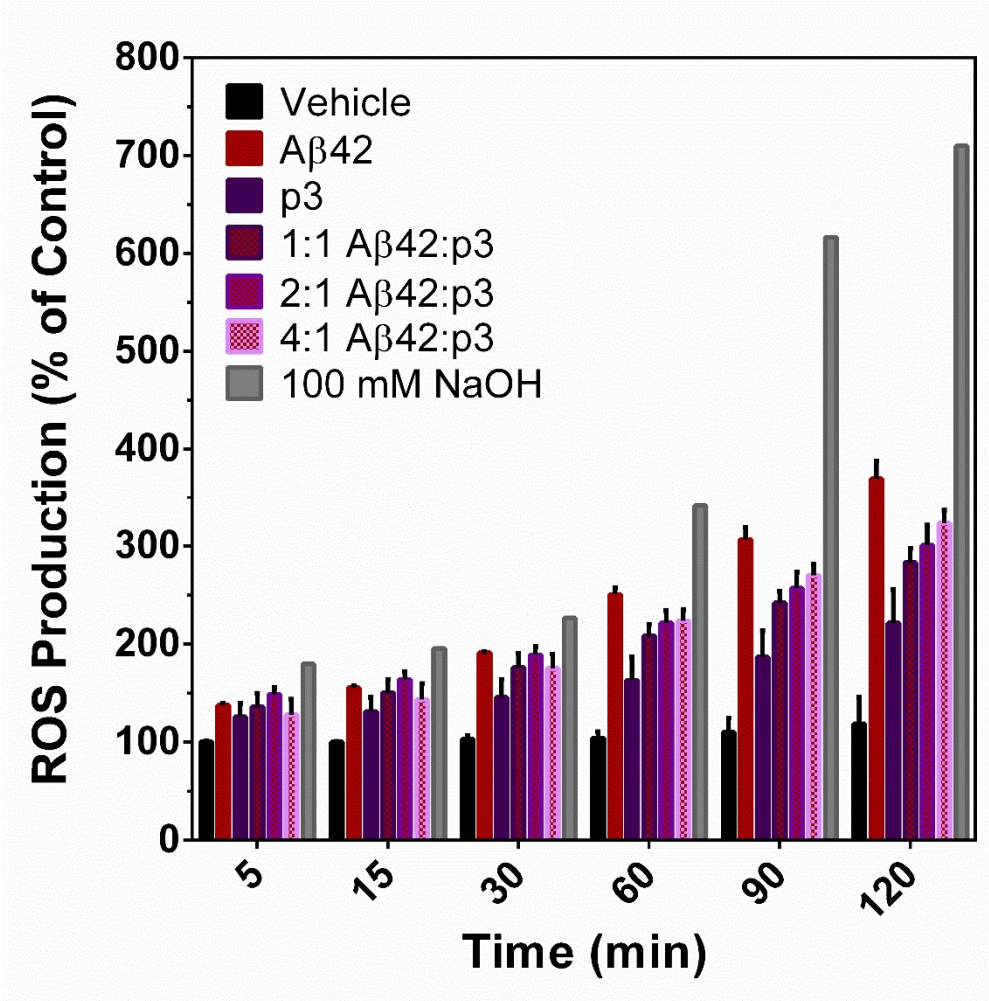

Figure S16. Effect of Aβ (50μM), p3 (50μM), 1:1 (50:50μM), 2:1 (50:25μM), 4:1 Aβ:p3 (50:12.5μM), and H2O2 (100mM) on production of ROS in SH-SY5Y cells (complementary to **Fig. 7C** in main text). Cells were plated at a density of 50,000 cells/well and allowed to adhere for 24h. Fluorescence signal of DCF was measured at 5, 30, 60, 90 and 120 minutes.

B.3.

New insights into differential aggregation of enantiomerically pure and racemic Aβ40 systems

Subrata Dutta,[a,†] Alejandro R. Foley,[a,†] Ariel J. Kuhn,[a,†] Benjamin Abrams,[b] Hsiau-Wei Lee,[a] and Jevgenij A. Raskatov[a,*]

[a] *Department of Chemistry and Biochemistry, 1156 High Street, University of California Santa Cruz, Santa Cruz, CA 95064, USA*

[b] *Department of Biomolecular Engineering, Life Sciences Microscopy Center, 1156 High Street, University of California Santa Cruz, Santa Cruz, CA 95064, USA*

[†] *Denotes equal contribution*

[*] *Correspondence should be addressed to: jraskato@ucsc.edu*

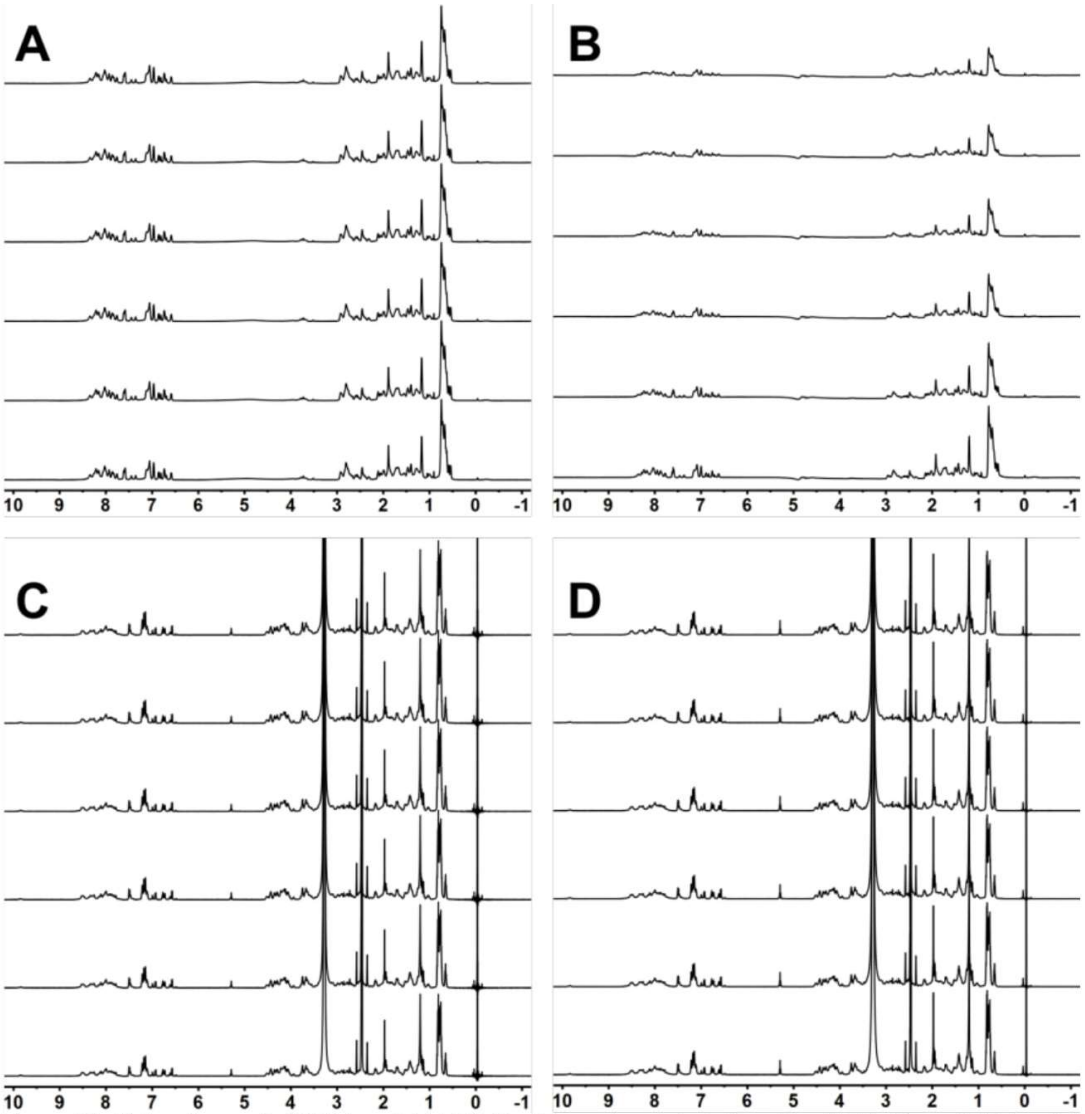

Figure S1. A) Enantiopure (L-)Aβ40 in a 9:1 H_2O/D_2O mixture, phosphate-buffered to pH 7.4; B) rac-Aβ40 in a 9:1 H_2O/D_2O mixture, phosphate-buffered to pH 7.4; C) L-Aβ40 in d_6-DMSO; D) rac-Aβ40 in d_6-DMSO. All ^1H NMR experiments were performed at 298 K with 160 μM total Aβ40 in all cases. The stacked spectra correspond, from lowest up, to t = 1, 9, 17, 25, 33 and 41 min. Racemic Aβ40 loses 61 % signal in water over that time period, whereas signal intensity is invariant in all other cases.

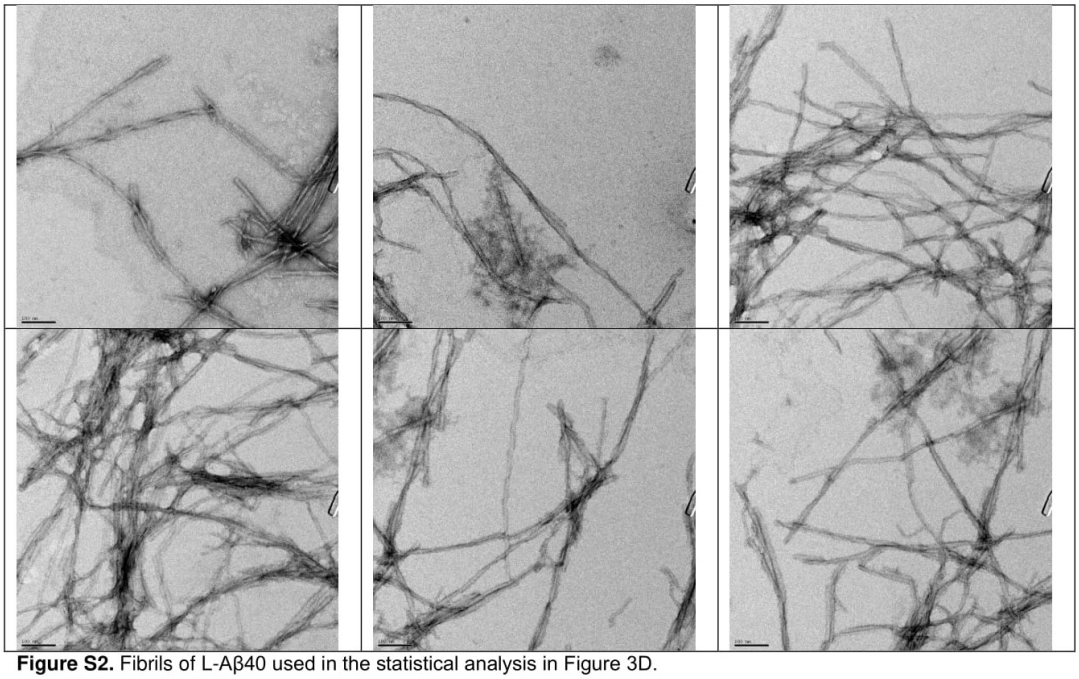

Figure S2. Fibrils of L-Aβ40 used in the statistical analysis in Figure 3D.

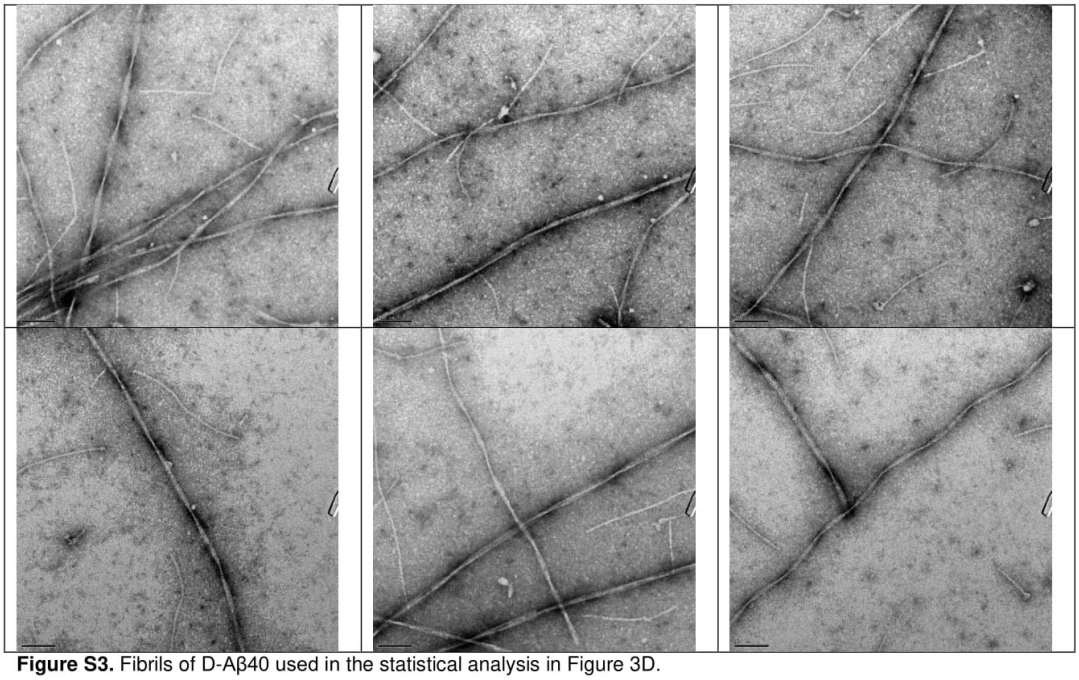

Figure S3. Fibrils of D-Aβ40 used in the statistical analysis in Figure 3D.

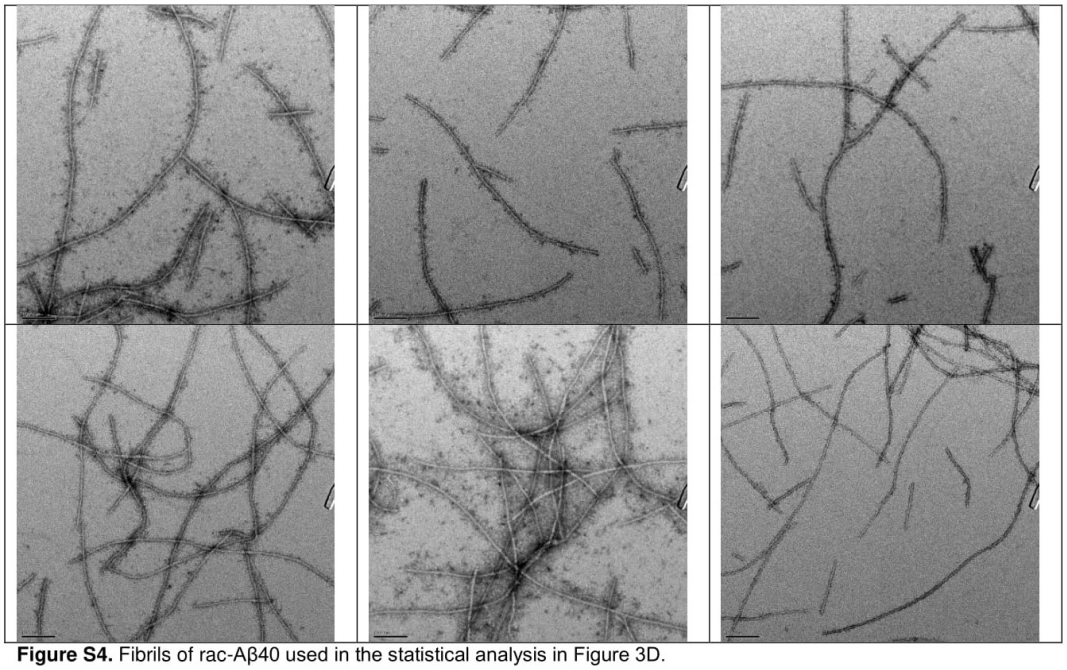

Figure S4. Fibrils of rac-Aβ40 used in the statistical analysis in Figure 3D.

DFT-optimized LVFFA:lvffa rippled parallel cross-β structure (*cf.* Figure 4)

188
symmetry c1

C	9.714220000	-1.313791000	1.432209000
C	8.638166000	-1.523183000	0.393099000
O	8.680427000	-0.956365000	-0.704045000
N	7.629391000	-2.350761000	0.724325000
C	6.531293000	-2.624044000	-0.196856000
C	5.332444000	-2.967098000	0.688972000
O	5.291094000	-4.033591000	1.296676000
N	4.381912000	-2.012923000	0.759018000
C	3.198788000	-2.168136000	1.574627000
C	1.958224000	-1.942119000	0.710374000
O	1.982868000	-1.204835000	-0.280122000
N	0.840077000	-2.564275000	1.119833000
C	-0.383267000	-2.507537000	0.343814000
C	-1.557549000	-2.656129000	1.302813000
O	-1.526298000	-3.490351000	2.204104000
N	-2.602410000	-1.852116000	1.032024000
C	-3.780144000	-1.794798000	1.867442000
C	-4.996338000	-1.663480000	0.958058000
O	-4.988009000	-0.819326000	0.057667000
N	-6.049000000	-2.446258000	1.219548000
C	-7.293306000	-2.335163000	0.474155000
C	-8.433595000	-2.496061000	1.476817000
O	-8.414004000	-3.418082000	2.287088000
N	-9.434445000	-1.607668000	1.348622000
O	-1.373138000	0.420563000	-0.369667000
C	-1.376324000	1.617480000	-0.680031000
C	-0.145674000	2.478326000	-0.429711000
N	1.035316000	1.679639000	-0.678937000
C	2.211601000	2.274446000	-0.968306000
O	2.344700000	3.492491000	-1.068626000
N	-2.433265000	2.245245000	-1.205314000
C	-3.726000000	1.613712000	-1.375622000
C	-4.802488000	2.610858000	-0.971544000
O	-4.698956000	3.797207000	-1.278020000
N	-5.882646000	2.079725000	-0.369708000
C	-7.112939000	2.842887000	-0.298623000
C	-8.281157000	1.864313000	-0.269823000
O	-8.151715000	0.741322000	0.217533000
N	-9.447342000	2.340154000	-0.729125000
C	3.369979000	1.317415000	-1.220757000
N	4.603545000	2.063728000	-1.077009000
C	5.681214000	1.560855000	-0.457742000
C	6.902531000	2.465886000	-0.336551000
N	7.962816000	1.829637000	-1.097195000
C	8.519888000	2.385037000	-2.196917000
C	9.577737000	1.537322000	-2.871157000
O	5.735146000	0.410700000	-0.008255000
O	8.227889000	3.507108000	-2.608379000
H	-10.198789000	-1.650263000	2.010257000
H	-10.266954000	1.747749000	-0.712075000
C	-7.395153000	-3.421272000	-0.597470000

H	-7.309726000	-1.344472000	0.015041000
H	-9.284091000	-0.745702000	0.827901000
C	-3.743262000	-0.547828000	2.783017000
H	-3.809039000	-2.708113000	2.466510000
H	-6.019713000	-3.132492000	1.965495000
C	-0.417301000	-3.642192000	-0.704005000
H	-0.417484000	-1.539246000	-0.157483000
H	-2.487077000	-1.117012000	0.334631000
C	3.202658000	-1.223897000	2.800249000
H	3.205712000	-3.202092000	1.932016000
H	0.855318000	-3.211981000	1.900465000
C	6.880123000	-3.759397000	-1.163882000
H	6.351337000	-1.697773000	-0.749606000
H	4.574074000	-1.114063000	0.316055000
H	7.671196000	-2.882047000	1.585063000
H	8.198972000	0.866009000	-0.854441000
C	3.233381000	0.638841000	-2.603559000
H	3.352815000	0.533406000	-0.462457000
H	0.992348000	0.670964000	-0.527183000
C	-3.954200000	1.226051000	-2.862655000
H	-3.768482000	0.722066000	-0.749466000
H	-5.931981000	1.071790000	-0.214059000
C	-0.159328000	3.019938000	1.021383000
H	-0.130766000	3.327248000	-1.120277000
H	-2.403728000	3.247096000	-1.370355000
C	7.258000000	2.621163000	1.150275000
H	6.718174000	3.440176000	-0.798459000
H	4.570710000	3.045051000	-1.329952000
C	-7.157827000	3.739672000	0.943625000
H	-7.175366000	3.465606000	-1.198821000
H	-9.514415000	3.231170000	-1.199892000
H	10.676255000	-1.603942000	1.003447000
H	9.764003000	-0.247026000	1.667870000
H	9.541232000	-1.876688000	2.350705000
H	9.322792000	1.429065000	-3.928068000
H	10.532197000	2.067997000	-2.813328000
H	9.680937000	0.552922000	-2.411524000
H	-6.573605000	-3.308501000	-1.311012000
H	-7.332249000	-4.411148000	-0.136030000
H	-8.346302000	-3.343315000	-1.132802000
H	0.446886000	-3.502520000	-1.362514000
H	-0.293462000	-4.594649000	-0.177700000
H	6.909979000	-4.701099000	-0.600361000
H	7.894412000	-3.560684000	-1.529204000
H	2.251234000	0.150221000	-2.602542000
H	-3.627498000	2.071410000	-3.477576000
H	-3.301203000	0.374588000	-3.082120000
H	-3.763412000	0.331490000	2.125597000
H	-4.657570000	-0.530575000	3.386121000
H	2.298155000	-1.461187000	3.376598000
H	-8.073377000	4.337123000	0.964142000
H	-7.110841000	3.125832000	1.847943000
H	-6.293963000	4.407793000	0.920360000
H	0.756647000	3.607441000	1.141105000
H	-0.103617000	2.166799000	1.706802000
H	7.747017000	1.693992000	1.479945000

H	6.324576000	2.697188000	1.723635000
C	-2.524189000	-0.522876000	3.667755000
C	-0.236634000	-0.521398000	5.294585000
C	-1.294594000	-0.077811000	3.168548000
C	-2.588760000	-0.974724000	4.988083000
C	-1.453893000	-0.978113000	5.796678000
C	-0.161778000	-0.068736000	3.978340000
H	-1.226136000	0.252082000	2.132866000
H	-3.538483000	-1.323833000	5.386173000
H	-1.522345000	-1.331578000	6.820924000
H	0.778780000	0.302257000	3.582414000
H	0.647471000	-0.513802000	5.924903000
C	-1.380798000	3.855274000	1.309549000
C	-3.700709000	5.371956000	1.730149000
C	-2.467256000	3.316294000	2.004117000
C	-1.471844000	5.163710000	0.825211000
C	-2.623832000	5.918691000	1.034599000
C	-3.621138000	4.067562000	2.214315000
H	-2.399857000	2.303256000	2.395092000
H	-0.630022000	5.594154000	0.286856000
H	-2.678464000	6.935699000	0.658596000
H	-4.455913000	3.634354000	2.757825000
H	-4.596413000	5.962585000	1.897735000
C	-1.704020000	-3.637356000	-1.489308000
C	-4.144002000	-3.549550000	-2.866527000
C	-1.903692000	-2.714249000	-2.520707000
C	-2.743933000	-4.505896000	-1.149531000
C	-3.957785000	-4.464641000	-1.832113000
C	-3.114013000	-2.672645000	-3.208456000
H	-1.102588000	-2.027897000	-2.787200000
H	-2.599938000	-5.215965000	-0.338537000
H	-4.755093000	-5.150025000	-1.559914000
H	-3.255196000	-1.960587000	-4.017004000
H	-5.086158000	-3.518450000	-3.407364000
C	-5.401300000	0.908214000	-3.153418000
C	-8.149291000	0.430437000	-3.458684000
C	-5.942930000	-0.340801000	-2.840363000
C	-6.250846000	1.910715000	-3.632936000
C	-7.616296000	1.677617000	-3.781095000
C	-7.307606000	-0.578443000	-2.993943000
H	-5.297452000	-1.116522000	-2.438699000
H	-5.839152000	2.890101000	-3.865761000
H	-8.263957000	2.470188000	-4.144608000
H	-7.715673000	-1.554507000	-2.746611000
H	-9.214049000	0.247598000	-3.567309000
C	5.941499000	-3.896367000	-2.369157000
H	5.918455000	-2.925377000	-2.886126000
C	4.507622000	-4.268877000	-1.980390000
H	4.501147000	-5.182667000	-1.374396000
H	3.906767000	-4.451522000	-2.877611000
H	4.008252000	-3.480773000	-1.407506000
C	6.507188000	-4.938463000	-3.335998000
H	7.523301000	-4.680343000	-3.651218000
H	5.882734000	-5.024153000	-4.230849000
H	6.542692000	-5.923440000	-2.855139000
C	8.134332000	3.830357000	1.494407000

H	7.553533000	4.734446000	1.261963000
C	9.435896000	3.885973000	0.692466000
H	9.996099000	2.948458000	0.796816000
H	10.068919000	4.700755000	1.060025000
H	9.250378000	4.057228000	-0.371515000
C	8.431326000	3.825989000	2.994818000
H	7.510262000	3.794600000	3.586164000
H	8.993708000	4.718797000	3.285622000
H	9.032954000	2.948058000	3.260145000
C	3.159414000	0.250766000	2.393619000
H	3.127107000	0.886334000	3.284625000
H	2.284178000	0.487924000	1.776426000
H	4.059326000	0.521374000	1.827505000
C	4.428071000	-1.510082000	3.667443000
H	4.397170000	-0.908938000	4.580898000
H	5.345824000	-1.255539000	3.124874000
H	4.480132000	-2.566500000	3.948369000
C	3.286581000	1.659058000	-3.739799000
H	2.515250000	2.428894000	-3.634362000
H	3.141523000	1.162170000	-4.703415000
H	4.263231000	2.155850000	-3.763326000
C	4.300209000	-0.441898000	-2.768183000
H	4.215090000	-1.187675000	-1.970379000
H	5.308286000	-0.011062000	-2.735156000
H	4.182016000	-0.951810000	-3.730170000

B.4.

CHEMBIOCHEM

Supporting Information

Chirality Dependence of Amyloid β Cellular Uptake and a New Mechanistic Perspective

Subrata Dutta,[a] Thomas S. Finn[+],[a] Ariel J. Kuhn[+],[a] Benjamin Abrams,[b] and Jevgenij A. Raskatov*[a]

cbic_201800708_sm_miscellaneous_information.pdf

CONTENTS PAGE

General experimental procedures	**Page 3**
Figure S1. HPLC and mass spectrum analysis of L-Aβ42 and D-Aβ42 peptides.	**Page 4**
Figure S2. HPLC and mass spectrum analysis of TAMRA labelled L-Aβ42 and D-Aβ42 peptides.	**Page 5**
Figure S3. HPLC and mass spectrum analysis of L-Aβ40 and D-Aβ40 peptides	**Page 6**
Figure S4. HPLC and mass spectrum analysis of TAMRA labelled L-Aβ40 and D-Aβ40 peptides	**Page 7**
Figure S5. TEM images of (L/D)-Aβ(40/42) and (L/D)-Aβ(40/42)-TAMRA following ThT fibril formation experiments	**Page 8**
Figure S6.. L-Aβ42 toxicity is not changed on N-terminal TAMRA addition.	**Page 8**
Figure S7. Intracellular co-localization of TAMRA labelled L/D-Aβ40/42 with Lysotracker Green in SH-SY5Y cells.	**Page 8**
Figure S8. Confocal images of SH-SY5Y cells dosed with (L/D)-Aβ42-TAMRA (15 h, 5 μM)	**Page 9**
Figure S9. Confocal images of PC12 cells dosed with (L/D)-Aβ42-TAMRA (2 h, 5 μM)	**Page 9**
Figure S10. Flow cytometry quantitation of TAMRA-labeled L- or D-Aβ42 uptake by SH-SY5Y and PC12 cells over a range of concentrations.	**Page 10**
Figure S11. Flow cytometry quantitation of (L/D)-Aβ42-TAMRA uptake by PC12 cells and rat hippocampal primary neurons.	**Page 10**
Figure S12. Flow cytometry quantitation of (L/D)-Aβ42-TAMRA uptake by SH-SY5Y cells at low temperature (4 °C).	**Page 10**
Flow cytometry quantitation of (L/D)-Aβ(40/42)-TAMRA uptake in SH-SY5Y and PC12 – individual replicates	**Page 11-17**
References	**Page 17**

WILEY-VCH

Experimental Procedures

Synthesis of unlabeled and TAMRA-labeled L-Aβ40/42 and D-Aβ40/42

L-Aβ40/42 and D-Aβ40/42 peptides were synthesized on TentaGel S PHB resin using Fmoc-based chemistry. Chemical modifications were performed following our previously published methods and protocols.[1] For TAMRA labeling, 50 mg of either L-Aβ40/42 or D-Aβ40/42 (~ 5 µmol) loaded resin (fully protected except the terminal primary amino group) was swelled by suspending the resin in 1 mL of dry DMF for 30 min. A mixture of 5(6)- carboxytetramethylrhodamine (TAMRA-COOH, 28 mg, 50 µmol) and (7-Azabenzotriazol-1-yloxy) tripyrrolidinophosphonium hexafluorophosphate (PyAOP, 31.3 mg, 50 µmol) was dissolved in 1 mL dry DMF and diisopropylethylamine (8.6 µL, 50 µmol) was added to each Aβ resin separately and each mixture was shaken for 24 h, filtered, washed with DMF (3 x 1 mL) and DCM (3 x 1 mL) and dried in vacuo for 30 min. All peptides were cleaved from solid support and deprotected with a reagent mixture containing trifluoroacetic acid (4 mL), 1, 2-diethanethiol (0.25 mL), tri-isopropylsilane (0.5 mL) and liquefied phenol (0.25 mL). All peptides were purified by HPLC, yielding purities exceeding 95% (Figure S1 to S4). The concentration of the resultant stock Aβ solutions was measured by nanodrop (ε = 1490 M^{-1} at 280 nm for unlabeled Aβ and ε = 99000 M^{-1} at 555 nm for TAMRA labeled Aβ).

Fibril formation assays

0.5 mg of either unlabeled or TAMRA-labeled L/D-Aβ42 was dissolved in 50 µL of cold 20 mM NaOH solution and sonicated for 30 s. Aβ solutions were then filtered through 100 kDa MWCO spin filter at 14000 g for 10 min. The concentration of the resultant stock solutions was measured by nanodrop (ε = 1490 M^{-1} at 280 nm for unlabeled Aβ and ε = 99000 M^{-1} at 555 nm for TAMRA labeled Aβ). The stock solutions were then diluted to 20 µM final concentration using 20 µM ThT in PBS in presence of 0.02 % NaN_3 for unlabeled Aβ and only PBS for TAMRA labeled Aβ. Aggregation of unlabeled and TAMRA labeled Aβ was monitored using ThT fluorescence (λ_{ex} = 440 nm, λ_{em} = 485 nm) and TAMRA fluorescence ((λ_{ex} = 550 nm, λ_{em} = 580 nm) at 37 °C every 5 min for 24h continuous shaking. All experiments were conducted in black clear bottom 96 well plates, sealed with optically clear adhesive film, and using the Biotek synergy HTX fluorescence plate reader for data collection. All experiments were run in quintuplicate.

TEM experiments

Samples of unlabeled or TAMRA labeled L/D-Aβ40/42 were taken at the end of the fibril formation assay. Each sample of 3 µL was spotted on a freshly glow-discharged carbon-coated electron microscopy grid (Ted Pella, Catalog No. 01701-F) and allowed to incubate for 1min at ambient temperature. The sample was then stained with uranyl acetate with 30 µL of 1 % uranyl acetate. Grids were stored at ambient temperature and imaged by using JEOL 1230 microscope at an accelerating voltage of 120 kV.

Cell culture and sample preparation.

Both Adhesive PC12 cells and Human neuroblastoma SH-SY5Y were purchased from ATCC. PC12 cells were cultured in F12K media supplemented with 2.5% fetal bovine serum, 12.5 % horse serum and 1% penicillin-streptamycin. Human neuroblastoma SH-SY5Y cells were cultured in 1:1 DMEM: F12 K media supplemented with 10% fetal bovine serum and 1% penicillin-streptamycin. For confocal experiments, cells were plated in a 8-well chamber slide (Ibidi µ slide) at a density of 20000 cells / well and allowed to adhere for 24 h before dosing. For flow cytometry experiments, cells were plated in a 6 well plate (Nunc) at a density of 500k/ well. All incubations occur at 37˚ C with 5% CO_2.

Confocal microscopy

SH-SY5Y or PC12 cells were plated in a 8-well chamber slide (Ibidi µ slide #80826) at a density of 20000 cells / well and allowed to adhere for 24 h before dosing. Each well contained 300 µL total volume. For Aβ dosing, a stock solution of 1 mg/mL TAMRA labeled Aβ was prepared for each and 6.8 µL of L/D-Aβ42 or 6.5 µL of L/D-Aβ40 solution was aliquoted in Eppendorfs and then lyophilized overnight. The peptides were then dissolved in 5 µL of 20 mM NaOH and diluted to a final concentration of 5 µM using 295 µL of F12K media containing 2.5% Fetal Bovine Serum and 12.5% Horse Serum for PC12 cells or 1:1 DMEM: F12K media supplemented with 10% fetal bovine serum for Sh-SY5Y cells. Original media was replaced with fresh media containing peptides and incubated for 2 h at 37˚ C. Cells were then washed with DPBS, and 5 µg/mL Hoechst 33342 in DPBS was added for 10 min before imaging. Confocal images were acquired on a Leica SP5 confocal microscope using a 63x/1.4-0.6 oil immersion objective. 405 nm laser was used for Hoechst 33342 and signal collected between 415 nm and 485 nm. For TAMRA: 543 nm laser (30% laser power, unless indicated otherwise) was used for excitation and signal was collected between 590 nm and 720 nm.

Flow cytometry

SH-SY5Y or PC12 cells were plated in a 6 well plate (Nunc) at a density of 500k cells/well and allowed to adhere for 24 h before dosing. Each well contained 2 mL total volume. For dosing, a stock solution of 1 mg/mL TAMRA labeled Aβ was prepared for each and 45 µL of L/D-Aβ42 or 43.5 µL of L/D-Aβ40 solution was aliquoted in Eppendorf and lyophilized overnight. The peptides were then dissolved in 30 µL of 20 mM NaOH and diluted to a final concentration of 5 µM using 1970 µL of F12-K media containing 2.5% Fetal Bovine Serum (FBS) and 12.5% Horse Serum (HS) for PC12 cells or 1:1 DMEM: F12 K media supplemented with 10% FBS for SH-SY5Y cells. Original media was then replaced with fresh media containing 5 µM peptides and incubated for 2 h at 37˚C. For control experiments, original media was replaced with only fresh media. After exposing the cells with 5 µM peptide for 2 hrs., the cells were washed with PBS (2 times), trypsinized, re-suspended in 1 mL cell culture media, centrifuged at 120 g for 10 minutes, re-suspended in 500 µL PBS containing 0.1% Live /Dead fixable violet dead cell staining dye (Thermofisher scientific, cat no. L34955) and analyzed by BD FACS Aria II flow cytometer. For each sample, 10000 cells were counted and analyzed. Live/Dead cell dye was excited by a 405 nm laser and fluorescence was detected through 450/30 nm filter. TAMRA was excited with a 571 nm laser and fluorescence was detected through 580/10 nm filter. The live cell counting gate was determined using Live/Dead cell dye (channel BV421-A in graphics below). Data were evaluated by the FlowJo software.

Rat hippocampal primary neuron culture and flow cytometry analysis

Rat hippocampal primary neurons were purchased from BrainBits and cultured in NbActive-1 media (BrainBits). To culture the neuron, a 6 well plate was coated with poly-D-lysine. For coating the 6 well plate, 1 ml of poly-D-lysine (50 µg/ml) was added into each well and incubated at room temperature for 2 h. After 2 h incubation, the poly-D-lysine was aspirated, rinsed with double distilled water and air-dried. Cells were then plated at a density of 1M cells/well in NbActive-1 media and incubated at 37˚ C. After 1 h incubation, 90% of the media was changed with fresh CO_2 equilibrated NbActive-1 media and incubated it for 7 days at 37˚ C. 50% of media was changed every 3 days with fresh CO_2 equilibrated media. After 7 days, neurons were dosed with 5 µM of L or D-Aβ42-TAMRA peptide in NbActive-1 media. For the control experiment, original media was replaced with only fresh media. After incubating the cells with 5 µM peptide for 2 h, the cells were washed twice with PBS, trypsinized, re-suspended in 1mL NBActive-1 media, centrifuged at 100 g for 5 minutes, re-suspended in 500 µL of PBS containing 0.1% Live /Dead fixable violet dead cell staining dye and analyzed by BD FACS Aria II flow cytometer, as described above for PC12 and SH-SY5Y.

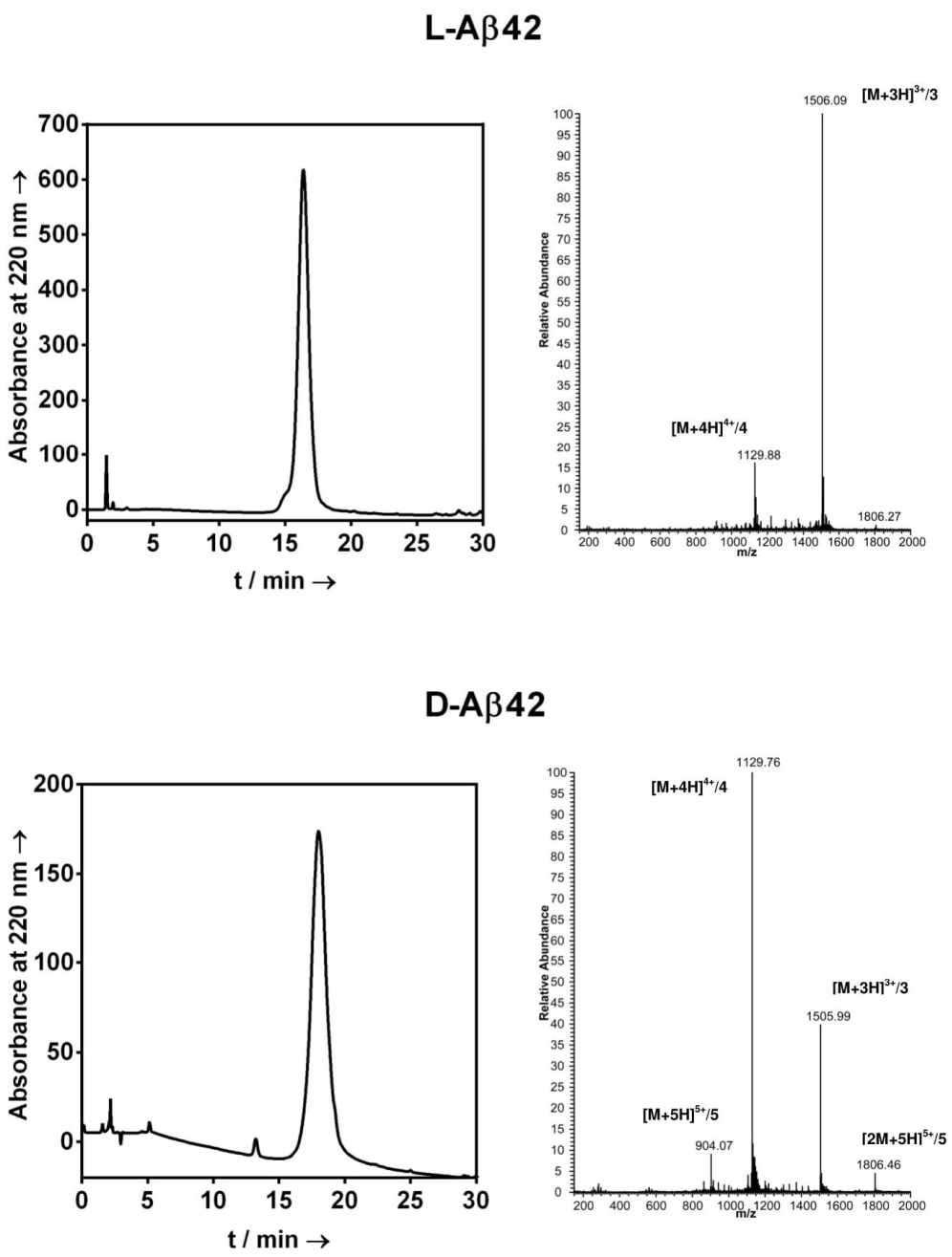

Figure S1. Analytical HPLC and mass spectrum analysis of the L-Aβ42 and D-Aβ42 peptide (representative examples). The purity of each peptide was >95%, determined *via* analytical HPLC, by integration of signals at 220 nm.

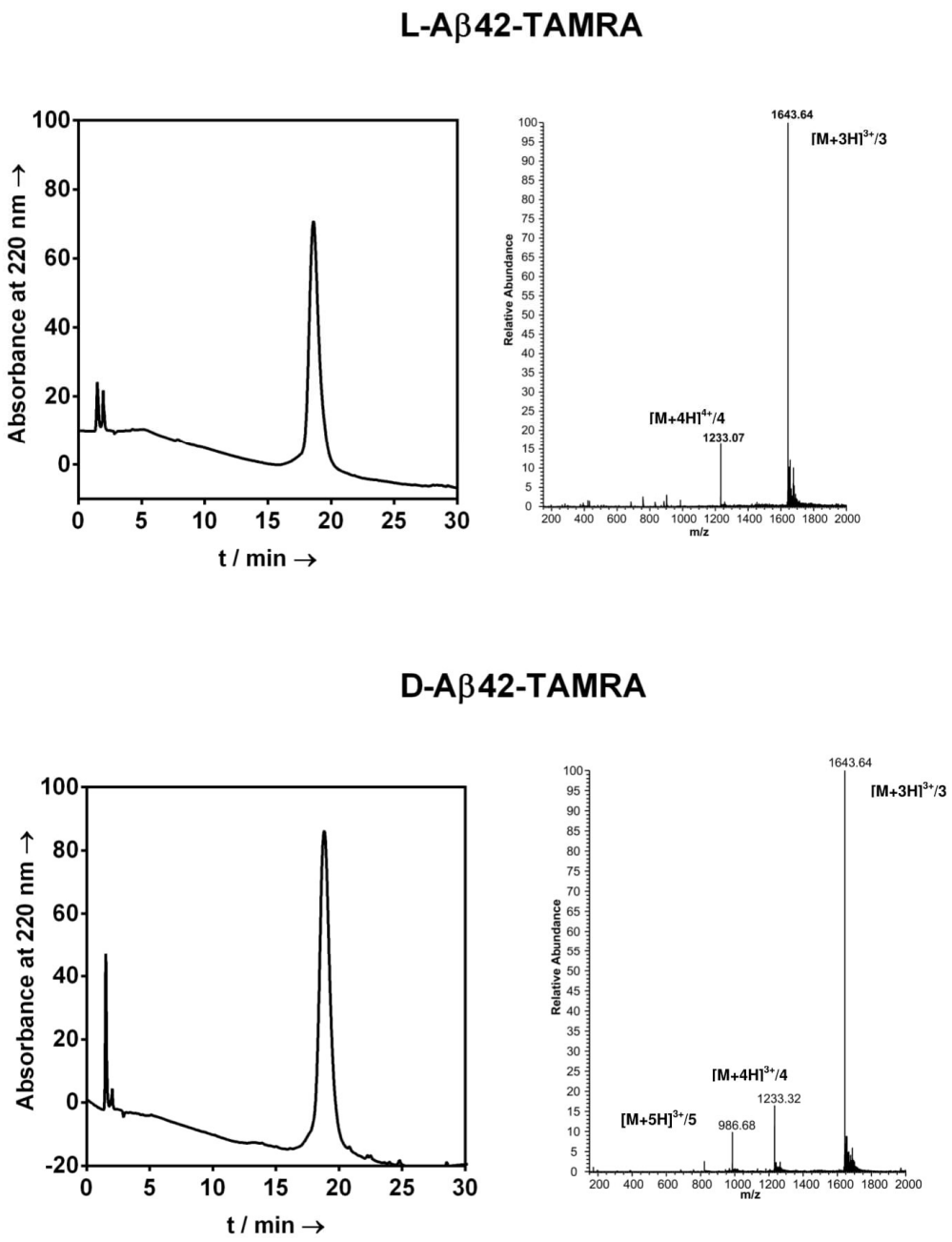

Figure S2. Analytical HPLC and mass spectrum analysis of the L-Aβ42-TAMRA and D-Aβ42-TAMRA peptide (representative examples). The purity of each peptide was >95%, determined *via* analytical HPLC, by integration of signals at 220 nm

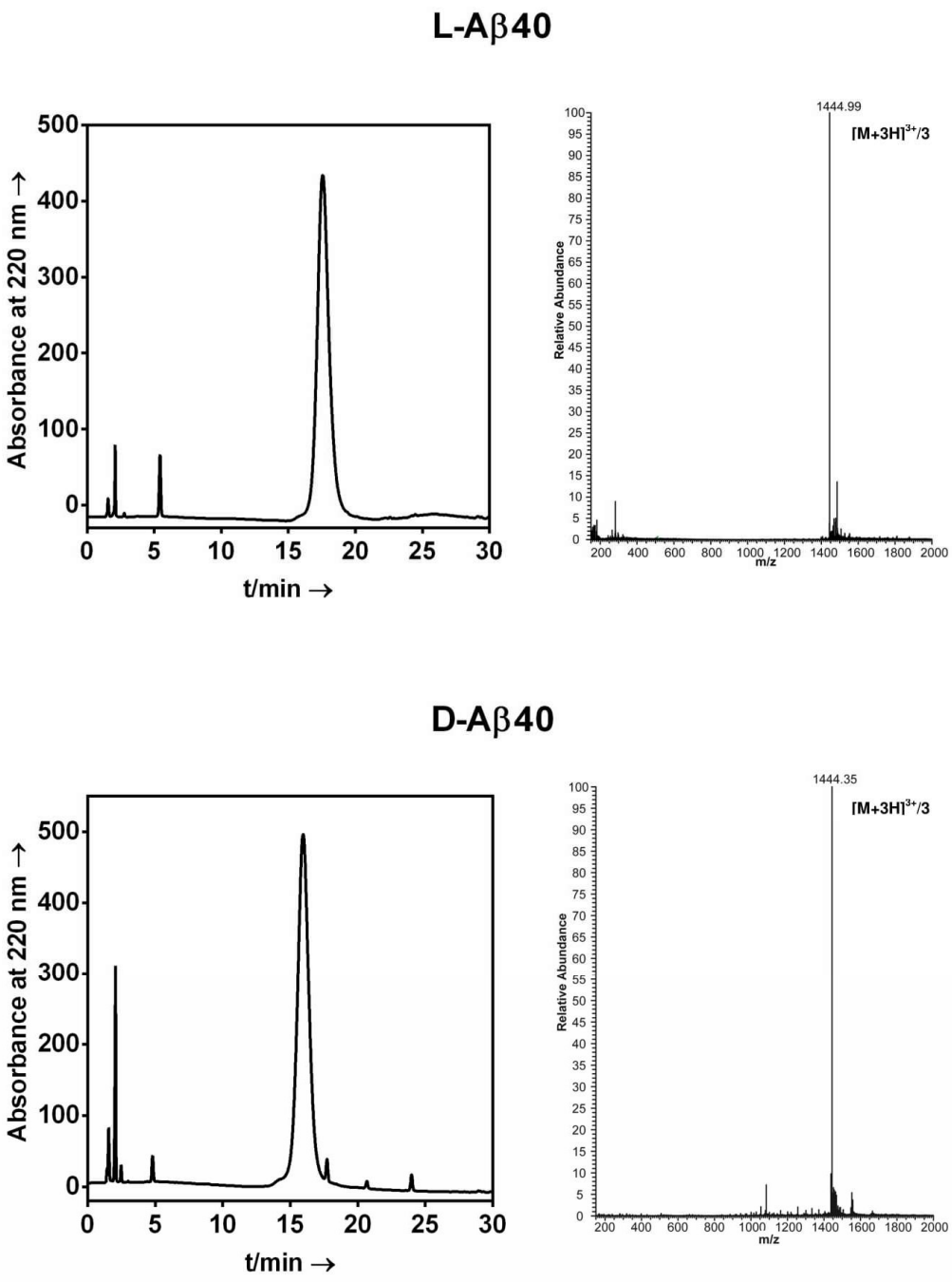

Figure S3. Analytical HPLC and mass spectrum analysis of the L-Aβ40 and D-Aβ40 peptide (representative examples). The purity of each peptide was >95%, determined *via* analytical HPLC, by integration of signals at 220 nm

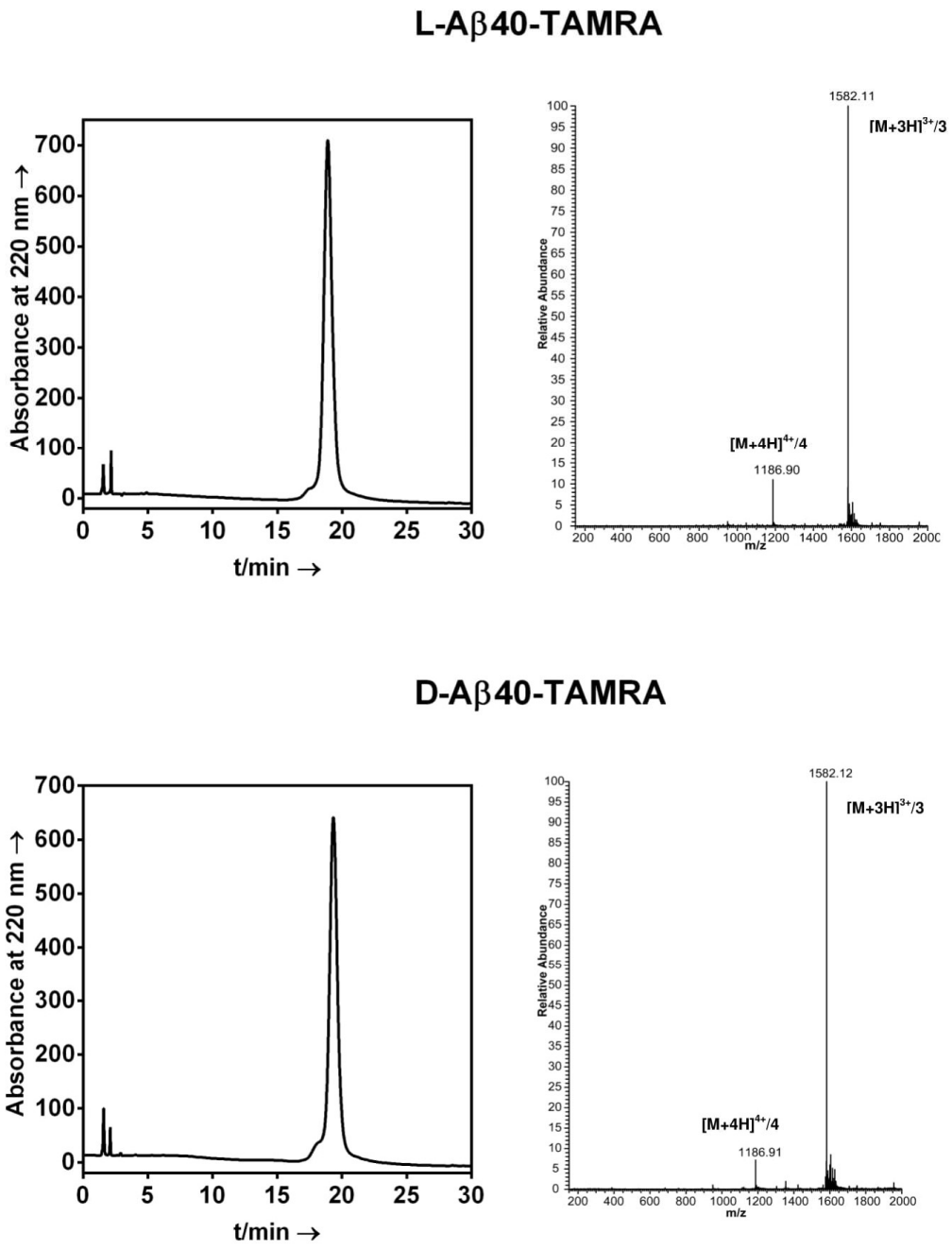

Figure S4. Analytical HPLC and mass spectrum analysis of the L-Aβ40-TAMRA and D-Aβ40-TAMRA peptide (representative examples). The purity of each peptide was >95%, determined *via* analytical HPLC, by integration of signals at 220 nm.

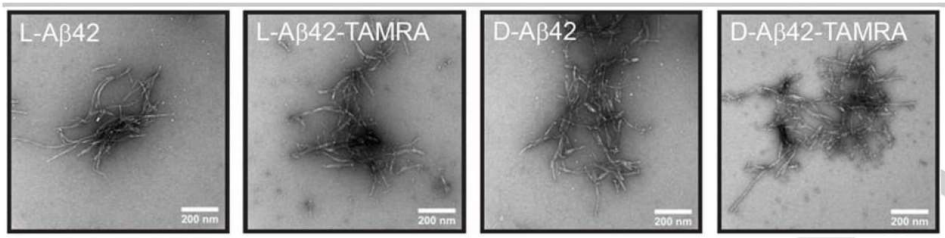

Figure S5. TEM images of (L/D)-Aβ(40/42) and (L/D)-Aβ(40/42)-TAMRA. Samples were taken directly from the ThT assays or TAMRA quenching assays (as appropriate) at the endpoint of the experiment. *Scale bars: 200 nm.*

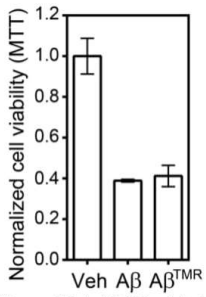

Figure S6. L-Aβ42 toxicity is not changed on N-terminal TAMRA addition. PC12 cells were incubated with 50 μM final L-Aβ42 peptide (either labelled or unlabelled, as indicated) for 3 days. See experimental procedures for further details.

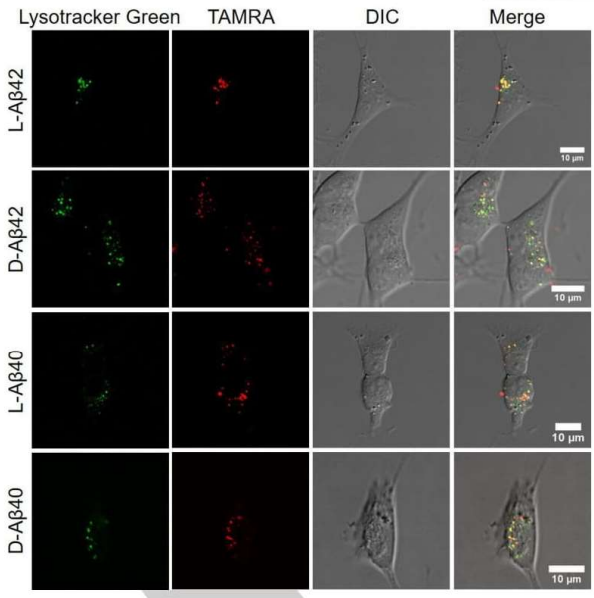

Figure S7. Intracellular co-localization of TAMRA labelled L/D-Aβ40/42 with Lysotracker Green in SH-SY5Y cells. The cells were incubated with Aβ peptide of 5 μM for 2 h, washed with fresh media and imaged 30 min after adding 50 nM Lysotracker Green. For L-Aβ40/42 peptide, 30% laser power was used and for D-Aβ40/42, 50% laser power was used, because reduced D-Aβ uptake precluded detection.

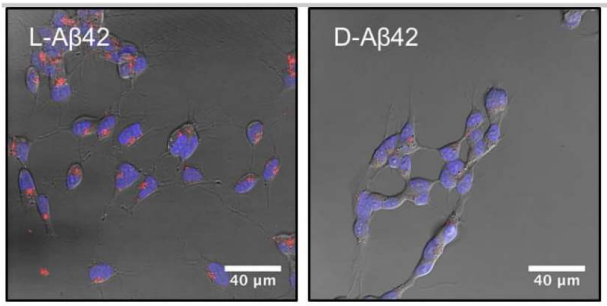

Figure S8. Confocal microscopy imaging of SH-SY5Y cells incubated with (L/D)-Aβ42-TAMRA, as indicated, at 5 µM for 15 h and rinsed with DPBS prior to imaging. TAMRA channel (Aβ uptake): excitation at 543 nm, emission over 590-720 nm; Hoechst 333420 channel (nuclear staining): excitation at 405 nm; emission over 415-485 nm.

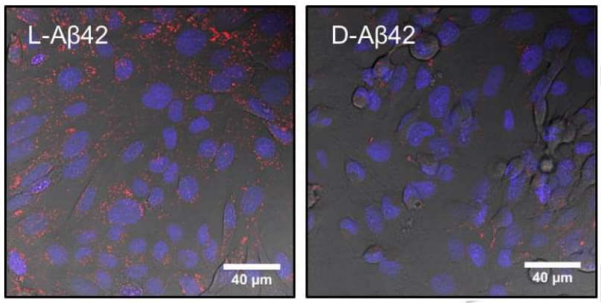

Figure S9. Confocal microscopy imaging of PC12 cells incubated with (L/D)-Aβ42-TAMRA, as indicated, at 5 µM for 2 h and rinsed with DPBS prior to imaging. TAMRA channel (Aβ uptake): excitation at 543 nm, emission over 590-720 nm; Hoechst 333420 channel (nuclear staining): excitation at 405 nm; emission over 415-485 nm. *Scalebar: 40 µm.*

WILEY-VCH

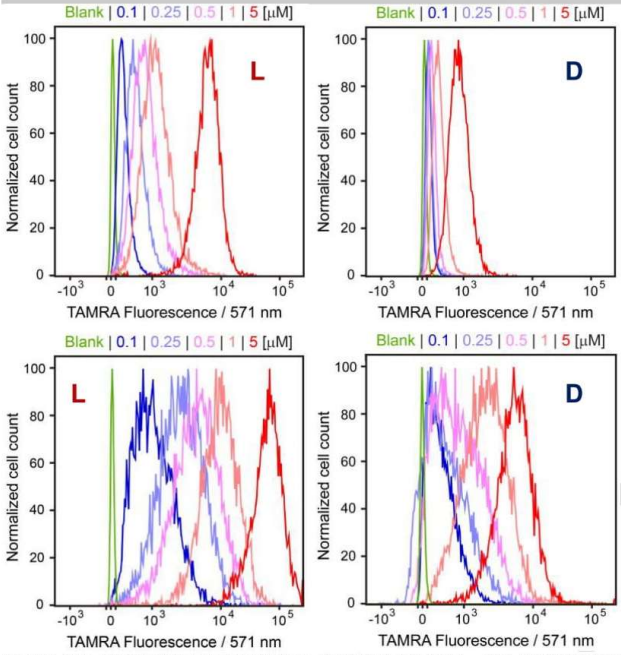

Figure S10. Flow cytometry quantitation of TAMRA-labeled L- or D-Aβ42 uptake by SH-SY5Y (top) and PC12 (bottom) cells over a range of concentrations reveals a consistent preference for cellular uptake of the L-stereoisomer. Cells were exposed to Aβ for 2 h, and then analyzed by flow cytometry (10,000 cells sampled per condition; only live cells selected for analysis; data analyzed using the FlowJo software package).

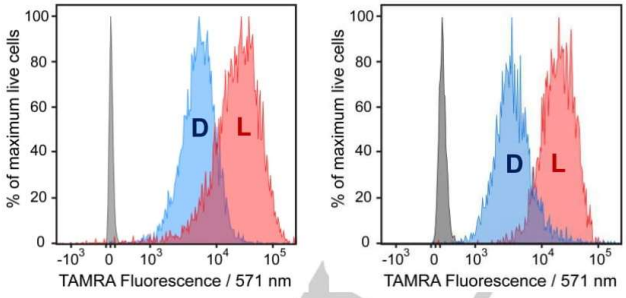

Figure S11. Flow cytometry quantitation of TAMRA-labeled L- or D-Aβ42 uptake by PC12 cells (left) and rat hippocampal primary neruons (right). Cells were exposed to 5 μM Aβ for 2 h, and then analyzed by flow cytometry (10,000 cells sampled per condition; only live cells selected for analysis; data analyzed using the FlowJo software package).

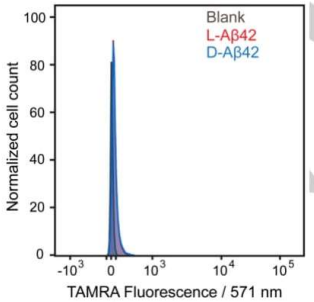

Figure S12. Flow cytometry quantitation of TAMRA-labeled L- or D-Aβ42 uptake by SH-SY5Y at low temperature. Cells were exposed to 5 μM Aβ for 2 h at 4 °C, and then analyzed by flow cytometry (10,000 cells sampled per condition; only live cells selected for analysis; data analyzed using the FlowJo software package).

SH-SY5Y flow cytometry – individual replicates: Blank

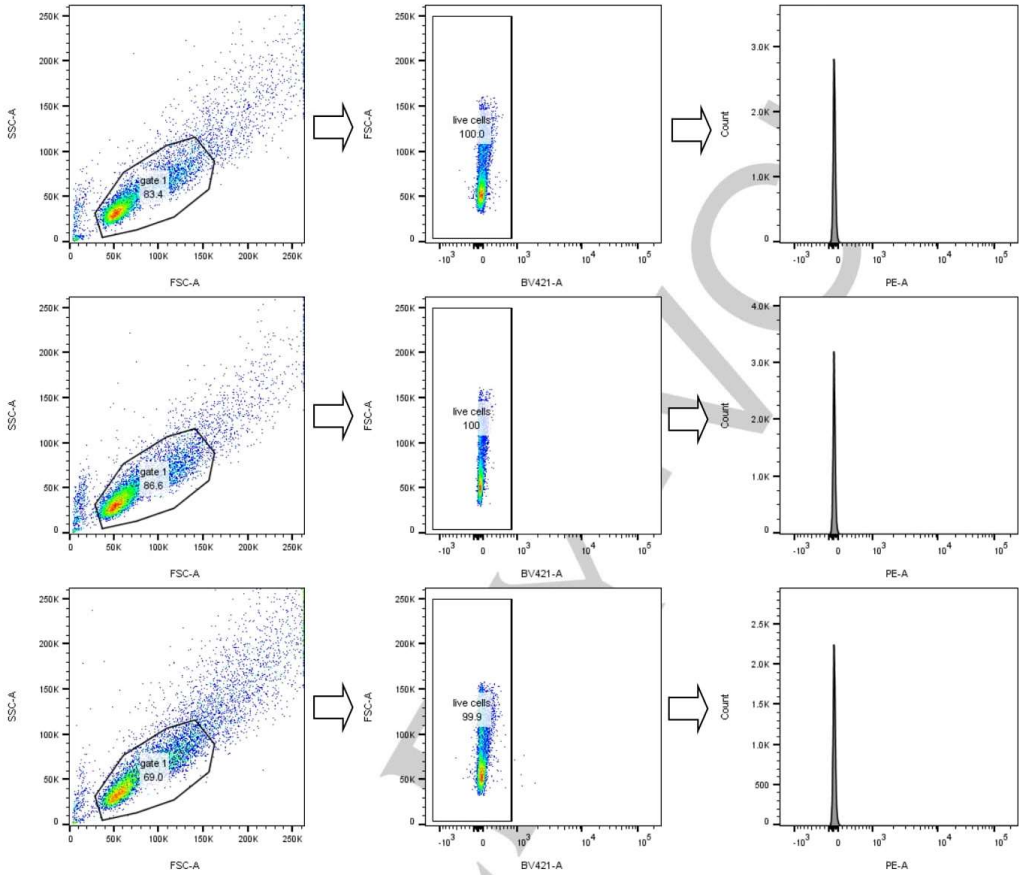

WILEY-VCH

SH-SY5Y flow cytometry – individual replicates: L-Aβ42

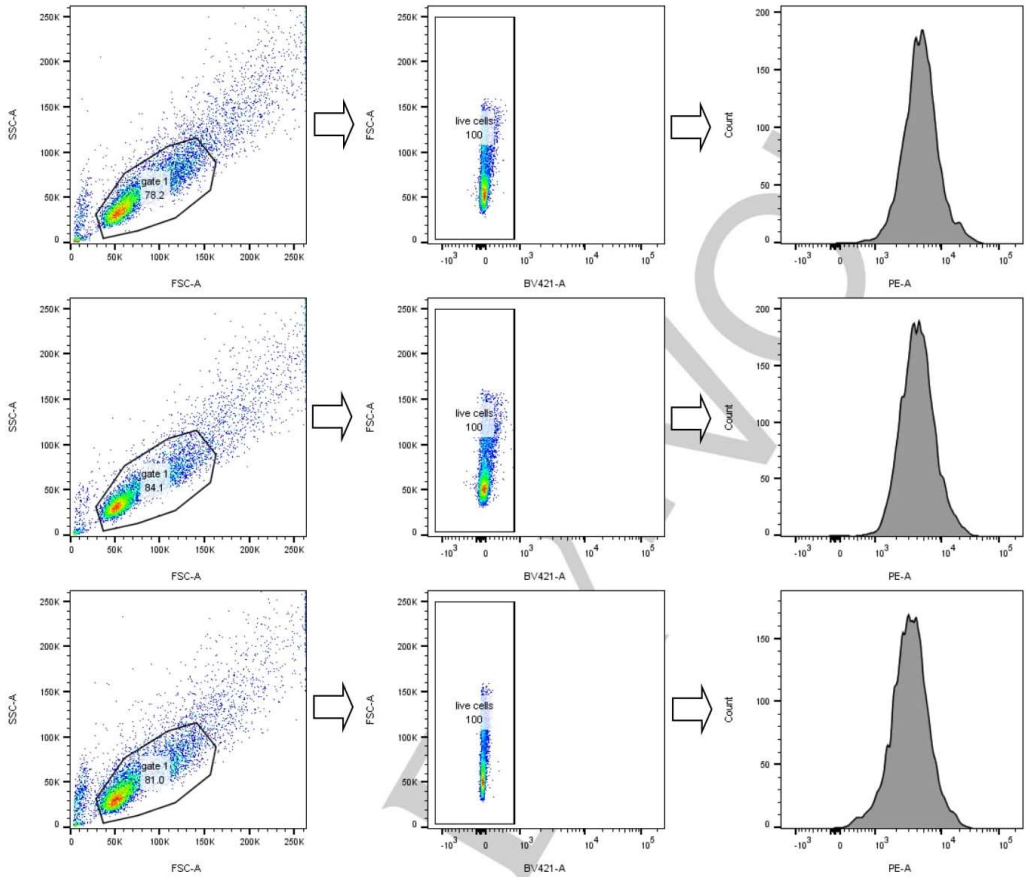

SH-SY5Y flow cytometry – individual replicates: D-Aβ42

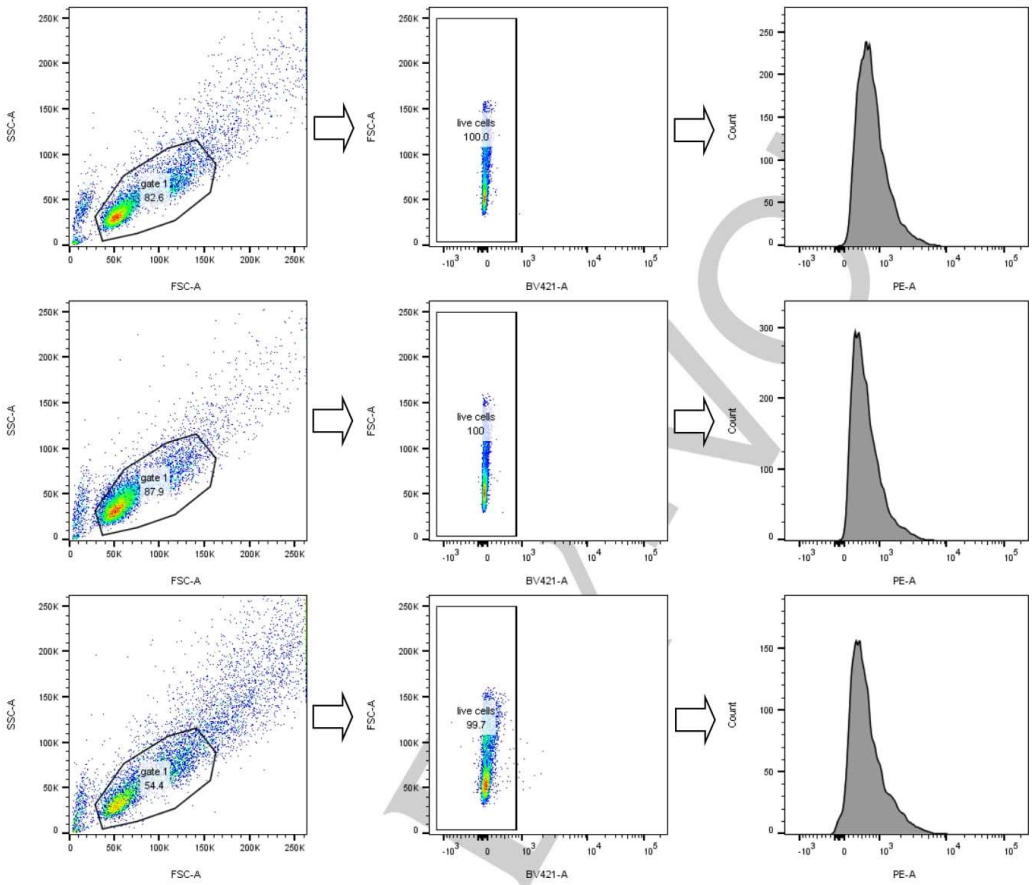

SH-SY5Y flow cytometry – individual replicates: L-Aβ40

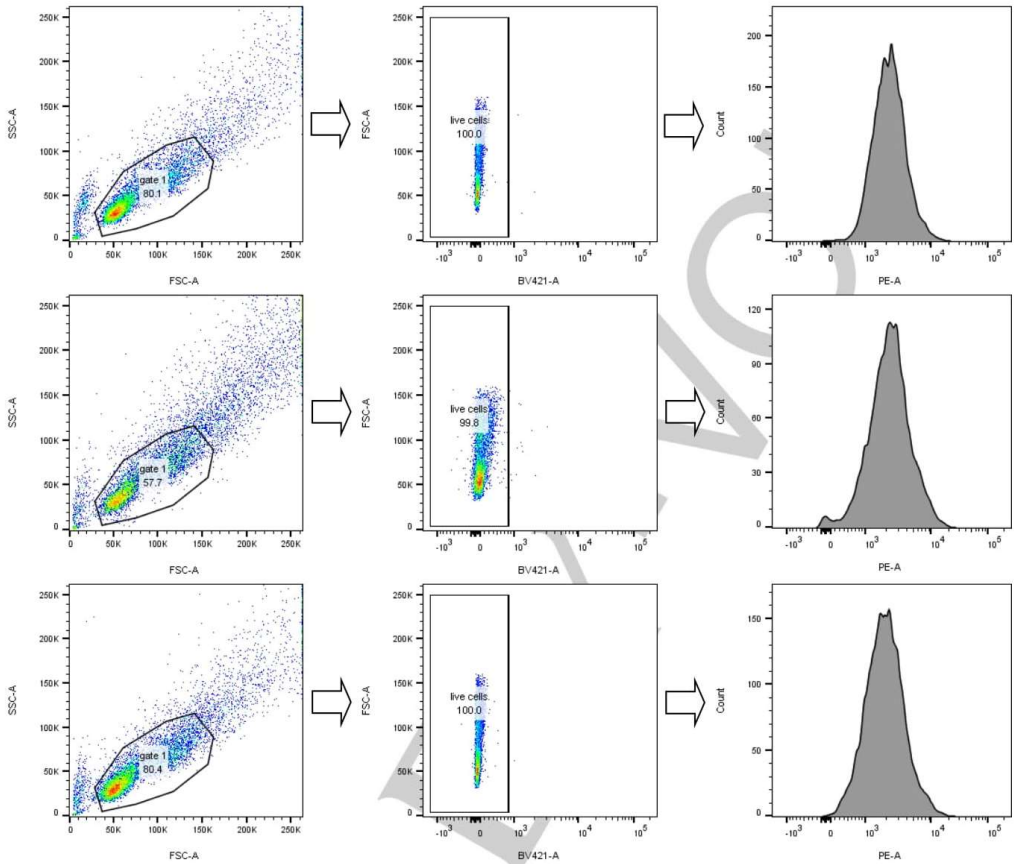

SH-SY5Y flow cytometry – individual replicates: D-Aβ40

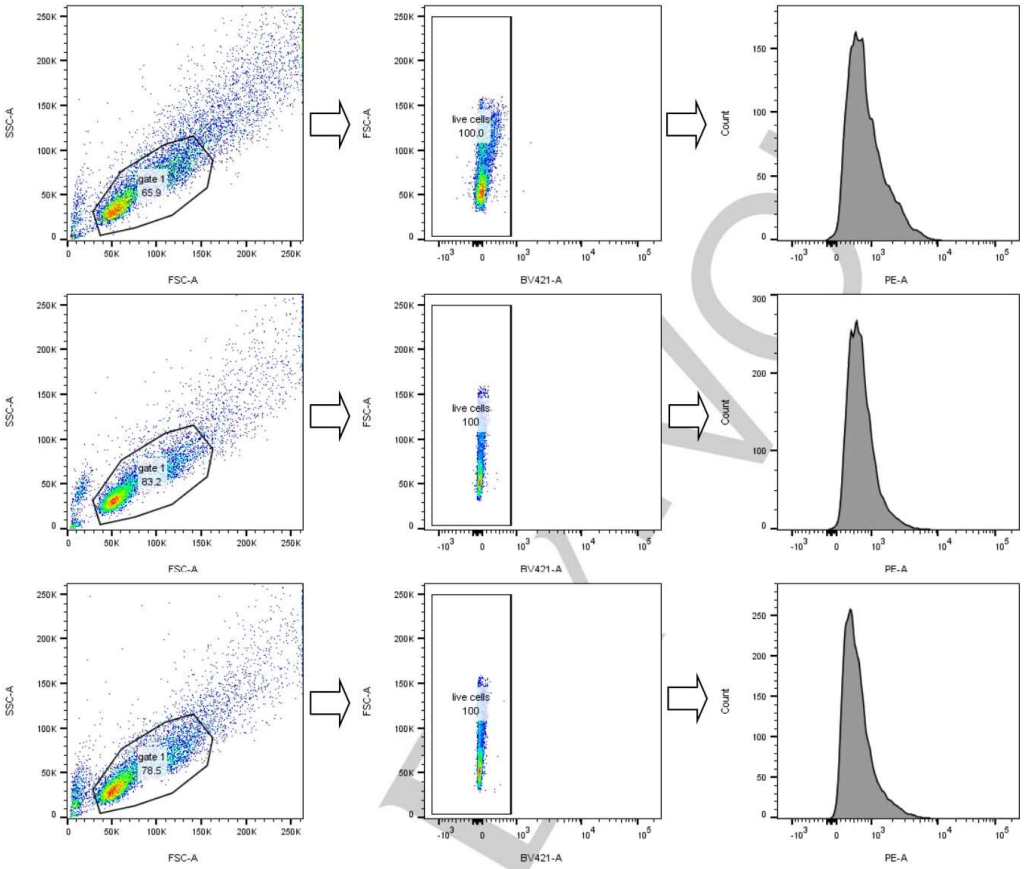

PC12 flow cytometry: Blank

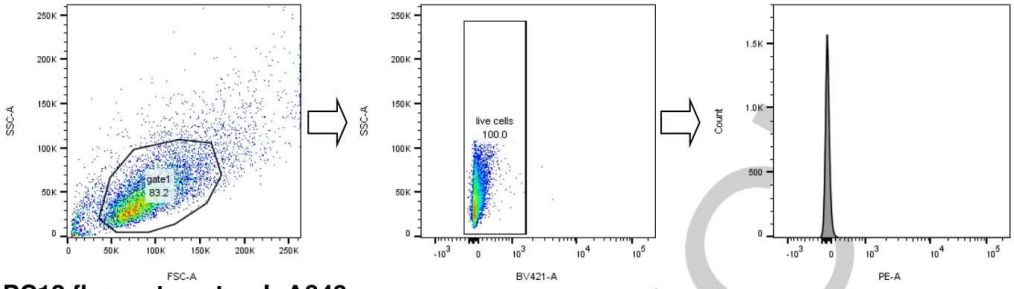

PC12 flow cytometry: L-Aβ42

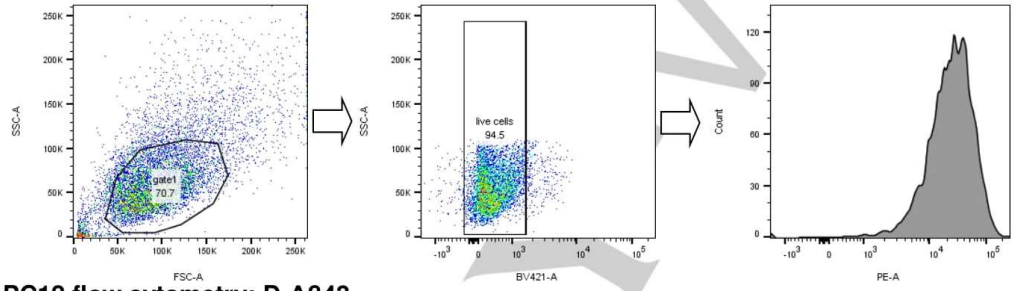

PC12 flow cytometry: D-Aβ42

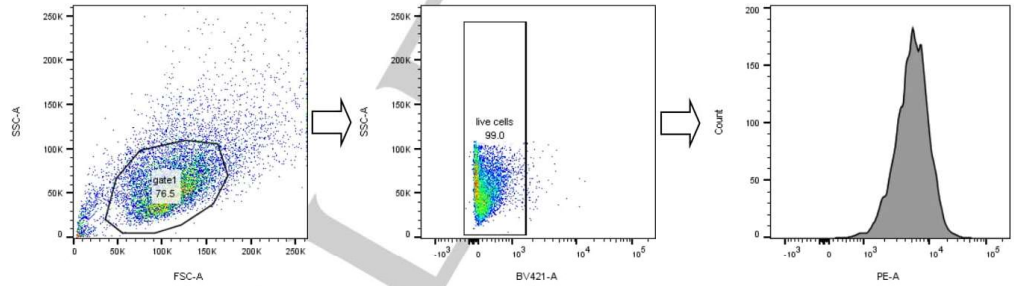

WILEY-VCH

Primary neuron flow cytometry: Blank

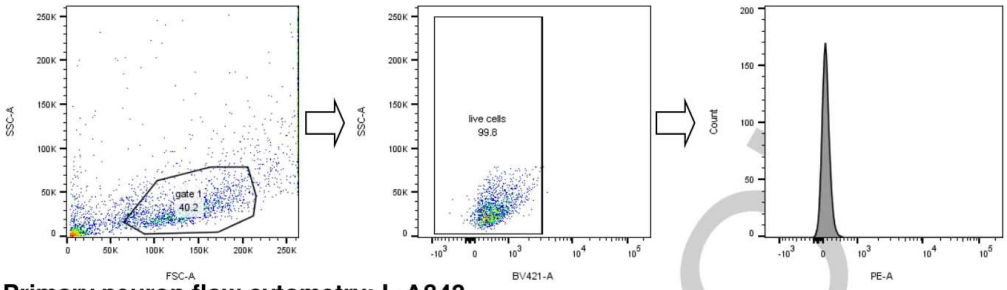

Primary neuron flow cytometry: L-Aβ42

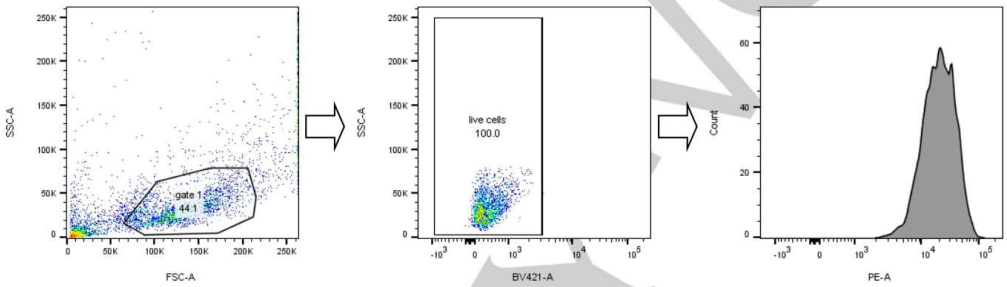

Primary neuron flow cytometry: D-Aβ42

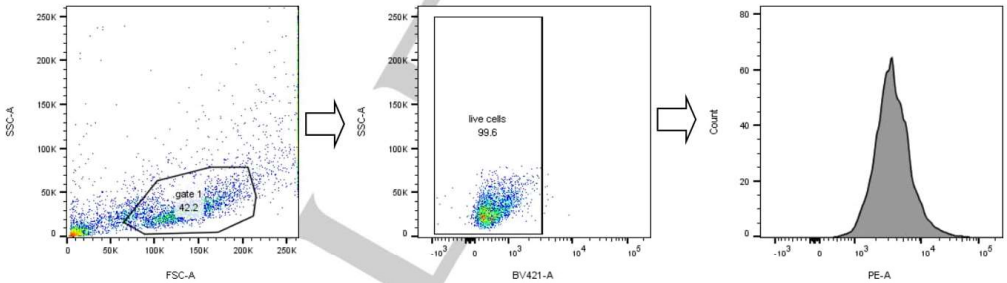

References

[1] S. Dutta, A. R. Foley, C. J. A. Warner, X. Zhang, M. Rolandi, B. Abrams and J. A. Raskatov, Angew. Chem. Int. Ed. 2017, 56, 11506-11510.

WILEY-VCH

B.5.

Electronic Supplementary Material (ESI) for Chemical Science.
This journal is © The Royal Society of Chemistry 2021

Supplementary Information for

A Crystal-Structural Study of Pauling-Corey Rippled Sheets

Ariel J. Kuhn,[a,♪] Beatriz Ehlke,[a,♪] Timothy C. Johnstone,[a]
Scott R. J. Oliver,[a] Jevgenij A. Raskatov[a,*]

* corresponding author; ♪ denotes equal contribution

Email: jraskato@ucsc.edu

This PDF file includes:

Figures S1 to S8
Tables S1 to S2
References

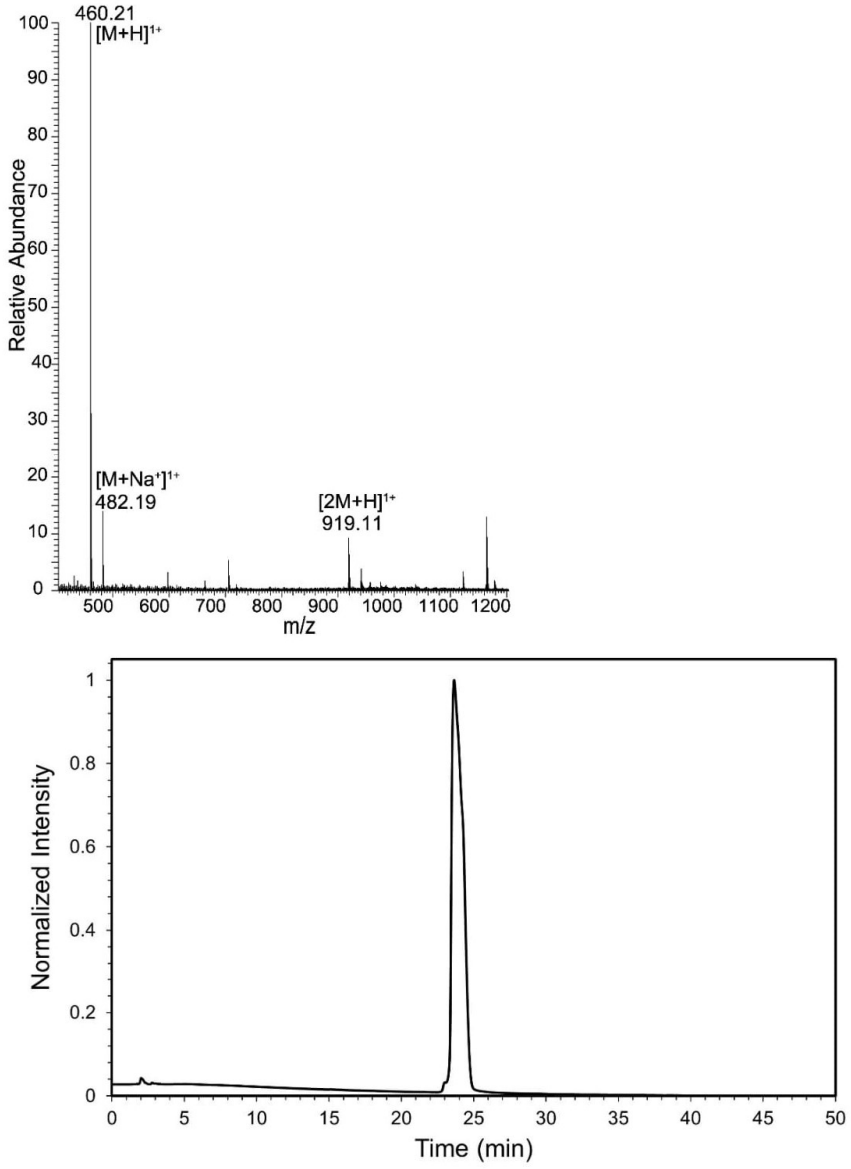

Fig. S1. Mass Spectrometry and HPLC characterization for NH_2-L-FFF-COOH.

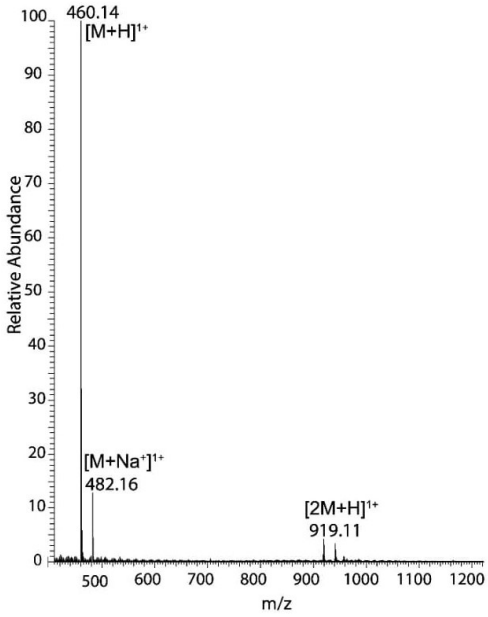

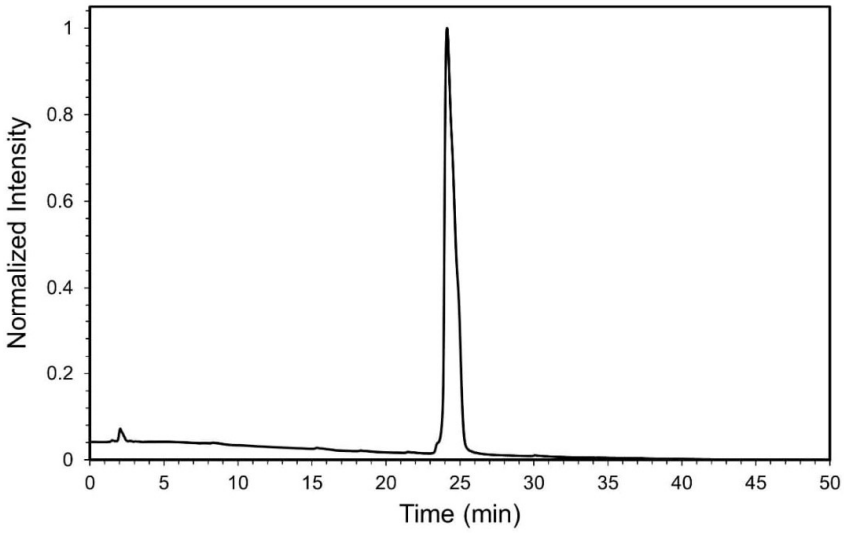

Fig. S2. Mass Spectrometry and HPLC characterization for NH_2-D-FFF-COOH.

Table S1. Crystallographic parameters

Compound	**Racemic triphenylalanine**
Formula	$C_{27}H_{29}N_3O_4$
FW	459.53
T (K)	100(2)
λ (Å)	1.54184
Crystal System	Monoclinic
Space group	$P2_1/c$
a (Å)	11.3563(5)
b (Å)	16.7472(6)
c (Å)	12.6545(6)
β (°)	101.483(4)
Volume (Å^3)	2358.54(18)
Z	4
ρ_{calc} (Mg/m^3)	1.294
Size (mm^3)	0.10 × 0.09 × 0.03
θ range (°)	4.44 – 67.06
Total data	23314
Unique data	4187
Parameters	323
Completeness	99.7%
R_{int}	5.00%
R_1 (I > 2σ)	4.43%
R_1 (all data)	5.54%
wR_2 (I > 2σ)	11.22%
wR_2 (all data)	11.81%
S	1.036
Min, max (e Å^{-3})	–0.279, 0.295

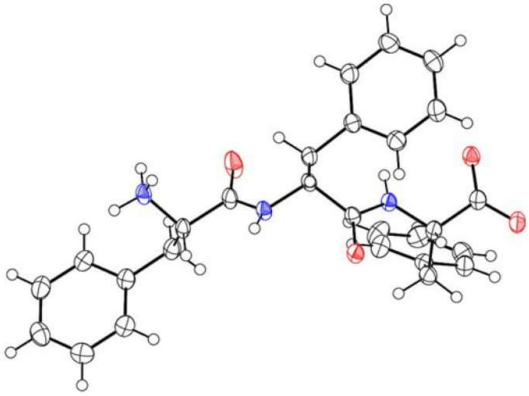

Fig. S3. Molecular graph of FFF with 50% thermal ellipsoids and H atoms shown as spheres of arbitrary radius. Color code: O red, N blue, C grey, H white.

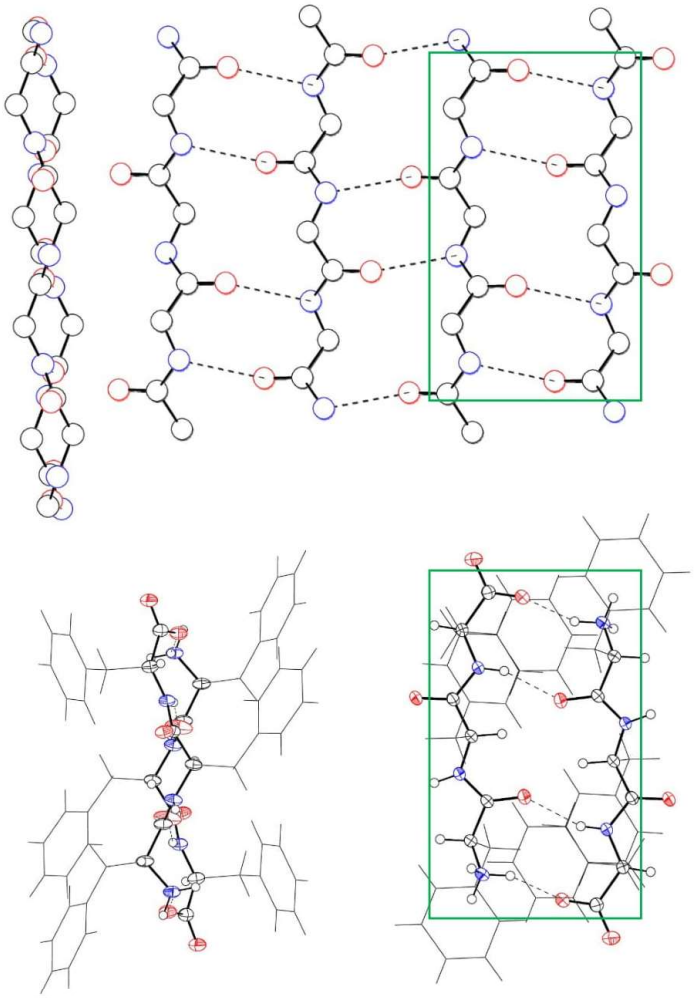

Fig. S4. *Top:* Side and top views of the rippled antiparallel sheet structure predicted by Pauling and Corey [cf. Figure 1 from *PNAS* **1953**, *39*, 253]. *Bottom:* Side and top views of the rippled sheet structure formed by FFF:fff. Atoms of the polypeptide backbone are shown as ellipsoids (non-H) or spheres of arbitrary radius (H). Side-chain atoms are shown as sticks. Color code: O red, N blue, C grey, H white. Hydrogen bonds are shown as dashed lines. Boxed in green is the similar motif from the predicted (top) and experimentally observed (bottom) structure.

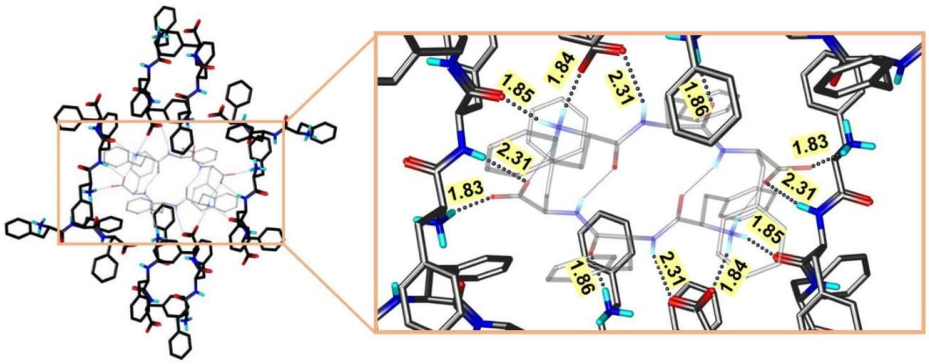

Fig. S5. The rippled antiparallel FFF:fff cross-β dimer shown in contact with its direct neighbors.

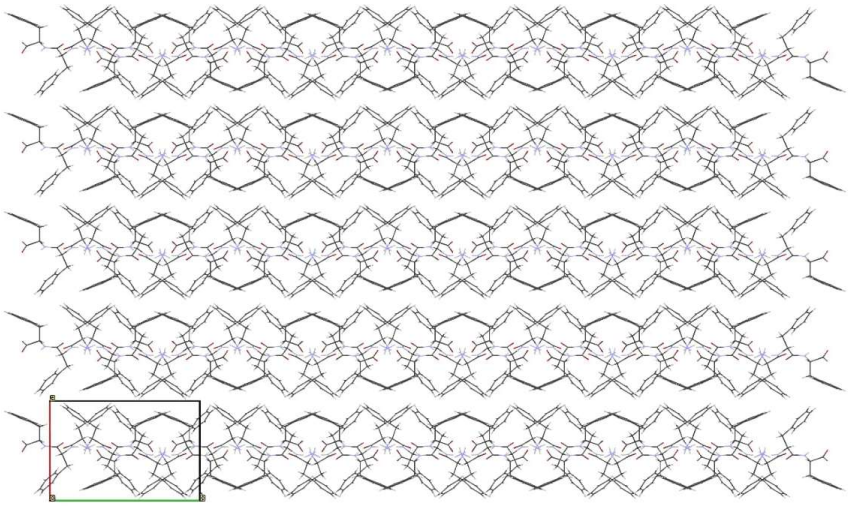

Fig. S6. Packing diagram of FFF:fff highlighting that the layer-to-layer distance is the crystallographic lattice parameter *a* = 11.3563(5) Å.

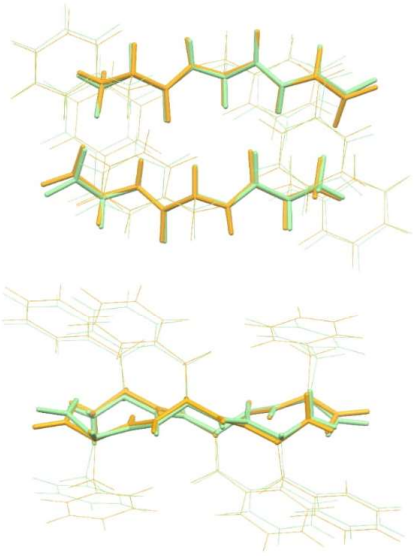

Fig. S7. Overlay of the crystallographic (orange) and the optimized (green; BP86-D3BJ/def2-SVP-CPCM$_{water}$) structure of the FFF:fff dimer. The polypeptide backbone is shown as thick sticks and the sidechains as thin sticks.

Table S2. Cartesian coordinates (Å) of the optimized (BP86-D3BJ/def2-SVP-CPCM$_{water}$) structure of FFF:fff.

N	4.09370415118074	12.55158927464286	8.01951364412157
H	3.96372050731073	11.87945342785070	8.89432214522468
H	3.67631800795364	13.45649622333425	8.29311390077636
H	5.10684826815001	12.72465726857804	7.86526886151337
O	4.68579699986856	10.00514061707158	7.08428367684645
C	4.21448263423020	10.83662052651225	6.28704928091444
C	3.40980475436177	12.02854135266891	6.80005942484666
H	3.38849381951550	12.83743527898451	6.04322345172614
C	1.97814220013488	11.57525758215830	7.15655122642748
H	1.54884004221062	11.10109355234939	6.25346523955252
H	2.05396185690734	10.79648718941633	7.94155838244508
C	1.09701622979355	12.71237139894564	7.62055690280438
C	1.09001748865928	13.10851995683912	8.97692250143198
H	1.71128992818933	12.55279025588311	9.70001424570751
C	0.29689600869346	14.19002383941204	9.39669431116368
H	0.30059192960416	14.48984062825498	10.45650801618807
C	-0.50386245035868	14.88372023555253	8.47211911233997
H	-1.12640255974232	15.72951255555404	8.80337394705965
C	-0.50629168506993	14.49105974185670	7.12126056936911
H	-1.13393642246107	15.02638237004613	6.39177196518855
C	0.29214352294006	13.41473994354018	6.69959318764820
H	0.28717212918944	13.10692663820845	5.64159702917600
N	4.34294104144003	10.71642127776430	4.95139847892585
H	4.02617325620660	11.45980460038944	4.32051429068197
O	4.39183936657579	10.13695537762992	2.13900493459608
C	4.53310543154521	9.25649096794045	3.00946511222600
C	5.11461928813669	9.61794373703439	4.38145018136459
H	5.03142864014147	8.76479723071096	5.07907335395468
C	6.60638929528331	10.03204527673807	4.24216281816270
H	6.66557687589099	10.81001469482846	3.45165198777844
H	6.89946224238773	10.50545984207140	5.19887788497200
C	7.54254308228714	8.88459583473587	3.94395032674684
C	7.58844472576498	8.28365432032168	2.66674556186903
H	6.94541458912158	8.66743223090499	1.86030598840700
C	8.45406241058803	7.20893971981611	2.40909750515203
H	8.45866869918136	6.74144750394299	1.41303033853607
C	9.30756466458947	6.72918695577871	3.41817773094835
H	9.98108783486585	5.88275984854788	3.21748271978528
C	9.27910482335856	7.32382914438217	4.69135159978216
H	9.93367021228568	6.94739162654751	5.49237800535179
C	8.39410679692009	8.38361619037178	4.95215142881515
H	8.36419766813895	8.83646995965917	5.95638546896319
N	4.27663118712145	7.94432643547798	2.83632745682123
H	4.39016191615368	7.30690269470780	3.64608983816175
O	5.36980195556720	5.51211468406074	2.26698208562355
O	5.09304882803972	5.85257505134016	0.05486234185960
C	4.90057255794537	6.14531097208455	1.25187163274656
C	3.97434193707562	7.35780504501355	1.54693871462719
H	4.15988268217939	8.13603868377272	0.78141118168691
C	2.48655619546023	6.92138841586021	1.42477292423107
H	1.85209546270454	7.81224356928512	1.60606231857112
H	2.32724214528117	6.59796256665133	0.37609533953726
C	2.11097727051036	5.80620589219198	2.37244680421324

C	2.28383758162549	4.45495364572536	1.99379188158820
H	2.67080634096225	4.22534617366592	0.98911503166958
C	1.97216973402590	3.41055767808345	2.87910349859398
H	2.11294850143188	2.36460126016809	2.56553803860911
C	1.48716530888976	3.70102699174574	4.17042290894159
H	1.23529636180071	2.88618588539751	4.86589264946698
C	1.31363145278839	5.04280868136374	4.55795607578832
H	0.92521192817041	5.27458827729304	5.56116588140656
C	1.62688866751194	6.08414190438623	3.66815534639682
H	1.50038556562449	7.13045249278436	3.98520466935573
N	4.74703122774710	4.19342206535575	4.38663953239223
H	4.86982114067797	4.86859999022297	3.51236735404479
H	5.16572951866549	3.29077403479728	4.10731414188434
H	3.73588967731612	4.01485485660771	4.54727049323470
O	4.16396127954101	6.74099311505567	5.31970178886795
C	4.63668287937818	5.91001586461808	6.11657509188658
C	5.43805826522110	4.71658749571353	5.60216894786604
H	5.46305755532070	3.90877021067308	6.35997761795219
C	6.86792610873869	5.16821719136807	5.23686214111084
H	7.30324336496732	5.64298378557832	6.13686772890228
H	6.78863229433642	5.94642718974931	4.45160130783574
C	7.74531512969249	4.02995894798071	4.76861216913461
C	7.74620225810931	3.63468321238378	3.41199288294599
H	7.12226633738760	4.19134827437473	2.69196386862010
C	8.53610557380459	2.55234105284025	2.98827944757836
H	8.52777712362381	2.25340164652189	1.92824534422122
C	9.33923708665485	1.85655064983315	3.90916358454985
H	9.95906506252588	1.00998479980240	3.57486101451993
C	9.34747886624511	2.24803499228983	5.26035139643555
H	9.97688767485362	1.71100378114162	5.98706279816186
C	8.55257204045476	3.32541707508023	5.68587348668957
H	8.56224206367965	3.63190721945685	6.74422251177071
N	4.51052720974095	6.03229462726670	7.45220154621982
H	4.82651042328429	5.28942368673009	8.08403981081477
O	4.45232595927066	6.60889428488492	10.26408493469117
C	4.30897502190871	7.49022987865021	9.39504697506979
C	3.73597511114322	7.13021966374973	8.01935926195330
H	3.82437115588301	7.98469998990265	7.32401109400939
C	2.24330073099328	6.71538912344956	8.14594351566544
H	2.17747246094972	5.93349904559341	8.93207273703793
H	1.95932459305754	6.24640532392327	7.18443283902556
C	1.30292448053796	7.86019962901400	8.44063142782111
C	1.24628926054932	8.45719361506985	9.71925040002921
H	1.88425058064177	8.07248796859544	10.52931357266964
C	0.37671889880669	9.52946860213518	9.97359028393214
H	0.36398847124617	9.99405460084568	10.97094721913926
C	-0.47041059278953	10.01046241701172	8.95970510299747
H	-1.14694010497439	10.85507471550927	9.15804996991875
C	-0.43155406803901	9.41947292909609	7.68513411129953
H	-1.08076873075477	9.79703992510457	6.88030795999379
C	0.45762561067833	8.36233045564615	7.42775676507842
H	0.49635272347544	7.91346605546526	6.42204849777097
N	4.55794847339994	8.80345073438008	9.57209305360787
H	4.44090072447028	9.44241168791802	8.76417612467272
O	3.45773153209174	11.23195820553672	10.13619692761770
O	3.72372766929813	10.89370536486153	12.35022202628192

10

C	3.92218845055026	10.60018630256060	11.15420196520344
C	4.85142631989578	9.38888224494806	10.86400355769733
H	4.66304253740939	8.60924727106737	11.62747022693811
C	6.33799403486710	9.82787788232499	10.99427526631197
H	6.97470662291954	8.93916325253939	10.81038900872820
H	6.49410552636178	10.14606052384495	12.04506325579148
C	6.71402078474572	10.94844574207184	10.05328804868640
C	6.54366053238547	12.29762245682966	10.44049823518437
H	6.15815230682130	12.52157842727393	11.44705665043399
C	6.85585320690155	13.34711395800373	9.56158813110815
H	6.71736316114667	14.39123957898378	9.88217394534763
C	7.33815102249408	13.06412388275726	8.26764787422629
H	7.58955393048688	13.88299875538902	7.57680417956278
C	7.50710227758705	11.72451427242645	7.87058479718694
H	7.88968207936726	11.49728715754806	6.86407916177420
C	7.19436456586794	10.67803224808990	8.75476176529525
H	7.31699362953703	9.63366286271353	8.42976376320827

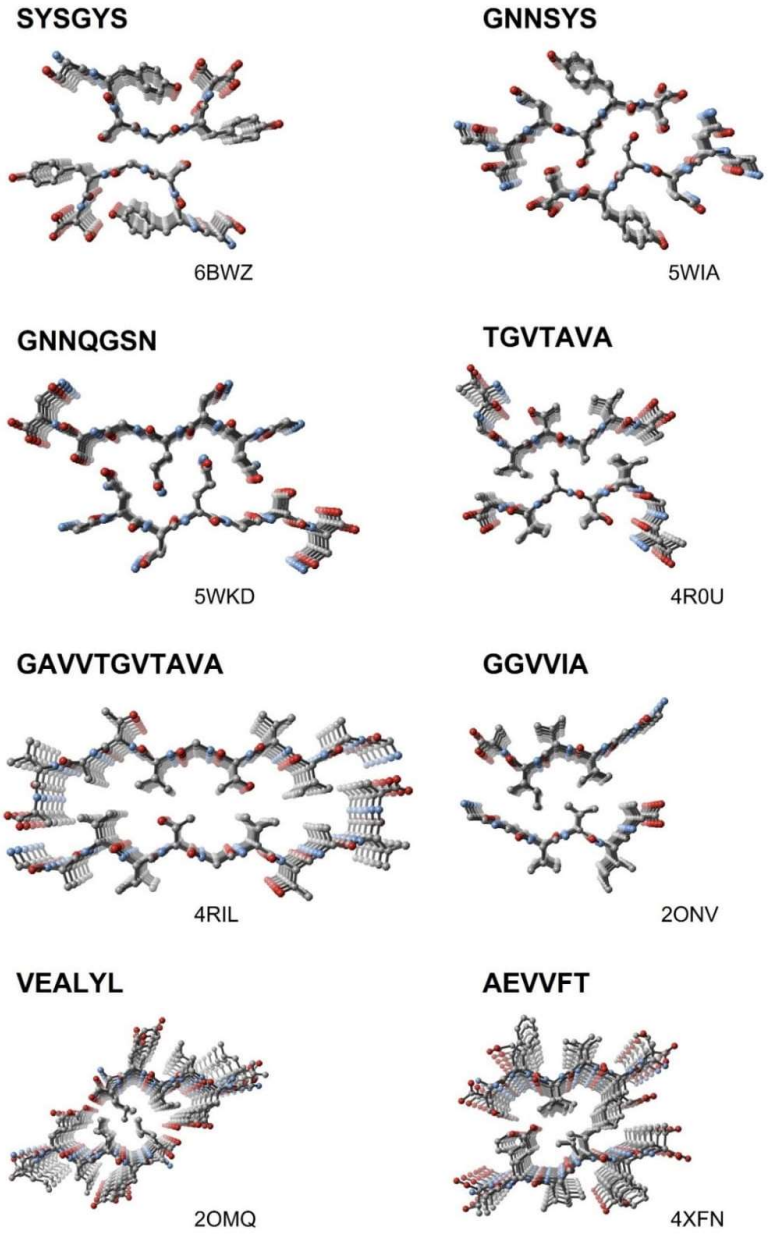

Fig. S8. Selected examples from Eisenberg and coworkers,(1–6) of fibrils formed by aggregating enantiopure peptides in which pleated β-sheets display one-dimensional, long-range order. Color code: C, gray; O, red; N, blue. Water molecules and hydrogens are omitted for clarity. PDB codes are displayed on the bottom right of each structure.

REFERENCES

1. M. P. Hughes, *et al.*, Atomic structures of low-complexity protein segments reveal kinked β sheets that assemble networks. *Science* **359**, 698-701 (2018).

2. E. L. Guenther, *et al.*, Atomic structures of TDP-43 LCD segments and insights into reversible or pathogenic aggregation. *Nat. Struct. Mol. Biol.* **25**, 463–471 (2018).

3. D. Li, *et al.*, Structure-Based Design of Functional Amyloid Materials. *J. Am. Chem. Soc.* **136**, 18044–18051 (2014).

4. J. A. Rodriguez, *et al.*, Structure of the toxic core of α-synuclein from invisible crystals. *Nature* **525**, 486–490 (2015).

5. M. R. Sawaya, *et al.*, Atomic structures of amyloid cross-β spines reveal varied steric zippers. *Nature* **447**, 453–457 (2007).

6. L. Saelices, *et al.*, Uncovering the Mechanism of Aggregation of Human Transthyretin. *J. Biol. Chem.* **290**, 28932–28943 (2015).